The use of computational fluid dynamics for the microbial assessment of food processing equipment

Asteriadou, Konstantia

Award date:
2005

Awarding institution:
University of Bath

The Use of Computational Fluid Dynamics for the microbial assessment of food processing equipment

Konstantia Asteriadou

A thesis submitted for the degree of Doctor of Philosophy

University of Bath

Department of Chemical Engineering

May 2005

ProQuest LLC
789 East Eisenhower Parkway
P.O. Box 1346
Ann Arbor, MI 48106-1346

Acknowledgements

The author would like to acknowledge the Marie Curie Fellowship Association for three years of financial support for the project. Thanks are given also to Unilever for the opportunity offered to carry out this work and the support offered, both financial and practical, for training and transportation between Bath, where experimental work was done, and Colworth House, where took place the computer based work. Special thanks to the technicians of the laboratory of the Chemical Engineering department in the University of Bath for the help they provided during the experimental work carried out there, and to the Unilever scientists, whose expertise contributed to the progress of this work through fruitful conversations and advise.

Summary

Hygienic design and manufacturing is very important especially for the food industry where consumers are involved and therefore the standards are very high and demanding. The combination of many parameters is essential for the correct operation of a production line in the food industry. Heating reassures sterilisation of product and equipment and cleaning follows for decontamination after a food product has gone through a process treatment. It is necessary to clean often in the food industry and improving the process can be crucial as far as it concerns energy and money saving while guaranteeing product quality. In addition, hygienically unsafe geometries are often encountered. Examples are: down-stands, up-stands, valves, locations of sensors and pipe couplings.

This thesis concerns the use of Computational Fluid Dynamics for the simulation of parameters that determine hygienic and safe operability of food processing. There are researchers that have worked on the CFD application for various products such as cans and pouches for sterilisation and sometimes including bacterial and nutritional information. Nevertheless, there was not strong temperature history dependence and heat transfer was mainly restricted to convection.

This work is built up gradually starting from temperature prediction distributions in a T-piece, where the horizontal part was at around 50°C and the vertical was just exposed to air temperature. This approach is taken because bacterial growth and inactivation is highly dependent on the temperature history of the product. Both Newtonian and non-Newtonian fluids are taken into account for different geometries. The predictions are supported by experiments that took place at the laboratory of the Chemical Engineering department of the University of Bath and by in-line measurements from a sterilisation Tube in Tube in Tube (TnTnT) heating unit at a Unilever factory.

Initially, steady state cases were examined that involved various flows: laminar, transitional and turbulent. Predictions were compared to experimental measurements and agreement was satisfactory. It depended on the accurate application of the code and the choice of the right CFD model that described the flow. For the T-piece, Newtonian fluid was used and various thicknesses of meshes were compared. It was shown that for higher amount of cells, solution in the vertical pipe was diverging more from the experimental values compared to the coarser mesh applied. The horizontal part of the configuration was insulated and the inlet temperature was maintained high and no significant heat losses were occurring to the environment. There was interaction between the bulk horizontal flow and the vertical pipe in the form of a recirculation zone that was extending further down the vertical tube as main flux was increasing. Thus, temperature was kept equal to the top (bulk flow) for longer as we were moving from laminar to turbulent flows.

The non-Newtonian flow was modelled in a TnTnT heat exchanger and bends were included as well. It was comprised of three heaters of 6m length each. The annular configuration, where the product was flowing is supposed to enhance heating compared to a simple Tube in Tube. There were in line measurements after each heating section from Pt-100 attached to the curved walls of the bends. Values taken from there were most likely affected by the heating medium supply, the entrance of which into the system was literally attached on the bends. Hence, conduction could have influenced values taken that were considerably higher than the predictions. However, there was very good agreement with the Pt-100 fixed at the end of the whole heating.

The model showed that there was mixing occurring in the bends, since the coldest zone of the product was exiting the bent parts at higher temperatures compared to the ones it was entering with.

Unsteady flows were also included in this work. Electrical conductivity was measured in the bottom of the T-piece in order to compare salt concentrations at steady state and again after cleaning the rig with deionised water for a certain period of time. The Species model was used in FLUENT so as to express the salt concentration. Fluent overestimated the height of measured concentration only by approximately 2cm in the vertical tube.

The last set of experiments involved bacterial kinetics. Ps. fluorescens was inoculated in Tryptone Soya Broth and was introduced into the rig. Various time periods and temperature conditions were applied in order to see the survival of the colonies, especially in the down-stand. Plating techniques and spectrophotometry were used to measure cell numbers. Cleaning followed with deionised water. Again, the species model was used for the simulation and a User Defined Function to express growth and inactivation of the bacteria. In that case the whole model was solved as unsteady since there was the reaction rate included all the time and cleaning took a specific period of time. The models used to express rates were inconsistent and convergence was difficult to achieve. Time step had to remain low and simulations took a long time. Nevertheless, agreement was satisfactory with only an inclination of maximum of two log orders in colony counts.

The above results support the use of CFD in assessing heating treatment and interaction of the product flow and cleaning solution with unhygienic geometries. Combination of engineering principles and microbiology methods is the way such issues should be approached for best results and CFD can incorporate both, with some necessary amendments. The models could be expanded to biofilm formation prediction, based on existing equations that combine bulk flow concentration and wall adherence. This could improve understanding concerning the whole behaviour of the flow and product and the risks to safety that a process line might be hiding.

Table of Contents

List of figures

List of tables

Nomenclature

A	constant value from equation (2.4.1)	~
A	maximum growth reached	[CFUml^{-1}time^{-1}]
a	sensitive volume of the cell	
A_{area}	surface area	[m^2]
A	constant in Jones and Walker model	~
A"	constant for the chemical reaction rate model	~
ah	average number of hits within the volume a	
$A_n(t)$	integral function of $\alpha_n(t)$	
b	constant for Bělehrádek models	~
b	constant from mixing length equation 2.4.11	~
B	constant in Jones and Walker model	~
B	mathematical parameter for Logistic and Gompertz equations	~
B	relative growth rate at time M for Zwietering model	[h^{-1}]
Br	Brinkman number	~
C	constant in Jones and Walker model	~
C	cook value	[h]
C	final log increase in bacterial numbers	
C'	constant in equation for natural convection heat transfer coefficient (eq. 3.2.1)	~
C_1	constant for the Davey model (eq. 2.8.3 and 2.8.10)	~
$C_{1\varepsilon}$	dimensionless constant for k-ε model from equation 2.4.18	~
$C_{2\varepsilon}$	dimensionless constant for k-ε model from equation 2.4.18	~
C_2	constant for the Davey model (eq. 2.8.3 and 2.8.10)	~
C_3	constant for the Davey model (eq. 2.8.10)	~
$C_{3\varepsilon}$	constant for k-ε model	~
C_A	concentration of component A	[kmolm^{-3}]
$C_{j,r}$	molar concentration of each reactant and product species j in reaction r	[kgmolm^{-3}]
C_o	constant for the Davey model (eq. 2.8.3 and 2.8.10)	~
c_p	specific heat	[kJkg^{-1}K^{-1}]
$C_{p,\alpha}$	air specific heat	[J kg^{-1} K^{-1}]
Cv	constant in eq. 3.1.9	~

C_μ	dimensionless constant for k-ε model from equation 2.4.16	~
d	constant for Bělehrádek models	~
D	constant in Jones and Walker model	~
D	log number of bacterial population at -∞	[h]
D_{10}	decimal reduction time when 10% of population survives	[h]
D_{90}	decimal reduction time when 90% of population is destroyed	[h]
D_e	equivalent diameter	[m]
dG/dt	per capita birth or growth rate in Jones and Walker model	[$cfuh^{-1}$]
Di,m	diffusion coefficient for species I in a mixture	[m^2s^{-1}]
dM/dt	per capita death or mortality rate in Jones and Walker model	[$cfuh^{-1}$]
D_o	decimal reduction time	[h]
D_T	decimal reduction time at temperature T	[h]
D_{Tr}	decimal reduction time at reference temperature T_r.	[h]
e	constant for eq. 2.8.7	~
e	deformation rate	[s^{-1}]
E	mean deformation of fluid element	[s^{-1}]
E_α	inactivation energy	[$kJmol^{-1}$]
f	constant for eq. 2.8.7	~
f	number of hits that fall within the volume a	~
$\vec{F}$	external body forces	
F	treatment time (lethality) at specific temperature	[h]
F(r,L)	treatment time at specific temperature at radial position r over axial length L	[h]
fibre	fibre content	~
F_{Tr}	thermal death rate	[h]
$\hat{F}(z)$	bulk lethality	
G_b	generation of turbulence kinetic energy due to buoyancy	
G_k	generation of turbulence kinetic energy due to the mean velocity gradients	
Gr	Grasshoff number	
G_T	bacterial generation time	[h]
G_ω	generation of ω	[$kg^2s^{-2}m^{-3}$].
h	average number of hits per unit volume	
h	heat transfer coefficient	[$Wm^{-2}K^{-1}$]
h	natural convection heat transfer coefficient	[$W\ m^{-2}\ K^{-1}$]

I	the unit tensor from eq. 3.1.3	
$\bar{j}_J$	diffusion flux of species j	[$kgm^{-2}s^{-1}$]
k	specific reaction rate constant	~
K	mean kinetic energy	[kgm^2s^{-1}]
k	turbulent kinetic energy	[kgm^2s^{-1}]
k_∞	reaction rate at infinite temperature	
k(t)	instantaneous kinetic energy	[kgm^2s^{-1}]
k'	inactivation rate constant	
$k_{b,r}$	backward rate constant for reaction r	
k_{eff}	effective thermal conductivity	[$Wm^{-1}K^{-1}$]
$k_{f,r}$	forward rate constant for reaction r	
k_t	turbulent thermal conductivity	[$Wm^{-1}K^{-1}$]
k_α	air thermal conductivity	[$W\ m^{-1}\ K^{-1}$]
l	length of surface for calculation of natural convection heat transfer coefficient	[m]
M	mathematical parameter for Logistic and Gompertz equations	
M	time at which culture achieves its maximum growth rate for Zwietering model	[h]
M_I	symbol denoting species i	
MW	molecular weight	[$kgmol^{-1}$]
N	bacterial population size	[CFU]
n	constant from mixing length equation 2.4.11	
n	constant in equation for natural convection heat transfer coefficient (eq. 3.2.1)	
N	number of chemical species in the system	
n	number of sensitive targets (eq. 2.6.19)	
n	power law flow behaviour index	~
No	bacterial population size at time zero	[CFU]
N_r	number of chemical species in reaction r	
N_t	surviving cell concentration	
p	pressure	[kPa, atm]
P(f)	poisson distribution	
Pr	Prandtl number	
$\dot{Q}$	fluid flux	[$kgm^{-1}s^{-1}$]
Q	volume fluid flux	[m^3s^{-1}]
r	radial coordinate	[m]
R	universal gas constant	[8.3143$kJkmol^{-1}K^{-1}$]

Re or N_{Re}	Reynolds number	~
r_e	equivalent radius	[m]
Ri	rate of prodaction by chemical reaction	
r_m	maximum absolute bacterial growth rate	[log(CFUml^{-1}h^{-1})]
Rε	extra term in RNG model making it more sensitive to rapid strains	
$\hat{R}_{i,r}$	Arrhenius molar rate of creation/destruction of species I in reaction r.	
S	deformation tensor in eq. 3.1.11	
S	surviving fraction at time t of homogeneous cell population from eq. 2.6.16	~
S_h	volumetric heat sources defined in heat transfer model in FLUENT	[kJm^{-3}s^{-1}]
Si	rate of creation by addition from dispersed face or user defined source	
S_k	user-defined source term.	
Sm	source of mass added to the continuous phase from dispersed second phase or any user-defined sources	
S_ε	user-defined source term.	
S_ω	user-defined source term	[kg^{2}s^{-2}m^{-3}].
T	temperature	[K or C]
t	time	[s or h or day]
T_{env}	environmental air's temperature	[K]
Tmin	theoritical minimum temperature for growth	[K]
To	biological zero for Bělehrádek models	[K]
T_{ref} or T_r	reference temperature for sterilisation treatment	[°C, °F]
T_{wall}	averaged temperature on wall surface	[K]
U	average value of velocity	[ms^{-1}]
u_{in}	inlet velocity	[ms^{-1}]
U_{ref}	reference mean flow velocity	[ms^{-1}]
u_{Ex}	velocity component in the X direction	[ms^{-1}]
u_{Ey}	velocity component in the Y direction	[ms^{-1}]
u_{Ez}	velocity component in the Z direction	[ms^{-1}]
u_z	velocity of flow in the X-direction parallel to a surface	[ms^{-1}]
x, y, z	flow directions	[m]
x_i	expected size of subpopulation from i-cell for Baranyi model	
Y	population density	[log(CFUml^{-1})]
Yi	mass fraction of species iMw,I molecular weight of species i	

Y_k	dissipation of k due to turbulence	[$kg^2s^{-2}m^{-3}$].
Y_M	contribution of the fluctuating dilatation in compressible turbulence to the overall dissipation rate	
Y_m	maximum population density	[$log(CFUml^{-1})$]
Y_ω	dissipation of ω due to turbulence	[$kg^2s^{-2}m^{-3}$].
z	number of degrees required to achieve a tenfold change of D_T values	[°C, °F]
z_q	z-value for the quality index	[°C, °F]
$\nabla \cdot \overline{\varphi}$	divergence of vector field ϕ	
$\nabla(\varphi)$	gradient of scalor function φ	

Greek

α	closure coefficient for k-w model from equation 2.4.22	~
α	constant for Bělehrádek models	~
α_b	time at which exponential growth phase ends from Buchanan and Cygnarowisz	[h]
α_k	inverse effective Prandtl number for k	~
$\alpha_n(t)$	adjustment function in Baranyi model (eq. 2.5.7)	
α_w	water activity	~
α_ε	inverse effective Prandtl numbers for ε	~
β	closure coefficient for k-w model from equation 2.4.22	~
β	constant in eq. 3.1.11	~
β	maximum specific death rate from eq. 2.6.16	[$time^{-1}$]
β	coefficient of cubical expansion	[K^{-1}]
β	consistency index	[$kgm^{-1}s^{-n}$]
β^*	closure coefficient for k-w model from equation 2.4.21	~
γ	strain rate	[s^{-1}]
Γ_k	effective diffusivity of k	[$kgm^{-1}s^{-1}$]
Γ_t	turbulent diffusivity	[m^2s^{-1}]
Γ_ω	effective diffusivity of ω	[$kgm^{-1}s^{-1}$]
ΔT	temperature difference between two locations	[K]
ε	rate of dissipation of turbulent kinetic energy for k-e model	[m^2s^{-3}]
η_0	constant in eq. 3.1.11	~

$\eta'_{j,r}$	forward rate exponent for each reactant and product species j in reaction r	~
$\eta''_{j,r}$	backward rate exponent for each reactant and product species j in reaction r	~
I	turbulence intensity	~
κ	thermal diffusivity	[ms^{-1}]
λ	lag time of bacterial growth	[h]
λ_b	lag time of bacterial growth from Buchanan and Cygnarowisz	[h]
μ	molecular viscosity	[$kgm^{-1}s^{-1}$]
μ_{eff}	effective viscosity	[$kgm^{-1}s^{-1}$]
μ_m	maximum specific growth rate of bacteria	[$CFUml^{-1}time^{-1}$]
μ_α	air dynamic viscosity	[N $m\ s^{-2}$]
μ_t	turbulent or eddy viscosity	[Pa s]
$\hat{\nu} = \mu_{eff} / \mu$		~
ν_t	kinematic turbulent or eddy viscosity	[m^2s^{-1}]
$\nu'_{i,r}$	stoichiometric coefficient for reactant i in reaction r	~
$\nu''_{i,r}$	stoichiometric coefficient for product i in reaction r	~
ρ	fluid density	[kgm^{-3}]
ρ_α	air density	[kgm^{-3}]
σ	closure coefficient for k-w model from equation 2.4.22	~
σ^*	closure coefficient for k-w model from equation 2.4.22	~
σ_ε	dimensionless constant for k-ε model from equation 2.4.18	~
σ_k	dimensionless constant for k-ε model from equation 2.4.17	~
σ_k	turbulent Prandtl number for turbulent kinetic energy	~
σ_t	turbulent Prandtl/Schmindt number	~
σ_ε	turbulent Prandtl number for the dissipation rate of turbulent kinetic energy	~
τ	measure of lag in killing from eq. 2.6.16	[h]
τ	viscous stress	[N or $kgm^{-1}s^{-2}$]
$\bar{\bar{\tau}}$	stress tensor from eq. 3.1.2	[$kgm^{-1}s^{-2}$]
$(\tau_{ij})_{eff}$	deviatoric stress tensor	[$kgm^{-1}s^{-2}$]
τ_i	lag time of individual i-cell	[h]
φ	flow property	

φ'	fluctuation of φ property	
$\dot{\varphi}_G$	generation rate for energy, mass or momentum	
ω	dissipation per unit turbulence kinetic energy	[kgs^{-1}]

Acronyms

G	Gompertz's model
ID	internal diameter
IS	Insoluble Solids
L	logistic's model
OD	outer diameter
SS	Soluble Solids

Abbreviations/subscripts

(r, t)	value at radial position r at time t
(r, z)	value at radial position r over axial length z
div	divergence of vector field ϕ
grad	gradient of scalor function φ
hor	of horizontal surface
i, j	subscripts showing dimensional position (e.g. when 1 then it is x direction)
max	maximum value of parameter
mol	molar property
T+z	conditions at temperature T+z
T-z	conditions at temperature T-z
ver	of vertical surface
w	water properties

1 Introduction

The food industry is continuing to experience the demands of increased consumer expectation and the opportunities and challenges of a competitive market. The objective is to deliver safe, more stable products. Currently, the trends ask for products, which are less microbiologically robust compared to the past. Less preservatives are demanded as well as natural tastes and textures. Although, at the same time, longer shelf life is expected and costs should stay to low enough levels for the products to be purchased. Another factor that puts pressure in the food industry is the authorities that come with regulations and checks on both products and lines. The industry increasingly needs to employ advanced manufacturing techniques, which allow greater process flexibility and reduced energy use and waste generation.

Hence, the pressure to improve hygiene standards from both consumers and legislation, is constant (Hasting, 1999). In the industry the production lines have to be interrupted in order to allow time for cleaning. Assuring the safety of food products becomes of critical importance. From an engineering prospect, a considerable amount of work on hygienic design has been done over the last 3 decades (EHEDG, 1993a; 1993b), leading to the provision of guidelines and regulations for food processing equipment. However, there have been few studies on the interactions between food products and food equipment and the effect of those on the residence time and temperature of the product

Therefore, it is of great importance to maintain safety during the processing of foods. This is directly linked to the possibility of microbial survival in the final product. This is avoided by treating the product at high temperatures for a certain period of time. The commonest processes for that are sterilisation and pasteurisation. These aim at achieving the required lethality. Many times though, they result in high nutritional losses (Bakalis et al., 2001). This is faced by high temperature and short time (HTST) processes that can give the same thermal process and less quality loss.

After a certain period of running a food production line, cleaning usually follows. The duration of cleaning depends on the kind of product and the contamination that might occur along with the cleaning conditions selected. Cleaning of closed process equipment (CIP) aims at disinfection and removal of possible bacterial attachment or any soiling created on the process equipment surfaces. The use of the adequate concentration of detergent, at a relatively high temperature is the chemical force that cleans a line. This, in combination with high velocities that achieve intense wall shear stresses, contribute to the detachment of soiling and the reassurance of a hygienically designed process.

Thus, from the above is concluded that it is important that the heating process is the correct one to give a safe product. Temperature and velocity should be adequate to kill pathogens and spoilage bacteria. Cleaning should be assessed to assure a disinfected line between productions. All these can lead to the design of a hygienically manufactured process that will give a safe product. Models and pilot plant experiments can contribute to the above, as well as collaboration between food microbiologists, engineers and chemists.

However, even if the above can be carried out successfully, there are sometimes parameters that are difficult to take into account. One of these parameters can be unhygienic features in the pipe geometry, such as down stands, up-stands or junctions that lead to dead ends. Other

examples can be valves, crevices and even surface roughness. These can be perfect locations for product entrapment and conditions can be created that may favour microbial growth. There is a high risk that there can be interaction between the bulk flow and these locations that can easily lead to contamination of the food product and withdrawal from the market with enormous economical losses for the companies, which can get worse if consumers' poisoning is involved.

The material chosen for the experiments in this work was stainless steel. Ideally, in the food industry it would be preferable to use smooth and free of crevice surfaces. A good example is glass, which has no cracks and it is even, transparent and hygienic. However, it is not recommended because it is expensive, has a low-pressure tolerance and breaks easily. The most useful material in processing is steel that can be treated e.g. by mechanical grinding.

Hence, it is important to have a good idea of what is going on in that kind of geometries and predict the effect they are going to have in the whole process domain. In this work, a Computational Fluid Dynamics (CFD) code is validated against experimental work carried out at the University of Bath using a T-piece as a dead end. Temperature and mass removal models are validated and compared to the experimental measurements of Newtonian fluids. Also, another model is developed of a Tube in Tube in Tube (TnTnT) heat exchanger in a factory of non-Newtonian processes. The code is a very good tool to simulate and visualise the conditions during the runs and offers the flexibility of adding one's own models of bacteria kinetics or other equations to describe different phenomena.

The next paragraphs of this chapter describe the importance of the problem and the necessity to control it.

1.1 Fouling and its implications

Fouling was always considered to be the major unresolved problem in heat transfer. The accumulation of deposits of unwanted material on the surfaces of processing equipment may cause a decline in its efficiency (de Jong, 1998):

- The fouling layer has a low thermal conductivity. So the resistance to heat transfer is increased and the effectiveness of e.g. heat exchangers is reduced.
- Deposition reduces the cross-sectional area. Thus, pressure drop increases across the apparatus.

Fouling of plant equipment results in increased cost of operation. Fouling costs, depending on the process, location and manpower. Major costs include (Pritchard, 1980):

- Loss of throughput: production losses during plant shut-downs due to fouling.
- Cost of cleaning equipment and chemicals.
- Capital expenditure including excess surface area, costs for stronger foundations, provisions for extra space, increased transport and installation costs and cleaning-in-place equipment.
- Extra fuel costs, which is needed to overcome the effects of fouling.

Problems in the line itself while it is on the run (I.F.A.C.T., 2003):

- Loss of energy,
- reduced flow,

- increased pressure
- Increased investment (e.g. replacement of equipment)
- Environmental problems: hazardous cleaning solution disposals, Increased costs of environmental regulations

According to the mechanism responsible for deposit generation, fouling has been classified into: crystallisation fouling, particulate fouling, chemical reaction fouling, corrosion fouling, biofouling and solidification (Mwaba, 2003; Thackery, 1980).

Crystallisation fouling is the deposition of a solid layer on a heat transfer surface, mainly resulting from the presence of dissolved inorganic salts in the flowing solution which become supersaturated under the process conditions. Typical scaling problems are calcium carbonate, calcium sulphate and silica deposits.

Particulate fouling (sedimentation) is the accumulation of solid particles suspended in a fluid onto a heat transfer surface. Suspended particles can be ambient pollutants (sand, silt, clay), upstream corrosion products, or products of chemical reactions occurring within the fluid.

Chemical reaction fouling involves deposits that are formed as the results of chemical reactions at the heat transfer surface. The heat exchanger surface material does not react itself, although it may act as a catalyst. This kind of fouling is a common problem in chemical process industries, oil refineries and dairy plants.

Corrosion fouling occurs when the heat exchanger material reacts with the fluid to form corrosion products on the heat transfer surface.

Biological fouling is the development and deposition of organic films consisting of microorganisms and their products (microbial fouling/biofilm).

Solidification (e.g. Freezing fouling) occurs on a cooled wall while the bulk liquid remains unsaturated. Freezing fouling describes the phenomenon whereby a layer is formed on a heat transfer surface which is colder than the bulk fluid (Fernandez-Torres, 2001)

Generally, several fouling mechanisms occur at the same time, nearly always being mutually reinforcing. One notable exception is particle deposition together with crystallisation, which weakens an otherwise tenacious scale.

The above fouling mechanisms generally occur in five consecutive steps (Mwaba, 2003):

1. **Initiation or delay period**. When a new or cleaned heat exchanger is put into operation, the initially high heat transfer coefficients may remain unchanged for some time. This delay period can be anything from a few seconds to several days. According to research results no delay period occurs for particulate fouling.
2. **Mass transport.** To form a deposit at the heat transfer surface, at least one key component has to be transported to it from the fluid bulk.
3. **Formation of the deposit.** After the foulant has been transported to the heat transfer surface, it must stick to the surface or react to give the deposit forming substance.
4. **Removal or auto-retardation**. Depending on the strength of the deposit, erosion occurs immediately after the first deposit has been laid down. Furthermore, several mechanisms exit which cause auto-retardation of the deposition process.

5. **Ageing**. Every deposit is subjected to this stage. This can increase the deposit strength by, for example, polymerisation, recrystallisation, or dehydration.

1.2 Fouling in the food industry

The food industry is of great importance for the economy of most of the countries. For that reason, food-processing science has developed a lot throughout the years so that the best combination of quality and quantity is achieved at the end of each process line. Maintaining high levels of food safety is essential for continued consumer confidence in the food industry and any failure of safety management can seriously affect the reputation of a product brand, or even the company itself. In comparison with other industries, where annual cleaning may be sufficient, it is common that in the food industry, like the dairy, cleaning might be necessary on a frequent basis (Chen et al, 1998) depending on the kind of flow of the product, on the viscosity and the surface of the devices used.

It has always been of great concern the hygienic function of a food industry especially when biological fouling is detected at some stage during the process of the product. If those microorganisms exist in the food industry they may cause spoilage or can be the cause of human illnesses. Some of the most common examples are *Streptococcus thermophilus, E. coli, Yersinia enterocolitica, Staphylococcus aureus* that grow during the milk processing or *Clostridium botulinum* in vegetable products (FDA/CFSAN, 2000).

Figure 1.2.1 shows the numbers of notified cases of Food Poisoning in Northern Ireland and England (FoodLink, 2003).

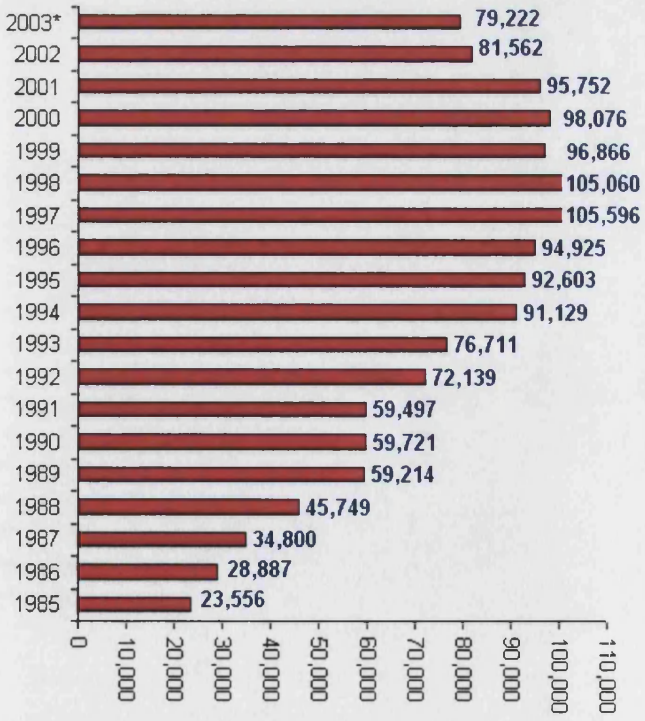

Figure 1.2.1: Number of notified cases of food poisoning (UK) (* denotes provisional figure)

This threat led the scientists to develop several mathematical models in order to predict the kinetics of those microorganisms during the processing of food. So there are many equations that describe the growth or the death of the bacteria in accordance with the change of temperature in the industrial equipment. These models are the basis of 'predictive microbiology' the concept of which is to give the correlation of the behaviour of the microorganisms to the environmental changes (McMeekin et al, 1993). This work is linked to the microbial fouling and the bacterial kinetics and behaviour.

1.3 Biofouling and connection to the food industry

Biofilms can develop on almost any surface exposed to an aqueous environment. However, biofilms can be quite troublesome in certain engineering systems. In water distribution systems and heat transfer equipment, for example, biofilms can cause substantial energy losses resulting from increased fluid frictional resistance and increased heat transfer resistance (Trulear and Characklis, 1982).

There were many researchers that looked into the biofilm formation and generally biological fouling. They tried to understand it for various products and conditions. Langeveld et al. (1995) found that strains were able to adhere and grow on the internal tube surface, the site being dependent on the wall temperature. As a result of release of bacteria from the walls, the bacteria cell concentration in the milk could increase up to a million-fold. Trulear and Characklis (1982) characterized the processes that take place during its formation

Microbial fouling often accelerates other types of fouling. For example, microbial fouling can increase the deleterious effects of sedimentation (or particulate) fouling by providing a more "absorbent" surface (Characklis and Cooksey, 1983)

Kirkpatrick et at (1980) presented a phenomenological model for development of biofilm in a circular tube and its effect on heat transfer. Both laminar and turbulent flow are examined and variations of fluid physical properties with temperature properties are included.

Others paid more attention to the surface characteristics and how these enhanced colonization or not in combination with operating conditions and control systems (Karlsson, 1999)

Lelievre et al (2002) modelled cleaning kinetics of stainless steel pipes soiled by Bacillus spores assuming competition between deposition and removal during a CIP procedure. A simple model (first order equation) was proven to fit the data well. The effect of the media used (milk or saline) during soiling, was found to be significant. Wall shear stress had a significant effect as well: the greater it was the faster the cleaning.

Wirtanen et al (1994) tested various parameters for estimating cleaning procedures in open systems in order to eliminate biofilms of *Bacillus subtilus, Listeria monocytogenes, Pediococcus pentosaceus* and *Pseudomonas fragi* on stainless steel surfaces. Statistical analysis showed that the roughness of the stainless steel surface is the most important factor in cleaning surfaces from biofilms. Many mathematical models developed to describe the biofilm formation link it to the bulk flow and growth there (de Jong et al, 2002)

Hasting (2002) indicated the necessity of good monitoring systems that can provide data also on optimization of cleaning, identification of deposits, fouling reduction, validation of cleaning.

Microbial growth is part of biological fouling, which is quite often encountered in the industry and can be very costly and dangerous especially in food production. The survival of the bacteria

is dependent on the temperature profile of the flow of the product. The temperature, in its turn, depends on the velocity. For these reasons it is important to have the correct predictions of the velocity and temperature so that the microbial kinetics can be as accurate as possible. Growth and adherence of bacteria to surfaces has led to consideration of the hygiene of surfaces, instruments and equipment in the food industry. This essentially affects the quality of the products processed. In process equipment, open or closed, biofilms have ideal opportunities to develop e.g. in bends, seals, crevices, dead ends and grooves. If the cleaning and sanitation are inadequate the above sources can cause contamination.

This is why there are systems applied to improve the microbial quality of food such as Good Manufacturing Practices (GMP), Hazard Analysis Critical Control Points (HACCP) and Microbial Risk Assessment (MRA) (den Aantrekker, 2002)

1.4 Aim of the thesis

The structure of this thesis is described below. Overall, the aim is to apply a CFD (Computational Fluid Dynamics) code, FLUENT, in order to predict temperature distribution, residence times and eventually microbial growth in the bulk flow in a geometry that comprises a down stand. Bacteria kinetics are temperature and time dependent. The code solutions were compared to experimental results as well. Good estimation of concentrations can be linked in the future to assessment of detachment/attachment on equipment surfaces. In general, the models developed can contribute to estimate the process line safety.

The models are based on the main flow and a set of various solutions are compared for varying flow of a Newtonian fluid in order to see how the code handles the flow in the dead end as well as the temperature distribution.

Another model presented in this work is the flow of a non-Newtonian fluid through a Tube in Tube in Tube heater where bends are included. The purpose is to check the heat transfer during the sterilization process in a food industry.

1.5 Structure of the thesis

The following chapter, number 2, gives a literature survey on the topics that were involved in this project. The importance of resolving the problems risky and unhygienic geometries may cause is highlighted in this section. The link between thermal processes, cleaning processes and various flows and bacterial kinetics is exlained. Later, in the same chapter, a brief description of the various flow options available in CFD and the models used to solve them is given. Bacterial kinetics and a various range of models developed to express them are mentioned together with their dependence on temperature and other parameters. The end of the chapter focuses on data found in the literature concerning *Ps. fluorescens*, which is the spoilage bacterium used here.

Chapter 3 summarizes the materials and methods that were used in this work. Therefore, FLUENT specifically is described and the way it solves flows, heat transfer and bacteria transport and kinetics, models that were chosen and why. Then, a report of the experimental set up and the techniques applied to take measurements in order to validate the models follows.

Chapter 4 is the first results chapter, providing the steady state flows both for Newtonian and non-Newtonian flows. This is followed by a comparison between experiments and models for the Newtonian flows and between factory measurements and models for non-Newtonian flow.

In chapter 5 the unsteady flows are described, where mass removal is included and bacterial kinetics are also integrated. First set is based on electrical conductivity measurements and the second on colony count techniques.

Chapter 6 is where general conclusions and comments on the thesis are made as well as some recommendations on how this work can be expanded and make its way towards more applications in the food industry.

2 Literature Review

Setting up a production line in a food factory is a major task that involves many aspects, which should be seriously taken into consideration every time.

First of all, all the equipment has to be hygienically installed according to regulations that exist in each country in order to avoid contact of the product with contamination sources (e.g. air or personnel).

Secondly the layout of the line should be the right one, given the adequate space for the machinery and the technicians to operate it safely and efficiently.

Third is the processes themselves. Depending on the outcome wanted, it has to be reassured that the product goes through the right conditions such as temperature, pressure etc., for the right amount of time so that it will not be damaged or mishandled.

Finally, control of all the operations of the line is necessary so as to avoid misfunctionality under the correct conditions. Automation of the processes should be working properly and keep the standards of the line.

From the above, it is quite obvious that hygienic and process design are very much linked and taking into account only one of them does not lead to the desirable results. It is completely irrelevant to obtain a perfectly safe flow of a food product within equipment that does not provide the right heating, cooling or holding conditions. Unhygienic configurations should be avoided (e.g. dead areas, geometries that are not aligned with the cleaning flow etc.) and at the same time monitoring of the operation has to be at an adequate level.

This chapter gives some key literature areas that are combined to achieve a safe and correct design of production line: geometries that should be avoided or, if not feasible, cleaned. Also processes such as heating, which aim to kill pathogens and cleaning that needs to be carried out to ensure the removal of possible formed biofilms. In this work the geometries on which models and experiments were based are a vertical T-piece and a Tube in Tube in Tube heat exchanger.

In the food industry contamination of a product may come from various microorganisms such as moulds, yeasts or bacteria. This work integrated spoilage bacteria issues. The survival of the bacteria is linked to the temperature and the residence time at the various temperatures during the processes. Hence, velocity, temperature and bacteria kinetics are strongly linked. All these are the concepts combined into simulations in a commercial CFD code, FLUENT, which applies the finite volume method. For this reason implementations of the CFD in the food industry are mentioned later on in the chapter. Laminar, turbulence and transitional flows were used for the models and experiments and the basic equations used for their modelling are referred. Later on some common bacteria kinetics models are mentioned with more extensive comments on the investigations made on the spoilage bacterium *Pseudomonas fluorescens*, which was used in this work.

2.1 Risky geometries in the food factory

It is quite common in the production lines to encounter pipework configurations that might form areas not aligned with the flow of the product. This could be because of a pressure gauge fitted in line, or any other measuring devices (fig. 2.1.1) (Hasting, 2002).

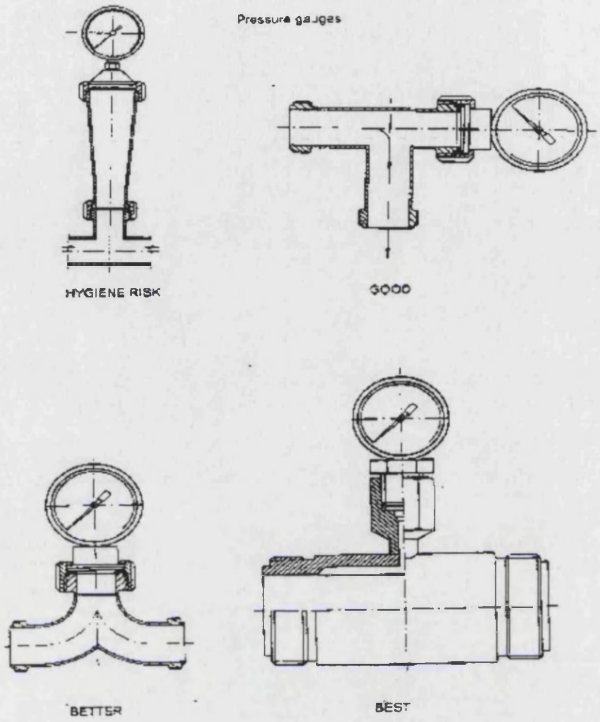

Figure. 2.1.1: Locations of a pressure gauge related to hygienic risk after .

Changing the flow, or even changing the processed product, may mean that some tubes are going to be sealed (fig. 2.1.2). This is the cause of stagnant area formation

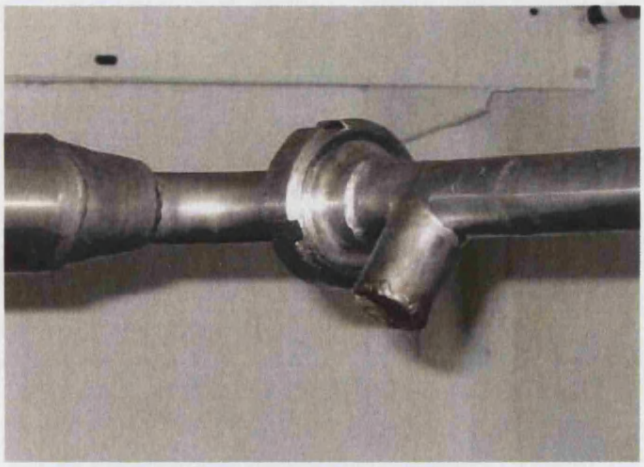

Figure. 2.1.2: Example of sealed pipe that might be source of contamination.

Also, opening or closing valves in order to direct the flow through different paths, can create dead spaces in the pipes just before the divergence occurs (fig. 2.13).

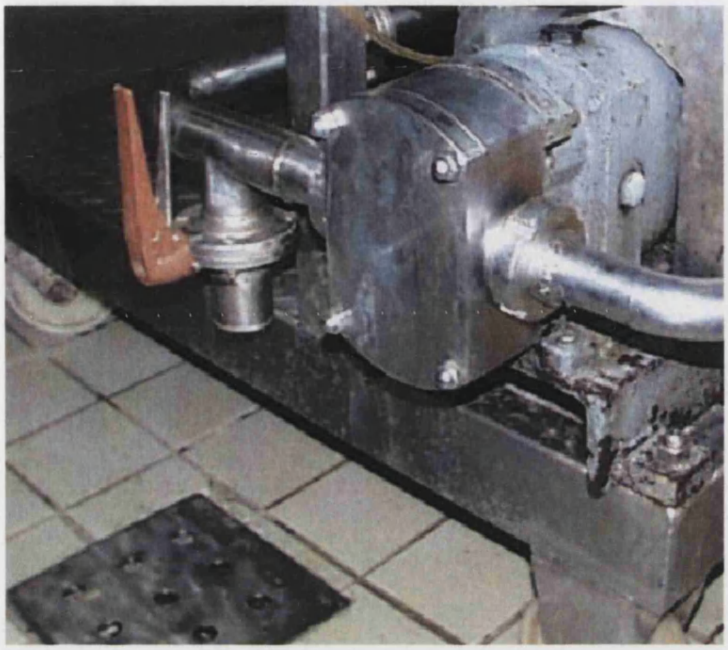

Figure. 2.1.3: Example of valve location that creates down stand T-piece shaped.

These areas end up trapping product. Stagnation is the following stage and, depending on the temperature, pH, water activity etc., we might have bacterial growth that due to the mass exchange with the bulk flow could end up in the product. This is the first difficulty that has to be taken into consideration when there is suspicion of risky geometries formed across the line. The second is to make sure that cleaning is going to be efficient enough to remove the entrapped product before the new production starts. Any residuals should be cleaned off in order to consider the line hygienic.

One could easily suggest trying and detaching these configurations from the lines. This cannot always be implemented for various reasons: usually there is no time since delays in production cost a lot of money to the factory. Interrupting production is a cause of great losses in earnings and always has to be kept to the minimum. Also, changes in the pipework or replacing equipment are options that cost a lot of money on their own since it requires dismantling the line or even buying new components. Cleaning time, on the other hand should be dropped down to a minimum so that again there will be more production time.

In a well-designed line, multiplication of microorganisms during processing is limited and in many cases frequent cleaning is not necessary. A well-designed line can be rapidly cleaned and decontaminated effectively. Reduced frequency of cleaning and shorter cleaning times will reduce production downtime (EHEDG, 1993a,b).

There are a few design lines to maintain hygienic aspect in tanks, pumps and pipework (Joint Technical Committee, FMF/FMA) including basic principles for design and materials of

constructions that show how and when some geometries are not, or less risky. Although, it is not always easy to know in advance and investigation or tests should be carried out. This is when CFD analysis can be a very useful tool to see the conditions inside a piece of equipment. It can give a good estimation of the critical point where contamination might occur and also the time of cleaning that is adequate and the velocity of the flows applied.

There are also a number of patents that have suggested fittings or couplings that minimise product entrapment between pipes of different dimensions, bends or any other changes in a plant. Applying protective layers onto vessels used in the food industry (such as milk and meat), is another method that has been invented so that microorganisms' adhesion is minimised (Van Leeuwen, 1996).

Campden association have also suggested design rules for liquid handling equipment in the food industry (Thorpe and Barker, 1988) such as various couplings, joints, flange assemblies, fittings, drainable arrangements, T-pieces etc.

Grasshoff (1992) has studied the flow behaviour of fluids in dead spaces and the influence of fluid movement on cleanability. He found that the fluid exchange and the local shear stress decrease very rapidly with increasing stagnant space depth. He found that the maximum permissible dead space depth is easily reached. The required rinsing times exceeded the time needed for the individual steps in programme controlled CIP. Some guidelines that could be given for fittings, gaskets and valves in order to limit contamination risks from the start are:

Fittings/gaskets

The technological development of fittings which, besides straight-lined pipes, are needed for the assembly of complex pipeline systems (T- and cross-pieces, bends, reduction pieces, sight glasses etc.) can be considered finished. Innovations might be done concerning the design of the sealing. The tightening of fitting/pipe is relatively uncomplicated, because it is a static problem. However, mounting of the gasket must be free of spaces with undefinable dead zones, which cannot be cleaned with CIP.

Valves

The influence of the spindle gasket on product carryover and recontamination determines the ideal gasket that some of the criteria it should meet are the following:

- completely accurate sealing in both directions
- sealing zone without any dead spaces
- slit-free fit in the housing
- low internal pressure force
- intensifying the pressure force by the system pressure
- good stripping off at the gasket lip
- high abrasion stability of the gliding area
- low frictional index
- chemical and thermal resistance

2.2 Thermal processes in the food industry

Heating has a great effect on the food properties. Various processing operations are based on heating, such as canning, baking and pasteurising. The above might aim to preservation (e.g. killing of bacteria, inactivating enzymes), physical changes (i.e. taste, flavour), structural changes (baking) or drying and frying where mass transfer is also occurring due to evaporation of moisture (Bakalis et al., 2001).

The heat processes devised to give different degrees of shelf life to food products are usually classified either as pasteurization or sterilization. The former is a partial treatment, that destroys only the more labile fraction of microbial population. The latter is a complete one, because the level of surviving organisms is lowered beyond any value detectable by usual analytical practices.

They are usually carried out in Heat Exchangers (HE) the most commons of which in the food industry are:

- Plate HE, used very often in the milk industry (Georgiadis and Macchietto, 1998a, 2000) and generally when low viscosity products are concerned (Christia et al., 2002; Robbins et al., 1999).
- Scraped surface HE are encountered mainly in the food industry for handling highly viscous fluids with complex rheology (cheese, fruit concentrate, ice cream, chocolate, particle containing products such as soups, sauces etc.) (Dumont et al., 2000; Wang et al, 2002, Russell et al., 1997; Loisel et al., 1997).
- Also, shell and tube HE are present in a big variety of dimensions in the food handling equipment (Georgiadis et al., 1998b).
- Double pipe HE (Tube in Tube) recommended for not very high flows.
- Triple pipe (Tube in Tube in Tube or TnTnT) where we achieve a large increase of the heat transfer area and better flow characteristics of the product (Rossi e Catelli web site).
- Other types that can be encountered are: platecoil, spiral, direct heat exchangers (Lazaridis, 2000).

There are many companies that are specialising in manufacturing that kind of equipment and are trying to achieve good performance both during heat transfer and cleaning (Alfa Laval web site; APV 1995; Rossi e Catelli, 2004)

The two treatments differ greatly in the size of (heat) applied. Pasteurization is usually done at temperatures lower than 80-100°C. Sterilization is applied at temperatures ranging from 115°C to 145°C (Casolari, 2002). The heat inactivation of bacteria is very dependent on the way in which the heat is applied. The temperature range and time scale (the total amount of heat/energy provided) are also critical parameters. The legislation for foods only covers the definitions of pasteurisation and sterilisation (Klijn et al., 2001).

2.2.1 Pasteurisation

The International Dairy Federation defines pasteurisation as 'a process by heat treatment with the aim of minimising possible health hazards arising from pathogenic micro-organisms and

extending keeping quality by reducing the number of spoilage microorganisms consistent with minimal chemical, physical and organoleptic changes in the product'. Pasteurization is usually applied to low-acid foods to kill the vegetative cells of the common pathogenic bacteria and to lower the contamination level of spoilage organisms growing under refrigerated conditions of storage (Klijn et al., 2001).

2.2.2 Sterilization

This heating process started in the canning industry. When a foodstuff is put into a container it will always contain microorganisms that would cause spoilage of the food, without having already been destroyed. In order for a food to be considered sterile the spores of a certain organism in it should reach a number that is safe. The aim in heat processed canned foods is the sterility of the most heat resistant microorganism that would cause spoilage (Ball and Olson, 1957).

Sterilization is employed to deprive microorganisms of their ability to multiply. Heat destruction of microorganisms is a gradual phenomenon: the longer the treatment time at lethal temperatures, the larger the number of killed microorganisms will be. The higher the treatment temperature:

1 - the shorter will be the time required to kill microorganisms;

2 - the lower the heat induced damage to food products.

Only Low Acid Foods, having pH higher than 4.6, must be sterilized, because all microorganisms are able to grow in such conditions. More acid products (pH equal or lower than 4.6) do not allow the growth of pathogenic sporeforming bacteria and in that case sterilization is not required (Casolari, 2002). The purpose of the Sterilization Process is the destruction of all pathogenic organisms together with spoilage/non-pathogenic microorganisms, to achieve the Safe Preservation at Room Temperature of treated products (longer shelf life). Food products processed to obtain the above are usually defined as 'commercially sterile'.

The sterilization is usually specified in terms of a decimal reduction. This is the number of powers of 10 that the number of organisms is to be reduced by. The most usual decimal reduction is a 12D reduction, i.e. $N_0/N=10^{12}$ and $\log N_0/N=12$. the sterilization time is often referred to as the "F number", which is the rate of thermal processing if very often quantified through the integrated lethality of a thermal process calculated by the following equation (Bakalis et al., 2001):

$$F = \int_0^t 10^{(T(t)-T_{ref})/z}\, dt \qquad (2.2.1)$$

where z is the increase in temperature that gives an increase in rate of a factor of 10 and T_{ref} is a reference temperature. F has the units of time being the length of time that the food would have to be held at the reference temperature to obtain the same effect as the actual process with T.

F is the product of the D-value and the decimal reduction. Thus, for a 12D reduction, F=12DT. Because *C. botulinum* is the basis of most food sterilizations, the F value is determined on the basis of a reference temperature of 121.1°C. In such cases F is usually designated as F_o.

The Sterilization Treatment by Heat [STH] is regarded as suitable if of size equivalent to F_o =10 at least (Casolari, 1994) or equal/higher than 8 (Stumbo et al., 1975). Fo value is the number of minutes the food is actually exposed at the Reference Sterilization Temperature of 250°F = 121.1°C. F_o does not refer to total, 'integrated heat' applied/received by the entire mass of product in the container or holding tube (that is the heat absorbed by the slowest-heating product at the center of the can or flowing at the center of the holding tube, plus the heat absorbed by the fast-heating product located at the periphery of the can, or of the holding tube). F_o refers to the amount of heat received by product located at the coldest point in the container heated inside a retort or hydrostatic sterilizer; or the fastest particle flowing in holding tube or plates of continuous sterilizers.

2.2.3 Laminar flows

Laminar flows are very common in the food industry when the above processes (pasteurisation, sterilization) are en route. This is mostly happening because we want to achieve the adequate residence time at the recommended temperature with the minimum energy cost and most likely the minimum equipment surface.

Also, a flow is almost necessarily laminar when non-Newtonian flows are considered. The products under process are highly viscous in those cases and it is very rare that high enough Reynolds numbers are achieved so that the flow can be considered other than laminar. Navier-Stokes, continuum and energy differential equations are solved in order to describe the flows (Brodkey and Hersey, 1988).

2.3 Cleaning in the food industry

Cleaning is an absolute necessity in the food industry, since deposits are quite likely to form and adhere on the equipment surface. This can have various consequences to the process. First of all it can be the perfect environment for microbial growth; secondly the thickness of the deposited layer can hinder the heat transfer and drop the overall heat transfer coefficient. This would mean higher energy consumption in order to achieve the required temperature in the product.

There are four factors that affect the overall cleaning process. When designing cleaning procedures these factors need to be thoroughly considered (Jennings, 1957; Bishop, 1997).

Time: The longer a cleaning solution remains in contact with the equipment surface, the greater the amount of food soil that is removed. Increasing time reduces the chemical concentration requirements.

Temperature: Soils are affected to varying degrees by temperature. In the presence of a cleaning solution most soils become more readily soluble as the temperature is increased.

Concentrations of chemicals: they vary depending on the chemical itself, type of food soil and the equipment to be cleaned. Concentration will normally be reduced as time and temperature are increased.

Mechanical Force: Mechanical force can be simple manual scrubbing with a brush or as complex as turbulent flow and pressure inside a pipeline. Mechanical force aids in soil removal and typically reduces time, temperature, and concentration requirements.

There are also five methods to achieve cleaning in the food industry (Jennings, 1957; Bishop, 1997)

Foam: Foam is produced through the introduction of air into a detergent solution as it is sprayed onto the surface to be cleaned. Foam cleaning will increase the contact time of the chemical solutions, allowing for improved cleaning with less mechanical force and temperature.

High Pressure: High pressure cleaning is used to increase the mechanical force, aiding in soil removal. In high pressure cleaning chemical detergents are often used along with increased temperature to make soil removal more effective.

Clean in Place (CIP): CIP cleaning is utilized to clean interior surfaces of tanks, pipelines etc. of liquid process equipment. A chemical solution is circulated through the process line and then returned to a central reservoir allowing to be reused. Time, temperature, and mechanical force are manipulated to achieve maximum cleaning.

Clean Out Of Place (COP): COP cleaning is utilized to clean parts of fillers and parts of other equipment which require disassembly for proper cleaning. Parts removed for cleaning are placed in a circulation tank and cleaned using a heated chemical solution and agitation.

Mechanical: Mechanical cleaning normally involves the use of a brush either by hand or a machine such as a floor scrubber. Mechanical cleaning uses friction for food soil removal.

There are two kinds of equipment that can be encountered in the food industry and cleaning will be treated differently. Open equipment is common in manufacturing of non-liquid foods. Closed equipment (pipes, tanks, heat exchangers) is cleaned with CIP procedures. CIP programmes are usually single-stage or two-stage cleaning procedures. Two-stage cleaning employs both acid and alkali, whereas in single-stage cleaning only one cleaning agent is used. In no heated surfaces is usually applied a single-stage process (with formulated alkaline detergents). In heated surfaces, where fouling is generally more severe, are applied two-stage alkali-acid procedure (Kane and Middlemiss, 1985; Grasshoff, 1989; Karlsson, 1999). The work presented here is based on the CIP necessities and closed pieces of equipment are taken into account. The models solved are based on the mass removal from a T-piece, due to flushing of the experimental rig with deionised water at high flow velocities.

There were many researchers that worked with cleaning and tried to improve cleaning by altering the four aforementioned factors. In the food industry one can find various residues like fat, protein, ash (milk residues) or water residues. This work is aiming to prove that CIP can be modeled and be used in the future to avoid or remove biofilms from process surfaces

On surfaces covered by flowing liquid, reversible adhesion is more probable than irreversible. An additional mechanism allows microorganisms to remain adhering: the production of a capsule of exocellular polymers (proteins, or, more frequently, polysaccharides). Polymer threads come close to the surface, where they adhere irreversibly. Firmly attached microorganisms can then multiply and colonize the surface within a matrix of the polymer, thus forming a "slime layer" (Grasshoff, 1992).

Concerning the primary step of adhesion, investigations with a variety of microorganisms confirm thermodynamic provisions: those with high free surface energy adhere to hydrophilic

materials, while those with low free surface energy adhere more to hydrophobic materials. If macromolecules which modify the apparent surface energy of materials are excreted by microorganisms, thermodynamic models remain valid provided the new state of the surface is considered. Two such cases have been reported: about the same adhesion extent, of the microorganism on various materials; and no adhesion on any materials.

Wirtanen et al (1994) tested various parameters for estimating cleaning procedures in open systems in order to eliminate biofilms of *Bacillus subtilus*, *Listeria monocytogenes*, *Pediococcus pentosaceus* and *Pseudomonas fragi* on stainless steel surfaces. With statistical analysis they showed that the roughness of the stainless steel surface is the most important factor in cleaning surfaces from biofilms.

Biofilm has been investigated industrially for years: (Characklis and Marshall, 1990; Panikov and Nikolaev, 2002). Growth of bacteria and adherence of them on the surfaces has led to consider that the hygiene of surfaces, instruments and equipment in the food industry essentially affects the quality of the products processed. In process equipment, open or closed, biofilm has ideal opportunities to develop e.g. bends, seals, crevices, dead ends and grooves. If the cleaning and sanitation are inadequate the above sources cause contamination.

Microorganisms of food products have varied classes of surface free energies. Bacteria have, in general, a high-energy surface, whereas moulds have a low one.

Many people have worked on CIP improvement and monitoring. Grasshoff (1994) investigated the multi-stage CIP process thoroughly for a dairy plant heat exchanger. He used computer imaging. It is considered as a first attempt to quantify the removal of encrusted deposits from a solid surface.

Gillham et al (1998) ran experiments in order to see the mechanisms involved in the alkali-based cleaning of whey protein deposits on stainless steel surfaces. They used rate, deposit surface and heat transfer techniques. The results showed that reaction and diffusive transport processes occurring in the swollen deposit layer determine the cleaning rate under conditions of steady pipe flow.

Bird and Espig (1998) investigated the removal of crude oil films from stainless steel surfaces using non-ionic surfactants at different temperatures. The cleaner used was alcohol ethoxylate. Plain water rinsing was not effective and followed Arrhenius kinetics. Surfactant cleaning deviated strongly from Arrhenius kinetics. At high surfactant concentrations a smooth curve is produced which appears to be physically controlled at high temperatures and a combination of chemically and diffusion controlled at low temperatures. A four step cleaning mechanism is postulated where the surface modification of the oil surfactant adsorption is the rate limiting step of the removal process. Also Bird and Bartlett (1995), elaborated on concentration and temperature optima during the removal of protein, starch and glucose for CIP processes.

2.3.1 Turbulent flows

When it comes to cleaning closed equipment, mechanical stress on the wall is of great importance. Such high forces are achieved only with turbulent flows. There is no dismantling of the line and flowrates should be adequate enough to perform complete cleaning.

Hence, high Reynolds numbers are necessary and equations that describe turbulent regimes are solved based on the mean values of properties (Brodkey and Hersey, 1988).

2.4 Computational Fluid Dynamics (CFD)

The aim of this work is the development of a modelling approach to predict the implications of processing on microbiological growth and hence the safety of food products. The tool used for this purpose is FLUENT, a commercial CFD (Computational Fluid Dynamics) code. CFD is widely applied in industry and has not been so far reported any use of it in combining engineering unit operations such as fluid flow and heat transfer with biological systems such as microbiological growth and death.

CFD is the analysis of systems involving fluid flow, heat transfer and associated phenomena such as chemical reactions by means of computer-based simulations. It is a very powerful technique and is used in a wide range of industrial and non-industrial application areas such as (Verteeg and Malalasekera, 1995):

Aerodynamics of aircraft and vehicles

Hydrodynamics of ships

Chemical process engineering

Environmental engineering

Biomedical engineering

Meteorology

The code is based on the finite volume method. This method was originally developed as a special finite difference formulation (e.g. Taylor series are used to generate finite difference approximations of derivatives of ϕ in terms of point samples of ϕ at each grid point that comprise the domain geometry.). The numerical algorithm consists of the following steps:

Integration of the governing equations of fluid flow over all the finite control volumes of the solution domain.

Discretisation involves the substitution of a variety of finite-difference-type approximations for the terms in the integrated equation representing flow processes such as convection, diffusion and sources. This converts the integral equations into a system of algebraic equations.

Solution of the algebraic equations achieved by an iterative method.

The first step distinguishes the finite volume method from all other CFD techniques. The resulting statements express the (exact) conservation of relevant properties for each finite size cell.

CFD codes contain discretisation techniques suitable for the treatment of the key transport phenomena, convection and diffusion as well as for the source terms and the rate of change with respect to the time. The underlying physical phenomena are complex and non-linear so an iterative solution approach is required.

In solving fluid flow problems we need to be aware that the underlying physics is complex and the results generated by a CFD code are at best as good as the physics (and chemistry) embedded in it.

Prior to setting up and running a CFD simulation there is a stage of identification and formulation of the flow problem in terms of the physical and chemical phenomena that need to be considered. A good understanding of the numerical solution is also crucial.

Three mathematical concepts are useful in determining the success or otherwise of such algorithms:

Convergence

Consistency

Stability

Convergence is the property of a numerical method to produce solution, which approaches the exact solution as the grid spacing, control volume size or element size is reduced to zero.

Consistent numerical schemes produce systems of algebraic equations which can be demonstrated to be equivalent to the original governing equation as the grid spacing tends to zero.

Stability is associated with damping of errors as the numerical method proceeds. If a technique is not stable even roundoff errors in the initial data can cause wild oscillations or divergence.

Convergence is usually very difficult to establish theoretically. The inability to prove conclusively that a numerical solution scheme is convergent should not be concerning since the process of making the mesh spacing very close to zero is not feasible on computing machines with a finite representation of numbers. Engineers need CFD codes that produce physically realistic results with good accuracy in simulations with finite, sometimes quite coarse, grids.

The finite volume approach guarantees local conservation of a fluid property ϕ for each control volume. Numerical schemes that possess the conservativeness property also ensure global conservation of the fluid property for the entire domain. The boundedness property is close to stability and requires that in a linear problem without sources the solution is bounded by the maximum and minimum boundary values of the flow variable.

All flow processes contain effects due to convection and diffusion. In diffusive phenomena a change of e.g. temperature at one location affects the temperature in more or less equal measure in all directions around it. Finite volume schemes with the transportiveness property must account for the directionality of influencing in terms of the relative strength of diffusion to convection.

Conservativeness, boundedness and transportiveness are designed into all finite volume schemes and have been widely shown to lead successful CFD simulations.

The solution algorithm is iterative in nature and in a converged solution the so-called residuals-measures of the overall conservation of the flow properties-are very small. Progress towards a converged solution can be greatly assisted by careful selection of the settings of various relaxation factors and acceleration devices.

2.4.1 The Benefits of CFD

Basically, the compelling reasons to use CFD are these three (FLUENT, 2004):

1. Insight

There are many devices and systems that are very difficult to prototype. Often, CFD analysis shows parts of the system or phenomena happening within the system that would not otherwise be visible through any other means. CFD gives a means of visualising and enhanced understanding of designs.

2. Foresight

Because CFD is a tool for predicting what will happen under a given set of circumstances, it can answer many hypothetical questions very quickly. Whenever you give the variables, it gives outcomes. In a short time, you can predict how your design will perform, and test many variations until you arrive at an optimal result.

3. Efficiency

Better and faster design or analysis leads to shorter design cycles. Time and money are saved. Products get to market faster. Equipment improvements are built and installed with minimal downtime. CFD is a tool for compressing the design and development cycle.

2.4.2 Planning a CFD Analysis

Before solving a problem using FLUENT, the following issues should be considered initially (FLUENT Inc 2001a):

Definition of the Modelling Goals: What specific results are required from the CFD model and how will they be used? What degree of accuracy is required from the model?

Choice of the Computational Model: In order to model a complete physical system it has to be chosen the way this system is going to be isolated. The computational domain has to be set, as long as the boundary conditions and the boundaries of the model. It has to be decided whether the problem will be modelled in two dimensions or in three-dimensional model.

Choice of Physical Models: The kind of flow should be considered: inviscid, laminar, or turbulent, if the flow is unsteady or steady, if heat transfer is important, whether the fluid will be treated as incompressible or compressible.

2.4.3 CFD in the food processing industry

Modelling of heating and CIP processes in the food industry may be just empirical correlations and graphical solutions, models with very simple approximations and uniform physicochemical properties, finite difference methods where the basic equations describing the process are descritised on a simple grid system and finite element or finite volume, which can cope with more complex geometries and more sensitive expressions for the properties of the products (Bakalis et al. 2001).

Technology's fast development has enabled the later methods to be more widely and more easily applied. The recent approaches of food processes with CFD methods show the flexibility and accuracy that can be achieved.

Over the last few years many attempts have been made to model food industry tasks using Computational Fluid Dynamics. Scott (1992) refers to spray dryer, which include recirculation zones and particle trajectories, mixing, where energy used should be reduced, refrigeration units, where mass transfer through evaporation and buoyancy induced flows should be taken into consideration. He also mentioned studies for clean room conditions, aseptic processing, rheological mechanisms of complex foods, in-container sterilisation and flow in pumps, valves and filling equipment. He also gives comparison between trials and CFD for a hydrostatic cooker. The comparison showed the obstacles when the conditions of the in line measurements and conditions are not well known to the CFD user. Scott and Richardson (1996) present three case studies related to non-Newtonian fluids in pipes: melted chocolate in a manifold and transport of material in a static mixer, showing benefits of CFD and mentioning future development requirements in order to be applied in the food industry more extensively. Later on (Scott and Richardson 1997) they published a review article mentioning several applications connected to the food industry, including (i) the prediction of air flows around buildings that showed that the method can be used to predict air flow movement inside items of food processing equipment, (ii) baking oven performance simulation with CFD in order to quantify heat and mass transfer to and from the product surface, (iii) the prediction of air and temperature distribution inside chillers and retail spray cabinets. Air was the first fluid that had its flow modelled for the food industry application improvements. Subsequently, models were developed for Newtonian and non-Newtonian fluids. Phase change has also been monitored, for equipment such as driers. Mixers and pumps have also been included in CFD modelling. They emphasise, though on the fact of showing confidence in the predictions. They suggest the enhanced use of a food properties database. Use of microbiological models is also mentioned, which is one of the attempts of this work as well.

Many groups studied the sterilisation of food products using finite element and finite volume methods. It was of great interest in the can industry the investigation of the coldest spot in a can. Kumar and Bhattacharya (1990) carried out a numerical simulation to study heating of canned viscous liquid food undergoing sterilization in a still retort, using FIDAP, a finite element code (FLUENT LTD.), to implement a finite element solution. The model liquid used had temperature dependent viscosity and only side wall heating with insulated top and bottom surfaces of the can was considered. They noticed the movements of the hot liquid and results indicated that the bottom of the can heated up at a slower rate than one could predict by assuming conduction heating. The slowest heating point was found to be at the bottom centre of the can, which was contrasting the centre line location predicted for pure conduction heating. The temperature difference from the bottom to the top of the geometry was high enough to indicate that the results are very sensitive to the assumptions made for the model. Later on, they (Kumar and Bhattacharya 1991a) used FIDAP to model transient natural convection heating of sodium carboxy-methyl cellulose in a still retort. The model liquid had temperature dependent and shear thinning viscosity. They found that there was no fixed point, which could be called the coldest point all times. They also modelled (Kumar and Bhattacharya 1991b) a tubular heat exchanger for sterilisation of a shear thinning product again. The analysis they made was based on a worst case scenario. They found the length of the heating section for a required lethality by solving the governing Partial Differential equations.

Verdoven et al. (1997) calculated the local surface heat transfer coefficient during thermal processing of foods of different shapes and for different heating conditions they used a

commercial code, CFX (CFX 4.1., Harwell, UK) for both laminar and turbulent flows around objects. They found that neglecting the local character of the surface heat transfer coefficients will lead to a higher estimation of the process lethality than in reality, because of the overprediction of the food temperature. Natural convection in a can of liquid food during sterilisation was simulated by Ghani et al. (1999a) solving the governing equations axisymmetrically using a commercial CFD package, PHOENIX. Density and viscosity of the model fluids (both Newtonian and non-Newtonian) were temperature dependent. They also (Ghani et al., 1999b) integrated an Arrhenius equation to the CFD code written in FORTRAN, in order to describe deactivation of bacteria during thermal sterilising:

$$k = Ae^{-E_a / RT} \qquad (2.4.1)$$

where k is the specific reaction rate constant, A is a constant, E_α is the inactivation energy, T is temperature and R is the universal gas constant. The above results were of great interest although there were no experiments mentioned that supported them.

Batch retorts were modelled by Varga et al (1999), calculating lethality distribution with F-value. They applied finite element method for the differential equations and boundary conditions comparing the results to experimental values. Later on Ghani et al. (2000) again worked on sterilization of soup pouches with transient three dimensional finite volume CFD models (PHOENIX) in order to establish the velocity, temperature profiles and the shape of the slowest heating zone comparing with temperatures taken in different locations in the pouch. The same team also (Ghani et al., 2001) worked on sterilization of a cherry juice can including bacteria inactivation and vitamin destruction kinetics. Dependence on temperature and flow are high and vary for bacteria and vitamins. They saw that sterilization temperature might vary depending on the quality required. One year later (Ghani et al., 2002a) they modelled sterilization in canned soup and the effect that would have a horizontal position of the can examining the movement of the slowest heated zone, concluding that heating is fastest in the vertical can. The rotational effect in canned food was also investigated (Ghani et al., 2003a) at a horizontal position and they found that the impact was quite significant since the slowest heating zone splits into two parts. They kept on with the CFD models in the pouches (Ghani et al., 2002b) extending the sterilisation considerations including inactivation kinetics of *Bacillus stearothermophilus* spores and getting good agreement with the bacteria counts. They also included (Ghani et al., 2002c) thermal destruction of Vitamin C in a carrot-orange soup pouch and validated taking measurements with high performance liquid chromatography and a titration method. Vitamin C concentration showed to depend on both temperature and velocity profiles with highest concentrations located to the almost stagnant zones. Farid and Ghani (2003) used PHOENIX to generate data in order to build a correlation to predict sterilisation times of liquid food in vertical and horizontal cans.

Sterilisation was also the area where Jung and Fryer (1999) applied FIDAP (finite element) for a flowing food fluid. Time-temperature profiles for laminar flows showed the potential errors that could be made when estimating the sterility and quality of a liquid food in a continuous flow sterilisation process.

Tewkesbury et al. (2000) used FIDAP (finite element code) to model the conduction cooling of chocolate through a polycarbonate mould. They applied temperature and cooling rate depended data for the specific heat of the chocolate and they found good agreement with experimental data. With that work they showed that a mathematical model can represent the behaviour of chocolate and fillings in commercial manufacture. Liao et al. (2000) used FIDAP

(finite element) to emphasise the importance of using accurate thermorheological behaviour of food in a tubular steriliser. They applied user subroutines of the non-Newtonian viscosity model of the starch containing fluid.

FLUENT, and other CFD codes have already been applied in the food industry for various processes like (FLUENT, 2003):

1) Equipment manufacturing (pumps, refrigerators, convection ovens, ventilation, industrial fryers, steamers, spray dryers etc.)

2) Mixing (laminar/turbulent mixing, blending, rheology changes etc)

3) Processing (pasteurisation/sterilization, baking, aseptic processing etc)

4) Packaging (film casting, bottle molding etc.)

Scott and Richardson (1997) report on some of the applications of CFD in general found in the food industry in recent years and aims to illustrate the benefits that can be achieved.

Initially, CFD was applied at the aerospace and automotive industries to predict airflow, for example, around planes and cars. Environmental studies have also used CFD for the prediction of airflows around buildings. Hence, it can be used for airflow movement inside items of food processing equipment. Baking ovens performance was simulated with CFD in order to quantify heat and mass transfer to and from the product surface. This was aiming to optimise the design of existing oven. Another application was prediction of air and temperature distribution inside chillers and retail spray cabinets.

Also, Clarke et al. (2002) made a CFD investigation of maldistribution effects on crude-oil fouling in Shell and Tube heat exchangers. This is related to the food industry as well since heat exchangers are very commonly encountered there and fouling is an important issue, especially when it comes to non-Newtonian flows. They discussed how complexity increases with number of grid-points. They developed a model of tubular exchanger including baffles and integrated into the code their own equations (named User Defined Functions) in order to describe the fouling increase.

Other applications for CFD modelling extrusion and die design, mixing operations and food safety, like in aseptic processing, have also been reported and it has been underlined the help that can be offered to guide experimental and pilot-plant work (Dhanasekharan et al. 2004)

Cleaning in Place of a T-piece and a 'test-cell' was modelled with CFX by Campden association (Hall et al., 1999) to determine efficiency after the process. They checked shear stress on the walls and they also measured log reduction number for biofilms after cleaning. It was demonstrated that log reduction increases with shear stress. They refer also to more models of butterfly valves and pipe couplings where flow at an angle occurs. They claim that CFD can be used to assess cleaning quantitatively as well comparing with EHEDG experiments and suggesting that development of a correlation between flow properties and cleaning would be a good tool.

CFD has also been used by Jensen and Friis (Friis and Jensen 2002) to model flows in upstands and valves during CIP flows. They used the finite volume method code STAR-CD. Validation was carried out using the standardized cleaning test proposed by the European Hygienic Engineering and Design Group (EHEDG). The controlling factors for cleaning were the shear stress and the nature and magnitude of recirculation zones. They concluded that CFD can be a qualitative tool for hygienic design and that complex geometries are not necessarily difficult to clean. Also, three dimensional modelling is suggested for turbulent flows in that kind of configurations. Later on (Jensen and Friis 2004a) they simulated flow in a mix-proof valve.

Flow patterns visualised by Laser Sheet Visualisation (LSV) were identified in the same regions by use of CFD. They compared various mesh and model set-ups and emphasised on the importance of resolving the flow in the near-wall region for modelling this kind of wall-bounded flows. They also worked (Jensen and Friis 2004b) on simulating the flow through a radial flowcell using STAR-CD. They showed that with appropriate models and mesh configuration, shear stress under transient flow could be estimated. They validated with the EHEDG test method.

Jensen (Jensen, 2002) showed, with various models run with STAR-CD, that by only measuring critical wall shear stress on spherical shaped valve houses it was not possible to predict cleanability. Other parameters that should be taken into account are: fluid exchange and flow patterns. Generally, he found that quantitative prediction of wall shear stress values for complex flows was quite difficult and the average values predicted by CFD could not justify all areas found cleaned or uncleaned by a standard EHEDG test for equipment that contains three dimensional flow phenomena.

Woodall (2000) achieved good agreement between simulations run with the CFD package CFX4 and experiments as far as it concerns CIP in T-pieces of various orientations and lengths when soiled with toothpaste.

Generally, so far CFD appears to be a good qualitative tool but still more work needs to be done and more ideas to be investigated probably with more enhanced models and correlations or maybe by taking better advantage of the existing CFD models and combinations of them.

2.4.4 Turbulence and its modelling

Turbulence has always been a difficult kind of flow to understand and modelling it is not an easy task. Eddy formation and boundary layers are critical and determine the equations that describe the various turbulent flows.

The nature of turbulent flow

In turbulent flow there is a complex interconnected series of circulating or eddy currents in the fluid, generally increasing in scale and intensity with increase of distance from any boundary surface. If, for steady state turbulent flow, the velocity is measured at any fixed point in the fluid, both its magnitude and direction will be found to vary in a random manner with time. This is because a random velocity component, attributable to the circulation of the fluid in the eddies, is superimposed on the steady state mean velocity. There is no net motion arising from the eddies and therefore their time average in any direction must be zero. The instantaneous magnitude and direction of velocity at any point is therefore the vector sum of the steady and fluctuating components.

If the magnitude of the fluctuating velocity component is the same in each of the three principal directions, the flow is termed *isotropic*. If they are different the flow is said to be *anisotropic*. Thus, if the root mean square values of the random velocity components in the X, Y and Z directions are respectively $\sqrt{\overline{u_{Ex}^2}}$, $\sqrt{\overline{u_{Ey}^2}}$, $\sqrt{\overline{u_{Ez}^2}}$; for isotropic turbulence:

$$\sqrt{\overline{u_{Ex}^2}} = \sqrt{\overline{u_{Ey}^2}} = \sqrt{\overline{u_{Ez}^2}}$$

There are two principal characteristics of turbulence. One is the *scale* which is a measure of the mean size of eddies, and the other is the *intensity* which is a function of the circulation velocity $\sqrt{\overline{u_E^2}}$ within the eddies. Both the scale and the intensity increase as the distance from a solid boundary becomes greater. During turbulent flow in a pipe, momentum is transferred from large eddies in the central core through successively smaller eddies as the walls are approached. Eventually, when the laminar sub-layer is reached, eddies die off completely. However, the **laminar sub-layer** should not be regarded as a completely discrete region, because there is evidence that from time to time eddies do penetrate and completely disturb it.

The intensity of turbulence I is defined as the ratio of the mean value of the fluctuating component of velocity to the steady state velocity. For flow in the X-direction parallel to a surface this may be written as:

$$I = \frac{\sqrt{\frac{1}{3}\left(\overline{u_{Ex}^2} + \overline{u_{Ey}^2} + \overline{u_{Ez}^2}\right)}}{u_x} \qquad (2.4.2)$$

The intensity of turbulence will vary with the geometry of the flow system.

The scale of turbulence is given approximately by the diameter of the eddy, or by the distance between the centres of successive eddies and is related to the dimensions of the system through which the fluid is flowing. The size of largest eddies is clearly limited by the diameter of the pipe or duct. As the wall is approached, their average size becomes less and momentum transfer takes place by interchange through a succession of eddies of progressively smaller size (down to about 1mm) until they finally die out as the laminar sub-layer is approached near the walls (Coulson and Richardson, 1995).

Turbulent intensity is linked to the kinetic energy and a reference mean flow velocity U_{ref} as follows (Verdteeg and Malalasekera, 1995):

$$I = \frac{\left(\frac{2}{3}k\right)^{1/2}}{U_{ref}} \qquad (2.4.3)$$

To illustrate the influence of turbulent fluctuations on the mean flow we consider the instantaneous continuity and Navier-Stokes equations for an incompressible flow with constant viscosity

The need for turbulence modelling

The instantaneous continuity and Navier-Stokes equations form a closed set of four equations with four unknowns u_x, u_y, u_z and p.

Engineers are content to focus their attention on certain mean quantities. However, in performing the time-averaging operation on the momentum equations we throw away all details concerning the state of the flow contained in the instantaneous fluctuations. As a result we obtain six additional unknowns, the Reynolds stresses, in the time averaged momentum equations. Similarly, time average scalar transport equations show extra terms containing $\overline{u_x'\varphi'}, \overline{u_y'\varphi'}, \overline{u_z'\varphi'}$.

By taking into account the mean values and the Reynold's stresses and after some algebraic work (Appendix 1) we obtain the transport equations for turbulent flows (Brodkey and Hershey, 1988):

the x-momentum is:

$$\rho\frac{\partial\overline{u}_x}{\partial t}+\rho(\overline{u}\cdot\nabla)\overline{u}_x=-\frac{\partial\overline{p}}{\partial x}+\mu\left(\nabla^2\overline{u}_x\right)-(\rho)\left(\frac{\partial}{\partial x}\left(\overline{u_x'^2}\right)+\frac{\partial}{\partial y}\left(\overline{u_x'u_y'}\right)+\frac{\partial}{\partial z}\left(\overline{u_x'u_z'}\right)\right) \tag{2.4.4}$$

the equation for heat transfer:

$$\rho c_p\frac{\partial\overline{T}}{\partial t}+\rho c_p(\overline{u}\cdot\nabla)\overline{T}=\dot{\overline{T}}_G+k\left(\nabla^2\overline{T}\right)-\rho c_p\left(\frac{\partial}{\partial x}\left(\overline{u_x'T'}\right)+\frac{\partial}{\partial y}\left(\overline{u_y'T'}\right)+\frac{\partial}{\partial z}\left(\overline{u_z'T'}\right)\right) \tag{2.4.5}$$

for the mass transfer

$$\frac{\partial\overline{C}_A}{\partial t}+(\overline{u}\cdot\nabla)\overline{C}_A=\overline{\dot{C}_{A,G}}+D\left(\nabla^2\overline{C}_A\right)-\left(\frac{\partial}{\partial x}\left(\overline{u_x'\,C_A'}\right)+\frac{\partial}{\partial y}\left(\overline{u_y'C_A'}\right)+\frac{\partial}{\partial z}\left(\overline{u_z'C_A'}\right)\right) \tag{2.4.6}$$

2.4.5 Turbulence models in CFD

A turbulence model is a computational procedure to close the system of mean flow equations so that a more or less wide variety of flow problems can be calculated. For most engineering purposes it is unnecessary to resolve the details of the turbulent fluctuations. Only the effects of the turbulence on the mean flow are usually sought. In particular, we always need expressions for the Reynolds stresses. In order to develop a useful model for a CFD code it must have wide applicability, be accurate, simple and economical to run. The most common turbulence models are classified below on table 2.4.1:

Table 2.4.1: CFD turbulence models.

Classical models	Based on (time-averaged) Reynolds equations 1. zero equation model-mixing length model 2. one-equation model Spalart-Allmaras (Wilcox, 1993) 3. two-equation model – k-ε model 4. two-equation model – k-ϖ (Wilcox, 1993) 5. Reynolds stress equation model 6. Algebraic stress model
Large eddy simulations	Based on space-filtered equations

Here we are going to refer in more detail only to the two equation models. Large eddy simulations are for very high Reynolds numbers, compute large eddies, model the small ones

and are very expensive computationally, for that reason they were not applied to solve the flows modelled. Reynolds stress equation model results have not yet been as much validated as the two-equation models and is very expensive computationally solving more differential equations. Algebraic equation models solve the Partial Differential Equations describing Reynolds stress transport to algebraic equations to be solved alongside the k and ε equations of the k-ε model.

Zero and one equation models are considered incomplete because they do not provide a turbulence length scale (Wilcox, 1988).

The Spalart-Allmaras one-equation model has been more recently developed and is mostly applied in free stream turbulent flows (not enclosed).

The classical models use the Reynolds equations and form the basis of turbulence calculations in currently available commercial CFD codes.

Of the classical models, the mixing length and k-ε models are presently the most widely used and validated. They are based on the presumption that there exists an analogy between the action of viscous stresses and Reynolds stresses on the mean flow. Both stresses appear on the right hand side of the momentum equation and in Newton's law of viscosity the viscous stresses are taken to be proportional to the rate of deformation of fluid elements. For an incompressible fluid this gives:

$$\tau_{ij} = \mu e_{ij} = \mu\left(\frac{\partial u_i}{\partial x_j} + \frac{\partial u_j}{\partial x_i}\right) \tag{2.4.7}$$

Subscripts show the dimensional position: i can be the x direction j the y. It is experimentally observed that turbulence decays unless there is shear in isothermal incompressible flows. Turbulence stresses are found to increase as the mean rate of deformation increases. It was proposed by Boussinesq (1877) that Reynolds stresses could be linked to mean rates of deformation:

$$\tau_{ij} = -\rho\overline{u_i' u_j'} = \mu_t\left(\frac{\partial U_i}{\partial x_j} + \frac{\partial U_j}{\partial x_i}\right) \tag{2.4.8}$$

where U shows here average values.

The right hand side is analogous to the previous formula except for the appearance of the turbulent or eddy viscosity μ_t [Pa s]. There is also a kinematic turbulent or eddy viscosity denoted by $\nu_t = \mu/\rho$ with dimensions m^2/s.

Turbulent transport of heat, mass and other scalar properties is modelled similarly. The above formula shows that turbulent momentum transport is assumed to be proportional to mean gradients of velocity (i.e. gradients of momentum per unit mass). By analogy, turbulent transport of a scalar is taken to be proportional to the gradient of the mean value of the transported quantity:

$$-\overline{\rho u_i' \varphi'} = \Gamma_t \frac{\partial \Phi}{\partial x_i} \tag{2.4.9}$$

where Γ_t is the turbulent diffusivity and Φ is the mean value of transported quantity φ.

Since turbulent transport of momentum and heat or mass is due to the same mechanism-eddy mixing-we expect that the value of the turbulent diffusivity is close to that of the turbulent viscocity. We introduce a turbulent Prandtl/Schmindt number defined as:

$$\sigma_t = \frac{\mu_t}{\Gamma_t} \tag{2.4.10}$$

Experiments in many flows have established that this ratio is often nearly constant. Most CFD procedures assume this to be the case and use values of around 1.

2.4.5.1 Mixing length models

These models attempt to describe the stresses by means of simple algebraic formulae for μ_t as a function of position:

$$\frac{\mu_t}{\mu} = by^{+n} \tag{2.4.11}$$

where μ is the molecular viscosity, b and *n* are constants, y is the distance from the wall and the superscript + indicates normalisation with respect to friction velocity and m. The application of this model is in simple engineering flows without recirculation or asymmetry (Grifoll and Giralt, 2000).

There is not going to be more expansion on this approach of turbulent flow, since the CFD solutions were obtained basically with the two equation models and their variations. It is popular in calculations of flows around wing sections.

2.4.5.2 Two-Equation Models

These models provide not only for computation of k, but also for the turbulence length scale or equivalent. Consequently, two-equation models are complete, i.e., can be used to predict properties of a given turbulent flow with no prior knowledge of the turbulence structure. They are, in fact, the simplest complete models of turbulence.

The starting point is the Boussinesq approximation.

<u>k-ε model</u>

The k-ε model is a more sophisticated and general, but also more costly, description of turbulence which allows for the effects of transport of turbulence properties by the mean flow and diffusion and for the production and destruction of turbulence. Two transport equations (partial differential equations or PDEs), one for the turbulent kinetic energy k and a further one for the rate of dissipation of turbulent kinetic energy ε, are solved.

The underlying assumption of both these models is that the turbulent viscosity μt is isotropic, i.e. that the ratio between Reynolds stress and mean rate of deformation is the same in all directions.

If convection and diffusion are not negligible-as is the case for example in recirculating flows-a compact algebraic prescription for the mixing length is no longer feasible. The mixing length model lacks this kind of generality. The k-ε model focuses on the mechanisms that affect the turbulent kinetic energy.

The instantaneous kinetic energy k(t) of a turbulent flow is the sum of the mean kinetic energy (Appendix 2)

$K=(1/2)(U_x^2+ U_y^2+ U_z^2)$ (2.4.12)

and the turbulent kinetic energy(Appendix3):

$$k=\frac{1}{2}\left(\overline{u_x'^2}+\overline{u_y'^2}+\overline{u_z'^2}\right) \quad (2.4.13)$$

$k(t) = K+k$ (2.4.14)

The k-ε model equations

The standard k-ε model (Launder and Spalding, 1974) has two model equations, one for k and one for ε.

We use k and ε to define velocity scale ϑ and length scale ℓ representative of the large scale turbulence as follows:

$$\vartheta = k^{1/2} \quad \ell = \frac{k^{3/2}}{\varepsilon} \quad (2.4.15)$$

Applying the same approach as in the mixing length model we specify the eddy viscosity as follows:

$$\mu_t = C\rho\vartheta\ell = \rho C_\mu \frac{k^2}{\varepsilon} \quad (2.4.16)$$

where C_μ is a dimensionless constant.

The standard model uses the following transport equations used for k and ε:

$$\frac{\partial(\rho k)}{\partial t}+div(\rho k\mathrm{U})=div\left[\frac{\mu_t}{\sigma_k}gradk\right]+2\mu_t E_{ij}\cdot E_{ij}-\rho\varepsilon \quad (2.4.17)$$

$$\frac{\partial(\rho\varepsilon)}{\partial t}+div(\rho\varepsilon\mathrm{U})=div\left(\frac{\mu_t}{\sigma_\varepsilon}grad\varepsilon\right)+C_{1\varepsilon}\frac{\varepsilon}{k}2\mu_t E_{ij}\cdot E_{ij}-C_{2\varepsilon}\rho\frac{\varepsilon^2}{k} \quad (2.4.18)$$

The rate of dissipation per unit mass, whose dimensions are m^2/s^3, is of vital importance in the study of turbulence dynamics and is denoted by

$$\varepsilon = 2\nu\overline{e'_{ij}\cdot e'_{ij}} \quad (2.4.19)$$

Where e' is the fluctuating component of the fluid element deformation.

It is always the main destruction term in the turbulent kinetic energy equation, of a similar order of magnitude to the production term and never negligible.

The equations contain five adjustable constants C_μ, σ_k, σ_ε, $C_{1\varepsilon}$ and $C_{2\varepsilon}$. The standard model employs values for the constants that from data fitting for a wide range of turbulent flows:

$C_\mu=0.09$, $\sigma_k=1.00$, $\sigma_\varepsilon=1.30$, $C_{1\varepsilon}=1.44$ and $C_{2\varepsilon}=1.92$

The k-ω model

Kolmogorov (1942) proposed the first two-equation model of turbulence. He chose the kinetic energy of the turbulence as one of his turbulence parameters and his second was the dissipation per unit turbulence kinetic energy, ω. In formulating his model Kolmogorov referred to ω as "the rate of dissipation of energy in unit volume and time". He also called it "some mean 'frequency' determined by $\omega = ck^{1/2}/l$, where c is a constant." On the one hand, the reciprocal of ω is the time scale on which dissipation of turbulence energy occurs. While the actual process of dissipation takes place in the smallest eddies, the rate of dissipation is the rate of transfer of turbulence kinetic energy to the smallest eddies. Hence, this rate is set by the properties of the large eddies and thus scales with k and l, wherefore ω is indirectly associated with dissipative processes.

The form of the equation for ω has changed as the k-ω model has evolved over the past five decades. A production term has been added by all model developers subsequent to Kolmogorov. Because it has been tested more extensively than any other k-ω model, we present the Wilcox (1988) model as the state of the art formulation.

Eddy viscosity

$$\mu_t = \rho k / \omega \tag{2.4.20}$$

Turbulence kinetic enegy

$$\frac{\partial(\rho k)}{\partial t} + div(\rho k \mathrm{U}) = div\left[\sigma^* \mu_t grad k\right] + 2\mu_t E_{ij} \cdot E_{ij} - \beta^* \rho k \omega \tag{2.4.21}$$

Specific dissipation rate

$$\frac{\partial(\rho \omega)}{\partial t} + div(\rho \omega \mathrm{U}) = div(\sigma \mu_t grad \varepsilon) + \alpha \frac{\omega}{k} 2\mu_t E_{ij} \cdot E_{ij} - \beta p \omega^2 \tag{2.4.22}$$

closure coefficients

$\alpha = 5/9$, $\beta = 3/40$, $\beta^* = 9/100$, $\sigma = ½$, $\sigma^* = ½$ (2.4.23)

2.4.5.3 Closure Coefficients

All of the two-equation models have closure coefficients that have been introduced in replacing unknown double and triple correlations with algebraic expressions involving known turbulence and mean-flow properties. The Wilcox k-ω model, for example, has five: α, β, β*, σ and σ*. The theory is not exact, but rather a model developed mainly on the strength of dimensional analysis. Consequently, the best we can do is to set the values of the closure coefficients to assure agreement with observed properties of turbulence (Wilcox, 1993).

2.4.6 Transitional flows

The point where instability first occurs is upstream of the point of transition to fully turbulent flow.

There are a number of common features in the transition processes (Verdteeg and Malalasekera, 1995):

(i) the amplification of initial mass disturbances

(ii) the development of areas with concentrated rotational structures

(iii) the formation of intense small scale motions and finally

(iv) the growth and merging of these areas of small scale motions into fully turbulent flows.

The forced transition to turbulence of laminar flows caused by strong external disturbances was shown (Hunt et al., 2001) to be highly dependent on their amplitude, location and type of flow. The transition to turbulence is strongly affected by factors such as pressure gradient, disturbance levels, wall roughness and heat transfer. The discussions only apply to subsonic incompressible flows.

Experiments showed that in pipe flows turbulent spots appear in the near wall region. Then, they grow, merge and fill the pipe leading to full turbulent slugs. In industrial pipe flows the intermittent formation of turbulent slugs takes place at Reynolds numbers around 2000 giving rise to alternate turbulent and laminar regions along the pipe.

Many commercially available general-purpose CFD procedures often ignore transition entirely and classify flows as either laminar or fully turbulent. The transition region often comprises only a very small fraction of the size of the flow domain and in those cases it is assumed that the errors made by neglecting its detailed structure are only small.

However, there were investigations of the existing turbulent models and how well they could describe the low Reynolds number turbulent flows. Wilcox (1994) made important progress in developing a transition model by showing that the low-Reynolds number k-ϖ model provides a reasonably accurate description for fully developed turbulent channel and pipe flow and or several transitional layers.

In cases of flow into a pipe with Reynolds numbers between 1500 and ~4000 the flow cannot be considered clearly, neither laminar nor fully turbulent. It is continuously in the transitional region and there are recently some 'mild' models suggested for its solution (FLUENT, 2001b).

2.5 Bacteria kinetics

A mathematical model is a set of assumptions, some of which can be formulated by equations describing mathematical relations between the introduced variables. In biology, the real system is extremely complex, so each model must inevitably include simplifications and/or assumptions. These could occur when one variable measures a feature that might be, in fact, a combination of several others, or when a variable is considered to be constant in time although it is time-dependent in reality. The extent of the above depends on theoretical and practical considerations such as the available mathematical techniques, computing power and data (Baranyi and Pin, 2001).

Mathematical models are frequently classified as mechanistic or empirical models. Empirical models are only expected to describe accurately a set of observations, without taking into account the fundamental mechanism by which these data are generated. A mechanistic model describes rather the process, either directly observable or unobservable, that generates those data (Baranyi and Pin 2001). In practice, among the models commonly used in predictive

microbiology, none are purely mechanistic, many have some underlying basis and some are simply curve-filling exercises that at the extreme are unique to the data used to generate the model (McMeekin et al., 2002). A mixture of the two is applied, possibly closer to one than the other (Baranyi and Pin, 2001).

Frequently, model development is an iterative process going through a 'learning curve', when initial, empirical models (describing observations purely quantitatively) can help to define certain qualitative features of a more mechanistic model to be developed. It is also desirable to embed the model into more general principles of science and to make it open to further developments as the quantity and quality of information about the system increases (Bakalis et al., 2001).

Description of the bacterial growth curve.

Since bacteria grow exponentially, it is often useful to plot the logarithm of the relative population size [y=ln(N/No)] against time. The 3 phases of the growth curve can be described by 3 parameters: the maximum specific growth rate μ_m, is defined as the tangent in the inflection point; the lag time, λ, is defined as the x-axis intercept of the tangent; and the asymptote [A=ln(N/No)] is the maximum value reached. Curves may show a decline. This kind of behaviour is called the death phase and is considered in a later paragraph in this chapter.

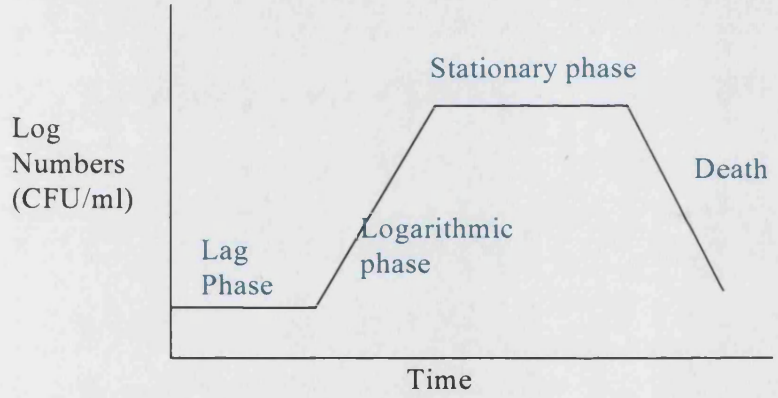

Figure: 2.5.1: Hypothetical bacterial growth curve

Models that describe the growth kinetics rate, can be called primary level models. Secondary level models describe the effect of some environmental conditions, such as temperature and pH, on growth parameters (Delignette-Muller, 1998; Ross and McMeekin 2003).

2.5.1 Primary models

There were several researchers that applied primary models in order to describe the growth and lag phase of various bacteria. Below we mention a few of them as examples of the kind of investigation that has been carried out in this area.

Zwietering et al, (1990) modified the growth models (sigmoidal curves) most commonly found in the literature so that they contain parameters with biological meaning rather than mathematical parameters.

Table 2.5.1: the modified models by Zwietering

Equation (y=)	Modified equation (y=)
Logistic: $\frac{\alpha}{[1+\exp(b-cx)]}$	$\frac{A}{\{1+\exp[\frac{4\mu_m}{A}(\lambda-t)+2]\}}$
Gompertz: $\alpha\exp[-\exp(b-cx)]$	$A\exp\{-\exp(\frac{\mu_m\cdot e}{A}(\lambda-t)+1]\}$
Richards: $\alpha\{1+u\exp[k(\tau-x)]\}^{-1/u}$	$A\{1+u\exp(1+u)\exp[\frac{\mu_m}{A}(1+u)^{\left(1+\frac{1}{u}\right)}(\lambda-t]\}^{-1/u}$
Stannard: $\alpha\{1+\exp[\frac{-(l+kx)}{p}]\}^{-p}$	$A\{1+u\exp(1+u)\exp[\frac{\mu_m}{A}(1+u)^{\left(1+\frac{1}{u}\right)}(\lambda-t)]\}^{-1/u}$
Schnute: $\left\{y_1^b+(y_2^b-y_1^b)\frac{1-\exp[-\alpha(t-\tau_1)]}{1-\exp[-\alpha(\tau_2-\tau_1)]}\right\}^{1/b}$	$\left(\mu_m\frac{1-b}{\alpha}\right)\left[\frac{1-b\exp(\alpha\lambda+1-b-\alpha t)}{1-b}\right]^{1/b}$

where e=exp(1) and u= shape parameter

Zwietering et al. (1990) compared several models statistically and found that, for *L. plantarum*, the Gompertz model was accepted in most cases. Also, from table 2.5.1 we can see that Richards and Stannard models are ending up to be the same after the modifications. The logistic model was not sufficient to describe the data (for *L. plantarum*). With the data of other microorganisms also, the Gompertz model provides a better fit to the growth curves than the rest.

Willocx et al (1993) used the logistic and Gompertz models in order to see the influence of temperature and carbon dioxide upon the growth of *Pseudomonas fluorescens*. The functions were modified to give the lag time and maximum absolute growth rate for R. fluorescens under controlled storage conditions. Expressions of lag time (h), maximum absolute growth rate (r_m) [log(cfu/ml)/h], maximum population density (Ym) [log(cfu/ml)] and generation time (G_T) h derived from logistic (L) and Gompertz (G) eq. parameters. Population density (Y) was expressed as [log(cfu/ml)]. They are given on table 2.5.2.

Table 2.5.2: Growth and lag models.

Growth parameters	Logistic Equation	Gompertz Eq.
Lag time	$\lambda_L = M - (2/B)$	$\lambda = M - (1/B)$
Max absolute growth rate	$r_{mL} = B.C/4$	$r_{mG} = B.C/e$
Max population density	$Y_{mL} = A + C$	$Y_{mG} = A + C$
Generation time at t = M	$G_{TL} = 4.\log(2)/B.C$	$G_{TG} = e.\log(2)/B.C$

In order to calculate directly the growth parameters they are substituted for the mathematical parameters B and M:

$$\text{Log}(N) = A + C/[1 + \exp((4.r_{mL}/C)(\lambda_L - t) + 2)] \text{ (modified logistic)} \quad (2.5.1)$$

$$\text{Log}(N) = A + C\exp[-\exp((e.r_{mG}/C)(\lambda_G - t) + 1)] \text{ (Gompertz)} \quad (2.5.2)$$

Jones and Walker (1993) developed a different mathematical model for bacterial growth, survival and death. Both birth and death control the size of a biological population. So, it follows that the rate at which population size changes, is dependent on both the 'birth' and 'death' rates. In mathematical terms, this can be represented by the following equation:

$$\frac{dN}{dt} = N\frac{dG}{dt} - N\frac{dM}{dt} \quad (2.5.3)$$

where N is the population size, t represents time, dG/dt is the per capita 'birth' or 'growth' rate and dM/dt is the per capita 'death' or 'mortality' rate.

By integrating the above equation for population size is given:

$$N=N_0 2^{(G(t)-M(t))} \quad (2.5.4)$$

Where:

$$G(t) = A(1-(1+(t/B)+(t/B)^2/2+(t/B)^3/6e^{-t/B}) \quad (2.5.5)$$

$$M(t) = e^{(t-D)/C}-e^{-(t-D)/C}-e^{-D/C}+e^{D/C} \quad (2.5.6)$$

and *A, B, C* and *D* are constants

They showed that this equation has the capacity to handle growth, survival and death rate.

2.5.1.1 Exponential phase in bacterial growth considering lag time

There are also models referred in the literature that comprise the lag phase as well, separately and not incorporated in the growth parameters only.

Baranyi et al (1993) described the lag phase as an adjustment period and for the lag-parameter they introduced a new definition. They applied an adjustment function of the form:

$$\alpha_n(t) = \frac{t^n}{\lambda^n + t^n} \tag{2.5.7}$$

Using the adjustment function they came up with the following model

$$y(t) = y_0 + \mu_{\max} A_n(t) - \ln\left(1 + \frac{(e^{\mu_{\max} A_n(t)}) - 1}{e^{-y_{\max} - y_0}}\right) \tag{2.5.8}$$

$A_n(t)$ is the integral function of α(t). The quantity μ(x) is called the specific growth rate.

Later Baranyi (2002) is using a stochastic birth model in order to study the lag distribution of the individual cells in a bacterial population. An integral formula is applied to transform the assumed lag distribution into a growth function describing the transition between lag and exponential phase of the cell population.

He assumed that once a cell divided, the subsequent daughter cells would be in exponential phase. At time t, the expected size of the subpopulation generated by the I-th cell is:

$$x_i = e^{\mu_{\max}(0, t-\tau_i)} \tag{2.5.9}$$

where τ_i the lag times of the individual cells.

Zwietering (1992), using a description of the growth curve like the Gompertz or logistics equations, the third derivative can be derived from these equations. Like Buchanan and Cygnarowisz (1990) he adopted the form of the Gompertz eq. as used by Gibson et al (1987):

$$y(t) = D_o + C\exp\{-\exp[B(t-M)]\} \tag{2.5.10}$$

Where: y(t)=log10 count at time t, D_o=log number at t=-∞, C=final log increase in bacterial numbers, M=time at which culture achieves its max. growth rate (h), B=relative growth rate at time M(1/h), t=time(h).

The conventional way of defining the lag time (λ) results in the following eq.

λ=M-(1/B) (2.5.11)

the definition of Buchanan and Cygnarowisz (1990):

λb=M-(0.96/B) (2.5.12)

Buchanan and Cygnarowisz also proposed that the end of the exponential growth phase can be calculated as the point where the third derivative of the growth model becomes zero for the 2nd time. It is called the time α_b:

$$\alpha_b = M - \frac{\ln(\frac{3-\sqrt{5}}{2})}{B} = M + \frac{0.96}{B} \quad (2.5.13)$$

Alternatively, the end of the exponential phase is defined as:

$$y = \frac{BC}{e} \cdot (t - M) + D + \frac{C}{e} \quad (2.5.14)$$

Zwietering et al. (1991) proposed an hyperbolic eq. to describe he natural logarithm of the lag time behaviour with temperature (Willocx et al., 1993):

Ln(λ) = p/(T-Tmin) (2.5.15)

λ = lag time (h)

p = hyperbolic regression parameter (K)

T = absolute temperature (K)

Tmin = theoritical min. temperature for growth (K)

Tmin is the theoretical min temperature for growth at which lag time is infinite.

2.5.2 Effect of temperature on microbial growth

These are part of the secondary models, as it has already been mentioned. Here we will refer only to the temperature dependent ones, since temperature is going to be the parameter, which will affect our experiments and simulations.

Two types of models have been proposed to describe the effect of temperature only on microbial growth (McMeekin et al., 1993).

2.5.2.1 Bělehrádek models

In 1926 Bělehrádek and Porodko independently published the same formula which described the duration (or rate) of biological reactions as functions of temperature (Ross, 1993):

$$y = \frac{\alpha}{T^b} \qquad (2.5.16)$$

y = duration of reaction

T = temperature in °C

α, b = constants to be fitted

Bělehrádek noted that the function often did not fit the data well at very low temperatures or at temperatures above the optimum for growth and he published a modified form of the equation This equation was written in the form now most widely used:

$$y = \frac{\alpha}{(T - T_o)^b} \qquad (2.5.17)$$

where

y = duration of reaction

T = temperature

T_o = a 'biological' zero

α , b = fitted parameters.

In modern notation, the Bělehrádek-type models can be written as expressions of the general form:

$$k = a(T - T_o)^d \qquad (2.5.18)$$

where

k = rate

α, d and T_o are parameters that need to be fitted.

2.5.2.2 Arrhenius type models

The second major grouping of models relating k to temperature is that of Arrhenius-type models and their extensions. The thermodynamic relationships underlying these models date back to the work of van't Hoff and Arrhenius on chemical reactions. The integrated form of the underlying differential equation results in the following empirical expression:

$$k = A\exp(-E_a / RT) \qquad (2.5.19)$$

where

k is the specific reaction rate constant,

E_a is the so-called 'activation energy' of the reaction system,

T is the absolute temperature,

R is the universal gas constant

A is the so-called 'collision factor'.

In bacterial growth systems, microbiologists have replaced k by a temperature characteristic μ or simply have interpreted k as a specific growth rate constant (McMeekin et al, 1993; Willocx et al., 1993).

2.5.3 Combined effect of temperature, water activity and other factors on Microbial Growth Rate

In many conditions, temperature is not the only factor that affects the rate of product deterioration. The combined effect of different factors often receives attention, but again this information is usually provided in the form of discrete values of the hurdles under consideration that will not permit growth to occur. The general conclusion is that the range of one factor permitting growth will be greatest at the optimum level of a second factor (McMeekin et al., 1993). Here models like that will not be mentioned although there are many of them mentioned in the literature, since the purpose of this work is the temperature dependence of the microbial kinetics and the rest of the factors are assumed to be constant.

2.5.4 Combining Engineering and Microbiological Modelling

Bellara et al. (2000) combined bacterial growth modelling with a heat transfer model describing the spatial temperature changes within a solid object. A finite difference scheme was used to model heat transfer in a vessel, where the model bacterium E. coli was, and bacterial growth was modelled as a function of temperature.

This study used the model of Baranyi and Roberts (1995) to fit experimental data for the growth of *E.coli* when grown at a constant temperature.

$$y(t) = y_0 + \mu_{max} A_n(t) - \ln\left(1 + \frac{(e^{\mu_{max} A_n(t)}) - 1}{e^{y_{max} - y_0}}\right) \quad (2.5.20)$$

They used the Ratkowsky's et al. (1982) model in order to describe the growth rate as a function of temperature. It's a linear relationship between the square root of the growth rate and the temperature (T):

$$\sqrt{\mu} = b(T - T_0) \quad (2.5.21)$$

where b is the regression coefficient and T_0 is the temperature value which is an intrinsic property of the bacteria.

For the temperature change in the vessel over time they used the energy equation for cylindrical co-ordinates:

$$\frac{\partial T}{\partial t} = \kappa\left[\frac{1}{r}\frac{\partial}{\partial r}\left(r\frac{\partial T}{\partial r}\right) + \frac{\partial^2 T}{\partial z^2}\right] \quad (2.5.22)$$

where κ is the thermal diffusivity, and r and z are the radial and axial co-ordinates respectively. The above equation was solved with the finite difference method. The temperature profile then predicted was used to calculate the microbial growth rates.

Zwietering and Hasting (1997a) used the program Simulink (a toolbox in the Matlab code) for the design of the bacterial kinetics depending on temperature. For both microbial growth and inactivation, first order kinetics are assumed, lag phases are neglected. So:

$r_n = \mu N$ and $r_n = -kN$ (#/gs) (2.5.23)

with μ the specific growth rate (s^{-1} or h^{-1}), r_n the organism production rate (if $r_n<0$ inactivation, with k the inactivation constant), N the concentration of micro-organisms (#/g) and # meaning number.

The assumption is made that lag is zero, which is the safest prediction and will occur in situations where the eventual contaminant has been in contact with the product before microbial growth and subsequent contamination. This can happen, for instance, if the contaminant comes from a stagnant area in the process line. They approached the kinetic data using the Ratkowsky model for growth:

$$\sqrt{\mu} = b(T - T_{min}) \quad (2.5.24)$$

A more detailed estimate of growth rate could be made by using the pH and water activity (α_w) of the product and calculate b on the basis of the below equation:

$$\mu = c(\alpha_w - \alpha_{w,\min})(pH - pH_{\min})(pH_{\max} - pH) \times (T - T_{\min})^2 \quad (2.5.25)$$

for inactivation rate:

$$k = k_\infty \exp\left(\frac{-E_\alpha}{RT}\right) \quad (2.5.26)$$

where k is the reaction rate (s^{-1}), k_∞ the reaction rate at infinite temperature, E_α the activation energy ($kJmol^{-1}$), R the universal gas constant ($kJ\ K^{-1}\ mol^{-1}$) and T the temperature in Kelvin.

They derived two organism balances, one for main product flow and one for dead space, both of which include a term for the exchange of micro-organisms from one to the other:

Also they used (Zwietering and Hasting, 1997b) the previous model considering two different configurations for temperature change and bacterial growth:

1) ideally mixed, continuous systems (both steady state and time-variant)
2) batch systems.

At this work they simulated also the effect of cooling on the temperature and on bacterial growth.

Considering the above applications, the square-root models have proven to be useful in predictive microbiology as well as other fields in biology. They fit the data well, are linear or close to linear and have good parameter estimation properties. Have interpretable parameters, are appropriate to the stochastic properties of the bacterial growth rates and are easy to use.

We cannot choose one of them based on actual numbers. The criteria can be only qualitative since the above mentioned models are presented to be applied satisfactorily but under different conditions each one of them. For instance the bacteria used every time vary and the temperature range is not the same in all experiments. So, the simple square root model is used in this work, since it seems to have a greater number of applications with acceptable results.

2.6 Inactivation theories

Generally, the models so far used cannot be applied widely and in any occasion with the same accuracy but they can describe pretty well the death of the microbes.

Microbial inactivation studies seem to be dominated by the exponential single hit and multitarget theories, the former being applied mostly to heat inactivation kinetics and the latter to microbial inactivation by radiators. However, both theories are unable to satisfactorily explain

some relevant experimental results, although they are valid enough to be of some predictive value in sterilisation technology (Casolari, 1988).

Survivor curves are usually described by plotting the logarithm of the number of microorganisms surviving (LogNs) against the size of treatment (S) (time, dose of radiation, concentration of the chemical lethal agent). The semilogarithmic plot of survivor curves may have various shapes such as convex, concave or linear.

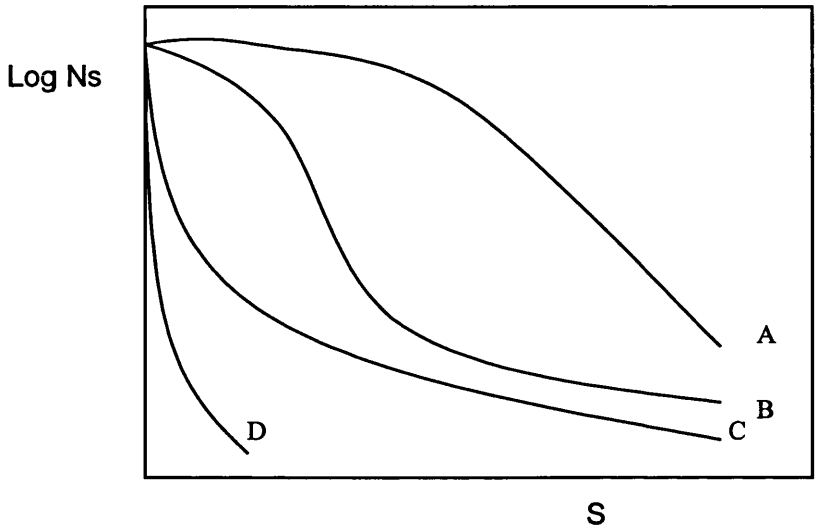

Figure 2.6.1: Shape of survivor curves of microorganisms treated with lethal agents: convex (A), sigmoid (B) and concave or continuously decreasing death rate curve (C and D). Ns is the concentration of survivors after the treatment size S.

Different shapes can be obtained (Casolari, 1988):

(1) under identical experimental conditions with different microorganisms or with the same organism in a different physiological condition (i.e., vegetative cell or spore, the former being in the lag or log phase, the later being activated or dormant, etc.);

(2) using the same population of organisms while changing the destructive potential of the applied lethal agent (viz., changing the treatment temperature or the concentration of the chemical lethal agent);

(3) using the same population of organisms while changing the environment in which the microorganisms are suspended or the culture medium employed etc.

Radiation inactivation studied show the typical convex survivor curve characterised by a more or less extended lag in inactivation at lower doses (shoulder), followed by a nearly exponential decay phase (figure 2.6.1(A)). Such a shape has also been found in heat inactivation experiments, although less frequently, and in microbial inactivation by chemical compounds.

The sigmoid shape is characterised by a more or less pronounced tail occurring after initial shoulder and exponential decay phases (figure 2.6.1(B)). Concave survivor curves characterised by a continuously decreasing death rate (CDDR) with increasing treatment time or size and often described as bi- or multiphasic, can be produced by many physical and chemical lethal agents.

There are few models that appear mostly in the literature and they are used to describe and predict microbial lethality.

2.6.1 Exponential model

According to the single hit theory, the death of microorganisms result from the inactivation of a single molecule or site per cell: the death rate is expected to be proportional to the number of organisms remaining alive and follows first order kinetics.

Plotting logarithm of surviving cell concentration, Nt, (Nt/g, Nt/ml, Nt/cm^2) against the time, t, or treatment at temperature T, a linear relationship is expected to occur:

$$Log_{10}N = Log_{10}N_o - k't \qquad (2.6.1)$$

where No is the concentration of the untreated population and k' is the inactivation rate constant. This type of plot is regarded as very convenient if the resistance of different microorganisms is to be compared. A parameter, called the decimal reduction time, is easily obtained from the regression coefficient k' and is denoted by D_{90}, D_{10}, or D_T:

$$D_T = 1/k' \qquad (2.6.2)$$

The use of D_{90} or D_{10}, refers to the fact that after a treatment time t = 1/k', 90% of the microbial population is destroyed or, alternatively, 10% of the population survives. In heat inactivation studies, D_T is preferred, where T is the treatment temperature.

In exponential form, equation 2.6.1 may be written:

$$N_t = N_o 10^{-k't} \qquad (2.6.3)$$

The value of D at the temperature T is specific to each type of microorganism, species, strain, physiological condition, environment etc (Casolari, 2002)

As for usual chemical reactions, the death rate of microorganisms increases with temperature, according to the Arrhenius law:

$$k = A \cdot e^{-E_a/RT} \qquad (2.6.4)$$

Thermobacteriologists prefer to link the effect of temperature upon the death rate of microorganisms to the parameter D [D = 2.3/k = 1/k'] of the equation 2.6.2 and 2.6.3:

$$D_T = D_{Tr} \cdot 10^{[T_r - T]/z} \quad (2.6.5)$$

where D_T and D_{Tr} are the D value at the temperature T and at the 'reference' temperature Tr, respectively; 'z' is the reciprocal of the rate of change of death rate with temperature, i.e., 'z' is the number of degrees [°C, °F] required to achieve a tenfold change of D_T values:

$$0.1D_{T-z} = D_T = 10D_{T+z} \quad (2.6.6)$$

Another term sometimes used is Q_{10}, which can be defined as the ratio of the thermal death constant at temperature T and the thermal death constant at (T+10)°C. With this definition, it can be shown that the product of the Z value and Q_{10} is a constant (Bull, 2002a)

Equation 2.6.5 can be written as:

$$\text{Log}D_T = \text{Log}D_{Tr} + [T_r - T]/z \quad (2.6.7)$$

After which :

$$z = [T_r - T]/ [\text{Log}D_T - \text{Log}D_{Tr}] \quad (2.6.8)$$

The value of z is characteristic to each microorganisms in a defined environmental condition and is parameter regarded as constant in the narrow range of temperature usually of relevance to the sterilisation purposes.

D and z are the two basic parameters defining completely the heat resistance characteristics of single microorganisms (Casolari, 2002).

There is another term in wide use, the F_{Tr} value. The F_{Tr} value is the thermal death time, i.e. the time required to kill all organisms in a population, measured at 121°C (reference temperature usually) (Bull, 2002b).

F is the treatment time at the temperature T applied for the sterilisation purposes. The *safety* is reached by applying F values high enough to destroy all pathogenic organisms. The preservation is obtained by applying F treatments high enough to destroy both pathogenic and spoilage microorganisms. In either case, the required F can be calculated by knowing:

Knowing the above quantities, the F at temperature T can be calculated by the following relationship:

$$F_T = D_T * nD \quad (2.6.9)$$

Where F_T is a multiple of the highest D_T recorded among D values of relevant spoilage and pathogenic organisms.

By changing the treatment temperature, the values of F = f(T) are obtained, by the following:

$$F = F_{Tr} * 10^{[Tr-T]/z} \quad (2.6.10)$$

Where F_{Tr} ir the treatment time at the reference temperature Tr (Casolari, 2002).

The integrated form of the above equation is also used. The rate of thermal processing commonly quantified through the integrated lethality of thermal process calculated using :

$$F = \int_0^t 10^{(T(t)-T_{ref})/z} dt \quad (2.6.11)$$

the concept of F value, originating from traditional canning, is also used in aseptic processing to describe microbial death. For the non- isothermal case of continuous flow the equation for the total lethality F at a radial position r over an axial length L, can be modified:

$$F(r,L) = \int_0^t 10^{(T(r,t)-T_r(r,t))/z} dt = \int_0^L 10^{(T(r,t)-T_r(r,t))/z} \left(\frac{1}{dz/dt}\right) dz = \int_0^t 10^{(T(r,t)-T_r(r,t))/z} \left(\frac{1}{u(r,z)}\right) dz \quad (2.6.12)$$

The lethality given by the above equation is used for the slowest heating zone, i.e. the centre line. Bulk (volume average) lethality is often estimated as follows:

$$\hat{F}(z) = \frac{\int_0^R F(r,z)u(r,z)2\pi dr}{\int_0^R u(r,z)2\pi dr} = \frac{\int_0^R F(r,z)u(r,z)2\pi dr}{\dot{Q}} \quad (2.6.13)$$

if the velocity and temperature fields are known, the above equation can be used to estimate the microbial death and the nutrient retention (Bakalis et al., 2001).

Jung and Fryer (1999) used the first order kinetics for computational modelling in a continuous sterilisation process. They used the CFD package FIDAP to simulate a laminar flow in a tube. Apart from the lethality, it was used also the 'cook value', *C*, which is an approximate measure of quality. So the equation used was:

$$C = \int_0^t 10^{\left(\frac{T^c(t)-T^c_{ref}}{z^c}\right)} dt \quad (2.6.14)$$

Hendrickx et al (1993) developed a computer program in order to model heat sterilisation of one-dimentional conduction-heated foods with negligible surface resistance to heat transfer. They *calculated the optimal sterilisation temperature* that results in a food product with minimum surface cook-value after achieving the desired degree of sterility, as a function of food properties (thermal diffusivity, z-value of the quality factor), processing conditions (dimensions and geometry of the food or container, initial temperature of the product, heating medium come-up-time) and processing criteria (target F_0-value). The optimal temperature was defined as the sterilising (holding) temperature which results in a product with a minimum surface cook-value. The objective function then becomes:

$$C = \int_0^t 10^{(T_s - T_{ref})/Z_q}\, dt \qquad (2.6.15)$$

where T_{ref} = 100^{0}C. T_s is the temperature at the surface as a function of time and Z_q is the z-value for the quality index.

2.6.1.1 Theoretical uncertainties.

Characteristically, the single-hit theory is applied to heat inactivation kinetics. Heat sterilisation technology is based on the tenet of exponential inactivation. If this order of death should be found to be invalid, the efficiency of the sterilisation process becomes questionable. First order kinetics are expected to be produced by unimolecular reactions, without regard to the underlying reasons (pseudo-first-order reaction, for instance) (Casolari, 1988). Generally, there have been many models developed that depend on the microorganism chosen and the environmental conditions such as temperature range at which the bacteria are exposed, pH of the medium where they grow in, water activity etc.

2.6.2 Logistic Model for Destruction of Bacteria

In the exponential models, each subpopulation of cells dies at a rate that is proportional to the subpopulation size at any time. There is no apparent limiting factor for killing and no initial lag in killing. If there is a lag in killing, then the survival curves are more complex and the exponential model will give a poor fit to the data. Logistic models may be used to analyse data from these complex survival curves for homogeneous as well as heterogeneous cell populations. In terms of surviving fraction S for a homogeneous cell population (Pruitt and Kamau, 1993):

$$S = \frac{1 + e^{-\beta\tau}}{1 + e^{\beta(t-\tau)}} \qquad (2.6.16)$$

where $S = x/x_o$ fraction surviving at any time t, β = maximum specific death rate and τ is a measure of lag in killing.

2.6.3 Other Models

There are some other models also mentioned in the literature taking into account different concepts or stages and conditions of the bacteria. We refer to some of them:

i) Smerage and Teixeira (1993) were based on the assumption that rate constants of activation and inactivation reactions may differ significantly. Inactivation rates of dormant and activated spores may differ and variations of all rate constants with temperature appear to be well described by Arrhenius equations. Apart from the classical model long used in thermal sterilisation, they considered the single species population to be a mix of dormant and activated, but otherwise homogeneous and viable, subpopulations and allow thermal activation of the dormant spores.

ii) Wang et al (2002) studied thermal death kinetics of insect pests. The fundamental 0.5th reaction model was suited for predicting the thermal death kinetics of codling moth larvae.

iii) Cohen et al (1998) dealt with colonies rather than with the bacteria themselves. He presented three models for growth of the bacterial colonies.

There are also other models developed that included dependence on other factors such as pH, water activity etc., (Davies, 1989) and various alterations (Chiruta, 1997; Gaillard, 1998).

2.6.4 Inactivation by radiation

The effects of ionising radiation upon microorganisms have led to the development of some very interesting models, usually described under the name of "target theory" (Casolari 1988).

The concept of microorganisms, or something inside microorganisms, as targets being hit by photons or particles, reflects quite closely what is believed to occur in radiological phenomena. The basic assumption of the "multiple hit" theory was that a single target must be hit n times before the organism is destroyed. If *a* is the sensitive volume of the cell and *h* the average number of hits per unit volume of the microbial suspension; then, *ah* is the average number of hits within the sensitive volume *a*. if the hits occur independently and at random, the probability that *f* hits fall within the volume *a* is given by the Poisson distribution:

$$P(f) = \exp(-ah) \cdot (ah)^f / f! \qquad (2.6.17)$$

If *n* is the number of hits required to inactivate a microorganism, then all cells receiving less than *n* hits will survive. The probability of survival is given by:

$$N_h / N_o = \exp(-ah) \sum_{0}^{n-1} (ah)^f / f! \qquad (2.6.18)$$

The second multiple hit hypothesis of the target theory follows directly from the exponential inactivation theory. If a population of organisms contains n sensitive targets that are inactivated

exponentially, the viability of the organism is ensured if fewer than n targets are hit. The probability that all the targets in such a group of *n* become inactivated is given by:

$$P(n) = (1-\exp(-kd))^n \qquad (2.6.19)$$

Both equations 2.6.18 and 2.6.19 describe convex curves, characterised by an initial shoulder followed by a nearly exponential behaviour at higher doses.

The multi target theory suggests a likely explanation of the observed variations in recovery rate in different environmental conditions. Under suitable environmental conditions the cell can recover.

2.6.4.1 Limitations of the theory

The target theory was developed to explain the shoulder in survivor curves of irradiated microorganisms. The single-hit survivor curve is a special case of the theory. However, the target theory does not explain other kind of survival curves occuring in many radiation inactivation experiments, such as true sigmoid curves, continuously decreasing death rate curves and curves with long tails. The advantage of the theory is that it suggests a multiplicity of events leading to death as a possible general mechanism of microbial inactivation.

2.6.5 Combination of Inactivation Kinetics and Engineering

Hasting et al. (2001) considered the heat resistance of Mycobacterium paratuberculosis in milk from an engineering perspective. They concluded that the thermal process delivered during milk pasteurisation is relatively unaffected by particle diameter. They expressed the inactivation of bacteria in the common way, as first order kinetics:

They used the D decimal reduction time that characterises the heat resistance of a micro-organism. The higher the value, the more heat resistant the organism. Also they included the z value, the second important parameter defining the heat resistance:

$$D(T) = D(T-z) \qquad (2.6.20)$$

Considering the clump of organisms as a sphere, they used the basic heat transfer equation for determining the temperature distribution in a sphere of radius r_o.

2.7 Comments on microbial kinetics models

Predictive microbiology is an area that is constantly being updated and many researchers have contributed. There has been created a number of software packages and on-line databases that give information on the growth of microbial organisms under various conditions.

ComBase, for instance, is a free web-based database of food microbiology data and a major international initiative to coordinate the collection of this data. The dataset consists of thousands of microbial growth and survival curves that are the basis for numerous microbial models used by industry, academia and government regulatory agencies (ComBase, 2004).

The US Department of Agriculture-Agricultural Research Service (USDA-ARS) Pathogen Modeling Program (PMP) is produced at the USDA-ARS Eastern Regional Research Center (ERRC) in Wyndmoor, Pennsylvania. The PMP is a package of models that can be used to predict the growth and inactivation of foodborne bacteria, primarily pathogens, under various environmental conditions (ERRC, 2004). The Food MicroModel database managed by the Institute of Food Research (IFR), sponsored by the UK government, is one of the largest systematically organised databases on pathogens' responses to food environments. It stores growth, survival and death data generated under a former Government-funded research and kinetic parameters collected from scientific literature (McClure et al., 1994), (Foods Standards Agency, 2004). The Seafood Spoilage and Safety Predictor (SSSP) software, which is an expanded version of SSP, becomes is available from www.dfu.min.dk/micro/sssp/. This software has been developed to predict shelf-life of seafood at constant and under fluctuating temperature storage conditions. The software can read data from different types of loggers and in this way evaluate the effect of fluctuating temperatures on shelf-life of seafood. Food Spoilage Predictor is commercial software developed at the University of Tasmania and models the effect of water activity and fluctuating temperatures on the psychrotrophic pseudomonad (Neumeyer et al., 1997; Ross and McMeekin, 2003).

In this work radiation is not going to be considered. The F and z values, although they have been widely used so far by industry in order to check if a product is safe, will not be applied here since the scope of this work is to try to have a clearer and closer view of the bacteria survival taking into account the temperature history of the product. The aim is to see if it is possible to spot the 'dangerous' areas where bacteria may accumulate, grow and end up in the bulk flow. The above models cannot be easily compared to each other since they were applied to different microorganisms. The first order kinetics have been applied most of the times for the mathematical expression of microbial death. So in the models that follow the Arrhenius equation is going to be used as well.

2.8 Pseudomonas Species

Pseudomonas species are very common in fresh foods because of their association with water, soil and vegetation. They commonly contaminate eggs, meat, milk, poultry, seafood and vegetatives. Many species are psychrotrophic and are, therefore, important spoilage microorganisms in refrigerated foods. Pseudomonas species have been isolated from many foods over the years: however, the species have not always been identified because of the difficulties in classification. There are many research papers that refer to unidentified Pseudomonas species rather than to specific species (Robinson et al., 2000).

2.8.1 Importance to the food industry

Many Ps. species, such as *Ps. fluorescent*, *Ps. fragi* and *Ps. maltphilia*, can degrade the globular casein proteins in milk, but not the whey proteins. Many of the proteases produced by

Ps. Species are stable to heat and survive ultra-high temperature (UHT) processing; thereby, causing problems in long shelf-life dairy products (cheeses, 'sterilised' self-stable milks).

2.8.2 Importance to the consumers

The growth of Ps. species in foods results in spoilage. Food that is spoiled is not harmful to eat; however, it will have a lower quality. Usually foods will have flavour, odour and textural changes that will cause consumers not to eat them.

2.8.3 Modelling *Ps. fluorescens* kinetics

P. fluorescens is a gram-negative rod and is usually responsible for food spoilage. It is aerobic and therefore requires an oxygen environment for growth and survival (Tyrer et al., 2004).

For this reason and the aforementioned on the previous pages, *Ps. fluorescens* has been investigated by many research groups and therefore was chosen as the model bacterium to validate the CFD simulations in this work. Also, it has been reported (Pereira et al., 2002; Allison et al., 1998; Panikov and Nikolaev, 2002) that these species form relatively easily biofilms, which is part of the future plans of this work. So, it can be a good suggestion to carry on from the suspensions to the adhesion on process surfaces. Of great importance is the fact that the specific bacterium is not a pathogen and can easily be handled in a chemical engineering environment laboratory where the experiments took place.

Willocx et al (1993) used the logistic and Gompertz primary models in order to see the influence of temperature and carbon dioxide upon the growth of *Pseudomonas Fluorescens*. The functions were modified to give the lag time and maximum absolute growth rate for Ps. fluorescens under controlled storage conditions. Expressions of lag time (h), maximum absolute growth rate (r_m) [log(cfu/ml)/h], maximum population density (Ym) [log(cfu/ml)] and generation time (G_T) h derived from logistic (L) and Gompertz (G) eq. parameters. Population density (Y) was expressed as [log(cfu/ml)].

$$\text{Log}(N) = A + C/[1 + \exp((4.r_{mL}/C)(\lambda_L - t) + 2)] \quad \text{(modified logistic)} \qquad (2.8.1)$$

$$\text{Log}(N) = A + C\exp[-\exp((e.r_{mG}/C)(\lambda_G - t) + 1)] \quad \text{(Gompertz)} \qquad (2.8.2)$$

They applied a linear, the Arrhenius and the square root model two both of them in order to see the dependence of growth on temperature.

The above survey showed that both growth models are useful and RSS showed that linear model was in better agreement with experiments at the range of temperature (4°-12°C).

Brunskill et al (1993) investigated the effect of salt, pH and temperature, separately and in combination on *Pseudomonas* spp. No single factor alone inhibited microbial growth, but when the combined effect of two or more factors was considered then growth would be reduced or inhibited. Different rates of growth occur, though, under different ranges of combined factors.

Ratkowsky et al. (1982) gave some data for the psychrophilic *Pseudomonas* for the square root rate describing the growth of the bacterium for various temperatures between 1°C and 44°C. They took 6 data sets on *Pseudomonas fluorescens*. They showed that the Arrhenius equation does not describe the growth of the above bacteria as well as the square root model. The

simple square root model $\sqrt{r} = b(T - T_0)$, where b is the slope of the regression line, T is the temperature and T_0 is a conceptual temperature of no metabolic significance. It is interesting that T_0 was independent of medium and aeration, indicating that it is an intrinsic property of the organism when growth conditions other than temperature are nonlimiting.

Daughtry et al. (1997) used the Chemical Reaction Rate theory model for growth and lag influenced by temperature in a wide range of foods and media including various strains of Ps.

Where the first model is the chemical reaction rate model and the second the Davey (Arrhenius model) one:

$$\ln k = A'' + B/T + C\ln T$$

$$\ln k = C_0 + C_1/T + C_2/T^2 \qquad (2.8.3)$$

McMeekin et al. (1993) worked on applying and comparing various temperature dependent models on bacteria. Organisms that are psychrotrophic and halotolerant, which include Pseudomonas species, are unaffected by water activity changes caused by partial freezing and continue to grow at a rate determined only by temperature. In that case, growth can be simply modelled by the simple square root model to the point at which growth stops (McMeekin and Franzmann, 1988)

They also fitted values for the extended (modified) Arrhenius (Davey's, 1989) model, which includes water activity dependence, on Pseudomonas strains.

Tyrer et al. (2004) used the modified Gompertz model (Zwietering et al., 1990) for accurate shelf life assessment. The models are used to describe the behaviour of microorganisms under different conditions like: temperature, pH, water activity or relative humidity and some additives. Several mathematical models are commonly used for modelling the growth of microorganisms, with much of the work up to date concentrating on pathogenic as opposed to spoilage organisms.

They isolated *Pseudomonas fl.* From chilled food and inoculated into ready-to-eat models and stored at 5, 10, 15 and 20°C. They used the non-linear modified Gompertz model and fitted it to the experimental data for the growth of the bacterium:

$$\log CFU/g = A \times \exp\left[-\exp\left(\frac{\mu_m \times \exp(1)}{A}\right)(\lambda - t) + 1\right] \qquad (2.8.4)$$

where A is the maximum population density (logCFU/g), μ_m is the maximum growth rate constant (h^{-1}), λ is the lag time (h) and t is the storage time (h). To find the relationship between storage temperature and each biological parameter for each organism, linear regression was carried out:

$$A = a + b*T \qquad (2.8.5)$$

where A the maximum population density (logCFU/g), a and b are constants and T is storage temperature.

$$\mu_m = c + d*T \qquad (2.8.6)$$

where μ_m is the maximum growth rate constant (1/day), c and d are constants and T is the storage temperature.

$$\lambda = e + f*T \quad (2.8.7)$$

λ is the lag time (day) e and f are constants and T is storage temperature.

Substituting to the first equation they get the secondary model:

$$\log CFU/g = (a+b*T)\times\exp\left[-\exp\left(\frac{(c+d*T)\times\exp(1)}{(a+b*T)}\right)\{(e+f*T)-t\}+1\right] \quad (2.8.8)$$

α = 10.83±0.43

b = 0.06±0.03

c = 0.01±0.001

d = 0.01±0.001

e = -35.76±6.61

f = 1.3±0.34

Chandler and McMeekin (1985), described the validation of the square root model in monitoring the shelf-life of pasteurised, homogenised milk where pseudomonas spp. were the major spoilage microorganisms. They concluded that a To of 264K curve can be used for temperatures even above 15°C.

Adair et al. (1988), compared the Schoolfield (1981) (non-linear Arrhenius) model and the Square Root model for law temperature bacterial growth predictions. They concluded that at low temperature range (minimum to optimum growth temperatures) and the whole biokinetic growth temperature range (minimum to maximum: up to 25°C) the Schoolfield model is the one that describes the kinetics best. They claimed that significant errors might result at low (chill) temperatures if the Square Root model is used. They included also *Ps. Fluorescens* in their study, since it is strongly psychrotrophic. Schoolfield model, although is quite complex and has many constants and parameters, is more reliable at low temperatures.

Ratkowsky et al., (1983) extended the square root model for various bacteria in order to cover the whole biokinetic temperature range. They included *Pseudomonas fluorescens*. The equation describing growth was:

$$\sqrt{k} = b(T - T_{min})\{1 - \exp[c(T - T_{max})]\}) \quad (2.8.9)$$

The constants b, c and T_{min}, T_{opt} and T_{max} were calculated by data of bacterial cultures. The parameters b and c were of less practical importance than T_{min} and T_{max} and were calculated from plots describing growth depending on temperature. For *Pseudomonas fluorescence*:

b = 0.03

c = 0.088

T_{min} = 279

T_{opt} = 312

T_{max} = 320

Chiruta et al. (1997) developed an inactivation model that includes the dependence of combined exposure temperature and medium pH on inactivation rates for three vegetative bacteria: *Listeria monicytogenes*, *Escherichia coli* and *Pseudomonas fluorescens* The rate

coefficient for thermal inactivation, k, can then be modelled by the suggested linear Arrhenius model of Davey (Davey, 1989):

$$Lnk = C_0 + (C_1/T) + C_2pH + C_3pH^2 \qquad (2.8.10)$$

Where C_0-C_3 are independent coefficients to be determined and for *Pseudomonas fluorescens* is: 116, -4168,-2.73 and 0.194 correspondingly for temperatures between 52-62°C and pH values between 5 and 6.5

In order to model growth of Ps. Fluorescens the above model of Ratkowsky et al. (1983) that covers the whole biokinetic temperature range was used. Lag time was not taken into account and it was intentionally avoided during the experiment, giving to the system the adequate amount of time to get used to sudden environmental changes during the preparation of the inocculum for the experiments such as dilutions into much bigger volumes.

For inactivation Chiruta's data was used assuming constant value for the pH of the medium where the bacteria were growing.

Conclusions of literature survey

In general, CFD has not been used extensively in the food research area and especially not under food manufacturing conditions. The fact that its wide use in other engineering areas has been proven reliable in most cases, allows us to make an attempt and apply it for hygienically risky geometries in connection to the food industry. Most of the CFD studies take into account only heat conduction and temperature gradient is not an issue. Also, the growth and inactivation models developed for bacteria are in most cases valid for specific media and conditions such as water activity, pH and short temperature range. In reality, during the food processing, these parameters vary and accuracy is very important when it comes to hygiene. Correct choice of flow pattern is an essential issue as well, when it comes to turbulent flows especially.

Geometries such as down stands, T-pieces and bends are difficult parts of a pipeline where flow cannot be easily predicted or solved analytically. CFD modelling has given a good approach to see the effect of shear stresses and product removal during Cleaning In Place in such configurations. This work is taking into account the temperature profile as well as product removal and bacterial counts, investigating more aspects of hygienic design and processing.

3 Materials and methods

This chapter describes the techniques used in this work in order to investigate applications of the finite volume method on processes in the food factory connected with hygienic design and its implications.

The performed simulations were supported by experimental work carried out in the chemical engineering department laboratory, at the University of Bath and by in line measurements of a tomato paste production line in a Unilever factory.

The experiments in the laboratory were based on a T-piece pointing downwards, which was connected with the necessary pipework, heater, pump and valves. Thermocouples were used to take temperature measurements and an electrical conductivity meter was used for measuring mass removal. Bacterial enumeration techniques were employed for the *Pseudomonas fluorescens* colonies that were inoculated in the rig in order to model kinetics and cleaning.

The measurements in the factory were taken from a Tube in Tube in Tube heater used for thick stream of tomato. Temperature was controlled automatically and also with some Pt100 thermocouples located at various points in the process.

3.1 Finite Volume Method for FLUENT

This CFD (Computational Fluid Dynamics) code, FLUENT, and its equations and models are used (for both low viscosity and high viscosity products) in order to model the flows in the T-piece and the heater. Below are given the equations the code applies for solving laminar flow, turbulent flows (only models used in this work), heat transfer and species transfer, which describes better the bacterial modelling, since it includes mixing and reaction options that can represent the microbial kinetics.

3.1.1 Modelling Laminar Flow in FLUENT

For all flows, FLUENT solves conservation equations for mass and momentum. For flows involving heat transfer, an additional equation for energy equation is solved. For flows involving species mixing or reactions, a species conservation equation is solved. Additional transport equations are also solved when the flow is turbulent.

In this section are presented the conservation equations for laminar flow (FLUENT, 2001a).

The mass conservation equation

For all flows, FLUENT solves conservation equations for mass and momentum. The equation for conservation of mass, or continuity equation, can be written as follows:

$$\frac{\partial \rho}{\partial t} + \nabla \cdot (\rho \vec{v}) = S_m \qquad (3.1.1)$$

It is the general form of the mass conservation equation. The source S_m is the mass added to the continuous phase from the dispersed second phase (e.g., due to vaporisation of liquid droplets) and any user-defined sources.

Momentum Conservation Equation

Conservation of momentum in an inertial (non-accelerating) reference frame is:

$$\frac{\partial}{\partial t}(\rho\vec{v}) + \nabla\cdot(\rho\vec{v}\vec{v}) = -\nabla p + \nabla\cdot(\bar{\bar{\tau}}) + \rho\vec{g} + \vec{F} \qquad (3.1.2)$$

where p is the static pressure, $\bar{\bar{\tau}}$ is the stress tensor (described below), and $\rho\vec{g}$ and $\vec{F}$ are the gravitational body force and external body forces (e.g. interaction with the dispersed phase), respectively. $\vec{F}$ also contains other model-dependent source terms such as user-defined sources.

The stress tensor $\bar{\bar{\tau}}$ is given by

$$\bar{\bar{\tau}} = \mu\left[\left(\nabla\vec{v} + \nabla\vec{v}^{T}\right) - \frac{2}{3}\nabla\cdot\vec{v}I\right] \qquad (3.1.3)$$

where μ is the molecular viscosity, I is the unit tensor, and the second term on the right hand side is the effect of volume dilation.

3.1.2 Modelling Turbulence in FLUENT

Fluctuating velocities characterise turbulent flows. These fluctuations mix transported quantities such as momentum, energy, and species concentration, and cause them to fluctuate as well. Since these fluctuations can be of small scale and high frequency, they are too expensive computationally to simulate directly in practical engineering calculations. Instead, the instantaneous governing equations can be time-averaged, ensemble-averaged, or otherwise manipulated to remove the small scales, resulting in a modified set of equations that are computationally less expensive to solve. However, the modified equations contain additional unknown variables, and turbulence models are needed to determine these variables in terms of known quantities.

FLUENT provides the following turbulence models:

- Spalart-Allmaras model
- k-ε models

- Standard k-ε model
- Renormalization-group (RNG) k-ε model
- Realizable k-ε model

- k-ω models
  - Standard k-ω model
  - Shear-stress transport (SST) k-ω model
- Reynolds stress model (RSM)
- Large eddy simulation (LES) model

The Spalart-Allmaras model is relatively new and cannot be relied on all types of complex engineering flows. It was designed specifically for engineering aerospace applications and is also used in turbomachinery. In FLUENT, the model has been implemented to use wall functions when the mesh resolution is not sufficiently fine. This might make it the best choice for relatively crude simulations on coarse meshes where accurate turbulent flow computations are not critical. Also, one-equation models usually do not cope rapidly with sudden changes in length scale.

The Reynolds Stress Model (RSM) is the most elaborate turbulence model that FLUENT provides. The RSM can describe the effects of streamline curvature, swirl, rotation, and rapid changes in strain rate in a more rigorous manner than one-equation and two-equation models and that enables it to give accurate predictions for complex flows. However, RSM predictions are not very reliable due to the closure assumptions employed to model various terms in the exact transport equations for the Reynolds stresses. The RSM might not always yield results that are clearly superior to the simpler models in all classes of flows to justify the additional computational expense.

LES model provides an alternative approach in which the large eddies are computed transiently using a set of "filtered" equations. Filtering is basically a manipulation of the exact Navier-Stokes equations to remove eddies that are smaller than the size of the filter, which is usually the mesh size. The filtering process creates additional unknown terms that must be modelled in order to achieve closure. It should, however, be mentioned that the application of LES to industrial fluid simulations is at a very initial stage (FLUENT, 2001a).

The simplest complete models of turbulence are the two-equation models. In those models, the solution of two separate transport equations allows the turbulent velocity and length scales to be independently determined.

The standard k-ε model in FLUENT is robust, economic and reasonably accurate for a wide range of turbulent flows, which explains its popularity in industrial flow and heat transfer simulations.

Two variants of this model are available in FLUENT: the RNG k-ε model and the realisable k-ε model. The RNG model is similar in form to the standard k-ε model, but includes the following refinements: The RNG model has an additional term in its ε equation that significantly improves the accuracy for rapidly distorted flows. The effect of swirl on turbulence is included in the RNG model, enhancing accuracy for swirling flows. The RNG theory provides an analytical formula for turbulent Prandtl numbers, while the standard model uses user-specified, constant values. While the standard k-ε model is a high-Reynolds-number model, the RNG theory provides an analytically derived differential formula for effective viscosity that accounts for low-Reynolds-number effects.

The realisable model is a relatively recent development and differs from the standard model in two important ways: the realisable contains a new formulation for the turbulent viscosity and a new transport equation for the dissipation rate, ε, has been derived from an exact equation for the transport of the mean-square vorticity fluctuation. The term "realisable" means that the model satisfies certain mathematical constraints on the Reynolds stresses, consistent with the physics of turbulent flows.

Both the realisable and RNG k-ε models have shown substantial improvements over the standard model where the flow features include strong streamline curvature, vortices, and rotation. Since the realisable model is still relatively new, it is not clear when it consistently outperforms the RNG model. However, initial studies have shown that the realisable model provides the best performance of all the k-ε model versions for several validations of separated flows and flows with complex secondary flow features and that it predicts more accurately the spreading rate of both planar and round jets. It could also perform better for flows involving rotation, boundary layers under strong adverse pressure gradients, separation, and recirculation. Since, there are no such flows as the above in the present work, the realisable model is not necessary to be used and only the standard and RNG with or without effective viscosity option on, depending on the flow, are compared.

The standard k-ω model in FLUENT is based on the Wilcox k-ω model (Wilcox, 1993), which incorporates modifications for low-Reynolds-number effects, compressibility, and shear flow spreading. The Wilcox model predicts free shear flow spreading rates that are in close agreement with measurements for far wakes, mixing layers, and plane, round, and radial jets, and is thus applicable to wall-bounded flows and free shear flows.

A variation of the standard k-ω model called the SST k-ω model is also available in FLUENT. The shear-stress transport (SST) k-ω model was developed by Menter (Menter, 1994) to combine the robust formulation of the k-ω model in the near-wall region with the free-stream independence of the k-ε model in the far field. To achieve this, the k-ε model is converted into a k-ω formulation. The SST model is similar to the standard model, but includes the following refinements:

- The standard k-ω model and the transformed k-ε model are both multiplied by a blending function and both models are added together. The blending function is designed to be one in the near-wall region, which activates the standard k-ω model, and zero away from the surface, which activates the transformed k-ε model.
- The SST model incorporates a damped cross-diffusion derivative term in the ω equation.
- The definition of the turbulent viscosity is modified to account for the transport of the turbulent shear stress.
- The modelling constants are different.

These features make the SST model more accurate and reliable for a wider class of flows (e.g., adverse pressure gradient flows, airfoils, transonic shock waves) than the standard k-ω model. Since flows in this work do not fall to the above categories, the SST model is taken into consideration only for modelling low-Reynolds turbulent flows.

The next section gives the equations that FLUENT applies for the 2-equation models chosen to solve the various flows. They were chosen according to the above qualitative criteria and they were compared amongst each other for temperature predictions and mass removal in the geometries modelled.

3.1.2.1 The Standard k-ε Model

The standard k-ε model is based on model transport equations for the turbulence kinetic energy, k, and its dissipation rate, ε. In the derivation of the k-ε model, it was assumed that the flow is fully turbulent, and the effects of molecular viscosity are negligible. It is therefore valid only for fully turbulent flows.

Transport Equations for the Standard k-ε Model

The turbulence kinetic energy, k, and its dissipation rate ε, are obtained from the following transport equations:

$$\frac{\partial}{\partial t}(\rho k)+\frac{\partial}{\partial x_i}(\rho k u_i)=\frac{\partial}{\partial x_j}\left[\left(\mu+\frac{\mu_t}{\sigma_k}\right)\frac{\partial k}{\partial x_j}\right]+G_k+G_b-\rho\varepsilon-Y_M+S_k \qquad (3.1.4)$$

and

$$\frac{\partial}{\partial t}(\rho \varepsilon)+\frac{\partial}{\partial x_i}(\rho \varepsilon u_i)=\frac{\partial}{\partial x_j}\left[\left(\mu+\frac{\mu_t}{\sigma_\varepsilon}\right)\frac{\partial \varepsilon}{\partial x_j}\right]+G_{1\varepsilon}\frac{\varepsilon}{k}(G_k+G_{3\varepsilon}G_b)-G_{2\varepsilon}\rho\frac{\varepsilon^2}{k}+S_\varepsilon \qquad (3.1.5)$$

G_k represents the generation of turbulence kinetic energy due to the mean velocity gradients (Appendix 4). G_b is the generation of turbulence kinetic energy due to buoyancy, calculated as described in Appendix 4. Y_M represents the contribution of the fluctuating dilatation in compressible turbulence to the overall dissipation rate, which will not be analysed further more since we are not going to deal with compressible flows. $C_{1\varepsilon}$, $C_{2\varepsilon}$, and $C_{3\varepsilon}$ are constants. σ_k and σ_ε are the turbulent Prandtl numbers for k and ε, respectively. S_k and S_ε are user-defined source terms.

Modelling the Turbulent Viscosity

The turbulent (or eddy) viscosity, μ_t, is computed by combining k and ε:

$$\mu_t=\rho C_\mu\frac{k^2}{\varepsilon} \qquad (3.1.6)$$

where C_μ is a constant.

Model Constants

The model constants $C_{1\varepsilon}$, $C_{2\varepsilon}$, C_μ, σ_κ and σ_ε have the following default values:

$C_{1\varepsilon}=1.44$, $C_{2\varepsilon}=1.92$, $C_\mu=0.09$, $\sigma_\kappa=1.0$ and $\sigma_\varepsilon=1.3$

These default values have been determined from experiments with air and water for fundamental turbulent shear flows. They have been found to work fairly well for a wide range of wall-bounded and free shear flows.

3.1.2.2 The RNG k-ε Model

The RNG-based k-ε turbulence model is derived from the instantaneous Navier-Stokes equations, using a mathematical technique called "renormalization group" (RNG) methods. The analytical derivation results in a model with constants different from those in the standard model, and additional terms and functions in the transport equations for k and ε.

Transport Equations for the RNG k-ε Model

The RNG model has a similar form to the standard model:

$$\frac{\partial}{\partial t}(\rho k)+\frac{\partial}{\partial x_i}(\rho k u_i)=\frac{\partial}{\partial x_j}\left(\alpha_k \mu_{eff}\frac{\partial k}{\partial x_j}\right)+G_k+G_b-\rho\varepsilon-Y_M+S_k \qquad (3.1.7)$$

and

$$\frac{\partial}{\partial t}(\rho \varepsilon)+\frac{\partial}{\partial x_i}(\rho \varepsilon u_i)=\frac{\partial}{\partial x_j}\left(\alpha_k \mu_{eff}\frac{\partial \varepsilon}{\partial x_j}\right)+G_{1\varepsilon}\frac{\varepsilon}{k}(G_k+G_{3\varepsilon}G_b)-G_{2\varepsilon}\rho\frac{\varepsilon^2}{k}-R_\varepsilon+S_\varepsilon \qquad (3.1.8)$$

In these equations, G_k represents the generation of turbulence kinetic energy due to the mean velocity gradients, calculated as described in Appendix 4. G_b is the generation of turbulence kinetic energy due to buoyancy, calculated as described in Appendix 4. Y_M represents the contribution of the fluctuating dilatation in compressible turbulence to the overall dissipation rate, which again will not be analysed since we are not having compressible flows. The quantities α_k and α_ε are the inverse effective Prandtl numbers for k and ε, respectively. S_k and S_ε are user-defined source terms.

Modelling the Effective Viscosity

The scale elimination procedure in RNG theory results in a differential equation for turbulent viscosity:

$$d\left(\frac{\rho^2 k}{\sqrt{\varepsilon\mu}}\right)=1.72\frac{\hat{\nu}}{\sqrt{\hat{\nu}^3-1+C_\nu}}d\hat{\nu} \qquad (3.1.9)$$

where

$$\hat{\nu}=\mu_{eff}/\mu \qquad (3.1.10)$$

$$C_\nu \approx 100$$

Equation 3.1.9 is integrated to obtain an accurate description of how the effective turbulent transport varies with the effective Reynolds number (or eddy scale), allowing the model to better handle low-Reynolds-number and near-wall flows.

In the high-Reynolds-number limit, equation 3.1.9 gives

$$\mu_t = \rho C_\mu \frac{k^2}{\varepsilon} \tag{3.1.6}$$

with $C\mu = 0.0845$.

The R_ε Term in the ε Equation

The main difference between the RNG and standard k-ε models is the additional term in the ε equation given by

$$R_\varepsilon = \frac{C_\mu \rho \eta^3 (1 - \eta/\eta_0)}{1 + \beta \eta^3} \frac{\varepsilon}{k} \tag{3.1.11}$$

where $\eta \equiv Sk/\varepsilon$ (S is the deformation tensor), $\eta_0 = 4.38$, $\beta = 0.012$.

This term makes RNG more sensitive to rapid strains depending on the η value.

Model Constants

The model constants $C_{1\varepsilon}$ and $C_{2\varepsilon}$ have values derived analytically by the RNG theory. These values, used by default in FLUENT, are:

$C_{1\varepsilon} = 1.42$ and $C_{2\varepsilon} = 1.68$.

3.1.2.3 Convective Heat and Mass Transfer Modelling in the k-ε Models

In FLUENT, turbulent heat transport is modeled using the concept of Reynolds' analogy to turbulent momentum transfer. The energy equation is thus given by the following:

$$\frac{\partial}{\partial t}(\rho E) + \frac{\partial}{\partial x_j}[u_i(\rho E + p)] = \frac{\partial}{\partial x_j}\left(k_{eff} \frac{\partial T}{\partial x_j} + u_i (\tau_{ij})_{eff} \right) + S_h \tag{3.1.12}$$

where E is the total energy, k_{eff} is the effective thermal conductivity, and $(\tau_{ij})_{eff}$ is the deviatoric stress tensor, defined as:

$$\left(\tau_{ij}\right)_{eff} = \mu_{eff}\left(\frac{\partial u_j}{\partial x_i} + \frac{\partial u_i}{\partial x_j}\right) - \frac{2}{3}\mu_{eff}\frac{\partial u_i}{\partial x_i}\delta_{ij} \qquad (3.1.13)$$

which is the Boussinesq hypothesis to relate the Reynolds stresses to the mean velocity gradients.

The term involving $(\tau_{ij})_{eff}$ represents the viscous heating.

For the standard k-ε model, the effective thermal conductivity is given by:

$$k_{eff} = k + \frac{c_p \mu_t}{\mathrm{Pr}_t} \qquad (3.1.14)$$

where k is the thermal conductivity.

For the RNG model, the effective thermal conductivity is:

$$k_{eff} = \alpha c_p \mu_{eff} \qquad (3.1.15)$$

where α is calculated as:

$$\left|\frac{\alpha - 1.3929}{\alpha_0 - 1.3929}\right|^{0.6321}\left|\frac{\alpha + 2.3929}{\alpha_0 + 2.3929}\right|^{0.3679} = \frac{\mu_{mol}}{\mu_{eff}} \qquad (3.1.16)$$

where $\alpha_0 = 1/\mathrm{Pr} = k/\mu c_p$.

3.1.2.4 The Standard k-ω Model

The standard k-ω model is based on model transport equations for the turbulence kinetic energy (k) and the specific dissipation rate (ω), which can also be considered as the ratio of ε to k (Wilcox, 1993).

Transport Equations for the Standard k-ω Model

The turbulence kinetic energy, k, and the specific dissipation rate, ω, are obtained from the following transport equations:

$$\frac{\partial}{\partial t}(\rho k) + \frac{\partial}{\partial x_i}(\rho k u_i) = \frac{\partial}{\partial x_j}\left(\Gamma_k \frac{\partial k}{\partial x_j}\right) + G_k - Y_k + S_k \qquad (3.1.17)$$

and

$$\frac{\partial}{\partial t}(\rho\omega)+\frac{\partial}{\partial x_i}(\rho\omega u_i)=\frac{\partial}{\partial x_j}\left(\Gamma_\omega\frac{\partial\omega}{\partial x_j}\right)+G_\omega-Y_\omega+S_\omega \quad (3.1.18)$$

In these equations, G_k represents the generation of turbulence kinetic energy due to mean velocity gradients. G_ω represents the generation of ω. Γ_k and Γ_ω represent the effective diffusivity of k and ω, respectively. Y_k and Y_ω represent the dissipation of k and ω due to turbulence. The above terms are described in Appendix 5. S_k and S_ω are user-defined source terms.

3.1.2.5 The Shear-Stress Transport (SST) k-ω Model

In addition to the standard k-ω model, FLUENT also provides a variation called the shear-stress transport (SST) k-ω model, so named because the definition of the turbulent viscosity is modified to account for the transport of the principal turbulent shear stress. The major differences between the SST model and the standard model are:

- gradual change from the standard model in the inner region of the boundary layer to a high-Reynolds-number version of the k-ε model in the outer part of the boundary layer
- modified turbulent viscosity formulation to account for the transport effects of the principal turbulent shear stress

Other modifications include the addition of a cross-diffusion term in the ω equation and a blending function to ensure that the model equations behave appropriately in both the near-wall and far-field zones.

Transport Equations for the SST k-ω Model

The SST model has a similar form to the standard k-ω model:

$$\frac{\partial}{\partial t}(\rho k)+\frac{\partial}{\partial x_i}(\rho k u_i)=\frac{\partial}{\partial x_j}\left(\Gamma_k\frac{\partial k}{\partial x_j}\right)+G_k-Y_k+S_k \quad (3.1.19)$$

and

$$\frac{\partial}{\partial t}(\rho\omega)+\frac{\partial}{\partial x_i}(\rho\omega u_i)=\frac{\partial}{\partial x_j}\left(\Gamma_\omega\frac{\partial\omega}{\partial x_j}\right)+G_\omega-Y_\omega+D_\omega+S_\omega \quad (3.1.20)$$

G_k represents the generation of turbulence kinetic energy due to mean velocity gradients, calculated as and G_ω represents the generation of ω. Γ_k and Γ_ω represent the effective diffusivity of k and ω, respectively. Y_k and Y_ω represent the dissipation of k and ω due to turbulence. D_ω represents the cross-diffusion term. All the above are described in Appendix 6. S_k and S_ω are user-defined source terms.

3.1.3 Modelling Heat Transfer in FLUENT

FLUENT solves the energy equation in the following form (FLUENT, 2001a):

$$\frac{\partial}{\partial t}(\rho E)+\nabla\cdot(\vec{\upsilon}(\rho E+p))=\nabla\cdot(k_{eff}\nabla T-\sum_j h_j\vec{J}_j+(\bar{\bar{\tau}}_{eff}\cdot\vec{\upsilon}))+S_h \qquad (3.1.21)$$

k_{eff}: is effective conductivity ($k+k_t$), where k_t is the turbulent thermal conductivity

$\vec{J}_j$: is the diffusion flux of species j

The first three terms on the right-hand side of the above equation represent energy transfer due to

conduction

species diffusion and

viscous dissipation respectively.

S_h: includes the heat of chemical reaction and any other volumetric heat sources that have been defined.

In equation 3.1.21

$$E=h-\frac{p}{\rho}+\frac{\upsilon^2}{2} \qquad (3.1.22)$$

where sensible enthalpy h is defined for incompressible flows as

$$h=\sum_j Y_j h_j+\frac{p}{\rho} \qquad (3.1.23)$$

In equation 3.1.23, Y_j is the mass fraction of species j and

$$h_j=\int_{T_{ref}}^{T} c_{p,j}dT \qquad (3.1.24)$$

where T_{ref} is 298.15 K.

Inclusion of Pressure Work and Kinetic Energy Terms

Equation 3.1.21 includes pressure work and kinetic energy terms, which are often negligible in incompressible flows and are not accounted for by default.

Inclusion of the Viscous Dissipation Terms

Equations 3.1.24 and 3.1.23 include viscous dissipation terms, which describe the thermal energy created by viscous shear in the flow. Viscous heating will be important when the Brinkman number, Br, approaches or exceeds unity, where

$$B_r = \frac{\mu U_e^2}{k\Delta T} \tag{3.1.25}$$

and ΔT represents the temperature difference in the system. In the models run in this work it is negligible.

Inclusion of the Species Diffusion Term

Equation 3.1.21 includes the effect of enthalpy transport due to species diffusion with the term

$$\nabla \cdot \left(\sum_j h_j \vec{J}_j \right)$$

Energy Sources Due to Reaction

Sources of energy, S_h, in equation 3.1.21 include the source of energy due to chemical reaction:

$$S_{h,r\times n} = -\sum_j \left(\frac{h_j^0}{M_j} + \int_{T_{ref,j}}^{T} c_{p,j} dT \right) R_j \tag{3.1.26}$$

where h_j^0 is the enthalpy of formation of species j and is the volumetric rate of creation of species j.

3.1.4 Modelling Bacteria Transport and Kinetics

The bacteria kinetics is modelled in FLUENT using the species model. The bacteria are so small that are not taken as separate particles but are considered to have the same properties as the bulk flow and do not affect the velocity profile.

FLUENT can model the mixing and transport of chemical species by solving conservation equations describing convection, diffusion, and reaction sources for each component species. Multiple simultaneous chemical reactions can be modelled, with reactions occurring in the bulk phase (volumetric reactions) and/or on wall or particle surfaces (FLUENT, 2000b). In this section species transport-modelling capabilities, both with and without reactions and the inputs provided when using the model are described.

In order to simulate the microbial kinetics the species transport model was enabled. Since the inactivation and growth rates of the bacteria were different from the rates available in the model, *UDFs (User Defined Functions)* were applied. A user-defined function, or UDF, is a function programmed by the user and can be dynamically loaded with the FLUENT solver to enhance the standard features of the code. UDFs are written in the C programming language. UDFs allow the user to customize FLUENT to fit particular modelling needs. It can either modify a variable already calculated in the solver, or one that the user would like to identify and keep track of.

The equations used in the Species transport model are explained below:

Species Transport Equations

When the conservation equations for chemical species are solved, FLUENT predicts the local mass fraction of each species, Y_i, through the solution of a convection-diffusion equation for the ith species. This conservation equation takes the following general form:

$$\frac{\partial}{\partial t}(\rho Y_i)+\nabla\cdot(\rho\vec{v}Y_i)=-\nabla\cdot\vec{J}_i+R_i+S_i \qquad (3.1.27)$$

where R_i is the net rate of production by chemical reaction and S_i is the rate of creation by addition from the dispersed phase plus any user-defined sources.

An equation of this form is solved for N-1 species where N is the total number of fluid phase chemical species present in the system. Since the mass fraction of the species must sum to unity, the N_{th} mass fraction is determined as one minus the sum of the N-1 solved mass fractions. To minimise numerical error, the N_{th} species should be selected as that species with the overall largest mass fraction, in our case is the fluid of the bulk flow (water/broth solution).

Mass Diffusion in Laminar Flows

In equation 3.1.27, $\vec{J}_i$ is the diffusion flux of species i, which arises due to concentration gradients. By default, FLUENT uses the dilute approximation, under which the diffusion flux can be written as

$$\vec{J}_i=-\rho D_{i,m}\nabla Y_i \qquad (3.1.28)$$

Here $D_{i,m}$ is the diffusion coefficient for species i in the mixture.

Mass Diffusion in Turbulent Flows

In turbulent flows, FLUENT computes the mass diffusion in the following form:

$$\vec{J}_i = -\left(\rho D_{i,m}\nabla Y_i + \frac{\mu_t}{Sc_t}\right)\nabla Y_i \qquad (3.1.29)$$

where is the turbulent Schmidt number, $\left(\frac{\mu_t}{\rho D_t}\right)$ (with a default setting of 0.7). Note that turbulent diffusion generally overwhelms laminar diffusion, and the specification of detailed laminar diffusion properties in turbulent flows is not warranted.

Diffusion at Inlets

Net transport of species at inlets consists of both the convection and diffusion components.

The Reaction Model used in FLUENT

FLUENT's reaction model computes the chemical source terms using Arrhenius expressions, and ignores the effects of turbulent fluctuations. Here, it is taken into account for the simulations that include growth and inactivation of *Ps. fluorescens*.

The system is described as it contains two components, the broth, which has water properties (aqueous solution), already in the FLUENT database, and the bacteria, which are assumed to have the same properties as the broth.

The net source of chemical species i due to reaction R_i is computed as the sum of the Arrhenius reaction source over the N_R reactions that the species participate in:

$$R_i = M_{w,i}\sum_{r=1}^{N_R}\hat{R}_{i,r} \qquad (3.1.30)$$

where $M_{w,i}$ is the molecular weight of species i and $\hat{R}_{i,r}$ is the Arrhenius molar rate of creation/destruction of species i in reaction r. Reaction here occurs in the continuous phase.

Consider the r_{th} reaction written in general form as follows:

$$\sum_{i=1}^{N} \nu'_{i,r} M_i \underset{k_{b,r}}{\overset{k_{f,r}}{\rightleftharpoons}} \sum_{i=1}^{N} \nu''_{i,r} M_i \qquad (3.1.31)$$

where

N = number of chemical species in the system

$\nu'_{i,r}$ = stoichiometric coefficient for reactant i in reaction r

$\nu''_{i,r}$ = stoichiometric coefficient for product i in reaction r

M_i = symbol denoting species i

$k_{f,r}$ = forward rate constant for reaction r

$k_{b,r}$ = backward rate constant for reaction r

The molar rate of creation/destruction of species i in reaction r (eq. 3.1.30) is given by

$$\hat{R}_{i,r} = \Gamma(\nu''_{i,r} - \nu'_{i,r})\left(k_{f,r} \prod_{j=1}^{N_r} [C_{j,r}]^{\eta'_{j,r}} - k_{b,r} \prod_{j=1}^{N_r} [C_{j,r}]^{\eta''_{j,r}} \right) \quad (3.1.32)$$

where

N_r = number of chemical species in reaction r

$C_{j,r}$ = molar concentration of each reactant and product species j in reaction r ($kgmol/m^3$)

$\eta'_{j,r}$ = forward rate exponent for each reactant and product species j in reaction r

$\eta''_{j,r}$ = backward rate exponent for each reactant and product species j in reaction r

In our case there are two species, the broth and the bacteria. The reaction was expressed as having one reactant component only with stoichiometric coefficient equal to one and forward rate component one as well. When cleaning is modelled, water is added as a component to the species at the inlet. Then, the reaction occurs at the rest of the geometry since the new fluid entering the domain consists only of water.

By default, FLUENT uses the Arrhenius expression to express the reaction rate. In our case we have a more complicated reaction that progresses differently depending on the temperature that is why a UDF is applied expressing the following kinetics models (Appendix 10):

Ratkowsky et al. (1983) extended square root model for various bacteria in order to cover the whole biokinetic temperature range. They included Pseudomonas fluorescens. The equation describing growth was:

$$\sqrt{k} = b(T - T_{min})\{1 - \exp[c(T - T_{max})]\} \quad (3.1.33)$$

The constants b, c and T_{min}, T_{opt} and T_{max} were calculated by data of bacterial cultures. The parameters b and c were of less practical importance than T_{min} and T_{max} and were calculated from plots describing growth depending on temperature. For *Pseudomonas fluorescence*:

b = 0.03

c = 0.088

T_{min} = 279

T_{opt} = 312

T_{max} = 320

Chiruta et al. (1997) developed an inactivation model that includes the dependence of combined exposure temperature and medium pH on inactivation rates for three vegetative bacteria: *Listeria monicytogenes*, *Escherichia coli* and *Pseudomonas fluorescens* The rate coefficient for thermal inactivation, k, can then be modelled by the suggested linear Arrhenius model of Davey (1989):

$$Lnk = C_0 + (C_1/T) + C_2pH + C_3pH^2 \quad (3.1.34)$$

Where C_0-C_3 are independent coefficients to be determined and for *Pseudomonas fluorescens* is: 116, -4168, -2.73 and 0.194 correspondingly for temperatures between 52-62°C and pH values between 5 and 6.5. The inactivation equation can take the Arrhenius form if pH if assumed constant:

$$k = e^{(C_0+C_2pH+C_3pH^2)} \cdot e^{C_1/T} \quad (3.1.35)$$

The above rates are integrated into the model with a UDF presented in Appendix 10.

Γ represents the net effect of third bodies on the reaction rate (Appendix 7).

3.2 Experimental set up

This paragraph describes the experiments that validated the models solved in FLUENT. There were various sets of experiments and models, the comparison of which aims at predicting various parameters and how they affect cleaning and microbial kinetics. Also, overall assessment of the hygienic design of various geometries using CFD is one of the major objectives of this work.

3.2.1 Rig

The experiments carried out in order to validate the models took place in the Chemical Engineering department laboratories in Bath. The rig set up is comprised of: a plate heat exchanger, a centrifugal pump, pipework of ½" (1.27cm) and 1" (2.54cm) external diameter, various valves (2 or 3 way), plastic tanks for supply, a magnetic flow meter, a cooling coil and thermocouples (fig. 3.2.1 (a) and (b)).

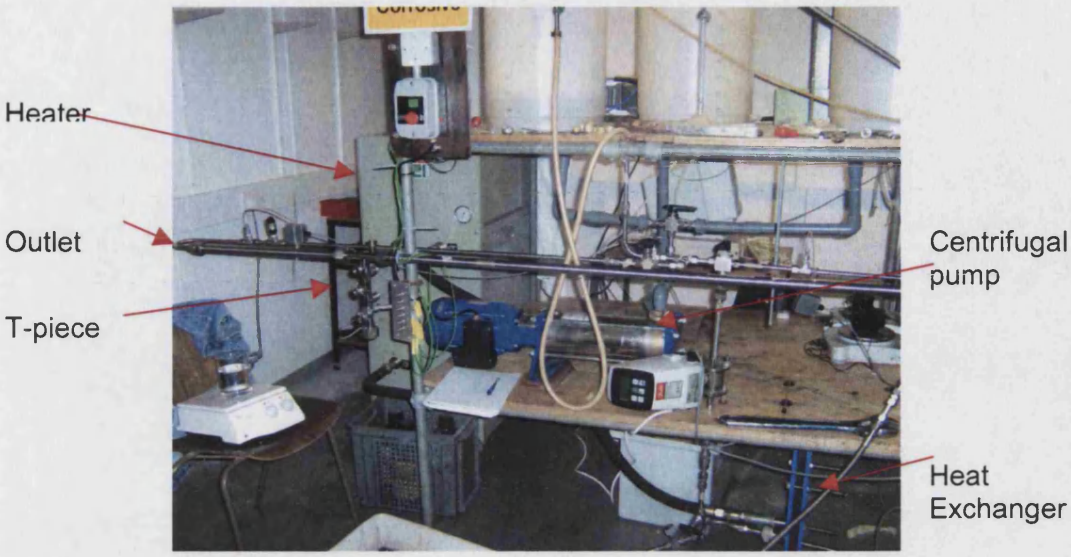

(a)

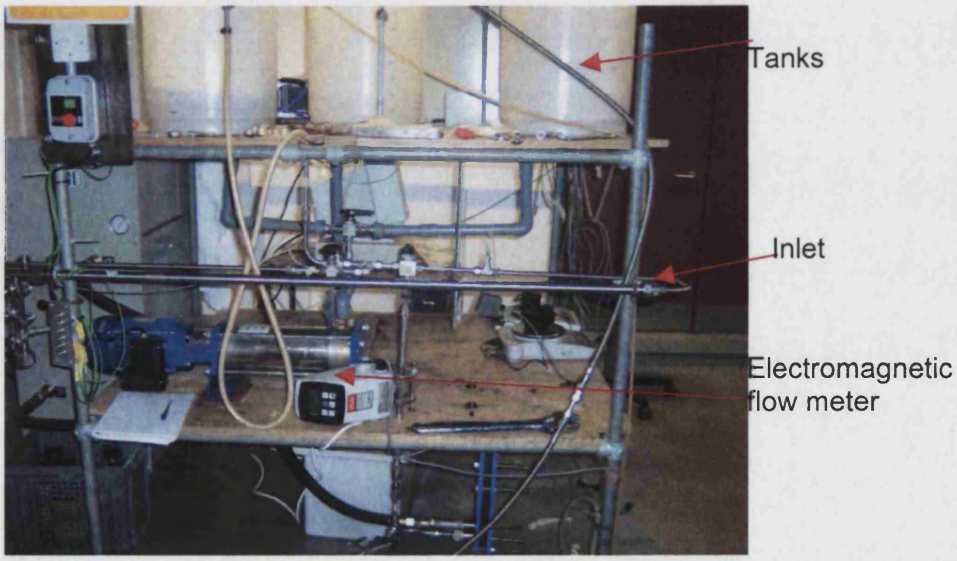

(b)

Figure 3.2.1 (a) and (b): Rig set up at the laboratory, showing the T-piece and various components.

Figure 3.2.2: Plate heat exchanger

Figure 3.2.3: Closer look at T-piece including thermocouples.

Below are described the major components of the configuration:

Heat exchanger (Sondex, 2000): Sondex plate heat exchanger, model S4IT9 where the heating medium is oil, supplied and recirculated by a heater.

Flow meter: MAGFLOW electromagnetic flow meter MAG 1100 DN15 designed for ½" pipe connection (Danfoss, 1997) and signal converter MAG 6000 (Danfoss, 1999)

Pump: electric vertical multistage centrifugal pump where all metal parts in contact with the pumped liquid are made of stainless steel. Model: SV211T15M with in-line oval flanges, single phase (Lowara, 1999).

The area of interest is a vertical T-junction in which the vertical arm is blocked, Fig (3.2.4), thus creating a potentially dead space where stagnant product may remain for extended periods of time.

The geometry that was modelled, is part of the rig. The dimensions are of 1" (0.0254m) external diameter and before and after the T-piece are 1.5 metres and 0.5 metre lengths of horizontal pipework correspondingly. The length of the dead-leg is 0.2325m, measured from the centre of the horizontal tube.

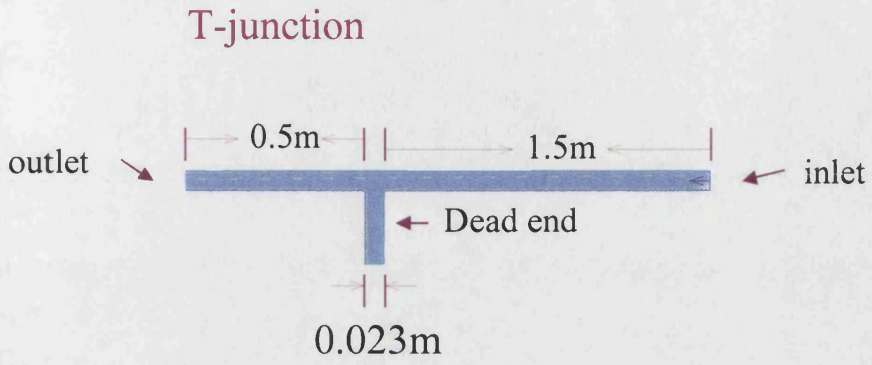

Figure 3.2.4: Schematic of the pipework geometry studied.

The horizontal pipe was insulated, so that constant temperatures can be maintained along its length. However, the vertical pipe is not lagged so there are heat losses to the air via natural convection around the T-piece. The equation used to calculate the natural convection heat transfer coefficient for horizontal pipes is the following (Coulson and Richardson, 1995):

$$\frac{hl}{k} = C'\left(\frac{\beta g \Delta T l^3 \rho^2}{\mu^2}\frac{C_p \mu}{k}\right)^n \qquad (3.2.1)$$

where C'=0.53 and n=0.25 are constants determined for horizontal cylinders and g is the gravitational acceleration.

For vertical surfaces:

$$h = \frac{k}{l}0.683 Gr^{0.25}\,\mathrm{Pr}^{0.25}\left(\frac{\mathrm{Pr}}{0.861+\mathrm{Pr}}\right)^{0.25} \qquad (3.2.2)$$

where:

h = natural convection heat transfer coefficient [W m^{-2} K^{-1}]

Pr = $C_p\mu/k$ (Prandtl number)

The physical properties of air: density ρ, specific heat C_p, viscosity μ and thermal conductivity k are calculated at the average temperature of the wall surface and the environmental temperature. They are taken from temperature dependent equations (R-theta, 2004):

$$\rho = \frac{351.99}{T} + \frac{344.84}{T^2} \qquad (3.2.3)$$

$$\mu = \frac{1.4592 \times 10^{-6} T^{1.5}}{109.1 + T} \quad (3.2.4)$$

$$k_f = \frac{0.002334 T^{1.5}}{164.54 + T} \quad (3.2.5)$$

$$C_p = 1030.5 - 0.19975T + 0.00039734T^2 + 0.83504 \times 10^{-7} T^3 \quad (3.2.6)$$

where:

ρ = density, [kg m^{-3}]

μ = dynamic viscosity, [N m s^{-2}]

k_f = fluid thermal conductivity, [W m^{-1} k^{-1}]

C_p = specific heat, [J kg^{-1} K^{-1}]

T = fluid temperature in Kelvins [K]

The coefficient of cubical expansion, β, is taken as 1/T, where T is the absolute temperature and I is the length of the vertical pipe. Also:

$$\Delta T = T_{wall} - T_{env} \quad (3.2.7)$$

Where T_{wall} is the averaged temperature on the wall and T_{env} is environmental air's temperature. In the experimental set-up are included; 6 type k 0.5mm thermocouples located down the centre of the vertical pipe at the following distances from the centre of the horizontal pipe: 0cm, 4cm, 6cm, 10cm, 14cm and 18cm. There were also two thermocouples fitted on the rig at the inlet and the outlet of the 1" inch pipe work.

Three sets of experiments were carried out in order to validate various modelling capabilities of the CFD code:

The *first set* of experiments was carried out under steady state conditions and the aim was to record the temperature distribution down the central axis of the T-piece and compare it with the values given by the CFD model. The flows were varying starting from laminar, moving on to transitional and finally highly turbulent at the maximum capacity of the pump. The temperature profiles from the thermocouples, in steady state, were compared with the prediction of the simulation. The temperature at the inlet of the horizontal part of the pipework was maintained at around 50°C, to provide a significant temperature difference from ambient conditions and hence create a temperature gradient down the unlagged pipe.

The *second set* of experiments was based on validating the code for removal kinetics and transient flows. The first part of the experimental protocol involved the establishment of steady state conditions of recirculation in the rig of a salt solution of known concentration. The temperature gradient was negligible since, by using a cooling coil, the temperature in the system was maintained at a value similar to the ambient temperature. Also, by keeping the temperature constant, any variation in the electrical conductivity with temperature was eliminated letting only the concentration to determine the values taken. Therefore conductivity

could be used to determine salt concentration. There was an electrical conductivity probe fitted at the bottom of the T-piece. The conductivity meter (Hanna instruments H8820N) was calibrated against the potassium chloride solution used. After steady state was accomplished, cleaning of the salt solution followed by flushing it out with clear water for a certain period of time. The two electrical conductivity values, before and after cleaning, are compared and thus the amount of salt removed is estimated.

The *third set* of experiments involved bacterial kinetics (fig. (3.2.5)). The steady state conditions were obtained recirculating broth which had been inoculated with *Ps. fluorescens* colonies. This species was chosen because it is spoilage bacteria suitable for use in the lab, which is not a microbiology one, where the use of pathogens is not allowed. Also, *Pseudomonas fluorescens* is very common in many food products (Cousin, 2000) and forms biofilms quite easily (Belova et al., 1995; Lindsay and von-Holy, 1998; Pereira et al., 2002), thus giving the opportunity to research biofilm formation. The tank used to supply the broth was aseptic to avoid any contamination in the system. For that reason it was not recommended to use the cooling coil in order to remove the heat introduced into the system from the pump. The media, Trypton Soya Broth (TSB) and Trypton Soya Agar (TSA) for the enumeration methods, were provided by Oxoid UK Limited.

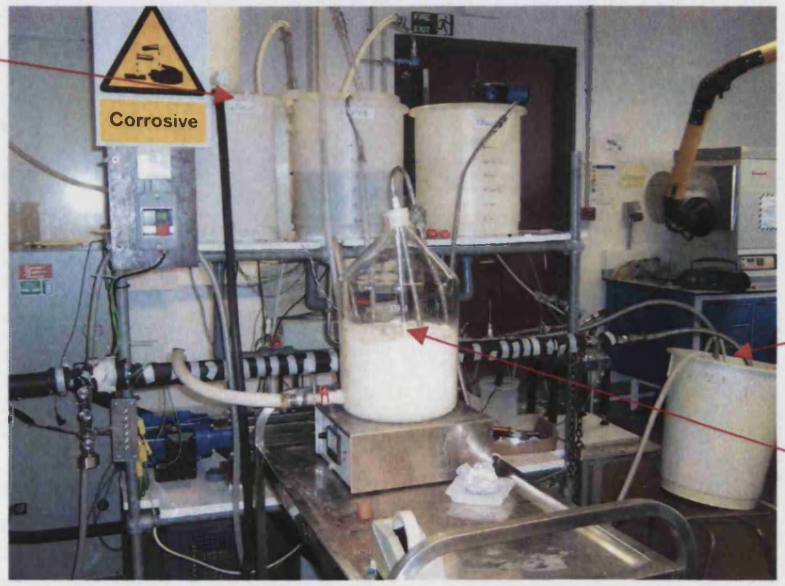

Figure 3.2.5: Modified rig for the bacteria experiments.

The bacteria were left overnight in 250ml flasks at 23°C. Then they were inoculated in the tank. The first experiments were ending up into high temperatures and in some cases the bacteria were killed since the system temperature went above 47°C, which is the maximum temperature above which growth stops for the specific bacterium and inactivation starts (Ratkowsky et al., 1983). Later on there was a stainless steel coil attached to the rig. This coil was emerged into a bucket where tab water was circulating (fig(3.2.5)). The aim of the cooling was to manage to keep the temperature in the horizontal tube at no more than 45°C and notice differences in the log numbers of the bacteria colonies. Initially, the bacteria in the tank had already reached the stationary phase, since they were left in there overnight, so there was no significant change or growth during the heating while the experiment was running for longer than two hours.

Following experiments included a holding period (lag time) after inoculating in the aseptic tank, so that the bacteria would just get used to the new conditions and reach the exponential phase without saturating the whole broth solution, once they are introduced to the rig.

3.3 Enumeration methods applied

The following paragraphs describe the techniques that were used in this project in the laboratory in order to get the microbial counts out of the rig, after circulating the broth for a certain amount of time under various temperature histories. Samples were taken also from the same areas in the rig after flushing out the broth with deionised water.

Methods applied were for viable counts and total counts. Brief descriptions of the methods and some advantages and disadvantages are given. It should be remembered that the experiments did not take place in a microbiology lab but in a chemical engineering one. Also, the exact amount of colonies is not of great importance. The log numbers are the ones that are taken into account and how CFD can predict the growth under favourable temperature conditions, the inactivation under high temperature and the removal under high turbulent flow. The bacteria are treated quite harshly: under stress in the pump or plate heat exchanger, through variable geometries (pipe expansions/contractions, valves). The conditions tried to resemble as much as possible heating treatment in a process line. For that reason, and in order to keep the reactions of the bacteria going, a UDF was applied that expresses the mass fraction of the *Ps. fluorescens* in the inlet to be read and used from the outlet (Appendix 3.E).

Enumeration methods can generally be classified as direct, where individual organisms are distinguished and counted (e.g. direct microscopy, plate counts, Coulter counter) or indirect in which some property of the total population (e.g. DNA, dry weight, optical density, impedance) (McMeekin et al.1993).

In this work plate count methods and optical density measurements were applied.

3.3.1 Spread-plate and pour plate techniques

To determine the number of viable cells, the serial dilution agar plate technique was used. It involves the serial dilution of a bacterial suspension in ¼ strength Ringer solutions, which serve as a diluent of known volume. Once diluted the suspensions are placed on suitable nutrient media (Tryptone Soya Agar was used in this work). The pour-plate technique is the procedure usually employed, where molten agar, cooled to 40-50°C, is poured into a petri-dish containing a specified amount (0.1ml) of the diluted sample. Following addition of the molten then cooled agar, the cover is replaced and the plate is gently rotated in a circular motion to achieve uniform distribution of microorganisms (Cappuccino and Sherman 2001). During spread-plate technique 0.1ml volume of sample is spread on the surface of pre-dried agar medium in a petri-dish and the medium is let to absorb the inoculum. The advantage over the pour plating is that there is no danger of killing the microorganisms with hot media (Messer et al., 2000). In the case of *Ps. fluorescens* the spread technique was used for the first experiments but was changed to pour plating because the colonies had the tendency to create spreaders in the film of water at the edge of the surface of the agar or between the agar and the dish.

Plating techniques are simple, sensitive and widely used to count bacteria and other microorganisms in samples of food, water and soil. Because it is not possible to be absolutely

certain that each colony arose from an individual cell, the results are often expressed in terms of Colony Forming Units (CFU) rather than the number of microorganisms (Prescott et al., 1999).

Advantages of the serial dilution-agar plate techniques are (Cappuccino and Sherman 2001):

- only viable cells are counted
- it allows isolation of descrete colonies that can be subcultured into pure cultures, which may then be easily studied and identified.
- Simple, sensitive and widely used (Prescott et al., 1999)

Disadvantages of this method are (Cappuccino and Sherman 2001):

- overnight incubation is necessary before colonies develop on the agar surface
- it is necessary to use more glassware in this procedure.
- the need for greater manipulation may result in erroneous counts due to errors in dilution or plating
- results are very dependent upon the skill and technique used by the plater

The dilutions were up to seven, depending on the condition of the bacteria when they were introduced into the system. So, when they were at the stationary phase we expect 10^8-10^9 cfu/ml. The last experiments were aimed at examining the bacterial kinetics while they were in the exponential phase. Up to five dilutions were used to count the concentration at the feeding and seven were used at the end of the experiment in order to observe the growth. After cleaning up to five dilutions were made for sampling at the T-piece and at the outlet and seven for the sample taken from the port closest to the bottom of the dead end.

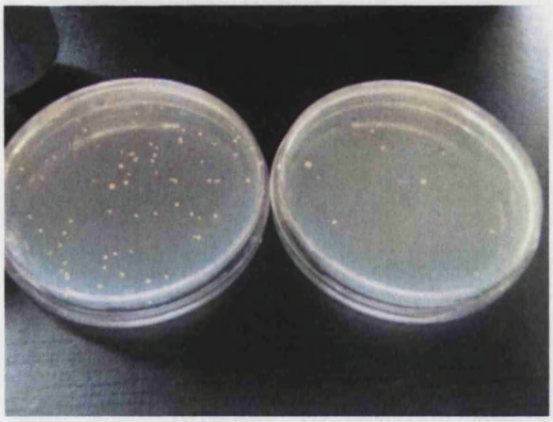

Figure 3.2.6: Petri-dishes after the experiment where a high temperature was reached in the horizontal pipe. Left petri-dish shows sample from the bottom of the T-piece and right one from the outlet of the geometry modelled. Both were at the 6^{th} dilution.

3.3.2 Optical Density - Spectrophotometer

More rapid, sensitive techniques depend upon the fact that microbial cells scatter light that strikes them. Because microbial cells in a population are of roughly constant size, the amount of

scattering is proportional to the concentration of cells present, size and shape of the bacteria, the relative refractive indices of the bacteria and the medium and the wavelength of the incident light. When the concentration of bacteria reaches about 10 million cells (10^7) per millilitre, the medium appears slightly cloudy or turbid. This property is recognised as turbidity and can be used to follow the increase in population density in a liquid medium using a spectrophotometer as detector (McMeekin et al., 1993). Further increases in concentration result in greater turbidity and less light is transmitted through the medium. The extent of light scattering can be measured by a spectrophotometer and is almost linearly related to bacterial concentration at low absorbance levels (Prescott et al., 1999).

Hence, increased turbidity in a culture is another index of growth. With turbidimetric instruments the amount of transmitted light decreases as the cell population increases and the decrease in radiant energy is converted to electrical energy and indicated on a galvanometer (Cappuccino Sherman, 2001).

Advantages of the method:

- rapid and simple (Cappuccino Sherman, 2001; Mcmeekin et al., 1993).
- Non-invasive allowing many measurements to be made on a single culture (Mcmeekin et al., 1993).

Disadvantages are: the limitation of its sensitivity, which is restricted to microbial suspensions of 10 million cells or greater and also the method may be used to enumerate the number of cells in a bacterial culture but the total count includes dead as well as living cells (Cappuccino Sherman, 2001). Also:

- relationship between concentration and absorbance/turbidity is only linear over a limited range, corresponding approximately to a tenfold increase in cell numbers (Mcmeekin et al., 1993).
- The lower limit of detection is of the order of 10^6 cells/ml and that under conditions permitting consistent growth the stationary phase is typically of the order of 10^9 cells/ml, the onset of the stationary phase is not easily measurable and lag time determinations can only be made on dense populations (Mcmeekin et al., 1993).

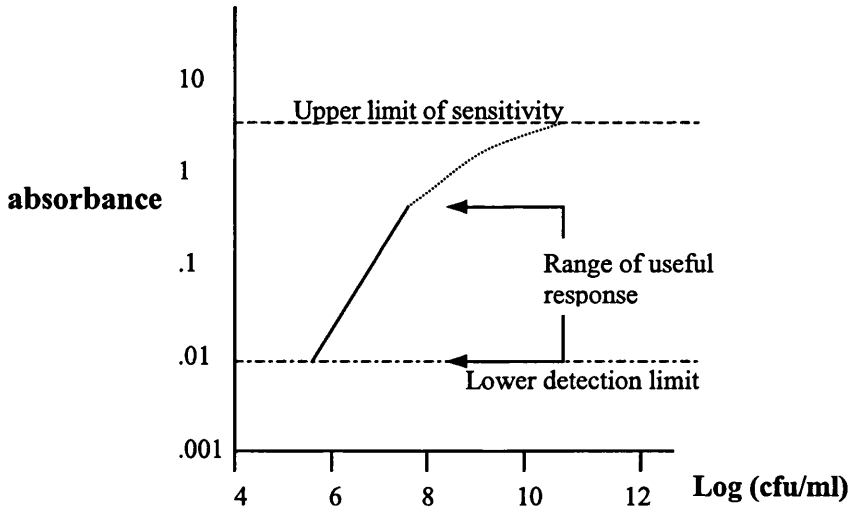

Figure 3.2.7: Plot showing absorbance-cell density relationship.

Though a linear relationship is predicted it is common to plot the variables as log absorbance versus log (cell density), so that data points are more evenly spaced. The relationship is only linear over a narrow range (~10^6-$10^{7.5}$) (fig 3.2.7).

Optical density values depend a lot on the characteristics of the organism, the medium and the geometry of the measuring system. Therefore, the system must be calibrated to absolute cell density if data are to be compared between systems. Here, zero optical density is set to pure deionised water and pure diluted broth and measurements against both are taking place most of the time for the absorption of the samples.

3.4 Non-Newtonian flows.

In this section a model based on a Unilever factory process of thick tomato paste in Greece is described. The heating is simulated, which takes place in a "Rossi e Catelli" tube in tube in tube (TnTnT) heat exchanger and the bent parts of the equipment are included in the model. The scope is to examine the flow pattern of the thick stream and the heat distribution.

3.4.1 Product description

The thick stream of tomato paste is a non-Newtonian fluid. Its viscosity follows the power-law equation:

$$\mu = \beta \cdot \gamma^{(n-1)} \tag{3.4.1}$$

where

β is the consistency index, γ is the strain rate and n is the power law index. The values used are (Dubbelman and van Dijk, 2004):

$$\beta = 0.0694 \cdot e^{\frac{2736.15}{T+273}} \tag{3.4.2}$$

and n=0.26.

The tomato product has 8% Insoluble Solids (IS) and 4.5% Soluble Solids (SS) and 5% brix (Dubbelman and van Dijk, 2004). The rest of the thermophysical properties are described by first order polynomial equations depending on temperature:

Density (Dubbelman and van Dijk, 2004):

$$\rho = (1009.9 - 0.46407)\cdot(1 - fibre) + (1488.3 - 0.219 \cdot T)\cdot fibre \text{ [kg m}^{-3}\text{]} \tag{3.4.3}$$

where *fibre* is the fibre content expressed as a percentage typical value of which is around 8%. The first part of the right hand side of the equation is the water content density and the other part is the fibre content density.

The specific heat and thermal conductivity were taken from measurements carried out in a Unilever laboratory in Colworth for various temperatures (Patrick, 2004):

$$k=0.11832+0.00155T \ [W\ m^{-1}K^{-1}] \quad (3.4.4)$$

$$Cp = 3.41265+1.61T \ [J\ gr^{-1}K^{-1}] \quad (3.4.5)$$

Where T is temperature.

3.4.2 Description of the TnTnT geometry

The configuration of the heater increases the heat transfer area (heating takes place from two sides, however the amount of shear is higher as well when compared to a normal TnT configuration). The product flows in a complex pattern compared to the heating medium, depending on the equipment set up, sometimes co-current, sometimes counter-current. However, heat transfer is always in counter-current mode. The heating section is described in fig. 3.2.8, where the dimensions and flow patterns are also depicted. The tomato product is in red colour and the heating medium in blue and dark blue, since it has two different entrances. The annulus through which the product flows is determined by the outer diameter of pipe 2 and the inner diameter of pipe 3:

Annulus = (Outer diameter pipe 3-Inner diameter pipe 2)/2=(99-73)/2=13 mm

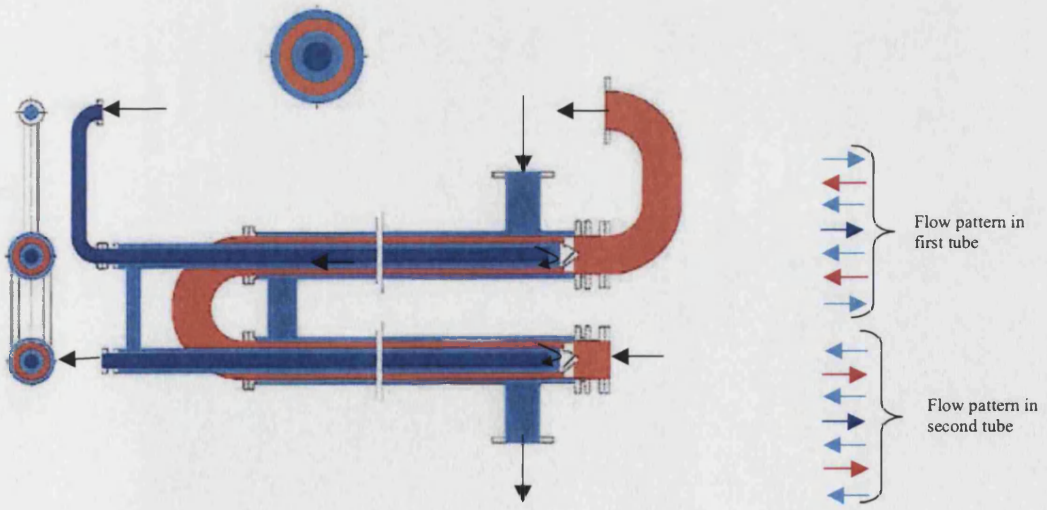

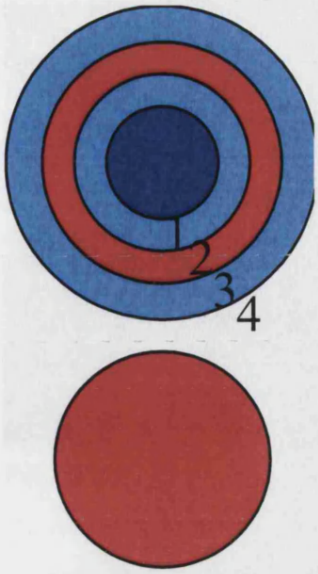

TNT Heating pipes dimensions:

Pipe 1:	Di = 42 mm, Do = 45 mm
Pipe 2:	Di = 70 mm, Do = 73 mm
Pipe 3:	Di = 99 mm, Do = 108 mm

Figure 3.2.8: Schematic of TnTnT heater.

3.4.3 Location of thermocouples

The results that came out of the simulation using FLUENT were compared to measurements taken at the plant. One set of measurements were given by Pt-100 attached to the curved walls of the bends after each heating section ("bend measurements") (fig. 3.2.9) during a trial.

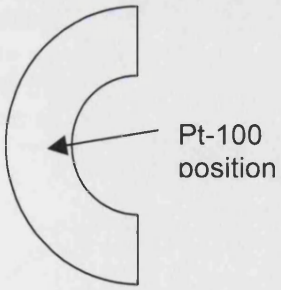

Figure 3.2.9: Stick-on Pt100s location.

Another set of temperature measurements was taken by a double sensor (double Pt100 probes set-point 106°C) (fig. 3.2.10) included in the machines by the manufacturers at the end of the whole heating set. The sensor gave the temperature in the centre of the flow at the exit and is referred to as the "operators measurements".

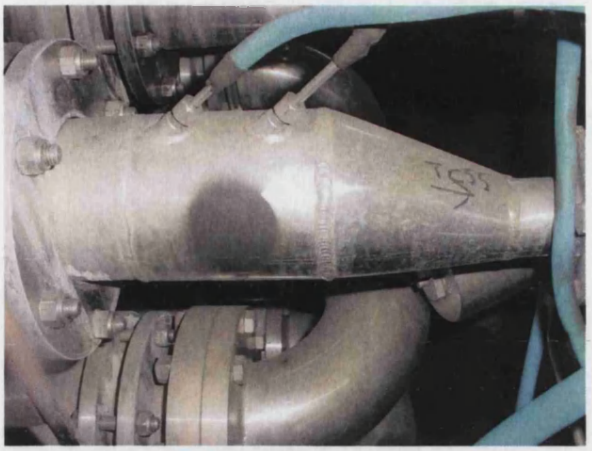

Figure 3.2.10: Double Pt100 probes.

3.4.4 Description of the model

The whole geometry of the heat exchangers was meshed in five sections: three heating TnTnT sections and two bends that connect them. In order to achieve greater accuracy the velocity and temperature distribution profiles of the thick stream flow at the outlet of each model were used as boundary conditions for the inlet of the next model. The code seemed to have difficulties in recognising velocity and temperature profiles when they led from a narrow area (annular entrance or exit) to a broader one (the inlet of the bend). For this reason, part of the heating section was attached to the bends section: twenty cm of heating on each end. In this way profiles were passed from annulus to annulus. So the TnTnT heating was 5.8 m for the first and third sections and 5.6 m for the second (fig. 3.2.11) with a total length of heating equal to 18 metres.

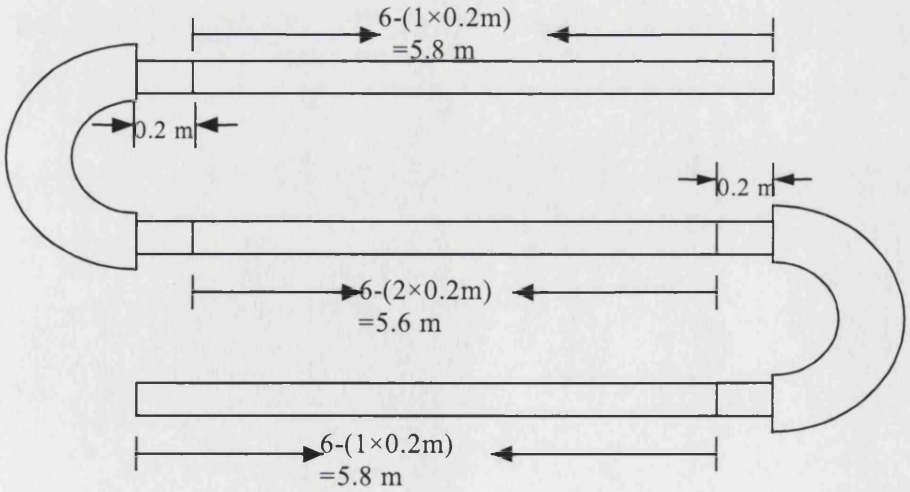

Figure 3.2.11: Schematic of the whole heating modelled in five parts.

The inlet temperature of the product is taken to be a constant value of 80°C (or 353 K). The flow of the heating medium is not modelled, since it is assumed that the temperature of the walls in contact with the heating source is constant equal to 130°C. This assumes that the controlling heat transfer resistance is on the product side.

Heat transfer to the environment occurs at the walls of the curved tubes and this was described using the natural convection option. The environmental temperature was assumed equal to 45°C (due to the fact that the trials were carried out in the summer period in Greece and that the area was already very hot since it's a sterilising unit). It is necessary to set the natural convection heat transfer coefficient that is used by the code to model the heat exchange between the bend wall surface and environmental air. The equation that describes the natural convection heat transfer coefficient for vertical plates and cylinders (Coulson et al., 1995) is:

$$h = \frac{k}{l} 0.683 Gr^{0.25} \Pr^{0.25} \left(\frac{\Pr}{0.861 + \Pr} \right)^{0.25} \tag{3.4.6}$$

where:

h = natural convection heat transfer coefficient [W m^{-2} K^{-1}]

Pr = $C_p \mu / k$ (Prandtl number)

The dimensions of the TnT are:

Outer tube: 108 mm OD and 99 mm ID

Inner tube: 73 mm OD and 70 mm ID.

Annular gap: (99-73)/2 = 13 mm.

The thick stream flow 3 tn hr^{-1}.

The velocity at the inlet: u_{in} = Q/A

Where Q is the volume flux in m^3 s^{-1} and

A is the cross sectional flow area

$$Q = \frac{3000}{\rho \times 3600} \frac{m^3}{\sec} = 0.00074 \frac{m^3}{\sec} \tag{3.4.7}$$

p is density at 80°C 1013 kg m^{-3}

$$A = \pi \times \frac{\left(0.099^2 - 0.073^2\right)}{4} m^2 = 0.00351 m^2 \tag{3.4.8}$$

$$u = 0.235\frac{m}{s}$$

The Reynolds number is calculated using the equivalent diameter:

$D_e = 4r_e = 4*(99-73)/4 = 26$ mm (3.4.9)

$$\mathrm{Re} = \frac{De \times u \times \rho}{\mu} = 0.133 \text{ (laminar flow)} \quad (3.4.10)$$

μ is viscosity at 80°C: 46.22 kg $m^{-1}sec^{-1}$.

The laminar flow model is therefore chosen in the code, because of the very low Reynolds number.

So, part of the experiments and the models aim at validating the code for temperature and residence time predictions in a risky hygienic geometry (dead-end) for a Newtonian fluid and in a production line heat exchanger for a non-Newtonian. The second set, where measurements of electrical conductivity take place, include transient flows and mass removal from the T-piece. In the end, microbial counts were taken after recirculation of inoculum in the rig and again after cleaning, in order to compare the kinetics with already existing models incorporated into the CFD code.

4 Steady State experiments and simulations: Results and Discussion

The work reported in this thesis consists both of experiments and computational fluid dynamics modelling. The aim was to validate the code, FLUENT, and CFD in general, for various processes that are directly linked to hygienic design and manufacturing in the food industry.

Initially the mesh is described, which was applied in GAMBIT. This is part of the CFD package as a preprocessor of the geometry. This is where a mesh can be applied or imported from a different CAD (Computer Aided Design) package.

The first set of results shows agreement between the models and the experiments as far as it concerns heating processes in steady state runs. The fluid used in the T-piece runs is water. In the experiments the variable parameter was the flow rate, which started at $150 l.h^{-1}$ for the first run and ended up at $1340 l.h^{-1}$ for the last run where the maximum power of the pump was used. The varying flux demonstrates how CFD handles heat transfer in that unusual geometry for flow regimes starting from laminar and moving on to transitional and fully turbulent flow using and comparing different models available in FLUENT. Part of the first set is the TnTnT heat exchanger as well, which is handling non-Newtonian fluids (thick tomato paste). There apart of the straight heating sections, the flow in the bends that connect them is examined as well.

The second set is dealing with mass removal and transient flows. The performance of the code is being tested for predicting concentrations of salt (Potassium Chloride) in the T-piece. Concentrations were measured via conductivity. However, conductivity is highly sensitive to temperature. To avoid complexity to tests, temperature gradients were minimised. The probe was calibrated against the salt for various dilutions. After achieving steady state, the rig is flushed out with deionised water and the salt removal is measured at a specific location close to the bottom of the T-piece. Two experiments take place for different initial potassium chloride concentrations and are compared with the models in FLUENT.

The third set of results provides the dimension of the project. The spoilage bacterium *Pseudomonas fluorescens* in Tryptone Soya Broth solution was used. The experiments take place under various temperature conditions in the T-piece and various concentrations of the bacteria when they are inoculated in the rig. Afterwards the rig is being cleaned with deionised water. The models involve both laminar/transitional and fully turbulent flow. Here we do not have steady states since the bacteria kinetics are rates that depend on residence time and temperature history. Hence, all cases are modelled transiently.

From the above we can summarise that the following results and comparisons deal with various fluxes (laminar to turbulence) and interaction with possible stagnant or low fluid velocities areas, transient bulk flows and bacteria kinetics integrated into FLUENT adjusting the tools available in the code. Also, UDFs (User Defined Functions) were applied in order to simulate more accurately the experimental conditions and convection and conduction were taken into account for the heat transfer phenomena.

All the models run were three-dimensional (3D). This chapter is dealing with the steady state solution models that are focusing mostly on the temperature distribution predictions.

4.1 GAMBIT: General

The mesh was applied in GAMBIT. GAMBIT is a software package designed to help analysts and designers build and mesh models for computational fluid dynamics (CFD) and other scientific applications. GAMBIT receives user input by means of its graphical user interface (GUI). The GAMBIT GUI makes the basic steps of building, meshing, and assigning zone types to a model simple and intuitive, yet it is versatile enough to accommodate a wide range of modelling applications (Fluent, 2001). It is a general preprocessor for CFD analysis. Apart from creating the mesh in it, it allows importing geometry from a third party CAD/CAE package, making modifications and also generating mesh. It also provides tools so that the user can check the quality of the mesh. It is important that the quality of the resulting mesh is checked, because properties such as skewness can greatly affect the accuracy and robustness of the CFD solution. GAMBIT provides several quality measures (sometimes called "metrics") with which the quality of the mesh can be assessed. In the case of skewness measures such as EquiAngle Skew and EquiSize Skew, for example, smaller values are more desirable (Fluent, 2001; Fluent, 2003). Further down the mesh that was applied for the T-piece and the TnTnT configurations is described.

4.1.1 Meshes

T-junction configuration

The T-piece geometry was adapted in Gambit in order to meet the requirements for the Cooper mesh scheme type (Gambit, 2001). In that scheme "source" faces are specified from where the mesh node patterns are swept through the volume. There were hexahedral elements that formed the volume mesh. The advantage of the hexahedral shapes and the cooper scheme are convenient for this type of flow in a pipe because they are aligned with the flux, when choosing as source faces the inlet and the outlet. Also a regular, structured grid of mesh elements was applied, so discrepancies were reduced to minimum and the quality of the mesh was the maximum possible (Gambit, 2001).

The grid interval size, which specifies the measurement unit for the mesh node spacing parameters, was set at 0.003mm. The number of cells is 57285 and 71369 nodes. This mesh is depicted on figure 4.1.1 (a) and (b).

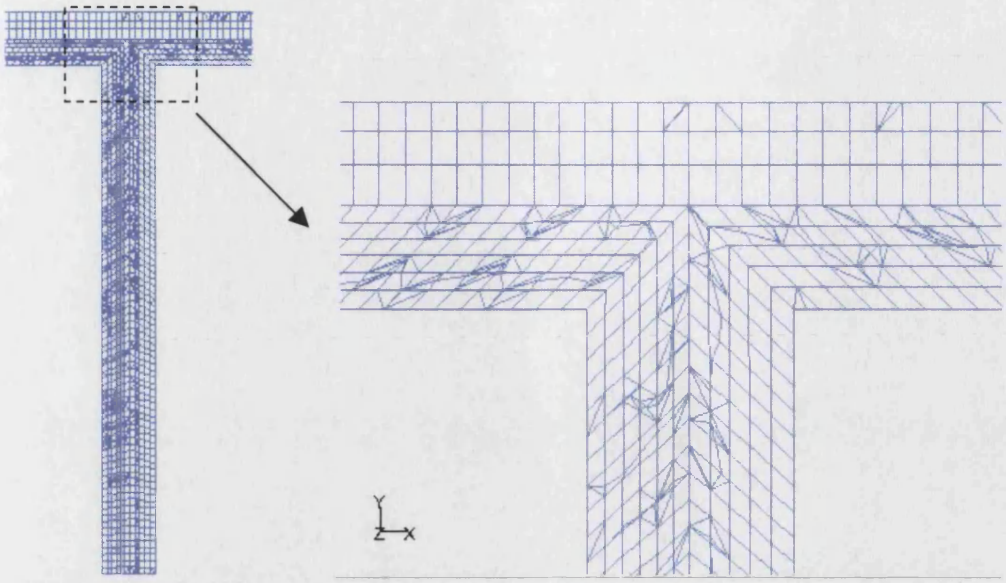

(a) (b)

Figure 4.1.1: Vertical cut surface showing grid with interval size 0.003m

There was another mesh applied of 0.002mm interval size and some turbulent flow models were compared to the coarser one. The results (paragraphs 4.2.1 and 4.2.4) did not favour in particular the finer one, when comparing the results in the vertical pipe, and the simulation was very expensive computationally to justify the use of such a huge number of cells (167512) (fig 4.1.2 (a) and (b))

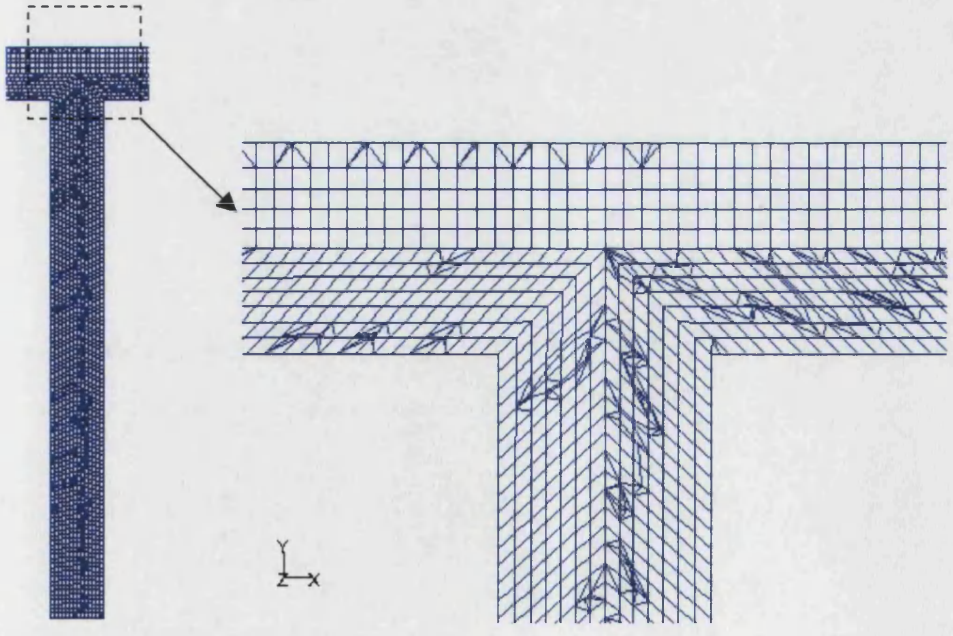

(a) (b)

Figure 4.1.2: Vertical cut surface showing grid with interval size 0.002m

For the TnTnT geometry, for both bends and straight sections, the Cooper scheme was applied as well with hexahedral shaped elements. The reasons are the same as in the T-piece geometry: flow alignment and more consistent mesh with better quality (minimum skewness) (fig 4.1.3, fig 4.1.4) For the straight heating sections of 5.8m the grids consists of 191360 cells and 210848 nodes. For the 5.6m one the meshing is composed of 184640 cells and 203456 nodes. The bend has 36576 cells and 38555 nodes.

Figure 4.1.3: Part of the geometry of the TnTnT meshed, including the inlet face.

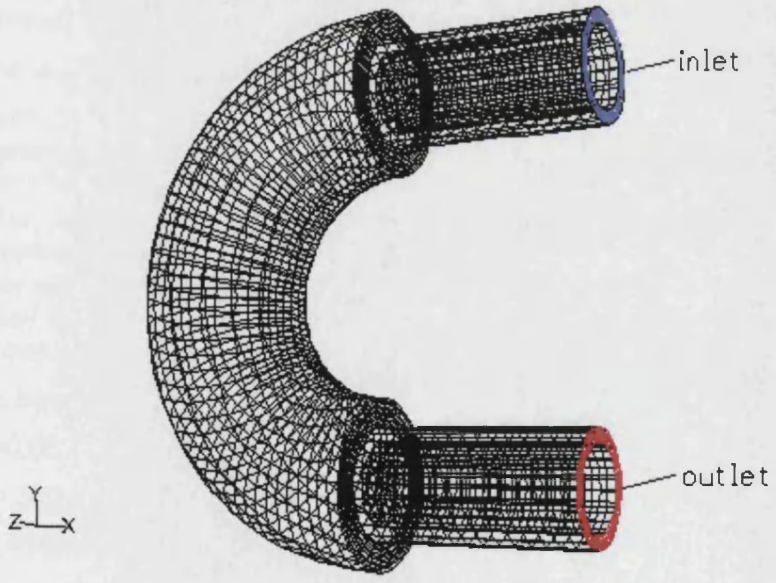

Figure 4.1.4: Mesh applied on one of the bends, where parts of the heating sections are attached as well, including the inlet and outlet faces.

4.2 Temperature and flow down the T-piece

The aim of the first set of experiments was validating the code for temperature distribution down the centre of the dead leg.

4.2.1 Flow of 150*l.h*$^{-1}$

The first water flux in the rig was maintained at around 150lt hr^{-1}. The velocity in the rig is:

$$u = \frac{Q}{A_{area}} \tag{4.2.1}$$

where Q is the fluid flux in m^3 s^{-1}.

A_{area} is the surface area of the inlet/outlet of the rig.

$Q=150*0.001/3600 = 4.167*10^{-5}$ [m^3 s^{-1}]

$A_{area}=\pi*d^2/4=3.14*0.0254^2/4=5*10^{-4}$ [m^2]

Where d is the diameter of the rig in metres

So, substituting to equation 4.2.1 we have:

u=0.082 [m s^{-1}]

The Reynolds number for the above flow is:

$$N_{\mathrm{Re}} = \frac{du\rho}{\mu} \tag{4.2.2}$$

where ρ: density of water 998 in kg m^3.

μ the viscosity of water 0.001 in kg m^{-1} s^{-1}

Reynolds number is then around 2000. As, has already been mentioned, flows of that range of Reynolds number are generally laminar but some new theories of low Reynolds turbulent flows claim that they are transitional and some not intensive turbulent models can describe them better. Hence, this experiment was simulated with laminar model, and the k-ε and k-ω with transitional flow options on. The models are compared to the experiment and amongst each other as far as it concern the temperature distribution in the centre of the T-piece. FLUENT is tested to validate how it copes with the vertical tube assuming, for example, turbulence in the horizontal pipe while not knowing the flow regime in the vertical.

The boundary conditions for the model are:

u_{in}=0.082 m s^{-1}

T_{in}= 322 K

T_{env}=297 K

h_{ver} = 4.59 Wm^{-2}K^{-1}.

h_{hor} = 2.78 Wm^{-2}K^{-1}.

Where u_{in} and T_{in} are velocity and temperature at the inlet of the horizontal tube and T_{env} is the temperature measured in the laboratory around the rig while the experiment was taking place.

h_{ver} and h_{hor} are the natural convection heat transfer coefficients for the vertical wall of the T-piece and the horizontal wall of the bulk flow, calculated from eq. 3.2.2 in paragraph 3.2.1.

The properties of the water are taken as constant from the FLUENT database as they do not vary significantly at the present temperature range, apart from the thermal conductivity (Lide, 1995):

$\rho_w = 998\ kgm^{-3}$

$C_{pw} = 4182j\ kg^{-1}K^{-1}$

$k_w = 0.25+0.001187*T\ Wm^{-1}K^{-1}$

$\mu_w = 0.001\ kgm^{-1}s^{-1}$

$MW = 18\ kgmol^{-1}$

Where ρ_w is water density, C_{pw} is specific heat of water, k_w is thermal conductivity of water μ_w is its viscosity and MW is its molecular weight.

The walls, which are made of stainless steel, have the following properties:

$\rho_w = 8030\ kgm^{-3}$

$C_{pw} = 502.48\ jkg^{-1}K^{-1}$

$k_w = 16.27\ Wm^{-1}K^{-1}$

Comparing various models

The first models for the $150l.h^{-1}$ flow were run for the coarser grid of interval size 0.003m. Laminar flow and the k-ε RNG and k-ω SST with transitional flow options on for low-Reynolds numbers were compared (fig. 4.2.1) against each other and to the experimental values from the 6 thermocouples down the T-piece. It can be observed that the laminar flow model and the k-ω SST show the best agreement with the experimental measurements. Can be concluded to use the k-ω SST model for similar flows (i.e. of that sort of Reynolds number in the fully developed flow) and further investigate further the model and compare between different grid sizes and adaptations. Also, the laminar flow model does predict well the temperature at the beginning of the vertical tube and at the point where the temperature starts to drop significantly. However, for the specific flow the difference between the laminar flow and the k-ω SST was very small. The k-ε RNG model is proven to overpredict the location of the point where temperature drops. It locates it approximately 4cm further down from the point given by the thermocouples.

It can be seen that the second thermocouple gives lower value than the third while the later is deeper down the pipe. This is not physically correct. It is probably an artefact of the experiment. After the run and the comparison in an EXCEL file, the thermocouple was removed and replaced by another one of the rest and several tests were carried out. While the rig was in operation, the thermocouple located at that point was being held stable manually. At the same time the values were being noticed on the computer where the thermocouples were connected. The temperature distribution was the one expected (with temperatures measured dropping slowly from the first to the third thermocouple). When the sensor in question was pushed slightly forwards or backwards, so that it will be closer to the walls, temperature was slightly dropping compared to the thermocouple positioned lower. Then, the initial one was placed back to the second port and behaviour was similar. Thus, it is most likely that is the pressure

developed into the rig, at that point, that is pushing the thermocouple closer to the walls, where the temperature is slightly lower.

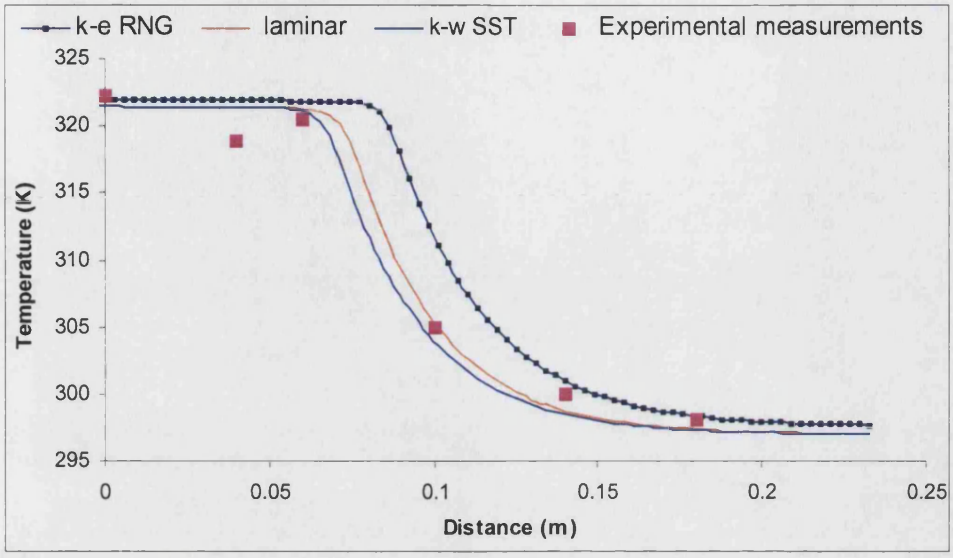

Figure 4.2.1: Comparison of temperature distribution down the central axis of the T-piece between various models and the experiment for 150lthr^{-1} using a Cooper grid of interval size 0.003m.

Further comparisons took place between the above chosen model (k-ω SST) and other models under changes of the mesh. Initially, the same interval size is maintained at the grid but it is adapted according to the y+ ($\equiv \rho u y / \mu$) values of the cells close to the wall. This is a non-dimensional parameter where u_T is friction velocity and y is distance from the wall.

So, calculation is run for as many iterations as it takes to accomplish steady state solution. Then, the grid is adapted at the cells that have y+ value between 1 and 5 (fig. 4.2.2), dividing each cell in two equal ones wherever the y+ has the above values.

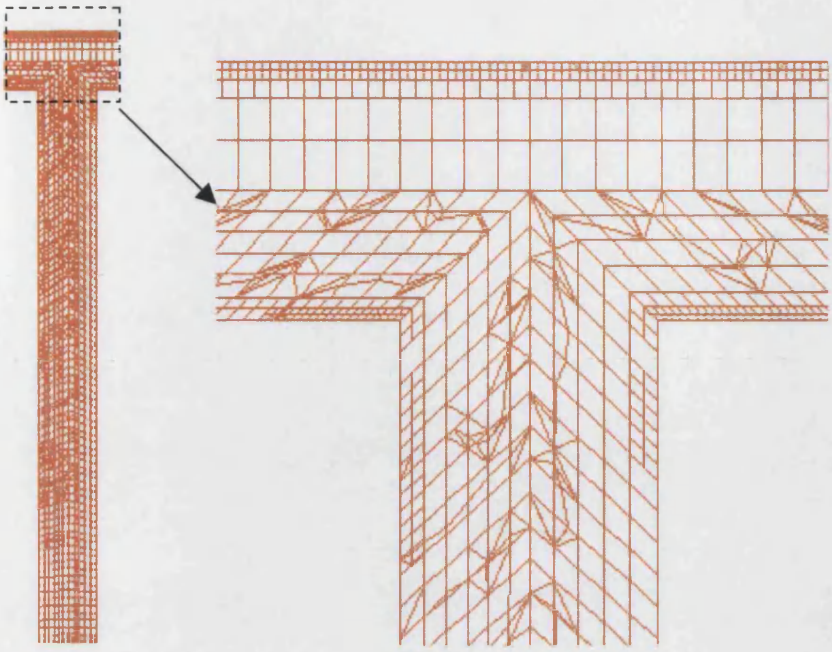

(a) (b)

Figure 4.2.2: Vertical cut surface showing the adapted grid with interval size 0.003m

Then the calculation is carried out for a finer mesh with interval size of 0.002m (fig 4.1.2). This is solved for both laminar flow and k-ω SST having on the option for transitional flows.

The comparison of the different grid modifications is shown on figure 4.2.3. All the new meshes were more expensive computationally comparing to the 0.003 without adaptation. The iterations took longer time with significant rise for the 0.002m interval size grid. Also, the new simulations demonstrate that the temperature is overestimated along the T-piece. Here, the difference is more profound between the laminar flow and the k-ω SST solutions for the new grid, with the first one giving the constant temperature plateau significantly extended. They overlap after approximately 17cm down the tube. The adapted grid of 0.003 size gives also an overrated profile but closer to the experimental values compared to the finer grid. So, all the new modifications in the grid overestimate the heat diffusion down the centre of the dead space. Nonetheless, they converge at the bottom of the geometry, which is the area where velocity is very low and heat is transferred basically with conduction within the liquid phase.

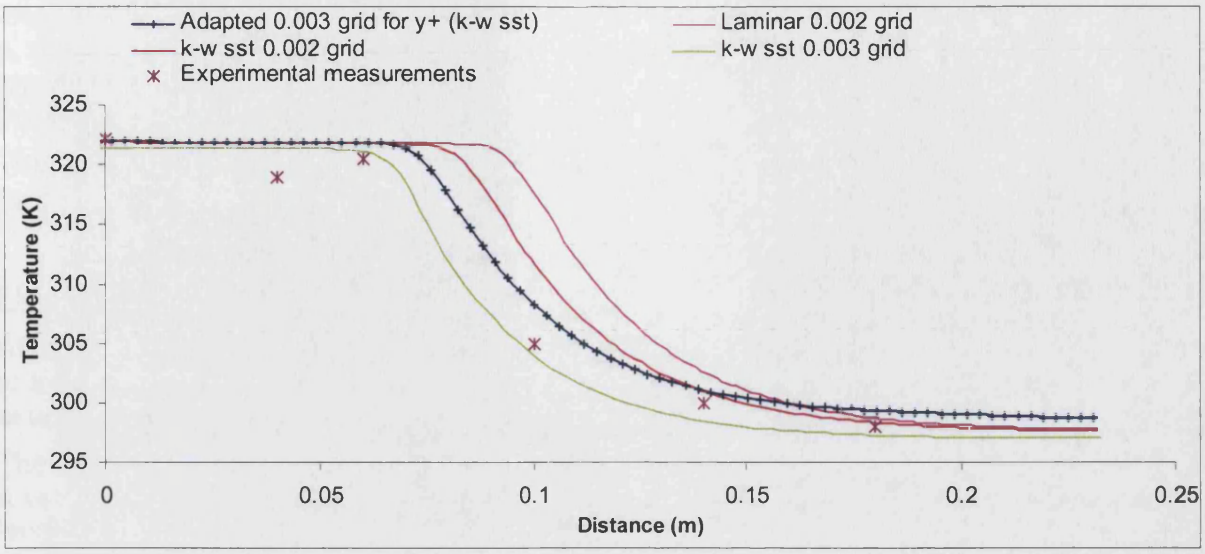

Figure 4.2.3: Comparison of temperature distribution down the central axis of the T-piece for 150lthr^{-1} using the Cooper grid of interval size 0.003m with and without adaptation and the Cooper grid of size 0.002m for the laminar and k-ω SST models.

This can be seen more clearly on figure 4.2.4, where temperature is given on the same plot with velocity along the centre of the pipe. It is after the first 7 cm where the velocity is practically zero and this is also the length where temperature gradient is the lowest (negative) because the values start dropping sharply. This means that the prevailing mechanism for heat diffusion is the conduction through the water volume.

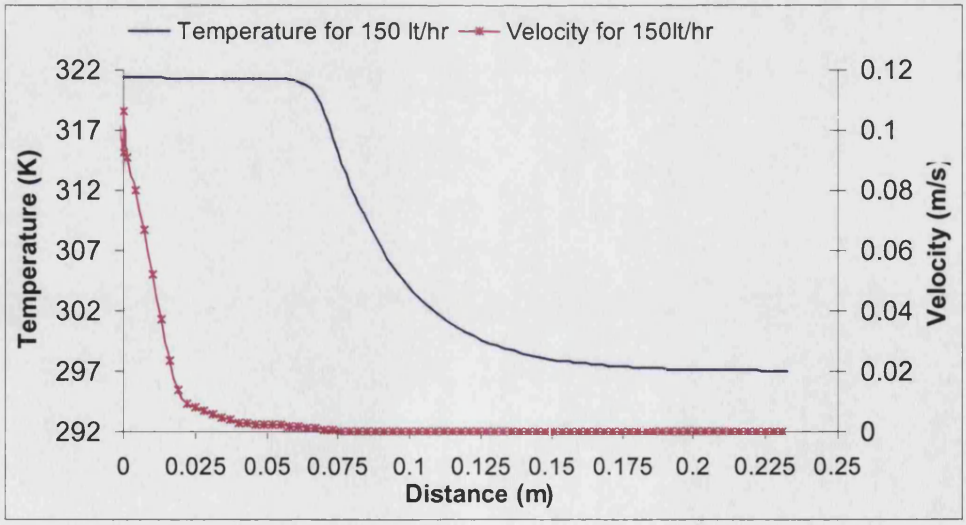

Figure 4.2.4: Temperature and velocity distribution down the central axis of the T-piece for the flow of 150lt hr^{-1}.

Generally, the above models used do not differ a lot between each other. They are transferring a similar profile of the temperature distribution further down the pipe. However, they show agreement in temperatures when conduction becomes more significant compared to forced convection.

The next paragraph is going to expand more in the flow in the pipe for this Reynolds number, having chosen the k-ω SST with the transitional option on.

Flow behaviour in the T-piece for 150$l.h^{-1}$.

After having selected the k-ω SST as the model to solve the specific or similar flows, according to the agreement the results gave with the experimental values, there is going to be some more extended description of the behaviour of the flow into the T-piece under the existing conditions.

The following figure (fig 4.2.5) is presenting the vectors according to the velocity magnitude on a vertical cut along the central axis of the T-piece. There are shown only the first 7-8cm of the length because after this depth velocity is practicaly zero and the vectors are hardly visible. This shows again that there is no motion after a certain, short, distance from the central point of the horizontal pipe. It is also quite clear the formation of a recirculation zone at the beginning of the vertical section. There, velocity is higher at the top and close to the right wall, and lower at the bottom of it. The whole eddy is slightly orientated towards the left side of the geometry, which is connected to the direction of the bulk flow. Hence, since the flux comes from the right, it is going to get carried away partly when it meets the gap and hits on the left wall at the beginning of the T-piece. That is why, it maintains most of the speed at that area.

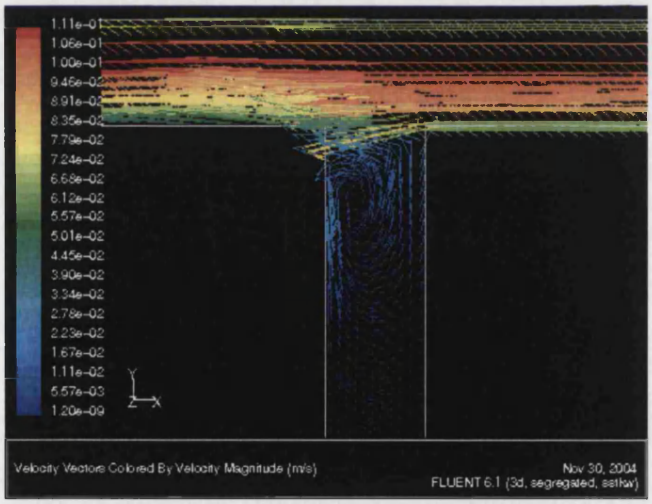

Figure 4.2.5: Velocity vectors of the 150$l.h^{-1}$ flow on vertical surface along the central axis of the T-piece.

It would probably not have the same effect, if the diameter of the vertical tube was bigger. After a certain value it is very likely that there would be no effect on the eddy formation. In this case the recirculation zone is "pushed" by the wall.

Figure 4.2.6 shows the velocity magnitude contours for a small range of values between 0.003 and 0.03ms^{-1}. Here we can see more clearly how the recirculation zone is towards the left side

of the pipe and how the velocity is a slightly higher on that side as well. In the centre of the eddy formed velocity has the minimum values.

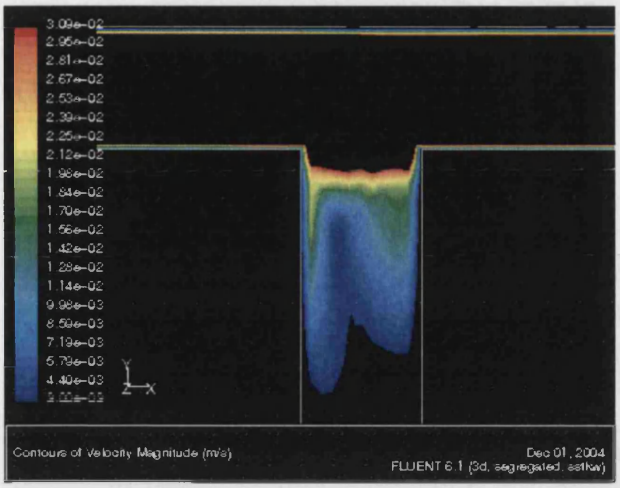

Figure 4.2.6: Velocity magnitude contours for a limited range of values close to the intersection.

The temperature profile in the centre of the dead-end has the values depicted in fig. 4.2.7, where temperature contours colour range accordingly. We can clearly see that it remains constant and equal to that in the horizontal pipe for the first centimetres. After there is a gradual drop (orange to light blue) and at the end the colour is only blue, which is the minimum temperature closest to the environmental, measured outside the rig (297.5K).

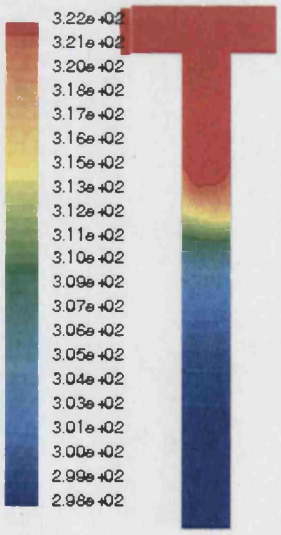

Figure 4.2.7: Contours of temperature on a vertical surface passing from the centre of the T-piece.

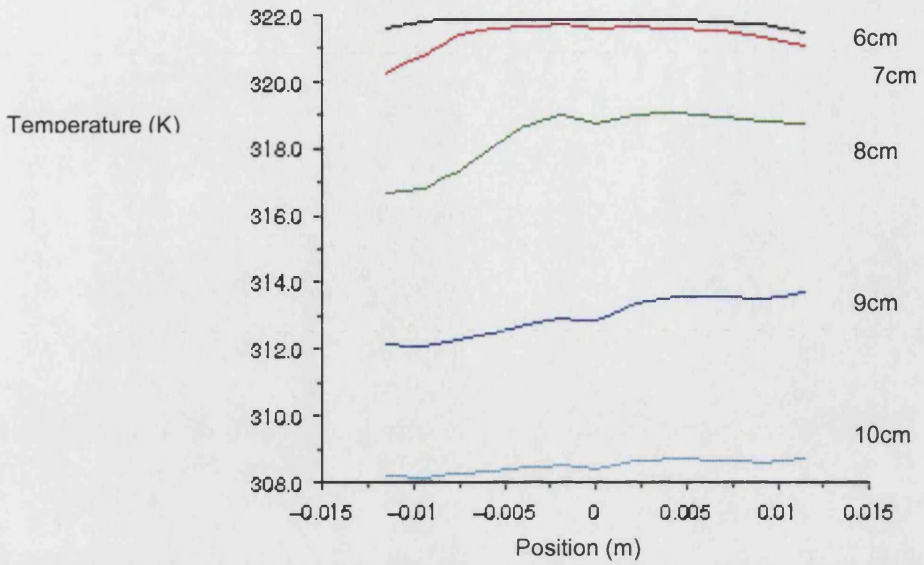

Figure 4.2.8: XY plot showing temperature profiles vertical to the T-piece at depths of 6, 7, 8, 9 and 10cm.

In the figure 4.2.8 there were selected lines that cross the down-stand vertically at various depths between 6 and 10cm. It can be noticed that temperature is not axisymmetrically along these lines. The recirculation effect takes place after the 7cm where we see that on the left values are slightly lower compared to those on the right of the lines chosen. On the left we have slightly higher velocities (fig 4.2.8), which means that residence time of the fluid is lower there and temperature should stay higher at that side. Nevertheless, this is not the case. This is understandable, if we notice the path lines of mass less particles colored by residence time and observe as well how the flow moves (fig. 4.2.9). After a certain point eddy breaks (~7cm) and moves downwards and passes from zones of low temperature since the interaction with the bulk flow is already stopped. This is why, although velocity is high, temperature does not remain high but drops. After 10cm this phenomenon dies out since velocity has already reached very low values and temperature is more homogeneous.

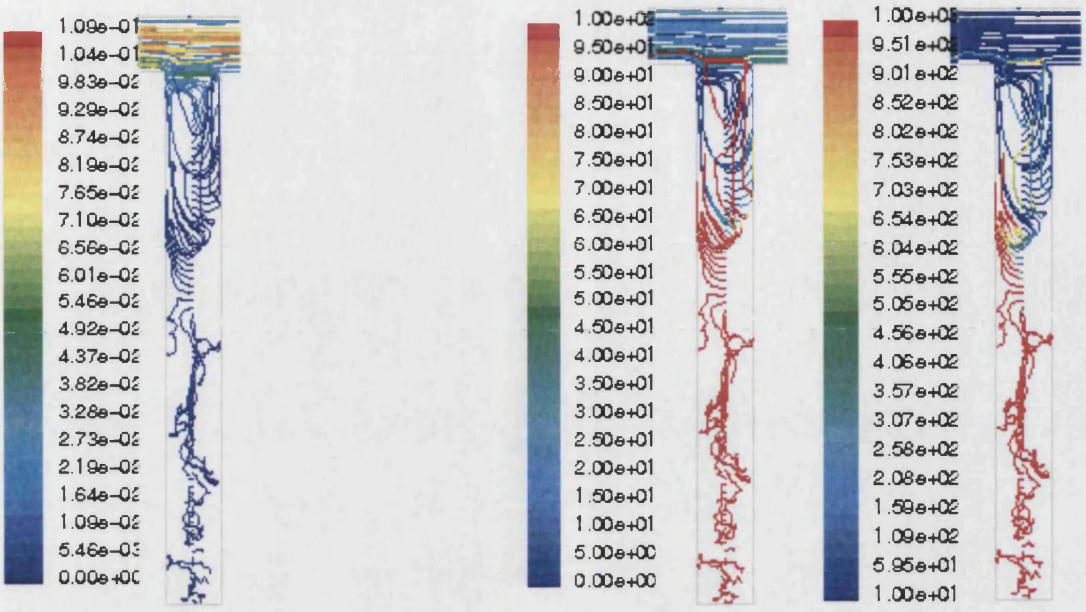

(a) (b) (c)

Figure 4.2.9: 150*l.h*$^{-1}$ flow path lines of massless particles released from the inlet and the central axis of the T-piece coloured by velocity magnitude (a) and residence time ranging between 1-100sec (b) and 1-1000 (c).

From the pictures that give the pathlines of massless particles that follow the flow (fig 4.2.9 (a) and (b)), we can take some information on the behaviour of the flow in the T-piece. A vertical line, which coincides with the central axis of the dead space, is chosen as the part of the geometry from where massless particles were released together as well with the inlet surface. Thus, this postprocessing option, available in FLUENT, allows the user to release particles that just follow the flow. The choice of this limited areas was made on purpose, otherwise the result would be very chaotic to try any kind of areas, such as a whole surface passing from the T-piece. Also, this vertical axis is considered sufficient to give a representative and understandable image of how the flow acts.

Fig 4.2.9 (a) shows path lines coloured by velocity magnitude. The eddy formation is more evident at the top of the tube after having observed the velocity vectors as well (fig 4.2.5). The sudden drop of the velocity is very clear, from red/orange colour in the centre of the horizontal pipe (0.09-0.1ms^{-1}) we pass to yellow and green, which declare lower velocity (0.05-0.09ms^{-1}), ending up in blue colour that corresponds to values between 0 and 0.01 ms^{-1}.

Likewise, we get the picture for the path lines coloured by residence time of the particles in seconds. There were two time ranges in order to show the residence time distribution on the areas of question. The first one allocates the path lines from between 0 and 100 seconds, the second between 0 and 1000 seconds. We see that the time the fluid remains into the tube is very short in the horizontal tube, which is just the time it takes to cross it (~10sec). As we look downwards in the T-piece we find also, together with the ones of minimum residence time of 10sec, there are some very small parts of the flow that have a longer stay, which is more likely due to the entrapment in the recirculation zone (yellow and green colours corresponding to 50-60sec). However, these parts manage to escape and end up into the bulk flow. In the flow below that depth path lines become suddenly red, equivalent to the maximum residence time

no matter which range we look at. Hence, this is more likely to mean that there we have stagnation until the very end of the vertical pipe and there is no interaction with the bulk flow.

Conclusions for the 150$l.h^{-1}$ flow.

From the comparisons made between the various models applied in order to solve the flow in FLUENT, we see that using a finer mesh rather that the one with interval size 0.003m, is not necessary. It is only enhancing the differences between using the laminar model and the k-ω SST with the transitional option selected. Otherwise, it is more expensive computationally and takes almost double the time to perform one iteration. Similarly, but with better agreement with the experimental measurements, it can be concluded that adapting the mesh and making it finer close to the wall, to see how the performance of the turbulent model is going to be affected, is not contributing to any significant changes of the final solution for validating temperature values into the centre of the T-piece. All these modifications of the grid would probably be of better application, if the near wall values and phenomena were of interest, such as shear stresses.

Furthermore, having observed that there is no significant difference between the laminar and the model, the k-ω SST is chosen since it includes the sensitivity of low Reynolds turbulent zones and offers a slightly better agreement with the temperature's dropping profile.

The behaviour of the water flowing into the T-piece is examined with the help of the post processing tools available in the code. Path lines coloured by velocity and residence time, velocity vectors and temperature vectors, as well as XY plots show that there is a recirculation zone that starts at the intersection of the two pipes and goes down for approximately 7.5cm. The fluid is forced to make a circular motion for a short while before re-entering into the bulk flow. From that point and downwards, the velocities are close to zero, residence time is very high and conductive forces within the fluid mainly lead temperature distribution mechanism. From all the above it is concluded that the product is practically stagnant in that area.

4.2.2 Flow of 300$l.h^{-1}$

The second experiment was carried out with flow at 300lh^{-1}. Velocity is 0.164ms^{-1} and Reynolds number approximately 4000. The flow is considered transitional in engineering books, but recent investigations in turbulence (Verdteeg and Malalasekera, 1995) consider it turbulent and various models are applied in finite element and finite volume methods in order to handle it. So, comparison was obtained between SST k-ω with transitional option activated, standard (STD) k-ω, which incorporates modifications for low Reynolds effects, and the k-ϵ standard and RNG models with the later used twice both for higher and low Reynolds number. Comparison is given on figure 4.2.10.

The boundary conditions for the model are:

u_{in}=0.164 m s^{-1}

T_{in}= 321 K

T_{env}=297.5 K

h_{ver} = 4.55 Wm^{-2}K^{-1}.

h_{hor} = 2.77 Wm^{-2}K^{-1}.

The properties of the water and steel walls are the same as the previous cases.

From figure (fig. 4.2.10), we can see that the k-ϵ RNG for low Re number is far away from the experimental curve. Generally, the differences in the predictions given by the rest are not especially pronounced. However, the k-ω STD and SST (transition checked), are overestimating a little bit the point where the temperature starts dropping. The k-ϵ models are behaving more according to the experimental data with the k-ϵ STD, which is not as aggressive as RNG, giving a slightly better agreement with the distribution given by the measurements. This model might not be as close as the one chosen for the 150lthr^{-1}, but comparing to the rest, the shape of the inclination is similar to the temperature distribution given by the thermocouples. Again, we see the artefact of the experiment as far as it concerns the second thermocouple.

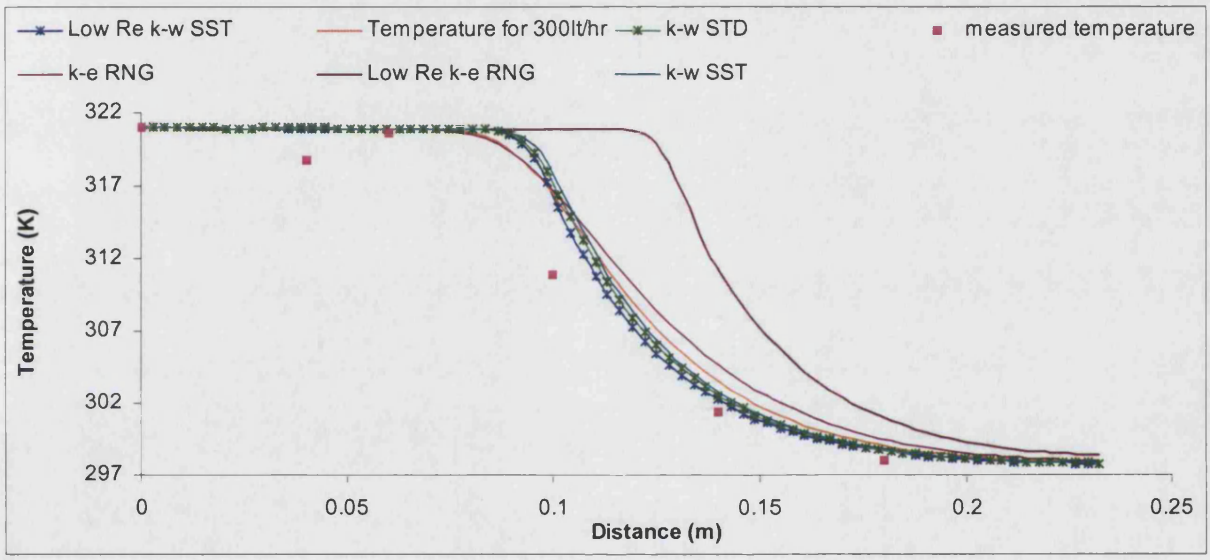

Figure 4.2.10: Comparison of temperature distribution down the central axis of the T-piece between various models and the experiment for the 300lthr^{-1}.

Comparison of temperature and velocity distribution down the centre of the vertical tube shows again how the sudden drop of the temperature starts when velocity is very low. From figure 4.2.11 we can say that this occurs at a depth of approximately 8cm, which is not very different from what was observed for the previous flow. However, this is going to be examined more thoroughly later.

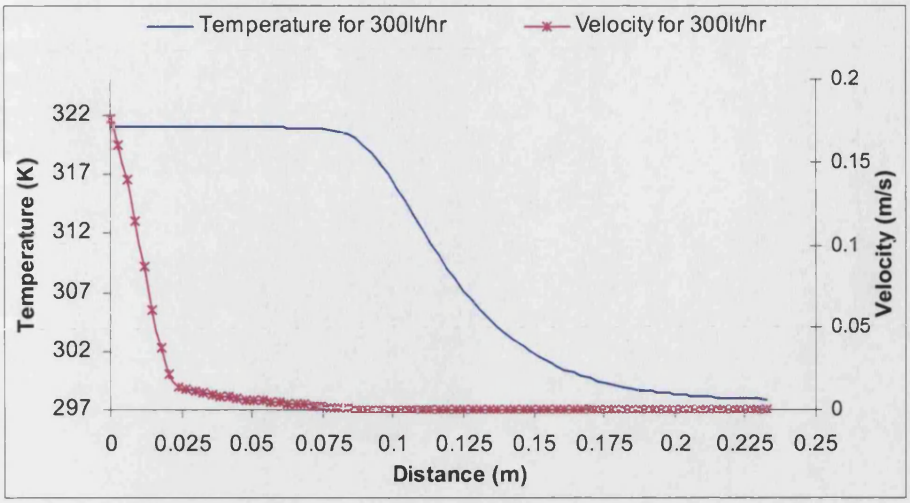

Figure 4.2.11: Temperature and velocity distribution down the central axis of the T-piece for the flow of 300lt hr^{-1}.

Observing the velocity vectors (fig 4.2.12) we see that there is again a recirculation zone at the intersection of the pipes but this time, although the centre of it is in the same, approximately, location as in the previous flow, its lower part is extended deeper down the tube. The vectors are visible down to a length of around 9cm, which shows that velocity magnitude is practically zero after that.

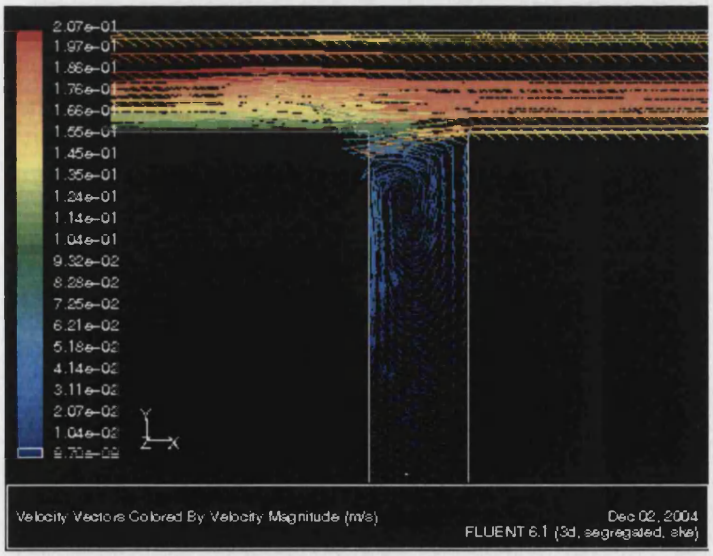

Figure 4.2.12: Velocity vectors of the 300 $lthr^{-1}$ flow on vertical surface along the central axis of the T-piece.

We can see how the eddy affects velocity profiles down the tube at various depths (fig 4.2.13, 4.2.14). Figure 4.2.13 shows velocity at 5, 6, 7 and 8cm. It is obvious that it is slightly higher on the left side as the fluid hits that side of the wall first, where it is slowed down while it returns

anti-clockwise. This goes on until approximately 7cm. Further down (fig 4.2.14) at the 8cm the profile looks more like parabolic, slightly placed on the left, with a sudden drop of one order of magnitude (from 0.001 to 0.0001ms^{-1}) at 9cm. At 10cm it is almost zero. So, for this flow, stagnant area starts to form after about 9cm. Until that point the fluid interacts with the bulk flow and works its way out of the T-piece again.

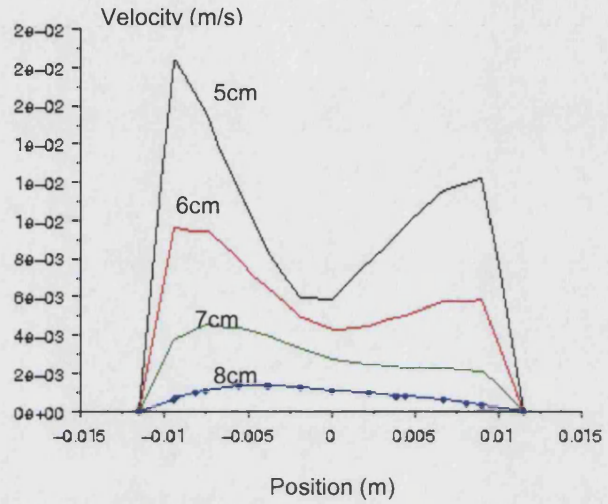

Figure 4.2.13: Velocity profiles at 5, 6, 7 and 8cm down the T-piece.

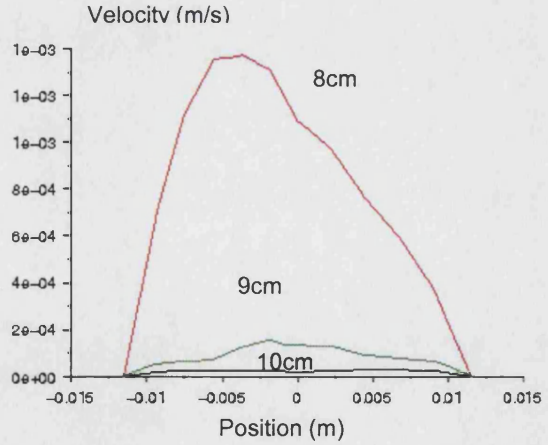

Figure 4.2.14: Velocity profiles at 8, 9, and 10cm down the T-piece.

The effect of the above velocity distribution on the temperature (fig 4.2.15) is similar to that for the lower flow of 150 $l.h^{-1}$, although smaller in magnitude. After 8cm temperature is just a little bit lower on the left compared to the right side of the diameter down the vertical pipe for about two centimetres until when the profile starts flattening at the 11th centimetre. Probably, the phenomenon is less pronounced here because the sudden change of the geometry from horizontal to vertical is not affecting the flow at that point.

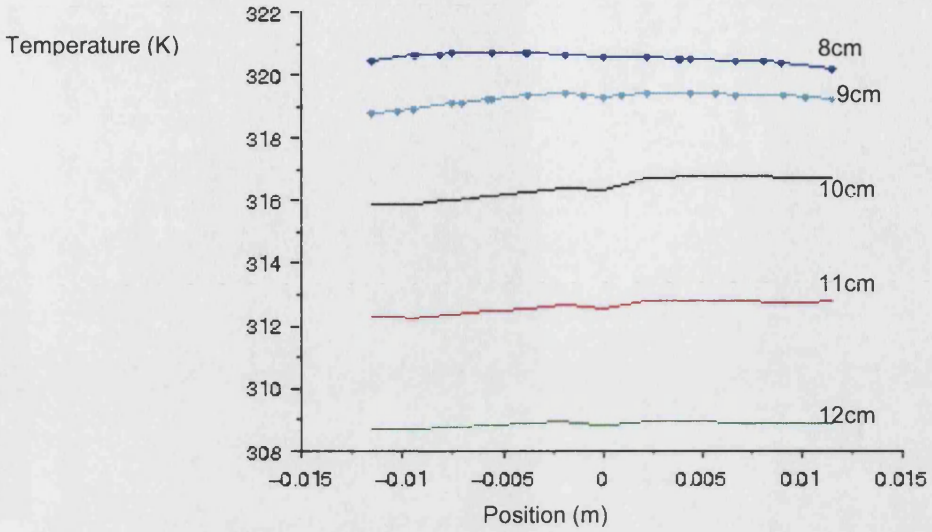

Figure 4.2.15: Temperature profiles for the 300lt^{-1} flow at 8, 9, 10, 11 and 12cm down the T-piece.

Path lines again show a better view of the flow behaviour. The eddy goes further down the pipe. Although the central part of the zone is not much more extended than in the previous flux, the effect is prolonged at the bottom and the velocities developed are high enough to force the fluid to come out again, even if it reaches 9cm in depth. On fig 4.2.16 (a) velocities are already one order of magnitude lower after a few centimetres, compared to the bulk horizontal flow (drops from 0.1 to 0.01ms^{-1}). Path lines of residence time (fig 4.2.16 (b) and (c)) show that around the 9cm the fluid is trying to make its way out. This is shown by the red colour (fig 4.2.16 (b)) of the path lines, which is the colour corresponding to the highest residence time of the fluid that manages to escape. From the fig 4.2.16 (c) we can see that this colour becomes orange discriminating it from the red that stays at the bottom of the T-piece after the 9-10 cm. Orange corresponds to approximately 800s (13.33min).

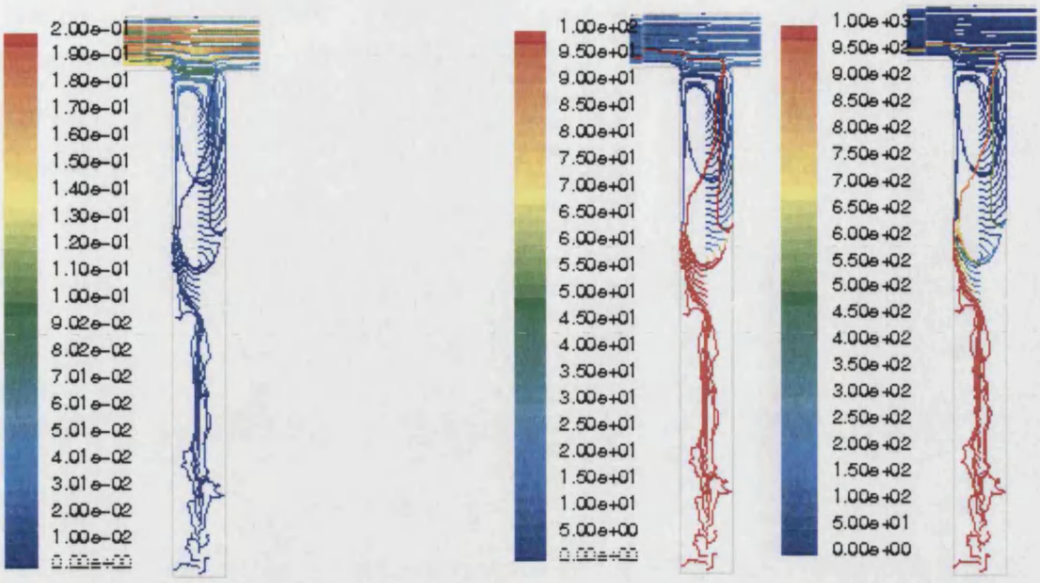

(a) (b) (c)

Figure 4.2.16: 300$l.h^{-1}$ flow path lines of massless particles released from the inlet and the central axis of the T-piece coloured by velocity magnitude (a) and residence time ranging between 1-100sec (b) and 1-1000sec (c).

Comments on the flow of 300$l.h^{-1}$.

The choice of the model that solves this flow best, was based more on qualitative rather than quantitative criteria and observations. The data from the thermocouples do not give a clear enough picture of the temperature drop profile after the third value. The k-e STD model, which is for fully developed turbulence, was chosen as the one that gives better agreement with the way that the temperature falls. The rest overestimate the point at which this drop starts to happen and give a sharper temperature gradient.

As far as it concerns velocity, there is again a recirculation zone formed that goes down the dead end to approximately 9cm. Temperature is affected slightly at those depths and it could be considered axisymmetric all the way down. It remains equal to the one in the main, horizontal flow, until the above depth, where velocity is still considerably high and allows interaction and exchange with the top.

Residence time at those points are quite high (more that 700s), which is almost the same amount of time as for the previous flow (fig 4.2.9 (b) and (c)). In the rest of the T-piece the fluid is trapped and temperature is close to the environmental value.

4.2.3 Flow of 600 $l.h^{-1}$

The third experiment was carried out with flow at 600$l.h^{-1}$. The Reynold's number is circa 8000. Flow is turbulent and comparison was obtained between SST k-ω, standard (STD) k-ω, k-ϵ standard and RNG model with the later used for higher Reynolds number. Comparison is given on figure 4.2.16. The properties of the water and steel walls are the same as for the previous flows.

The boundary conditions for the model are:

u_{in}=0.336ms^{-1}

T_{in}= 322K

T_{env}=298K

h_{ver} = 4.55Wm^{-2}K^{-1}.

h_{hor} = 2.77Wm^{-2}K^{-1}.

What can be noticed while comparing the models to the experiment (fig 4.2.17) is that the difference again is not so pronounced. The drop starts at the 4th thermocouple (10cm). Generally, all of them give a similar profile of the temperature down the pipe. Only the k-ω SST gives a little bit further down the drop point by approximately 2cm than the experiment. The same, but closer to the 4th thermocouple's location, is happening with the k-ω STD. Both of them give a sharper exponential dropping profile with a very good agreement at the bottom of the tube. The k-ε models look very alike, with the same predictions for almost 14cm and then the RNG slightly over estimates the values. Both of them give higher values after the 12th centimetre compared to the k-ω models, but the shape of the curve provides a better match of the shape of the experimental profile. After these 12cm predictions tend to follow the same shape as experimental results but are advanced approximately 2cm down the tube.

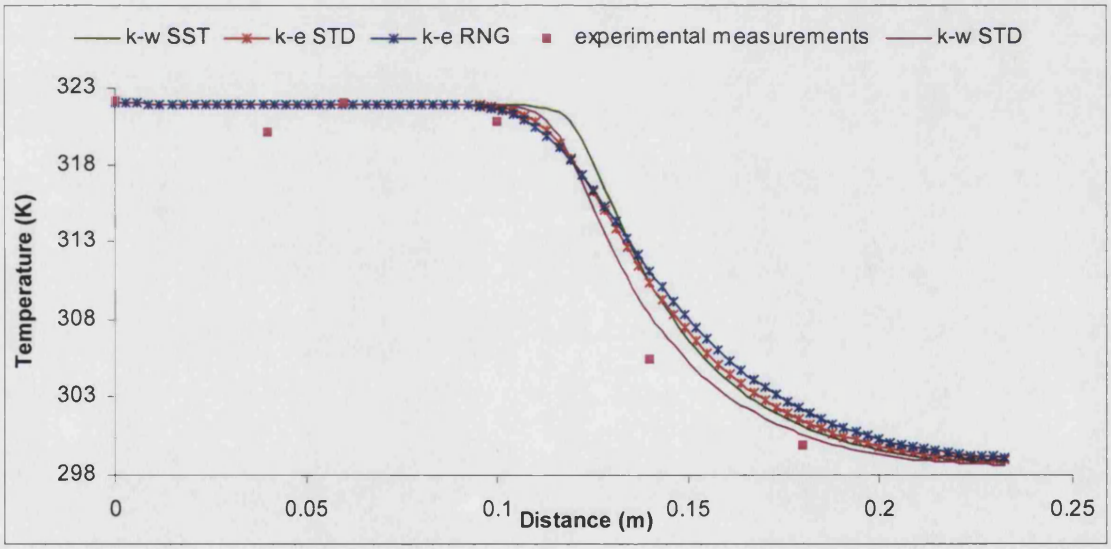

Figure 4.2.17: Comparison of temperature distribution down the central axis of the T-piece between various models and the experiment for the 600lthr^{-1}.

Figure 4.2.18 is a plot of temperature and velocity values along the central axis of the T-piece. There is noticed the sudden drop that happens just after the 10cm, which corresponds to practical zeroing of the velocity.

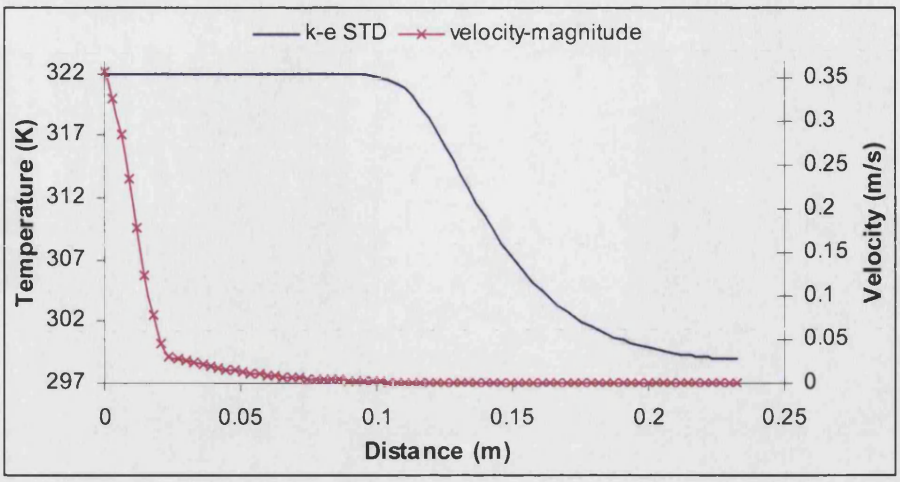

Figure 4.2.18: Temperature and velocity distribution down the central axis of the T-piece for the flow of 600$l.h^{-1}$.

Velocity vectors (fig 4.2.19) give the formation of the recirculation zone. Again, the centre of it starts just underneath the merging of the two pipes. The whole zone is going further down the pipe at approximately 11cm, where the vectors can barely be seen and, by looking at the coloured bar, correspond to velocities below 0.01ms^{-1}.

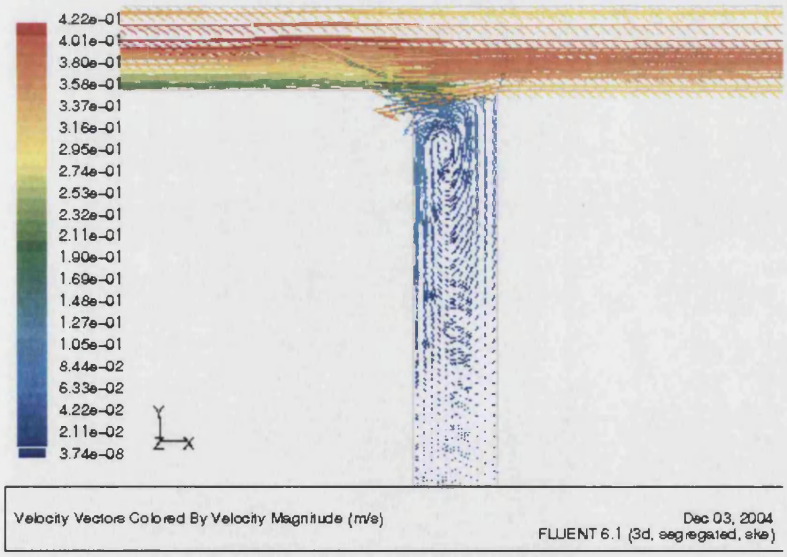

Figure 4.2.19: Velocity vectors of the 600 lthr^{-1} flow on vertical surface along the central axis of the T-piece.

The eddy formation affects again the velocity until a depth of 8cm, where we have the slightly higher velocities on the left (fig 4.2.20). It ceases at the 10cm where we get the parabolic profile (fig 4.2.21). After that point velocity drops suddenly over only one centimeter from 0.002 to 0.0002ms^{-1}. After that, the velocity profile is almost a straight line and the values practically zero, so stagnation zone starts.

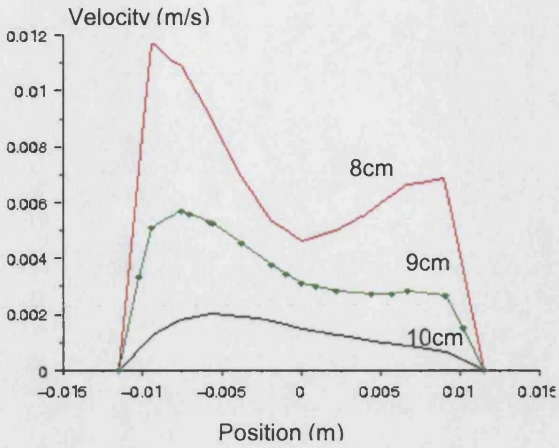

Figure 4.2.20: Velocity profiles at 8, 9 and 10cm down the T-piece.

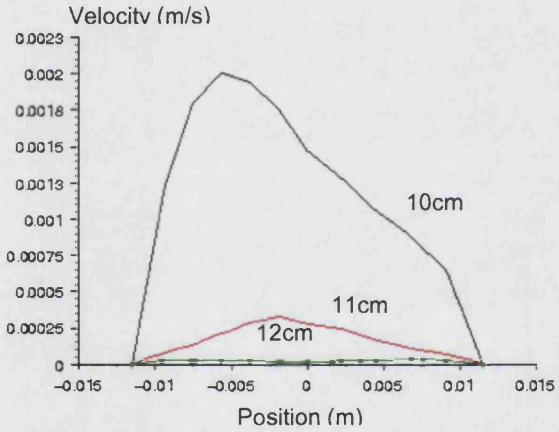

Figure 4.2.21: Velocity profiles at 10, 11 and 12cm down the T-piece

This time, the effect on the temperature profile is even less prominent. It appears slightly after the 12th and 13th cm profiles (fig 4.2.22). This time the distance from the intersection is even larger.

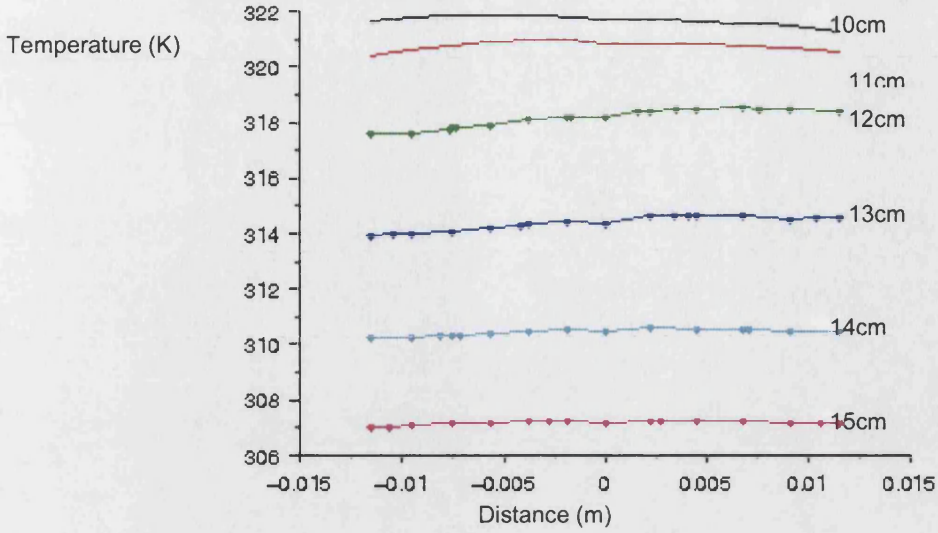

Figure 4.2.22: Temperature profiles for the 600$l.h^{-1}$ flow at 10, 11, 12, 13, 14 and 15cm down the T-piece.

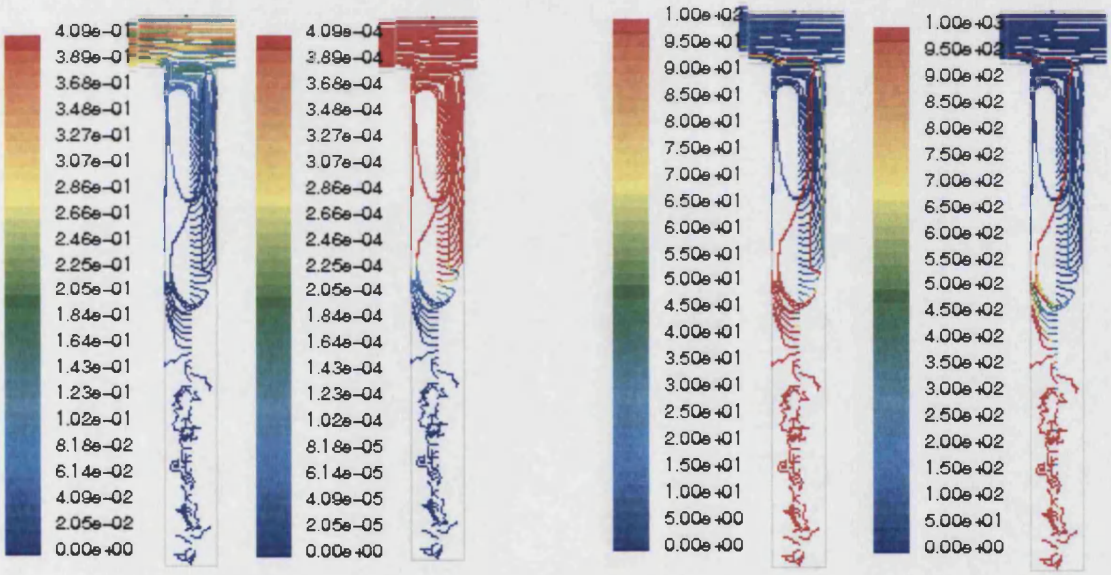

Figure 4.2.23: 600$l.h^{-1}$ flow path lines of mass less particles released from the inlet and the central axis of the T-piece coloured by velocity magnitude ranging between 0-0.409ms^{-1} (a) and 0-0.01ms^{-1} (b) and residence time ranging between 1-100sec (c) and 1-1000 (d).

Drawing the path lines of velocity (fig 4.2.23 (a) and (b)) and residence time (fig 4.2.23 (c) and (d)) of mass less particles released from the inlet of the rig and the vertical axis along the T-piece, we can see once more how velocity values drop after 11cm down the pipe. Also fig 4.2.23 (b) shows where and how velocities slow down quite suddenly at that depth, moving from red colours to yellow, green and eventually blue within one centimetre corresponding to at least one order of magnitude drop. There the swirling shape of the eddy brakes and some particles return upwards and the rest go to the bottom of the geometry where they are trapped

and remain. There the eddy does not have any effect. That is why at the base of the swirl we see very high and low residence times (fig 4.2.23 (d)). We can observe that, until the 5th or 6th cm, the fluid, being trapped in the eddy, is forced to remain for longer swirling around in a longer and narrower circle compared to the previous flows.

Comments on the flow of 600$l.h^{-1}$.

For this flow the choice of model best describing the flow in the dead end is based on qualitative rather than quantitative criteria. The temperature profile predicted by the k-ε STD model should still be transferred a couple of centimetres upwards, in order to describe it more accurately. The k-ω models might give a better agreement at the bottom but the shape of the curve shows a different and steeper fall of values.

There is mass exchange between the vertical pipe and the horizontal up to a depth of approximately 11-11.5cm. Below that point velocity is negligible.

Temperature, in general, is uniform until the 10th to 11th centimetre and on the whole is also axi-symmetric throughout the whole length of the T-piece.

It is also noticed that at the area where the eddy is formed there is more fluid recirculating until its escape to the top of the pipe. So, the momentum is significantly higher and more mass is pushed up.

4.2.4 Flow of 1000$l.h^{-1}$

A much higher flow of 1000$l.h^{-1}$ was obtained in the stainless steel rig and Reynolds' number was approximately 13000. Flow was turbulent and comparison was obtained between SST k-ω, standard (STD) k-ω, k-ϵ standard and RNG models (fig 4.2.24).

The boundary conditions for the model are:

u_{in}=0.56ms^{-1}

T_{in}= 321K

T_{env} = 297K

h_{ver} = 4.55Wm^{-2}K^{-1}.

h_{hor} = 2.77Wm^{-2}K^{-1}.

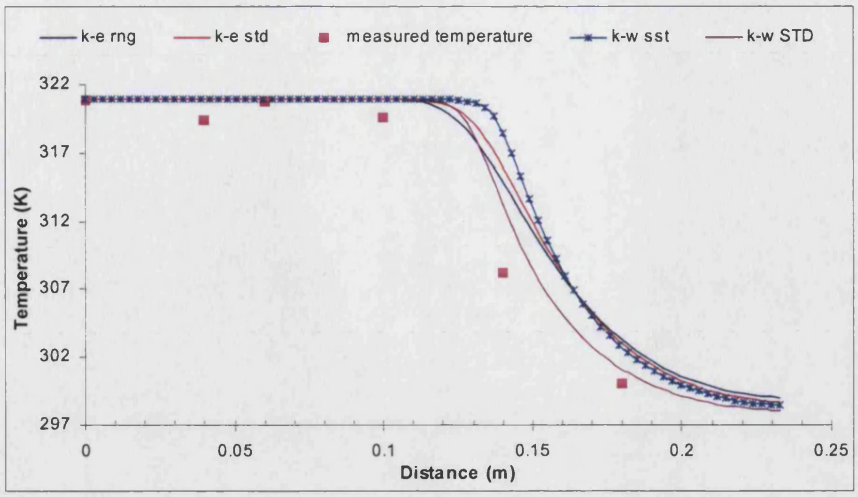

Figure 4.2.24: Comparison of temperature distribution down the central axis of the T-piece between various models and the experiment for the $1000l.h^{-1}$ (interval size 0.003).

The models used to solve this kind of flow are compared on figure 4.2.24. All of them are fairly close to each other with the k-ω models demonstrating a big difference amongst each other to the overall profile of the temperature drop. In the meanwhile the k-ω STD is pretty close to the prediction of the dropping point and comes in good agreement with the k-ε models as well. Nevertheless, it gives a steeper description of the drop compared to the one given by the thermocouples. As in the previous flow of the $600l.h^{-1}$, the k-ε models are closer to the shape of the temperature distribution with the k-ε- RNG giving a slightly better behaviour at the point where the decrease starts.

In order to get an idea of how a turbulence model behaves with a finer grid we solve the k-e RNG for a mesh of interval size equal to 0.002m (fig 4.2.25). It is quite clear the deviation of the finer grid and the over estimation of the whole profile compared to a coarser and less rigid one.

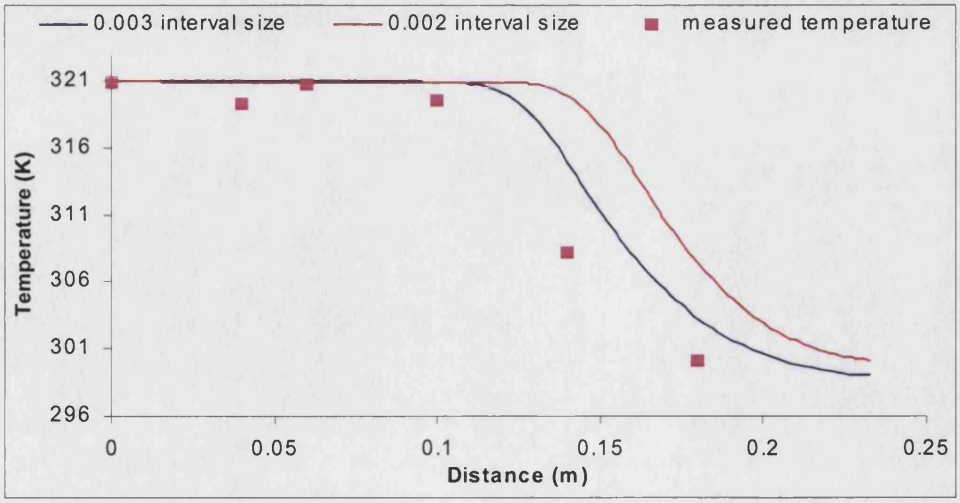

Figure 4.2.25: Comparison of k-e RNG models to the experiment for two grids with interval size of 0.003 and 0.002.

Taking a look at the velocity distribution together with the temperature (fig 4.2.26 (a)) we can see that the sudden drop of both starts at around 12cm. Choosing a shorter range of velocity values (fig 4.2.26(b)) we see that the vertical drop of velocity by almost two orders of magnitude happens at around 15cm.

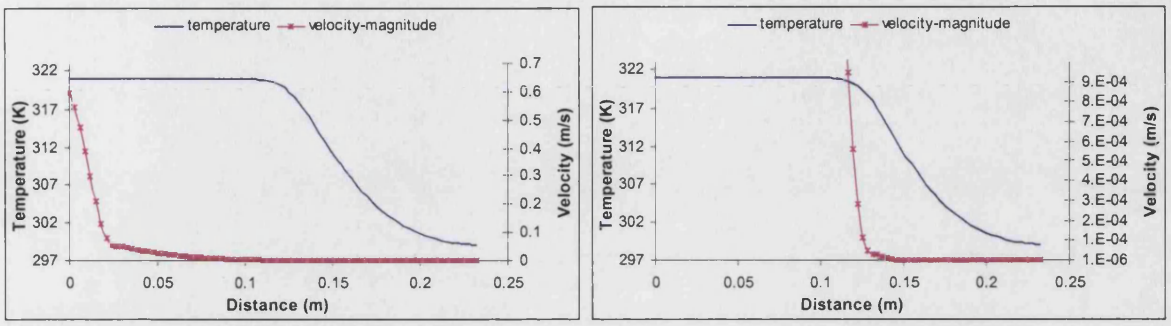

(a) (b)

Figure 4.2.26: Temperature and velocity distribution down the central axis of the T-piece for the flow of 1000$l.h^{-1}$ for different velocity ranges.

By comparing the profiles of the velocity at various depths down the T-piece (fig 4.2.27 and 4.2.28) it is observed that on the 10th and 11th cm the velocity is slightly higher on the left than the right hand side, due to the recirculation zone, as explained previously for the other flows. Further down a similar distribution is noticed, although not that pronounced, with velocity being a bit higher on the right side this time. This probably happens because of the smaller eddy formed under the first one (fig 4.2.29). This appeared to the other flows as well (fig 4.2.14, 4.2.21), although not that strongly and without such effects on the velocity.

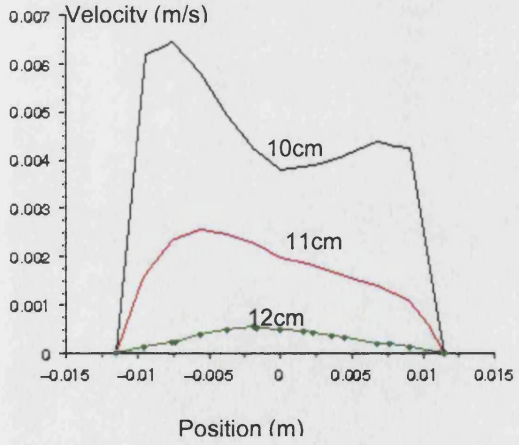

Figure 4.2.27: Velocity profiles at 10, 11 and 12cm down the T-piece.

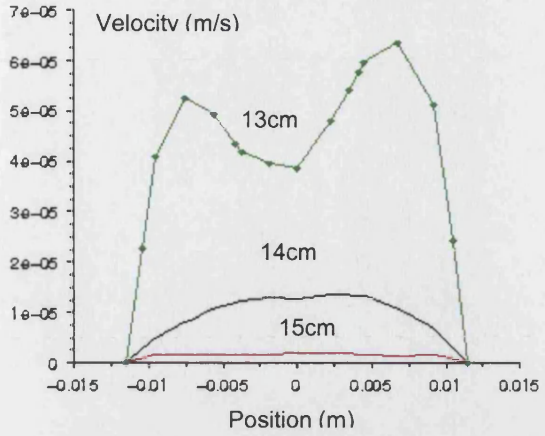

Figure 4.2.28: Velocity profiles at 13, 14 and 15cm down the T-piece.

This time, a closer look is taken to the path lines coloured by velocity magnitude (fig 4.2.29 (a) and (b)). By changing the range of values we see how the colours change gradually in a short space. The recirculation zone detaches from the rest of the volume after approximately 15cm. Also it is noticeable how much stronger this zone is by creating a longer and narrower eddy that goes deeper down forcing the creation of another smaller one (or probably the same one including rotation around the y-axis) that pushes the fluid at the other side (left), from the centre, before bringing it up from the right side again.

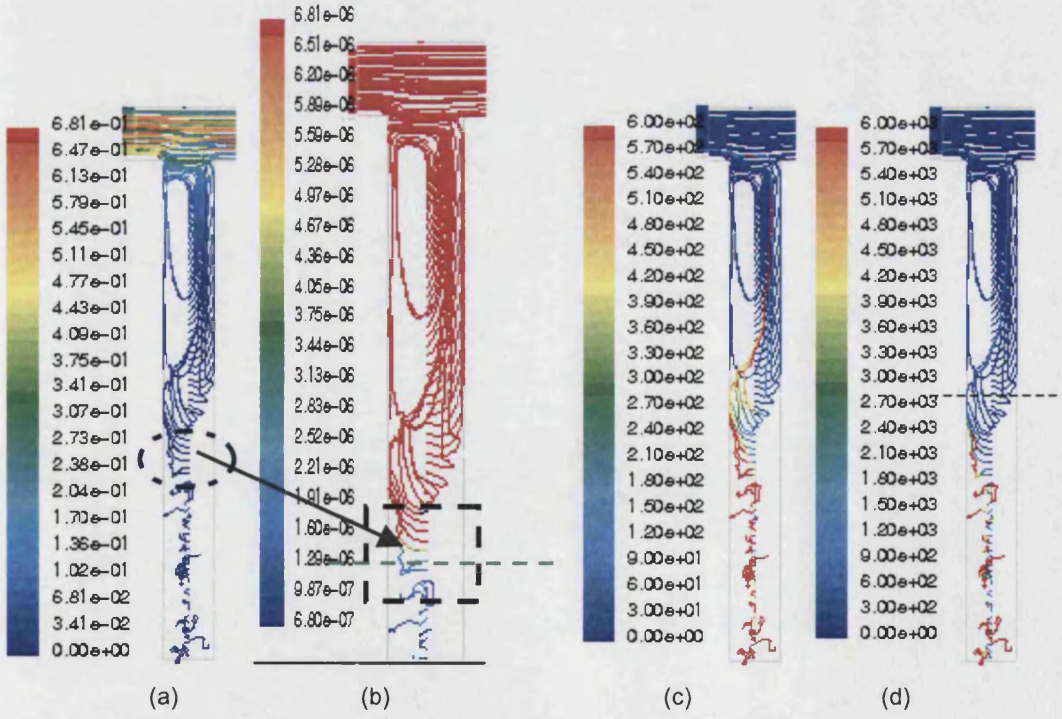

Figure 4.2.29: 1000*l.h*$^{-1}$ flow path lines of mass less particles released from the inlet and the central axis of the T-piece coloured by velocity magnitude ranging between 0-0.681ms^{-1} (a) and 6.8 10^{-7}-6.8 10^{-6}ms^{-1} (b) and residence time ranging between 1-600sec (c) and 1-6000 (d).

Comments on the flow of 1000$l.h^{-1}$.

The flow here is of high Reynolds number and the k-e RNG seemed to cope better with the flow. The criteria are not based on exact matching with the values measured. Generally, so far, the higher the bulk flow the more difficult for the code to predict the conditions in the T-piece.

Application of a finer mesh gave higher temperatures, which probably means that the coupling with the main flow becomes stronger.

Although, not much deeper compared to the previous flow, the recirculation is quite strongly influencing the whole flow, especially right before the 15th cm point, where the velocity becomes negligible. There, an eddy of smaller scale is formed causing a more sudden twist on the right.

4.2.5 Flow of 1340$l.h^{-1}$

Once more, using water in the stainless steel rig we proceed obtaining the much higher flow of 1340$l.h^{-1}$. Reynolds' number is approximately 17000. Flow is turbulent and comparison was obtained between SST k-ω, standard (STD) k-ω, k-ϵ standard and RNG models (fig 4.2.30).

The boundary conditions for the model are:

u_{in}=0.75ms^{-1}

T_{in}= 321.5K

T_{env} = 297K

h_{ver} = 4.5Wm^{-2}K^{-1}.

h_{hor} = 2.77Wm^{-2}K^{-1}.

The flow is not very much higher than the previous values. It is important though to investigate this value since it is the maximum capacity that the pump can achieve and is going to be subsequently used for the unsteady flow conditions. The same models are compared (fig 4.2.30) and the k-ε RNG seems again to better represent the dropping profile, with an overestimation of the location of the starting point of approximately 2cm.

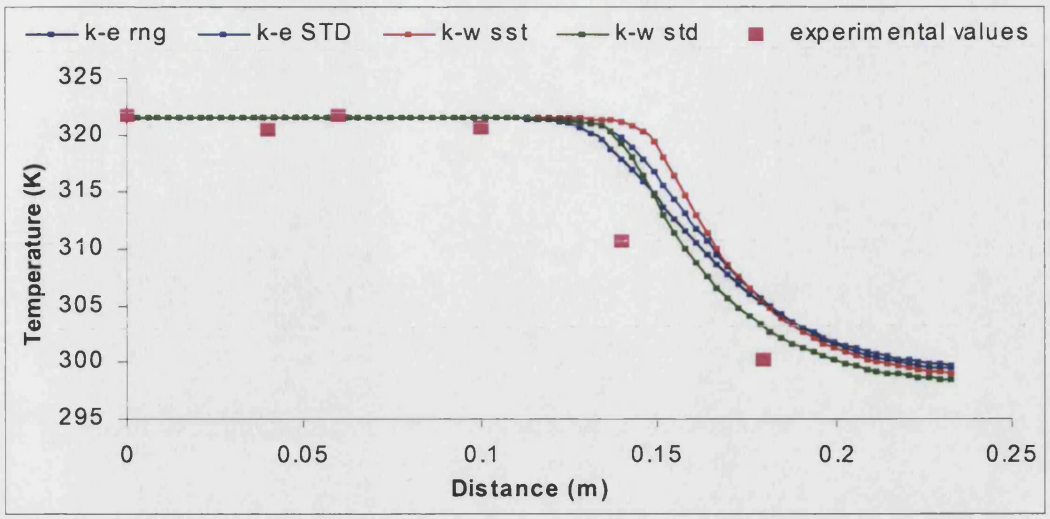

Figure 4.2.30: Comparison of temperature distribution down the central axis of the T-piece between various models and the experiment for the 1340 $lthr^{-1}$.

Velocity drops from $10^{-4}ms^{-1}$ to $10^{-6}ms^{-1}$ just after 15cm (fig 4.2.31). This can be verified by the velocity profiles at various depths in the T-piece (fig 4.2.32), where we can also see how the drop occurs from the 14th to the 16th centimetre. Also on figures 4.2.32 and 4.2.33 we have an effect similar to the one for the $1000lthr^{-1}$ flow. It is a little bit higher on the left compared to the right side of the diameter and further down it is the other way around since the eddy changes direction and goes first towards the left wall before turning to the right and forcing itself upwards.

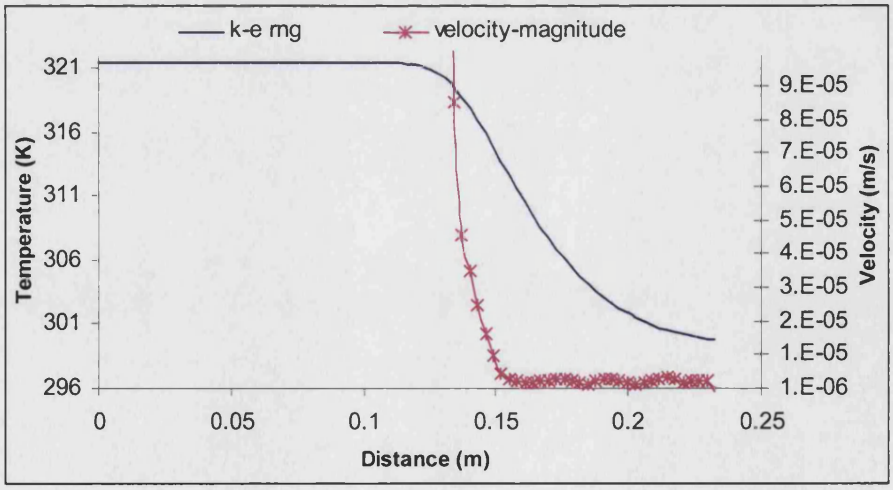

Figure 4.2.31: Temperature and velocity distribution down the central axis of the T-piece for the flow of $1340l.h^{-1}$.

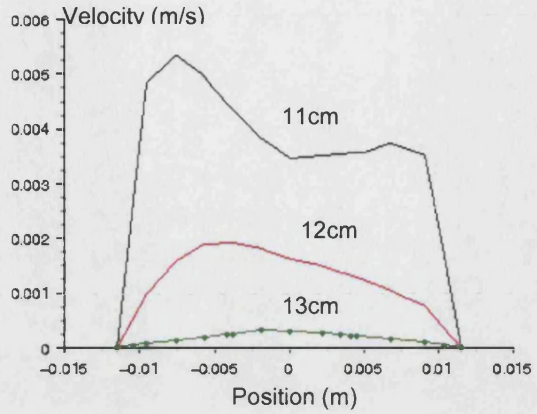

Figure 4.2.32: Velocity profiles at 11, 12 and 13cm down the T-piece.

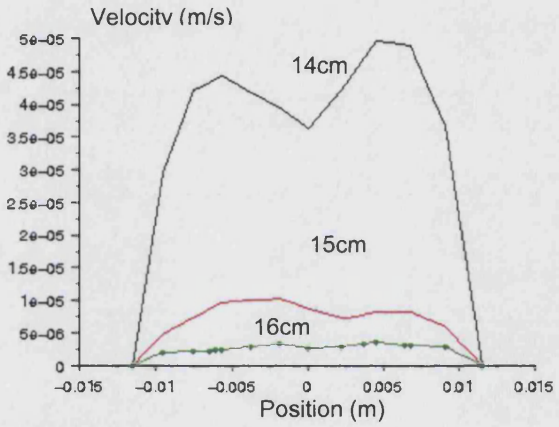

Figure 4.2.33: Velocity profiles at 14, 15 and 16cm down the T-piece.

The path lines of the massless particles (fig 4.2.34) demonstrate very clearly how the recirculation zone is shaped. It seems to be having a larger distorted shape, which is not so different from the previous flow, although maybe a little more pronounced. The detachment of the recirculation zone happens at around 16cm and the residence time is increasing by orders of magnitude of seconds after that threshold, choosing two different time scales (fig 4.2.34 (c) and (d)).

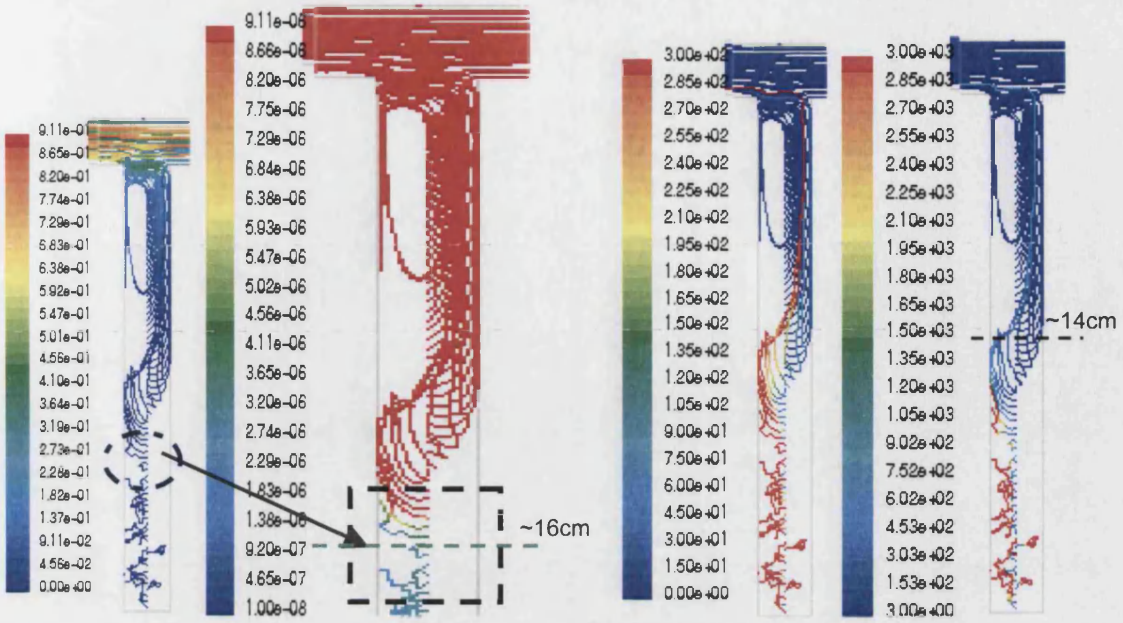

Figure 4.2.34: 1340$l.h^{-1}$ flow path lines of mass less particles released from the inlet and the central axis of the T-piece coloured by velocity magnitude ranging between 0 and 0.911ms^{-1} (a) and 10^{-8}-9.11 10^{-8}ms^{-1} (b) and residence time ranging between 1-300sec (c) and 1-3000sec (d).

Comments on the flow of 1340$l.h^{-1}$.

The specific flux is not much higher than the previous one. That is why the stagnant area begins no more than one centimetre further down. Time recirculation zone is larger and the rotation of it is stronger.

4.2.6 Flow and temperature: general comments

The flows modelled above show clearly that the higher the inlet velocity the more heat penetrates into the T-piece (fig 4.2.35 and 4.2.36). We notice that while moving from laminar to fully turbulent flow, velocity does not increase significantly into the vertical pipe but the recirculation zone increases its depth and interaction with the bulk flow is stronger. The temperature profiles show that after 600lthr^{-1} the threshold of a steep drop is not far from the one of the maximum flow of 1340$l.h^{-1}$, although that flux is more than double. The difference is more profound between the 300 and 600$l.h^{-1}$. Hence, despite the fully developed turbulent flow, the interaction gets more difficult to interpret in the dead leg as we examine the flow further down.

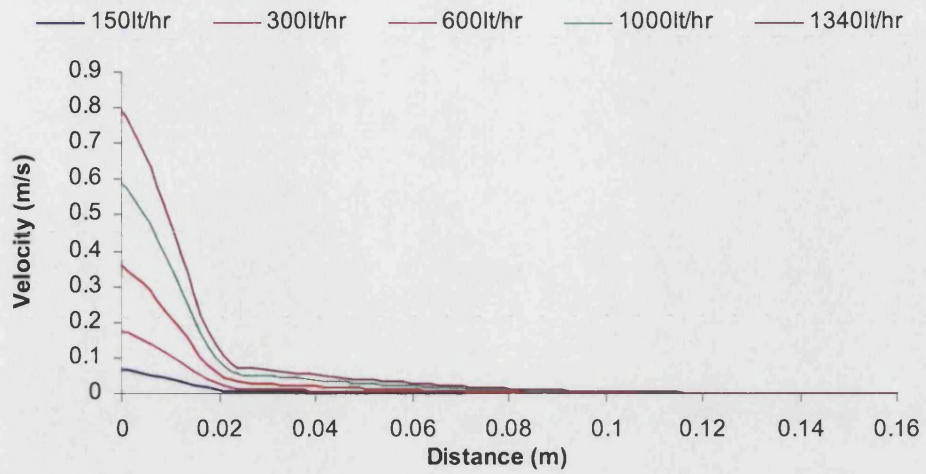

Figure 4.2.35: Velocity distribution along the centre of the T area for different flows

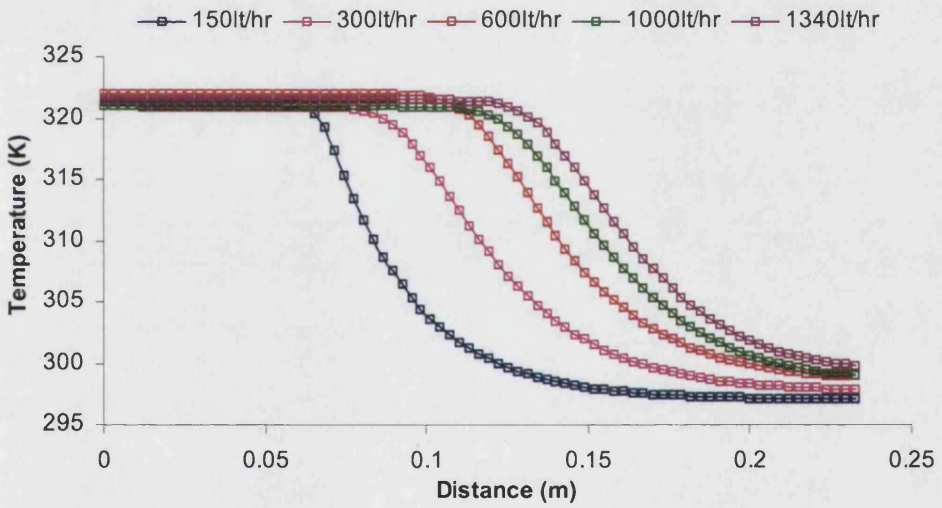

Figure 4.2.36: Temperature distribution along the centre of the T area for different flows.

Contours of temperature for the various flows on a vertical cut surface along the dead space (fig 4.2.37) can give a better image of the temperature. The aim was to try and keep the inlet temperature constant for all experiments and under similar environmental conditions in order to achieve comparable results. Lower flows could not be achieved due to necessity of more means of temperature measurement, especially close to the merging of the two tubes that could not be fit on the T-piece. Also, higher flows were not possible, as the pump was operating at its maximum flow rate. From the analysis that preceded, we can conclude that the specific geometry would not be cleaned under the current flows since there is always a stagnant area formed that traps fluid at relatively low temperatures. So, the specific T-piece examined would be considered hygienically risky under the conditions tested. In figure 4.2.37 are added the contour plots for higher inlet velocities of $1ms^{-1}$, $1.5ms^{-1}$ and $3ms^{-1}$. These were just modelled

and no experimental data exist for comparison. Drop of temperature is almost linear at the beginning but then it ceases the fast decrease and is more exponential.

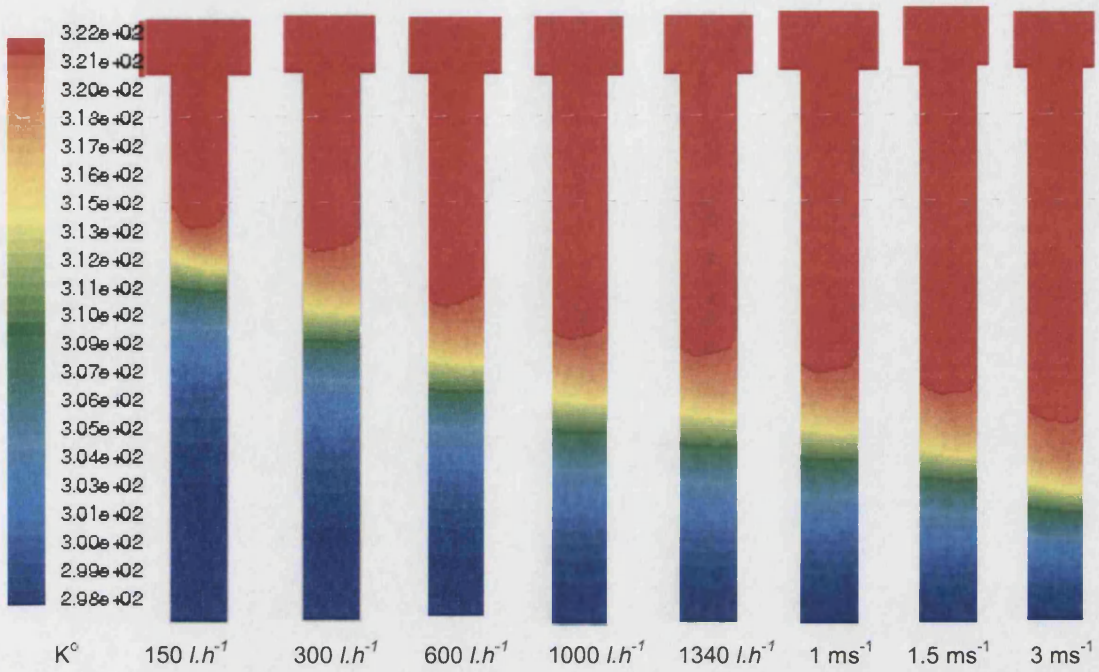

Figure 4.2.37: Contours of temperature along the dead leg for various flows.

Examining the distributions of figure 4.2.36 in more detail, we can attempt to develop a mathematical rule or maybe a model that correlates the inlet velocity (independent variable) to the temperatures down the specific T-piece. Hence, the temperature can be connected to the flowmetric rate. This is going to be applicable only for water, or may be for Newtonian fluids and for the specific geometry examined (same diameter for both pipes), although it can be applied for various lengths of the particular vertical pipe.

The flows taken into account were: 150lthr^{-1}, 300lthr^{-1}, 600lthr^{-1}, 1000lthr^{-1} and 1340lthr^{-1}. The last one is the maximum flow that could be achieved with the existing pump (Lowara SV211T15M) and correspondent pressure drop constraints.

On table 4.2.1 are displayed the difference between the trendline, fitting the experimental measurements, and the prediction down the T-piece. The comparison is presented as the area laying between the two series of data for each case, using figures: 4.2.1, 4.2.10, 4.2.17, 4.2.25 andf 4.2.30. The minus sign for the first flow shows that values predicted are mostly lower than the ones measured. It is noticed that the higher the flow the bigger the difference with the two last ones demonstrating similar values where the same models was used. The same is observed with 300 and 600$l.h^{-1}$ where again the same k-ε STD was applied.

Table 4.2.1: Integrals' differences between predictions and measurements.

Flow [$l.h^{-1}$]	150	300	600	1000	1340
Area [cm^2]	**-1.2**	**3.5**	**3.7**	**5.3**	**5.2**

Relating temperature down the T-piece to inlet velocity

Temperature distribution down the T-piece has approximately the shape shown below (fig 4.2.38) for all flow rates that were examined, where at the beginning of the vertical tube temperature is equal to the inlet temperature, T_{in}, since the horizontal pipe is insulated, and remains constant for a distance ε down the T-piece. After that the drop is exponential until it reaches values very close to the environmental temperature, T_{env}, which is the temperature of the air outside the tube. As the flow gets higher, the threshold value ε increases, which means that heat diffuses in the tube more as flow goes from laminar to turbulent.

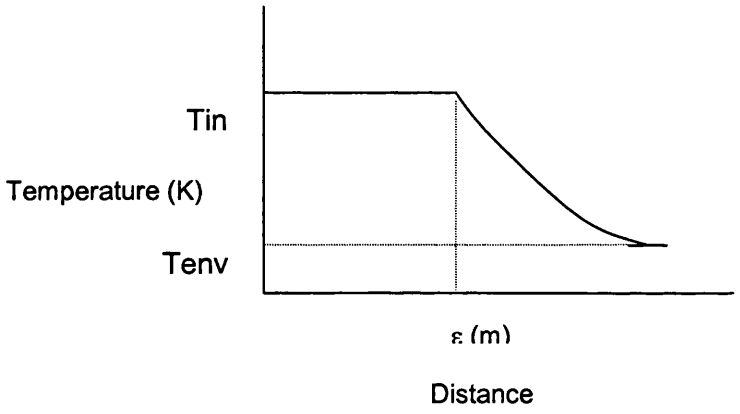

Figure 4.2.38: Shape of temperature drop in the central axis of the T-piece.

The equation that describes the temperature distribution down the tube has the following form:

$$T = T_{in} \qquad 0 \le x \le \varepsilon \text{ and}$$

$$T = \left(T_{in} - T_{env}\right) \cdot e^{-B(x-\varepsilon)} + T_{env} \qquad x \ge \varepsilon \qquad (4.2.3)$$

where T_{in} is the temperature at the inlet of the flow and consequently the one at the beginning of the T-piece, because of the insulation. T_{env} is the air temperature; B [m^{-1}] is the pre-exponential factor of the exponential equation and ε [m] is the distance down the pipe where temperature starts to drop. The above equation is valid for values of x higher that ε.

Correlating all inlet velocities with the constants B and ε, we notice that we can take an expression of the following form:

$$y = \alpha + \beta \cdot \gamma^{x} \qquad (4.2.4)$$

where y is either B or ε , x is the inlet velocity and α, β, γ are the constants of the above three parameter asymptotic regression model.

For B we had $\alpha_B = 23.3$, $\beta_B = 35.01$ and $\gamma_B = 5.29\ 10^{-5}$, or better in order to smoother constants we can express it as an exponential model.

$$B = 23.3 + 35.01\ e^{(-9.84Uin)} \qquad (4.2.5)$$

For ε values were $\alpha_\varepsilon = 0.14$, $\beta_\varepsilon = -0.1$ and $\gamma_\varepsilon = 0.0136$

So,

$$\varepsilon = 0.14 - 0.1\ e^{(-4.3Uin)} \qquad (4.2.6)$$

Another correlation that can be checked is the ratio of average velocity of the flow to the maximum against the Reynolds number of the flow (fig. 4.2.39). Chemical engineering handbooks state that for a flow in a pipe the maximum this value can reach is approximately 0.82 for a Reynolds' number of 10^5 (Coulson and Richardson, 1996).

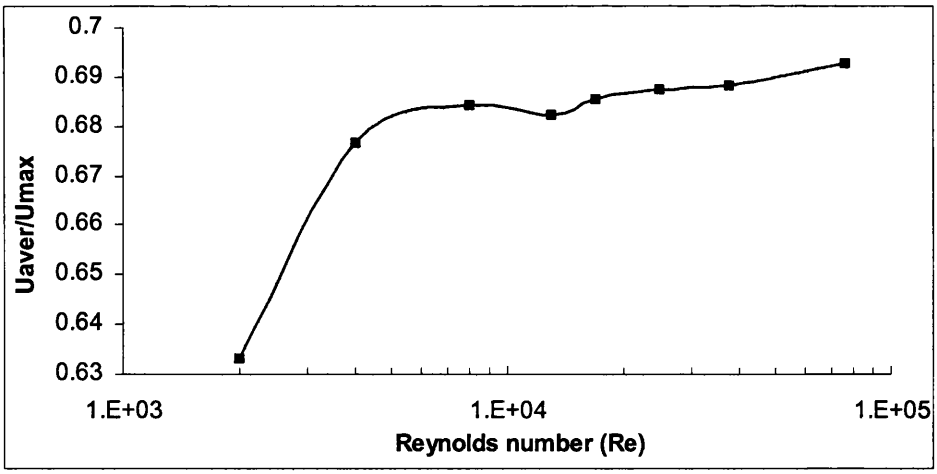

Figure 4.2.39: Variations of Uaver/Umax measured at the outlet of the geometry against Reynolds' number for the modelled flows.

Literature says that for Re between 2000 and 4000 there is a sharp increase of the ratio, which is the case in the models done here. The rest get close to an asymptote but still below the 0.82 ratio, although Re values are high. Probably this shows the different way CFD approaches flows with the various models available depending on the turbulence intensity.

4.3 Sterilisation processing for a non-Newtonial fluid

Carrying on from the previous models based on steady state heating processes, in this section is presented the simulation of the Tube in Tube in Tube (TnTnT) heat exchanger in the tomato paste factory in Greece. As already was mentioned, the whole geometry consists of three heating sections of 6m each and two bends of 180° that connect them. The bends do not have the shape of an annulus in their interior. Instead, they are like simple bent tubes that are not heated.

Figure 6 shows the wall mesh applied on the bend and the 20cm parts attached to the inlet and outlet of the bent part of the pipe work. So the actual inlet and outlet of the model are annular areas that after 20 cm lead to the bent tube.

4.3.1 Initial, boundary conditions

The inlet temperature of the product is taken constant equal to 80°C (or 353 K) (Dubbelman and van Dijk., 2003). The flow of the heating medium is not modelled, since it is assumed that the temperature of the walls in contact with the heating source is constant equal to 130°C (Dubbelman and van Dijk., 2003). This assumes that the controlling heat transfer resistance is on the product side.

Heat transfer to the environment occurs at the walls of the curved tubes and this was described using the natural convection option. The environmental temperature was assumed equal to 45°C (due to the fact that the trials were carried out in the summer period in Greece and that the area was already very hot since it's a sterilising unit). It is necessary to set the natural convection heat transfer coefficient that is used by the code to model the heat exchange between the wall surface and environmental air. The equation used is given in paragraph 3.4.6. Thermophysical properties of the product are taken from experimental results (Patrick, 2003):

Reynolds number is 0.133, calculated from equation 3.4.10, and so the flow is laminar.

$D_e = 4r_e = 4*(99-73)/4 = 26$ mm. (4.3.1)

$$\mathrm{Re} = \frac{De \times u \times \rho}{\mu} = 0.133 \text{ (laminar flow)} \quad (4.3.2)$$

μ is viscosity at 80°C: 46.22 kg/m/sec (Dubbelman S., van Dijk M., 2003).

The results are separated in the ones that are on the TnTnT heaters and the ones that are observed for the flow in the bends:

4.3.2 Results and comparison

The Pt-100s attached on the walls of the bends measured the temperature continuously for one day while the line was running. The temperature traces of figure 4.3.1 show the temperature

history against time these bend thermocouples measured. On the same graph the operators' measurements are shown and the modelled ones: mass averaged temperature at the end of the whole heating process and the ones on the outer side of the inner walls of the bends. We can see that there are big differences between the bend measurements and the modelled temperature. It can also be observed that the temperature is higher after the second heating section compared to the third. If this is correct, there could be systematic errors in the thermocouples such as calibration or the fixing of them on the bends. Alternatively, the heating medium itself, despite the control systems, may not be distributed homogeneously in the different heating sections.

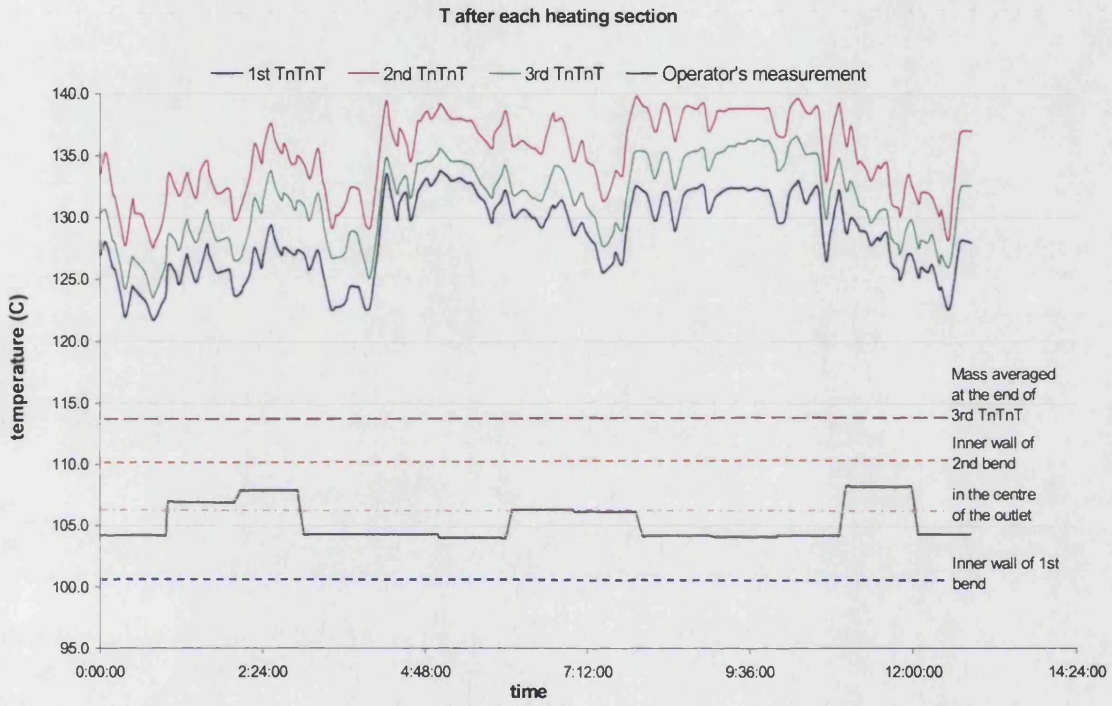

Figure 4.3.1: Comparison between in line measurements and model.

After visiting the plant and observing the actual heating unit, it was noticed that the heating medium was entering the system from locations that were in contact with the interior of the bends (fig 4.3.2). Since the measurements were taken on the surface of the bends it is logical that due to the fast heat conduction in stainless steel, the temperature distribution on the bend fluctuates arbitrarily and could justify the peculiar differences between the 2^{nd} and the 3^{rd} heating sections by the control system. Additionally, there were some measurements taken with infrared and showed that the temperature on the outer wall of the bend was higher than the inner one. This could not be the case in the product itself, since the distance the fluid has to travel on the inner wall is shorter than the other side, which leads to less heat losses. Nevertheless, if there is a very hot stream, literally, attached to that side of the pipe, like in this case, then it makes sense that locally we have that divergence in the temperature values. Also, there was rejection of heating medium in the form of steam in the environment. This was again occurring very close to the heating system and could as well affect the measurements.

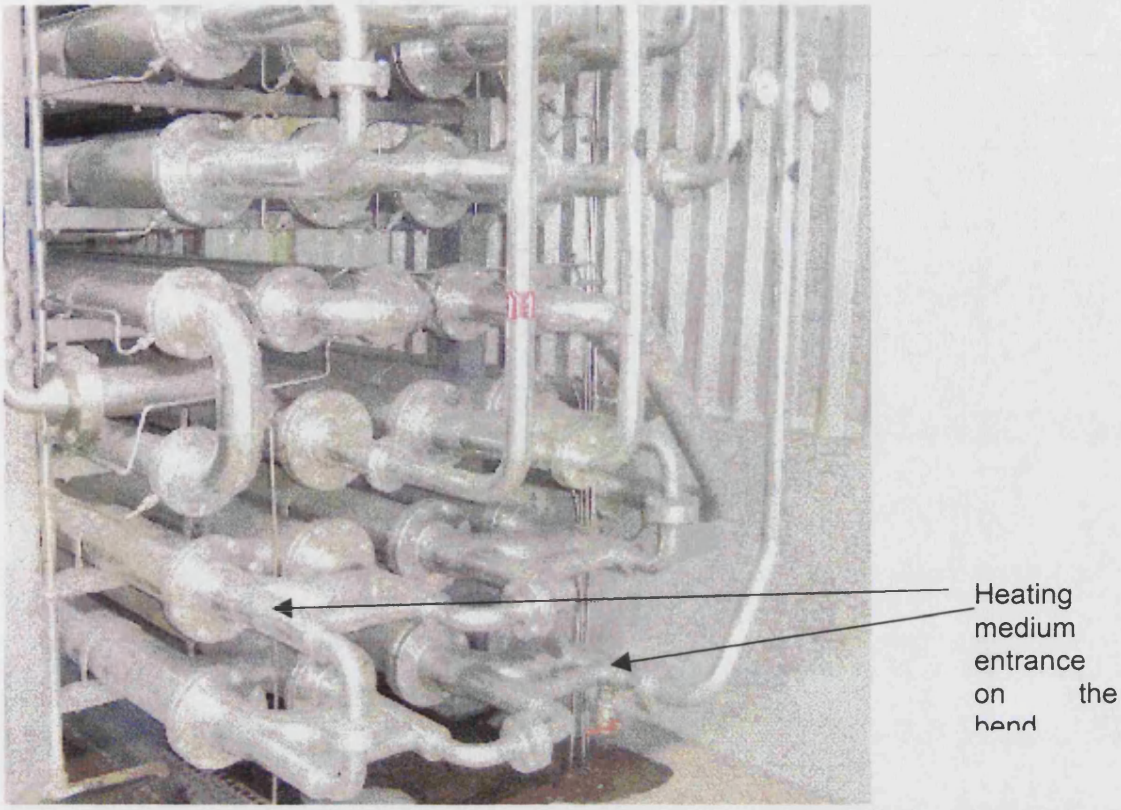

Figure 4.3.2: Rossi e Catelli TnTnT heaters showing heating medium entry. The picture includes holding and cooling system, which was not modelled.

We can also notice that the same kinds of oscillations (fig 4.3.1) are happening at the same time for all three of heating sections. This occurs because the heating medium system was trying to maintain temperature via feedback, by adjusting the flow in the same mode for the whole heating system. The averaged temperatures for the three indicators are 129°C, 135°C and 131°C. The operators' averaged is 105°C.

The values predicted from the model are quite different. The solution obtained was for steady state. In the centre of the outlet after the 18m of heating, the modelled temperature is 106°C, which is just one degree higher than the one measured at the plant. Also the rest of the predicted temperatures on the walls of the bends are lower than the ones given from the bend measurements because of the aforementioned reasons.

4.3.2.1 Heating Sections

The velocity distribution along the centre of the annular area for the three TnTnT heat exchangers takes a lot of computational time to converge. This is due to the fact that the TnTnT section is 6m long and there is a temperature gradient. When the difference between wall and product temperature is minimised then flow field solution converges much faster. The mean central velocity tends to increase overall along the whole heating area, which is expected since the product becomes less viscous as temperature increases (fig 4.3.3). The sudden drops and rises of the velocity are due to the fact that the product goes through expansions and contractions at the inlets and outlets of the bends.

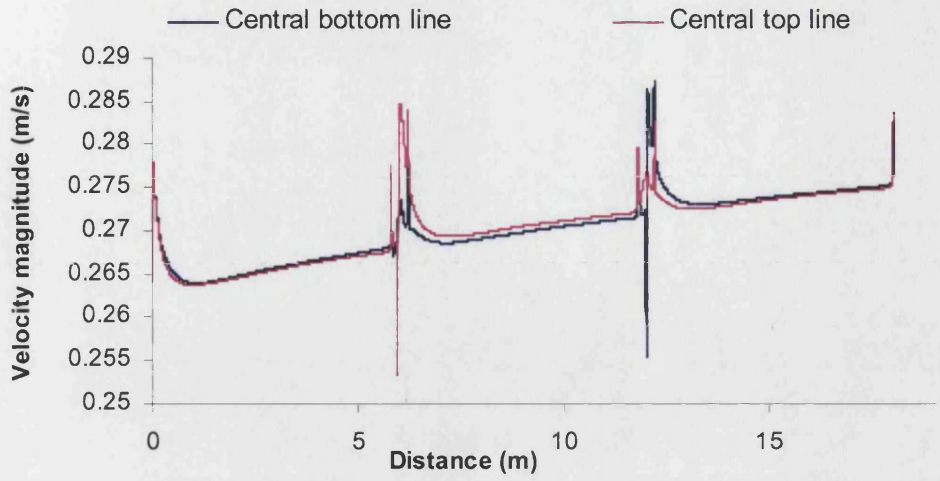

Figure 4.3.3: Modelled velocity distribution along the annular flow

Temperature distributions for the same areas as on figure 4.3.3, are depicted on the plot of figure 4.3.4, where we can also see with green colour the mass averaged temperature at the end of the 18m. The dark coloured line is along the centre of the bottom of the flow and the purple coloured along the centre of the top (diametrically opposite). At the end of each heating section we see that there is mixing in the bend that follows, since the next heating section starts with a higher temperature compared to the exit value from the previous section. In the first heating TnTnT section the temperatures are practically the same for both top and bottom with a very slight increasing tendency along the bottom line. The rest of the heating sections do not show the same correlation with velocity distribution since velocity seems consistent. Also, passing through the bend, the product changes orientation and the bottom becomes the top and vice versa. That is why the temperature starts higher at the top for the first one, in the second heater the temperature is higher at the bottom and in the third it is higher at the top again.

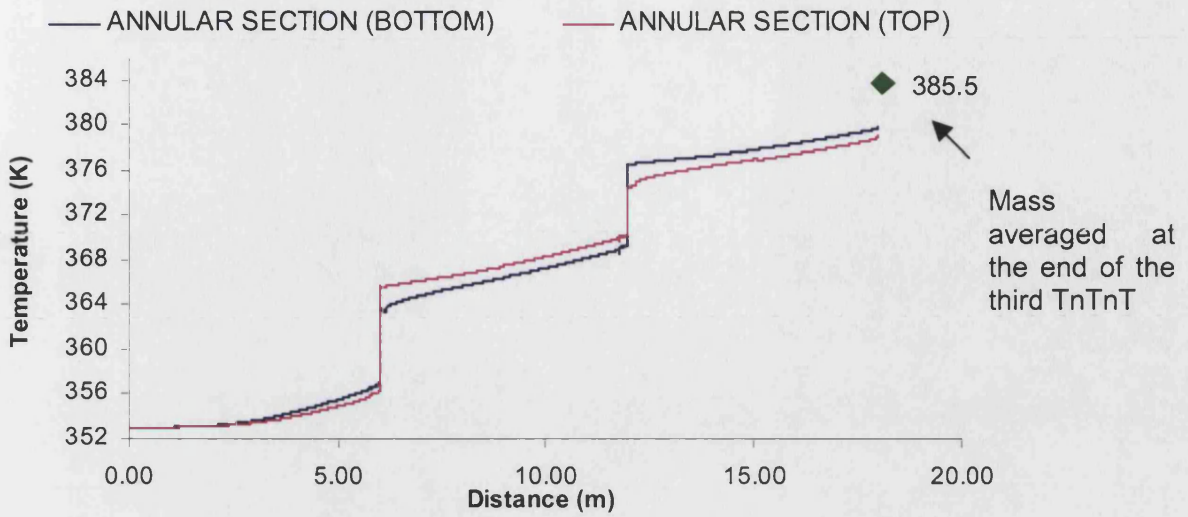

Figure 4.3.4: Temperature distribution along the annular flow.

Figures 4.3.5 and 4.3.6 show velocity and temperature profiles across the centre and the outlet on an axis perpendicular to the 1st heater of the first 5.8m of heating. Generally, velocity is slightly higher at the outlet when we look at both, the bottom (lower) and the topside. It is so small that it can be considered to be a computational fluctuation and does not need to be taken into account.

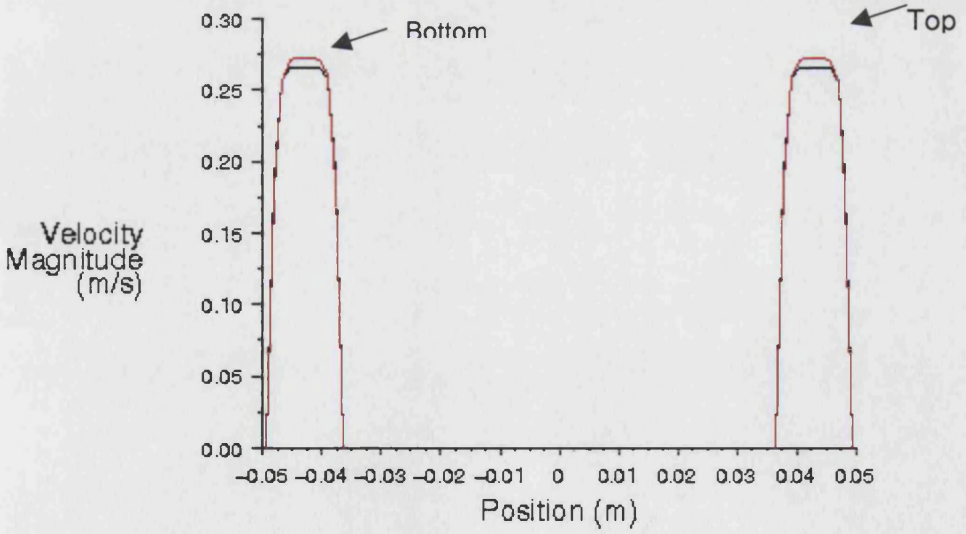

Figure 4.3.5: velocity profile at the centre (black line) and outlet (red line) of the first TnTnT on an axis perpendicular to the 1st heater.

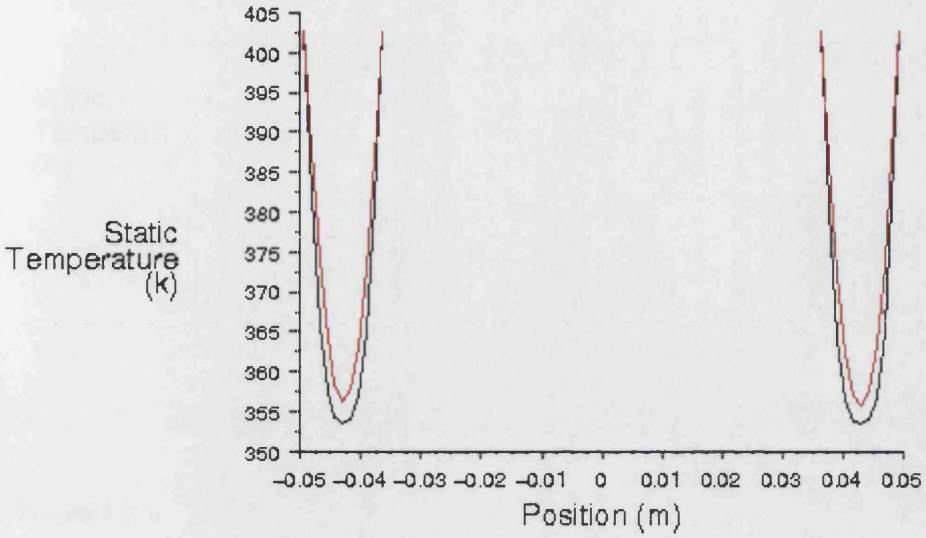

Figure 4.3.6 velocity profile at the centre (black line) and outlet (red line) of the first TnTnT on an axis perpendicular to the 1st heater.

Figure 4.3.8 follows the temperature as it rises from the inlet to the outlet (from right to left side of the plot) of the first modelled heating section. The areas chosen are depicted on the schematic of figure 4.3.7.

Figure 4.3.7: Areas chosen for plot of fig. 4.3.8.

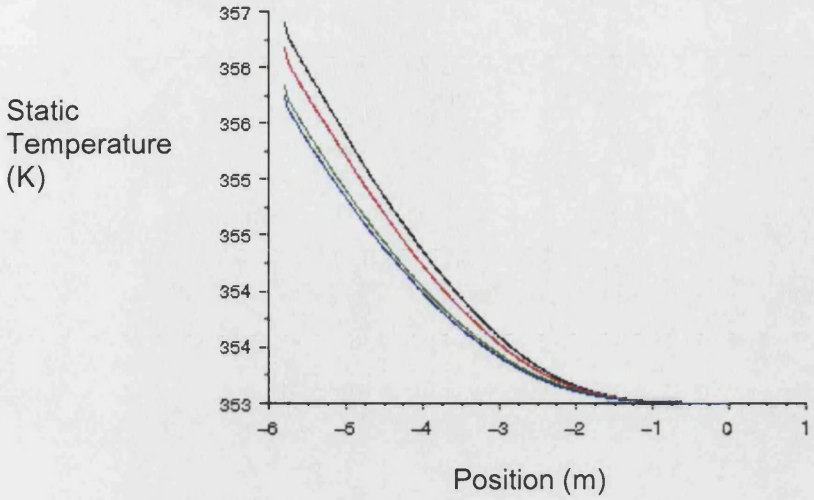

Figure 4.3.8: Temperature distribution at various lines along the central flow for the first heating section, where red is 1, blue is 2, green is 3 and black is 4.

Similar to figure 4.3.8 are the ones for the third heater (fig 4.3.9). We see that temperature profiles remained on the same position for the left and right side of the annulus but the top and bottom changed places because of the pass through the bend, as already explained.

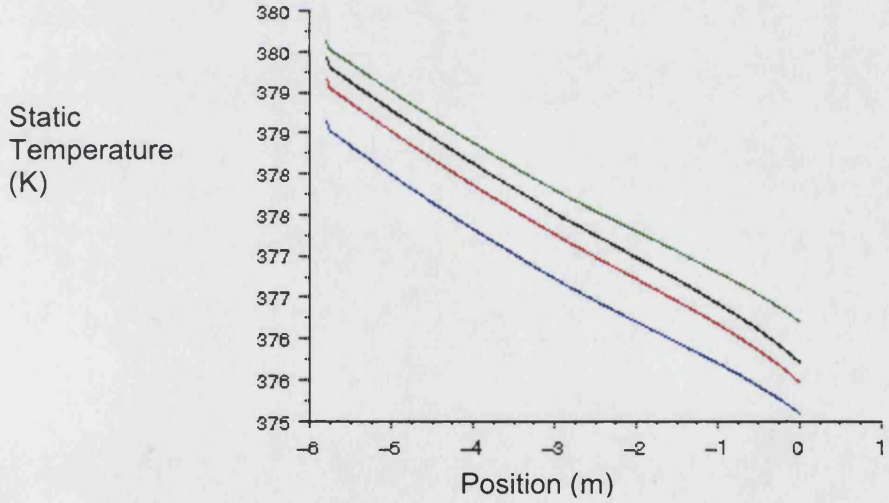

Figure 4.3.9: Velocity (a) and temperature (b) in the 3rd heater for various lines along it, where blue is the top, green is the bottom, black is on the left side and red on the right.

Shear stresses on the walls (fig 4.3.10) are depicted with filled contours for inner and outer walls for the first TnTnT heat exchanger with maximum values 900Pas. The colour change of the contours shows that there is a higher shear stress developed on the inner walls the differences being greater in the 2nd and 3rd heaters (fig 4.3.11 and 4.3.12) where the shear stress stays relatively high for longer as well. In addition the shear stress drops as the product moves through the annulus and is heated up.

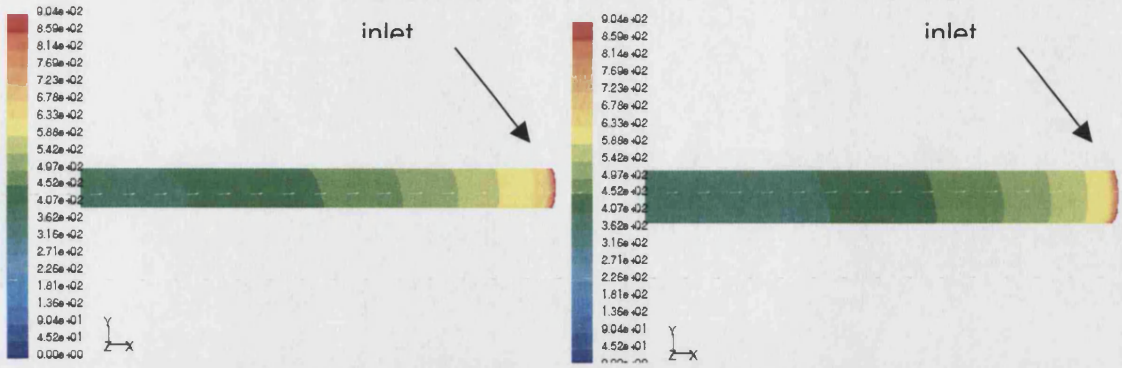

(a) (b)

Figure 4.3.10: Shear stress contours for the inner (a) and outer (b) wall of the first TnTnT section

On figure 4.3.11 the above effect is more profound, as far as it concerns the entrance. The overall values of the stresses are much lower and the maximum at the inlet is around 400Pas. It is also noticeable that the wall shear stress drops differently on the outer and inner wall. The contours have opposite orientations.

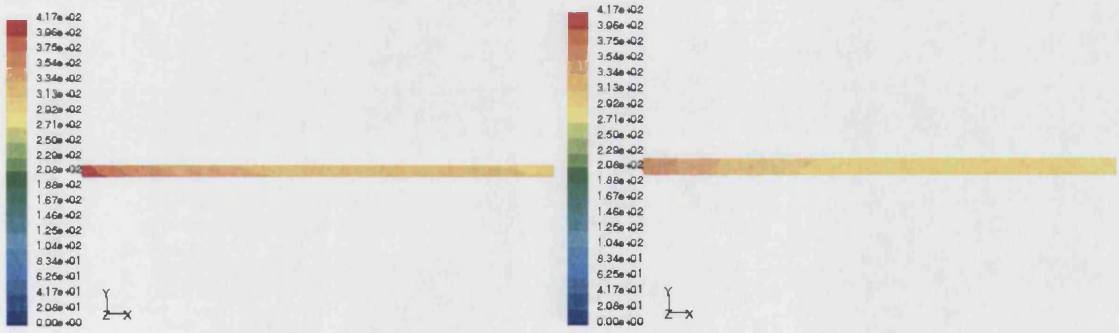

(a) (b)

Figure 4.3.11: Shear stress contours for the inner (a) and outer (b) wall of the second TnTnT section

Similar observations are made for the third and last part of heating section (fig 4.3.12). Again the inner wall seems to keep higher values for longer and for both areas maximum numbers are at around 360Pas. The contours show again opposite orientations. The observation is that the product is going through high shear at the entrances, which is expected since it is forced to move from a wide space (bend) to a much narrower (annulus). Nevertheless, these high wall stresses drop significantly once the product starts heating up after the first heating section from 900 to 400Pa.

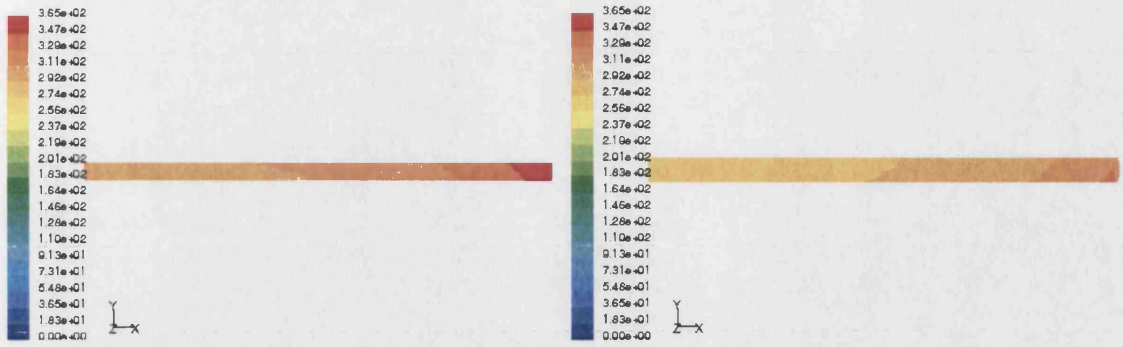

(a) (b)

Figure 4.3.12: Shear stress contours for the inner (a) and outer (b) wall of the third TnTnT section

Selecting lines attached on the inner (black lines) and outer (red lines) walls of all three heating sections at the upper part of the annulus we can take plots of wall shear stresses given on figures 4.3.13. We distinguish the values much clearer and we see how they drop. For the first one it starts with around 900Pas and at the end of the 5.8 meters reaches 300Pas. The drop is sharper at the beginning where from 900 goes to 650Pas almost straight after the entrance. This case is either because we start from a constrained annular entrance or it is just computational fluctuation in the model until it settles to the continuous drop.

Moreover, the drop has similar shape for the second heater (5.6m). The values are overall higher for the inner wall than the outer, whereas in the first heater numbers were approximately the same on both sides. So, for the inner boundary wall, shear stress starts from 400 to drop to 310Pas and for the outer from 380 to 290Pas.

Similarly, with even bigger differences between the two lines of the third heating section, wall shear stress drops from 370 to 290 and from 325 to 270Pas.

In general, the shear stress drops along the heating length. It is the sudden contractions the product goes through when it moves from the bend to the annulus areas that cause these stresses to increase.

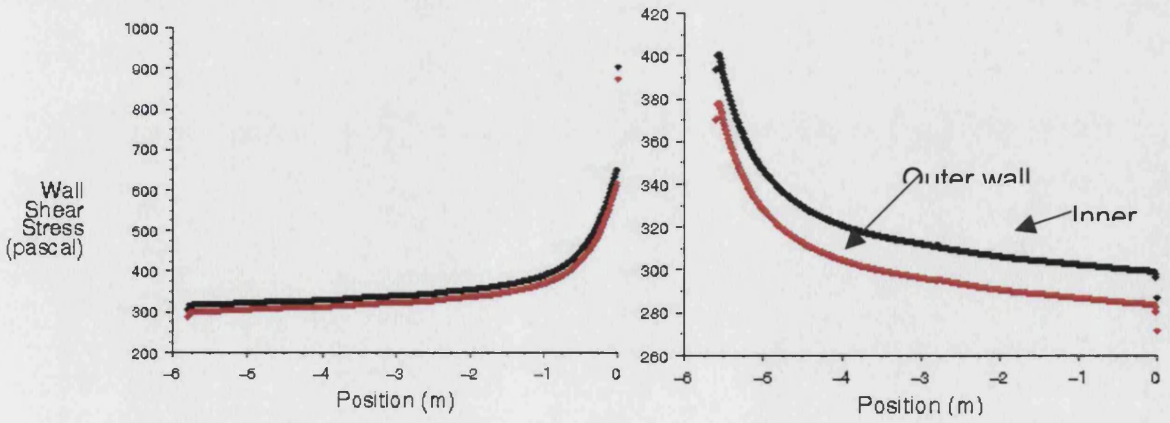

(a) (b)

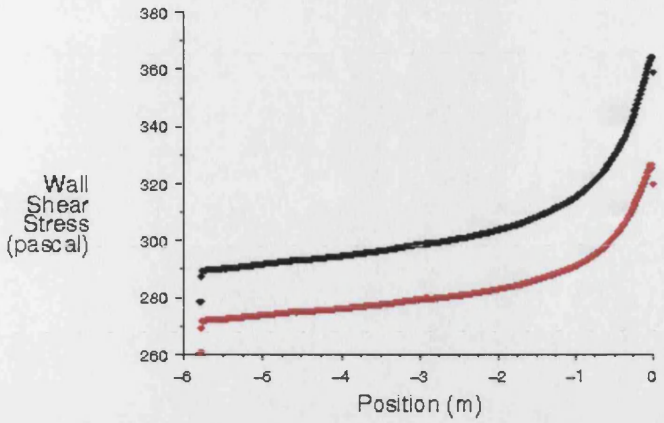

(c)

Figure 4.3.13: Shear stress along the annulus for the inner (black line) and outer (red line) wall of the 1st (a), 2nd (b) and 3rd (c) TnTnT section.

4.3.2.2 Bends

1st bend

Starting with the first bend, there were lines selected in the geometry that pass from the centre top and bottom of the attached 20cm of heating sections and continue all the way into the bend until the outer wall in both cases. So, on figure 4.3.14 we can see four lines where one pair is for the inlet (red, green) and outlet (black, blue) of the geometry. It is easily noticed that in the parts of the lines that correspond to the 20cm of the heaters temperatures are demonstrating a straight plateau. Also the bottom becomes the top moving from inlet to outlet (red to blue, green to black) transferring the higher values from the bottom to the top. The blue and red lines are longer since they cover larger area of the bend (inlet bottom and outlet top) before they reach the wall. The sudden changes for all of them imply that there is mixing between the part of the product that is in the centre of the annulus and the part that is close to the heated walls. Hence, it finally comes out at higher temperatures.

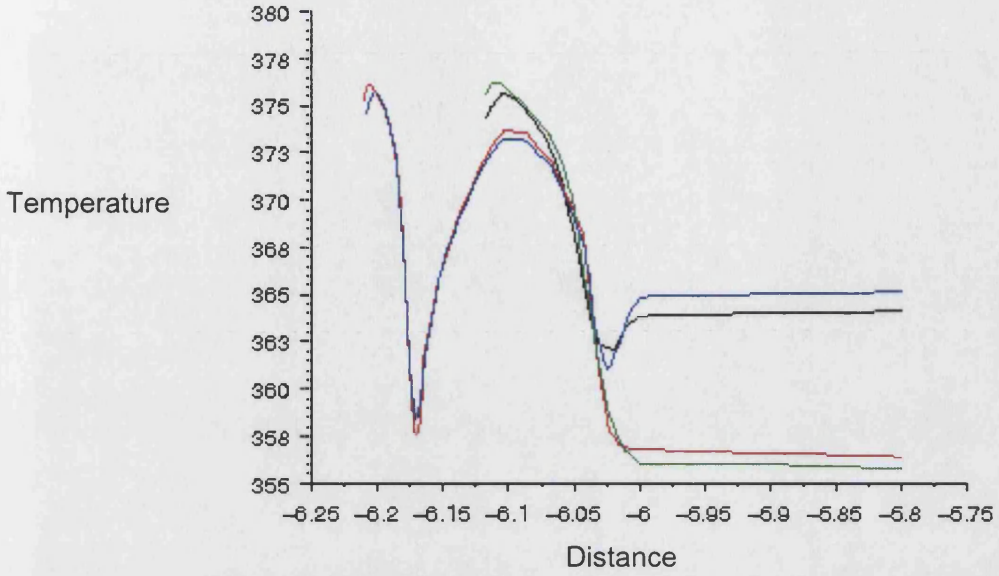

Figure 4.3.14: Temperature distribution in the bend on axis selected in the centre of the annular area for the top and bottom of it, where red is in the inlet bottom, green inlet top, black outlet bottom and blue outlet top.

Contours of temperature on the walls of the whole bend geometry (fig 4.3.15) give a better image of the situation in the bend. Reminding that the outside temperature is set to be 45°C (318K), we see that on the wall the temperature is not showing big variations. However, after the end of the first heater the temperature is dropping to 379-381K (green colour), which is higher by approximately two degrees comparing to the main surface of the bend (374.5-377K). Towards the exit and on the outer bend surface, is around 372-374K, which is the lowest temperature on the bent part. Once more, it is noticeable the dark blue colour on the inlet and the lighter on the outlet that corresponds to higher values according to the colours bar on the left.

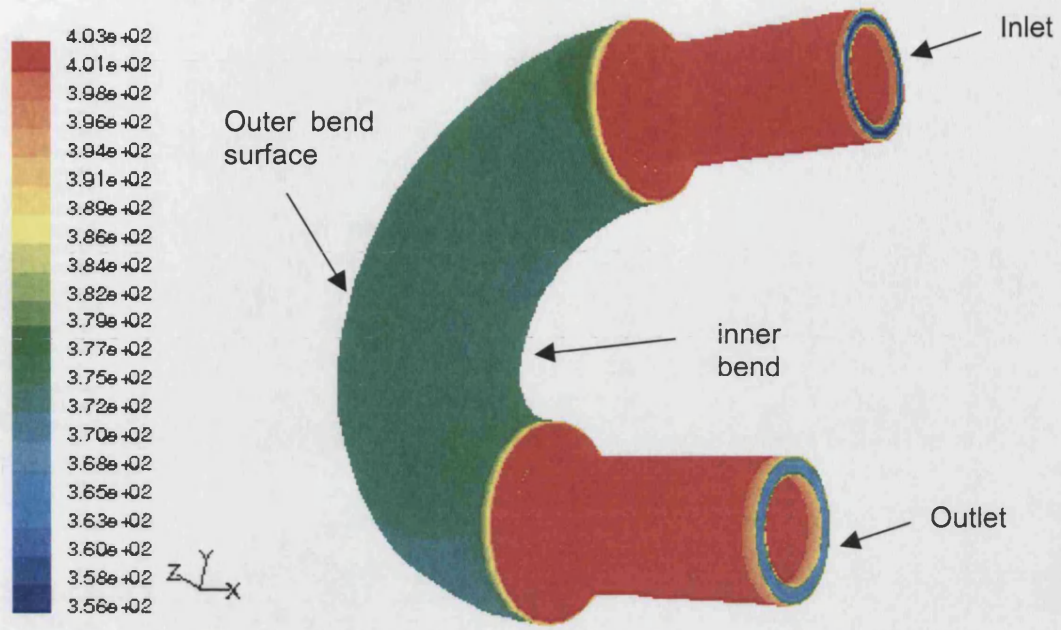

Figure 4.3.15: Temperature contours on the walls of the first bend.

By observing the path lines of mass less particles, released from the inlet, coloured by residence time (i.e. each particle's path line changes colour according to the residence time of the product at a specific location) that follow the flow on figure 4.3.16 the racetrack effect can be noticed. This means that the closer to the inner bend wall the stream flows the sooner it will reach the outlet. Also, the mass close to the outer wall surface has a higher residence time than that of the inner wall. The differences are more pronounced at the beginning of the bend moving on until the middle and then, towards the end, the residence time is becoming high for the entire product that flows and is in touch with the walls. The flow is that slow that when part of it is exiting the bend some of it has not even completed the curve. Additional comments can be made on the bottom at the end of the turn where a quite large volume of red (high residence time) path lines can be observed. This might be a characteristic of the flow that contributes to the lower temperature at that area, as seen on figure 4.3.15.

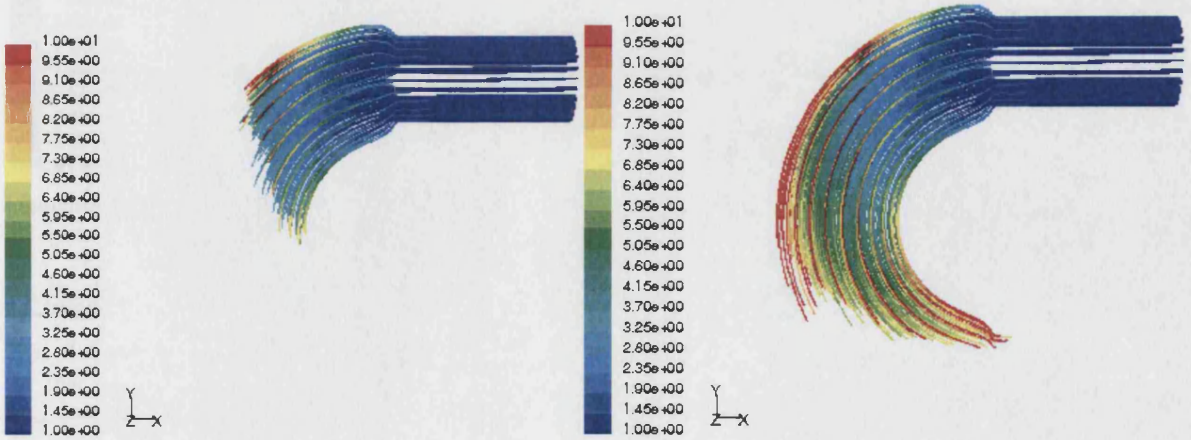

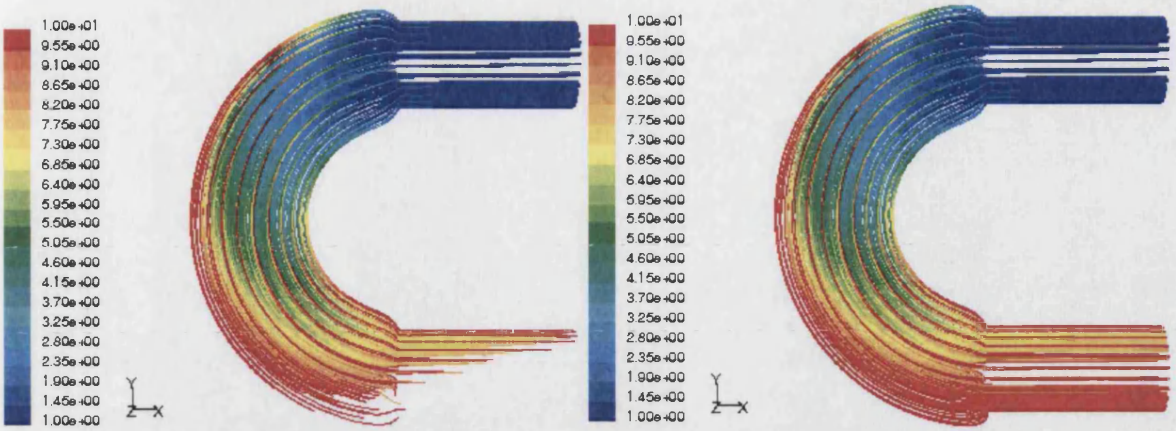

Figure 4.3.16: Path lines of mass less particles that follow the flow in the bend coloured by residence time.

Shear stress filled contours (fig. 4.3.17) show that on the inner wall the values are higher (~175-200Pas) compared to the outer (~125-150Pas). So, on the walls of the first bend the difference is around 50 Pas. The maximum shear stress appears at the beginning of the second heating section and is approximately 400Pas. The outlet of the first heater gives lower values but still higher compared to the bend walls. As expected, expansions in the flow minimise the wall stresses to practically zero and the contraction that leads to the second heater is a big and sudden change for the product.

Figure 4.3.17: Contours of wall shear stress on the first bend

2nd bend

The difference between the two connection bends is that they were modelled in such way that for the first one the inlet is at the top and for the second it is at the bottom. So, in the second one the flow moves upwards. The behaviour of the product is not much different, considering also the fact that velocity is not varying significantly throughout the whole configuration. Again, temperature contours (fig 4.3.18) show a region of high temperature as soon as the product

enters the bend. The green colour that corresponds to this represends approximately 384-386K. The rest of the bend wall is quite stable to around 382-384K and again as it approaches the exit the temperature drops to around 380-382K (light blue coloured).

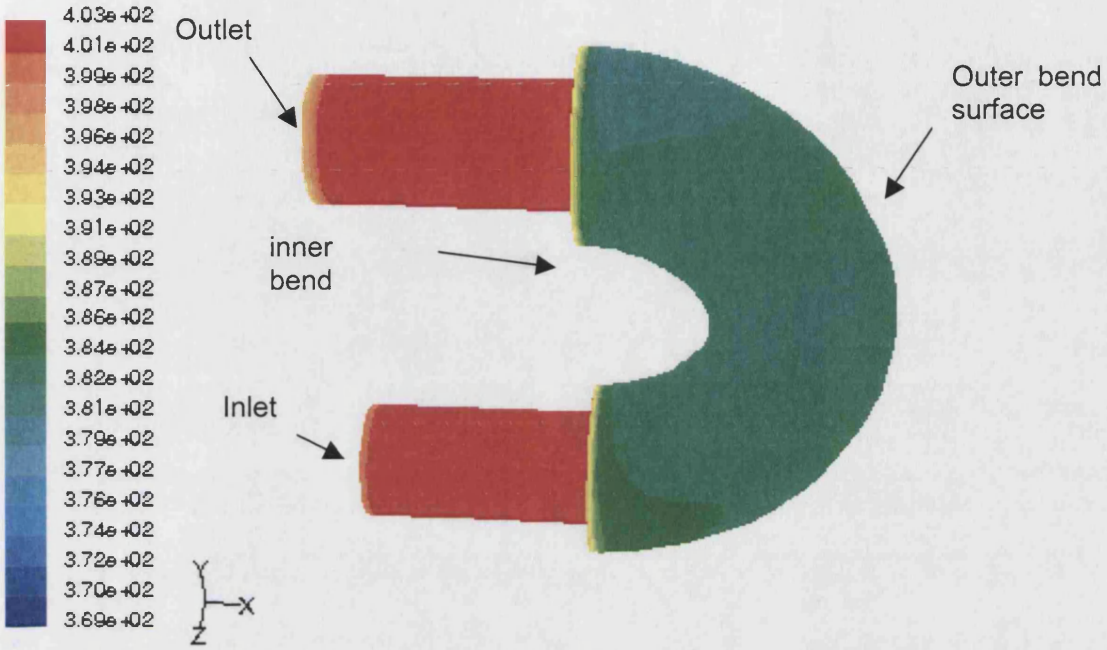

Figure 4.3.18: Temperature contours on the walls of the first bend.

The path lines of mass less particles (fig 4.3.19) show now a different behaviour to the direction. Now the product comes from the bottom end of the bend and moves its way to the top. Again the race track effect takes place with the product closer to the inner wall moving faster than the rest. Gravity is not affecting the flow by dragging it backwards or causing any noticeable delays. The path lines are given based on the same residence time scale as was done for the first one so that they are comparable. There is no evident difference, apart from possible longer residence towards the end of the flow, if it is determined that the density of the red lines is higher at the exit. Once again, the large volume of red path lines at the top of the bend before entering the heater explains the lower temperatures in that area.

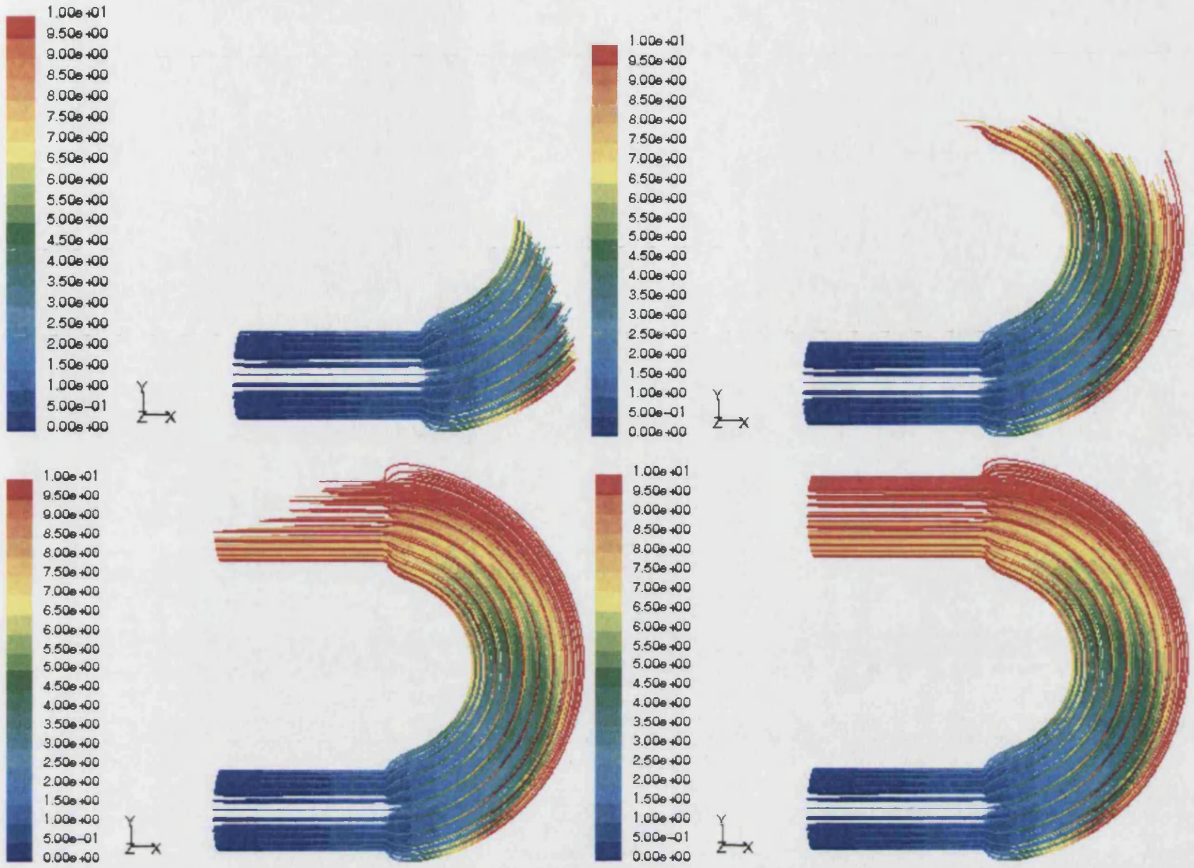

Figure 4.3.19: Path lines of massless particles that follow the flow in the bend coloured by residence time.

The contours of wall shear stresses on the second bend (fig 4.3.20) have similar distribution, although lower values, to the first bend. Thus, the inner wall shows a variation of 147-168Pas, the outer 105-126Pas and the outlet straight after the bend on the wall of the beginning of the third heater is 357-378Pas. The difference between the inner and outer wall surface is approximately 40Pas, just below the corresponding value for the first bend (fig 4.3.17). Generally, values are slightly but not significantly lower.

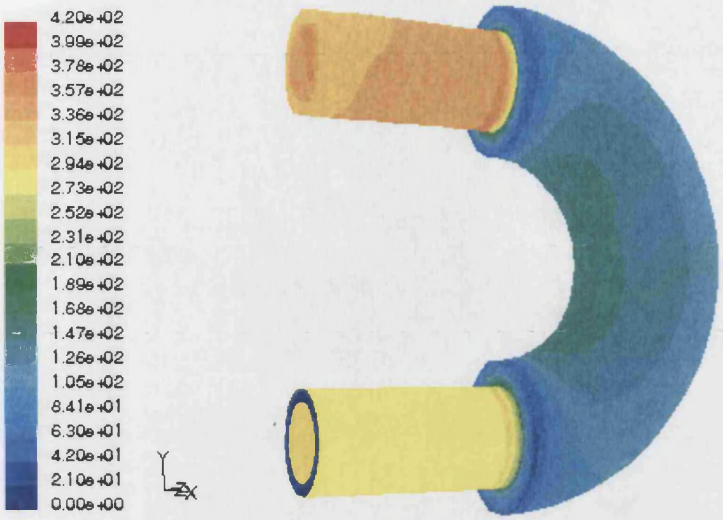

Figure 4.3.20: Contours of wall shear stress on the second bend

4.3.3 Conclusions for the shear thinning flow model

The agreement between the model and the real in line measurements taken on the bend while the production was in progress is not very satisfactory. Nevertheless, the operator's measurement at the end of the heating is very close to the final temperature given by the CFD model. This is very encouraging; since this sensor is taking values from inside the geometry, directly in contact with the product, while the Pt100s are attached on the walls of the bends assuming that they correspond to the internal temperatures. Having inspected the configuration of the heating in combination with the way the heating medium is supplied, the inconsistency of the measurements can be explained. It is more likely due to the conduction that takes place since the entry of the heating medium to the system is occurring from tubes ending on the bends.

Generally, the product has plug flow in the tubes and at the bends there is mixing (or/and conduction) which contributes to the better distribution of heat. That is why it always enters a subsequent heater with a higher temperature in the centre of the flow, compared to the value when it left the previous one. There were no stagnant areas found in the bent tubes and temperature was distributed smoothly.

4.4 Comments on Steady State models

This chapter described the steady state models that were carried out and are linked to the thermal processes in the food industry for Newtonian and non-Newtonian fluids. The agreement so far is acceptable and describes the temperatures in a very satisfactory qualitative way. This is especially so in the T-piece, where the conditions cannot be assumed or predicted and the only flow parameters are set in the horizontal pipe. Simulations were fairly quick for the down stand as well as for the bends, in order to obtain convergence. The straight TnTnT heaters were more expensive computationally due to the much higher amount of cells. Every time the solution obtained was quite straightforward, without complexities. Experimental set up difficulties resulted from the fact that CFD modelling had to be kept in mind so that boundary

conditions could be simulated especially the maintenance of a constant temperature at the inlet of the rig.

The next chapter deals with transient flows. Initially steady flow conditions are achieved and cleaning follows with deionised water at high velocities. Two set of experiments took place in the rig: one based on electrical conductivity measurements and the other on bacteria counts in order to assess mass removal from the T-piece.

5 Transient experiments and simulations: Results and discussion

This chapter describes experiments and simulations that were aimed at examining transitional flows. The experiments consisted of two parts: firstly extended runs to establish a specific temperature and flow regime and then cleaning the rig for a particular period of time under known temperature and flux of deionised water. Accordingly, the simulations were comprised of two parts: first the solution of the desired regime was obtained and, later, using this solution every time as initial condition into the rig, inlet and boundary fields were set in order to start the second part of the transient computation. Results were compared to the experimental measurements.

The first set of experiments carried out was based upon electrical conductivity measurements, which were taken at a distance of approximately 8cm from the bottom of the T-piece. The probe was calibrated at various temperatures and concentrations of Potassium Chloride. Conductivity was measured once close to the bottom of the T-piece when steady state was accomplished and afterwards when cleaning was finished. The species model is used so as to express the concentration of the salt in the solution.

The second set of experiments was based on microbial counts using *Pseudomonas fluorescens* was used as the spoilage bacterium. It was inoculated into the rig into Tryptone Soya Broth (TSB). Sterilised needles and syringes were used for sampling from ports on the vertical pipe. Samples were taken after cleaning as well from the same ports. Pour and spread plate techniques were applied in order to estimate concentrations of bacteria together with some spectrophotometry measurements. Those experiments were simulated with FLUENT using the species model in order to describe bacterial concentrations and reactions, the rate of which was integrated into the solution with the help of a UDF. Both parts of the simulation were transient, since microbial kinetics are time and temperature dependent.

5.1 Electrical Conductivity based measurements

There were two experiments carried out under similar velocity and temperature conditions but different initial concentrations of salt. This part of the work is the first attempt to simulate the CIP principles. The aim was to check if CFD can predict mass removal from the specific geometry. In the experiments the concentrations were measured by measuring the electrical conductivity of the solution using a probe that was placed in an upward position at the bottom of the T piece. The value of electrical conductivity was taken at a distance of approximately 8cm from the end of the vertical pipe and 15.5cm from the centre of the bulk flow.

After establishing steady state conditions in the T-junction, cleaning was simulated using only water under highly turbulent flow conditions ($N_{Re}\approx17000$). Results of the simulation were compared with experiments carried out using Potassium Chloride solution that was flushed out with deionised water. The velocity of the cleaning water was $0.75ms^{-1}$.

The model predictions were compared with the experimental results. The predicted concentrations were in good agreement with the electrical conductivity measurements from the probe. These results showed that mass removal can be predicted and hence the implications of

equipment geometry on removal of materials during the cleaning process. This model offers the potential to be used to assess the risks of microbial growth, inactivation and removal after cleaning process equipment by understanding the interaction of cleaning fluids with the equipment being cleaned.

5.1.1 Experimental set up modifications

There were two experiments that took place: one with salt concentration of $5mgl^{-1}$ ($0.005gl^{-1}$) and another one of $2.5mgl^{-1}$ ($0.0025gl^{-1}$). In both cases, steady state was established with flow of $500lthr^{-1}$ (or $0.5m^3h^{-1}$). Afterwards, the rig was cleaned for 3.5min flushing through the system deionised water at the maximum flow possible which was approximately $1320l.h^{-1}$. The removal of the salt solution was measured by comparing the electrical conductivity values before and after the flushing. A probe was fitted at the bottom of the dead leg (fig 5.1.1) and was taking measurements on the central axis of the geometry, just below the 5^{th} thermocouple. The probe was calibrated for various temperatures and salt concentrations in order to estimate the remaining salt (Appendix 9).

In general, the rig configuration remained the same as it was described in chapter 4. Only the thermocouple at the bottom of the vertical pipe was removed so that it would not interfere with the probe measurements. The temperature gradient was minimised in order to avoid fluctuations of the electrical conductivity, which is quite sensitive to temperature changes. Also, for the cleaning there were two tanks of approximately 20lt capacity each (fig 5.1.2) that were used to supply water of high velocity into the system.

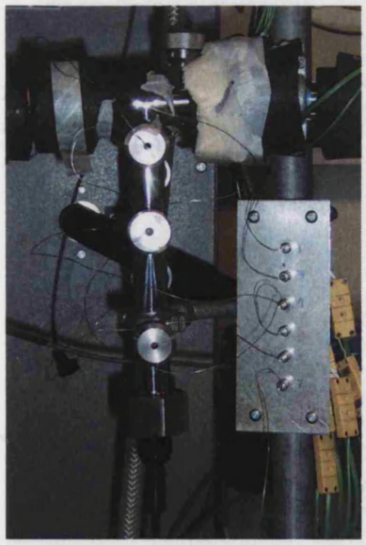

Figure 5.1.1: Probe location for electrical conductivity experiments

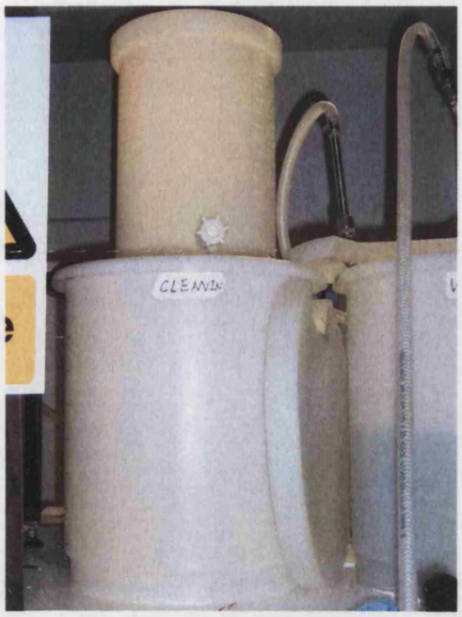

Figure 5.1.2: Tanks used for cleaning.

5.1.2 First electrical conductivity experiment and model

During the first experiment flow was $500 l.h^{-1}$ in order to establish steady state. Cleaning was carried out at the highest flow that could be obtained, $1320 l.h^{-1}$ ($N_{Re} \approx 17000$). The salt content was described by using the species model where the mass fraction at the inlet is set.

The temperature distribution down the centre of the vertical pipe is compared to the measurements taken during the experiments. From the same area were also taken the predicted values of the KCl concentration both at steady state and after flushing for 3.5 minutes.

The properties of the water and steel walls are the same as for the previous flows.

The boundary conditions for the steady state model are:

$u_{in}=0.336 ms^{-1}$

$T_{in}= 297.5K$

$T_{env}=292.5K$

$h_{ver} = 5.7 Wm^{-2}K^{-1}$.

$h_{hor} = 2.4 Wm^{-2}K^{-1}$.

Hence, steady state was accomplished with salt concentration of $0.005 gl^{-1}$ and inlet temperature of 297.5K. At the end of the run, the concentration is the same throughout the whole rig and equal to the aforementioned number. The temperature difference between the top and the bottom of the T-piece was kept low in order to avoid errors due to the electrical conductivity probe sensitivity. Figure 5.1.3 shows the agreement of the model with the experiment for the temperature distribution. It is satisfactory and similar to the $600 l.h^{-1}$ that, as explained in paragraph 4.2.3, is a similar profile with a slight offset on the right. The thermocouples used are five this time since one of them was removed to allow space for the conductivity probe.

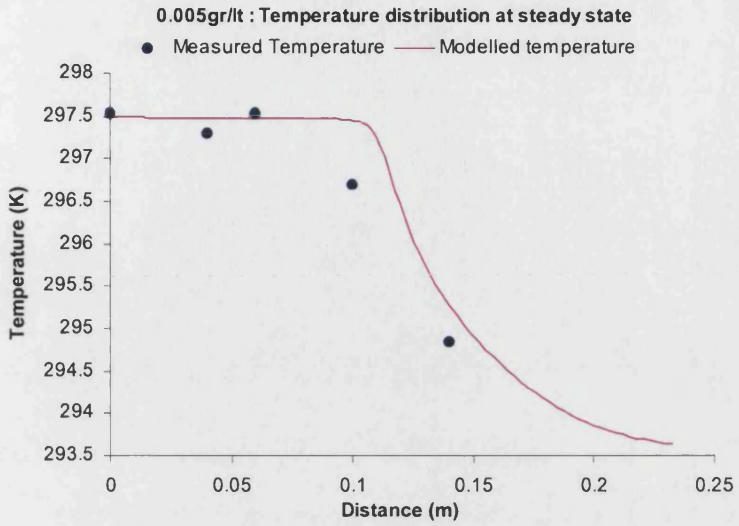

Figure 5.1.3: Temperature distribution comparison between model and 1st experiment in the centre of the vertical tube before cleaning.

At steady state, the temperature given by the 5th thermocouple (the closest to the electrical conductivity probe) is just below 295K. The electrical conductivity measured before the cleaning, assuming at 295K, was 5.9mScm^{-1}.

Again, temperature dropping point is where velocity becomes very low as well (fig 5.1.4), similar to the remarks made for the steady state flows in chapter 4 (e.g fig : 4.2.18, 4.2.26, 4.2.31).

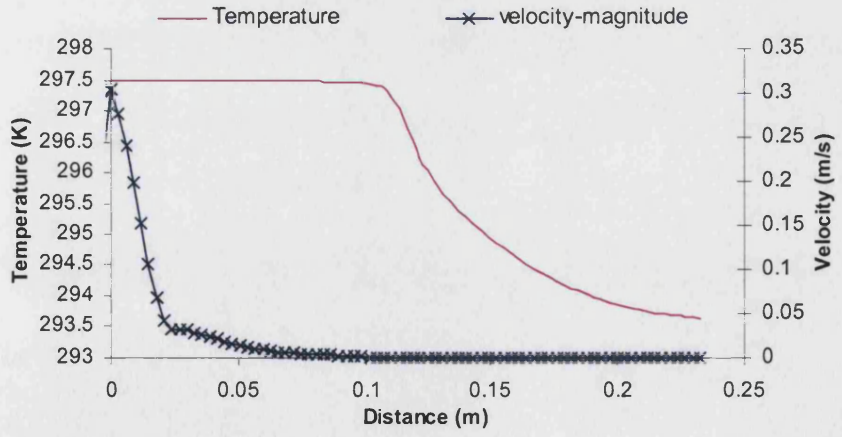

Figure 5.1.4: Velocity and temperature distribution predicted down the T-piece for first experiment steady state

Cleaning follows with deionised water and carries on for 3.5min. The boundary conditions for this part of the model are:

$u_{in} = 0.74ms^{-1}$

$T_{in} = 291.5K$

$T_{env} = 292.5K$

$h_{ver} = 2.55Wm^{-2}K^{-1}$.

$h_{hor} = 1.9Wm^{-2}K^{-1}$.

Water flow rate is $1320l.h^{-1}$, which is the maximum flow obtained with the existing conditions and is fully turbulent. The water was coming from the supply of the two tanks used from quite high above the rig. Again the temperature gradient was low, as it can be observed on figure 5.1.5. Between the top and the bottom of the vertical pipe the difference is only 3.5 degrees. The agreement with the model is very good. We see that at the bottom the temperature remains high and, specifically, below the 15cm the profile is the same as in figure 5.1.4. The water has not reached that area and the 3.5min of flushing is not enough time to affect the temperature due to conduction.

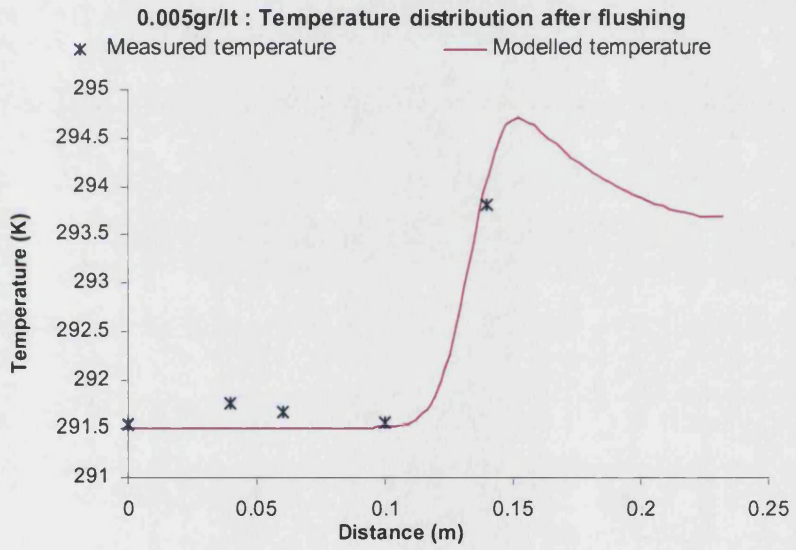

Figure 5.1.5: Temperature distribution comparison between model and 1st experiment in the centre of the vertical tube after cleaning.

After flushing, temperature measured by the 5th thermocouple is just below 294K. The highest maintained temperature is at 15.2cm (fig 5.1.6). At a first look this is approximately where the interaction between the bulk flow and the vertical tube stops, since velocity drops quite suddenly at that point. Noticing fig 4.2.30, from paragraph 4.2.5, it can be seen that this height is approximately where the velocity becomes practically zero for the slightly higher flow of $1340l.h^{-1}$, although for that steady state flow the drop is steeper. Later on, in the same paragraph, are compared the velocity and residence time path lines in order to get a better idea of the transient flow.

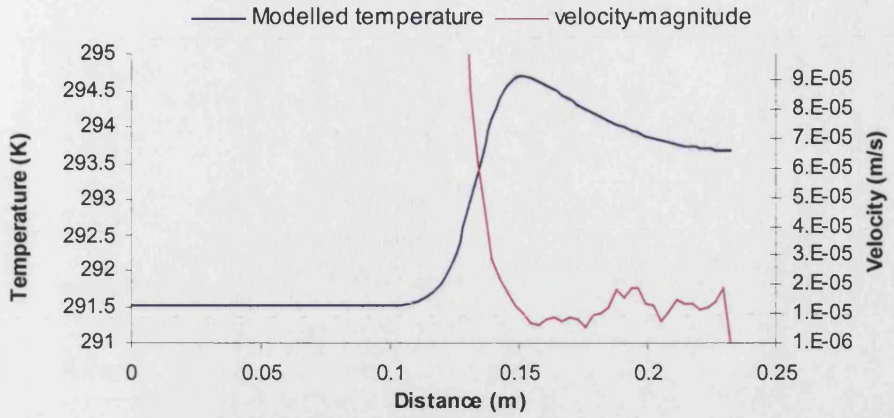

Figure 5.1.6: Temperature distribution compared to the point where velocity drops significantly.

So, the calibration curve for 294K given in the appendix 9 can be used in order to see the relationship between conductivity and concentration. The electrical conductivity measured before and after the cleaning was 5.9mScm^{-1} and 2.84mScm^{-1} correspondingly. Figure 9.1 in Appendix 9 shows that for 294K and 2.84mScm^{-1} concentration is approximately 0.0019gl^{-1}. The probe measures that at around 8cm from the bottom or 15.5cm from the top. The above concentration of 0.0019gl^{-1} corresponds to approximately 13.5cm from the top of the t-piece (fig. 5.1.7), according to the model. So the code overestimates the height of the removal by almost 2cm.

This can be accepted, considering that the electrical conductivity probe is one for laboratory use and not an industrial one that is fitted in-line. Thus, sensitivity to fast changes is not very high. Also the exact location point of measuring the values with the probe cannot be determined with accuracy during the experiment. We can see from figure 5.1.7 that between 0.1m and 0.15m the concentration changes rapidly and small movements of the probe could give different measured values. Moving the probe though was not feasible, since the pressure developed down there was pushing the probe out of the system and had to be very steadily fixed in the pipe. So it was constrained to take measurements at one place.

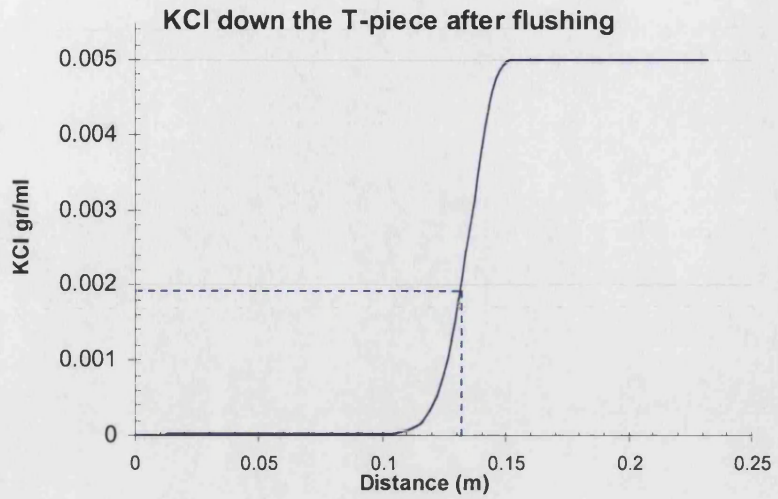

Figure 5.1.7: KCl mass concentration down the centre of the T-piece for the1st experiment predicted by FLUENT.

At the outlet of the rig the conductivity was measured after the end of the experiment and was equal to 0.52mScm^{-1} at 291.5K. This was achieved by taking a sample from the outlet and removing the probe from the dead end in order to find out the value. This was very close to the deioniser indication at that time, where the water was taken from.

On figure 5.1.8 contours of static temperature on a vertical surface cut along the centre of the dead leg show the distribution at steady state, just before cleaning starts.

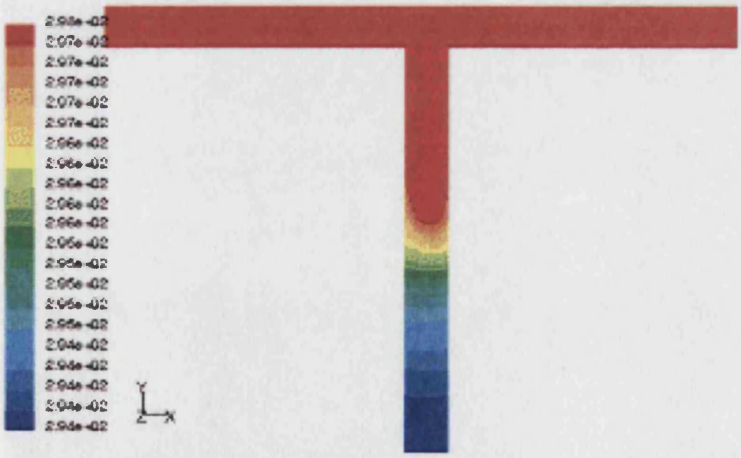

Figure 5.1.8: Contours of static temperature on a vertical cut surface across the T-piece at steady state for the 1st experiment

Later on, on figure 5.1.9, contours of the same area and magnitude are depicted for 1.5s, 2s, 3s, 5s, 10s, 16s, 1min and 3.5min. It can be observed that the temperature drops as time passes and goes down to lower depths. Looking at the temperature contours at 3.5min in combination with figure 5.1.5, we can see how the KCl solution is trapped at the bottom of the

T-piece. Also, once the water is into the T-piece, it penetrates the down stand slowly and takes time to reach lower depths. After 10s is starting getting into the vertical pipe and then it takes 60sec to reach the centre of it. Between 60sec and 3.5min the difference of the depth in the pipe is very small. Hence, it would take much longer time and higher fluxes in order to clean the whole length.

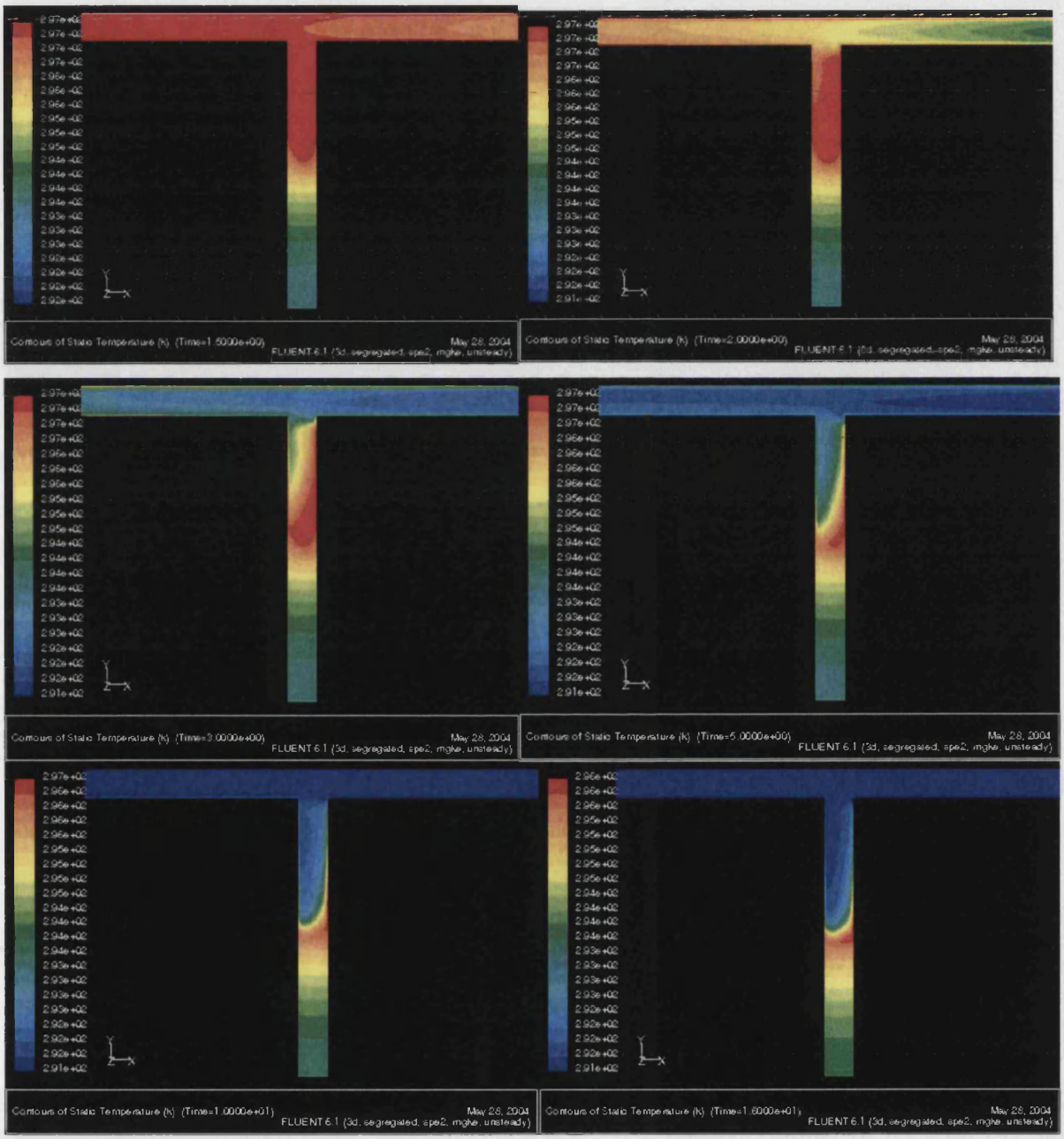

(continues in next page)

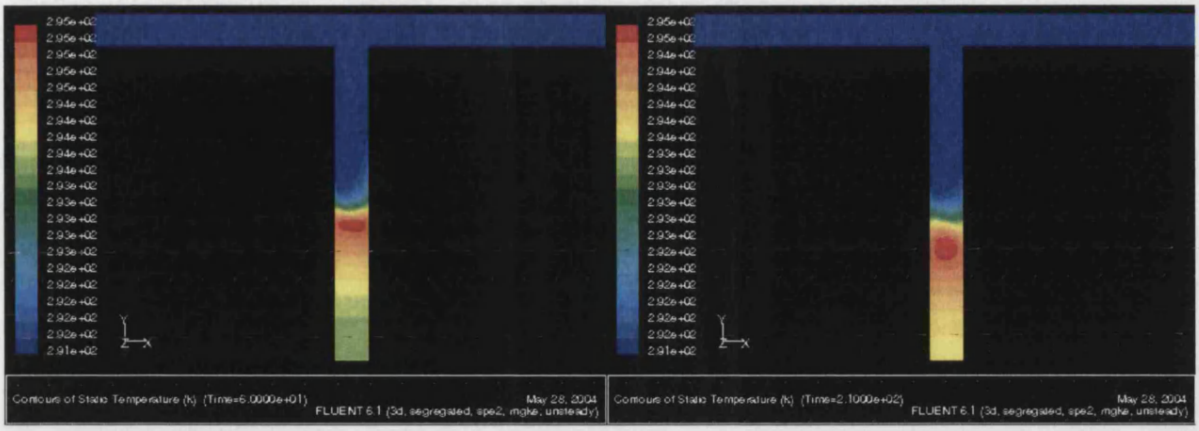

Figure 5.1.9: Contours of static temperature in the central area of the vertical tube for 1st experiment at different time steps of cleaning.

For the same time steps we can see the mass fraction of KCl at the same area of the geometry (figure 5.1.10). It can be noticed that concentration drops as time passes and so the solution is removed form the T-junction. Between 1 minute (60sec) and 3.5 minutes the difference is not that big. The images show that there is a part of the geometry where a kind of mixing area exists, during that period, above which the solution is almost free of salt. This shows that the interaction with the bulk flow becomes stronger as time passes, although slower, since the threshold of the mixing area goes down very slowly. Turbulence goes deeper into the dead leg area and cleans it better at that flow. Also, the removal happened towards the end of the flushing time, since it was observed during the experiment that the electrical conductivity was not changing, not until 3.5min had elapsed.

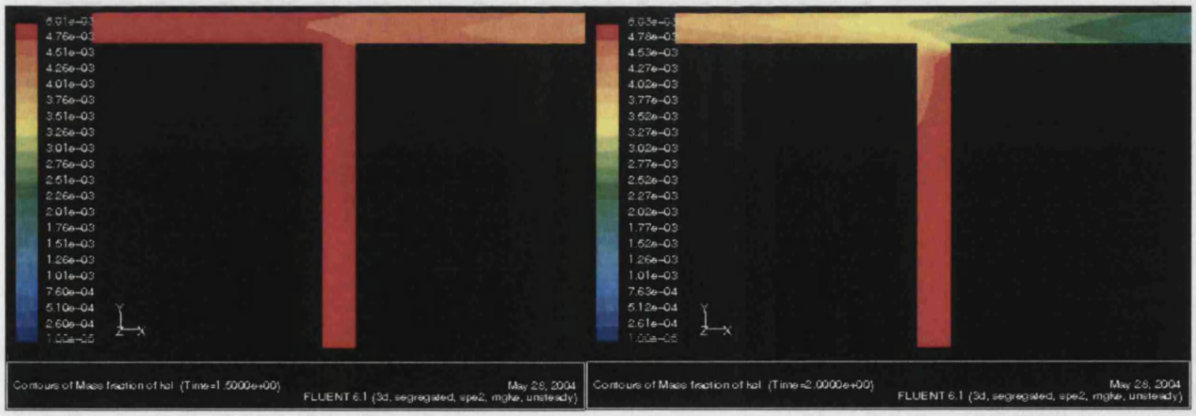

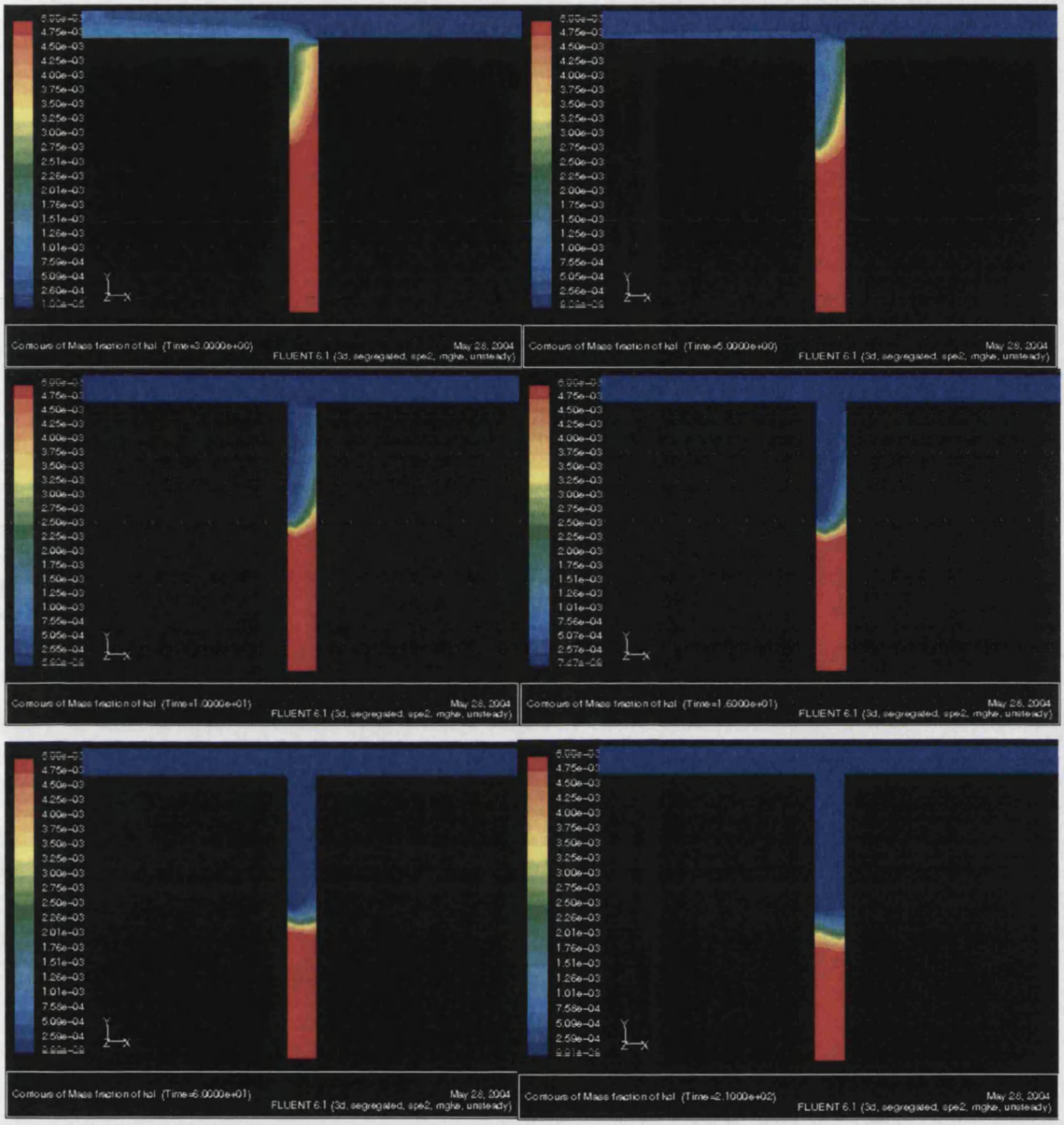

Figure 5.1.10: Contours of mass fractions in the central area of the vertical tube for 1st experiment at different time steps of cleaning.

Figure 5.1.11 shows the comparison between the path lines of the specific transient model of cleaning at 1320$l.h^{-1}$ and the steady state one of 1340$l.h^{-1}$ described in paragraph 4.2.5, accepting that the comparison is feasible since the flows are very close to each other and the differences in the parameters that transfer phenomena depend on, such as velocity and residence time are not significant. We notice that maximum velocity is slightly lower now since the bulk flow inlet velocity is lower as well. The shape of the eddy formed is similar for both cases, although we notice that there is more contact with the left wall. This effect is probably due to the fact that the flow is not completely developed yet and because the fluid entering the

vertical pipe meets the volume already there and carries it away. Due to this sweeping and the unsteady flow we note that this recirculation stops at around 14.5-15cm, which is slightly higher compared with 16cm in the case of the steady state of 1340$l.h^{-1}$ where the eddy separates from the stagnant area.

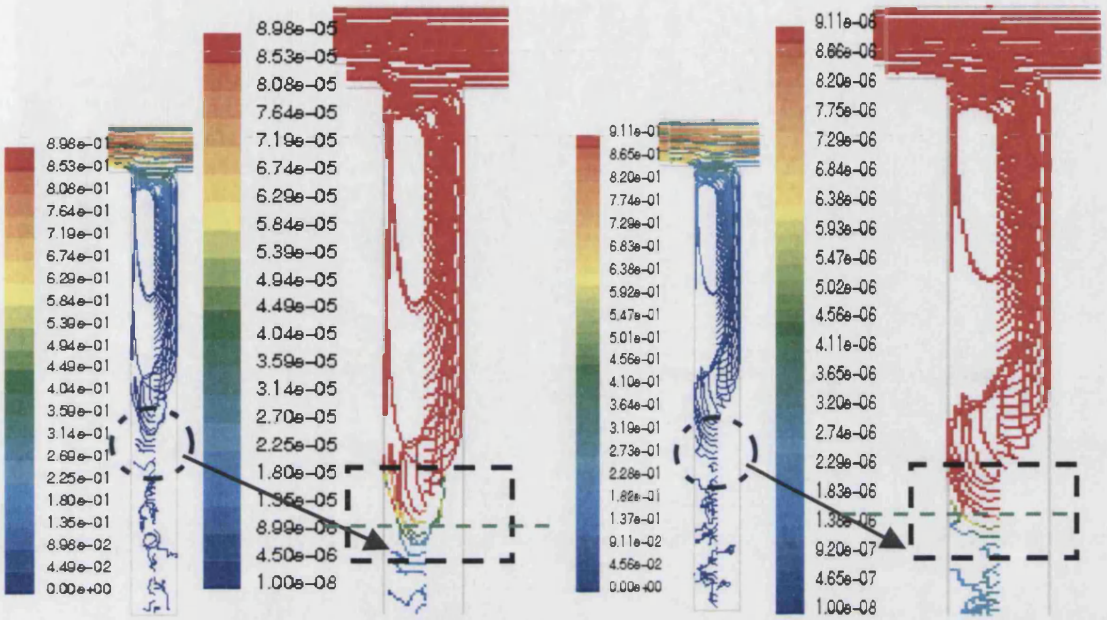

(a) (b)

Figure 5.1.11: Comparison between path lines coloured by velocity magnitude released from a vertical line coinciding with the central axis of the down stand and the inlet surface for the transient cleaning of 1320lthr^{-1} (a) and the steady state of 1340lthr^{-1} (b).

Similar conclusions can be drawn by observing the path lines coloured with the same residence time limits (figure 5.1.12). We see that the eddy is cut off from the bottom and creates a stagnant area further down the tube at steady state. Some particles at the end of the recirculation zone, in the transient flow, seem to have the tendency to escape but the high residence time and the incomplete paths show that they remain there.

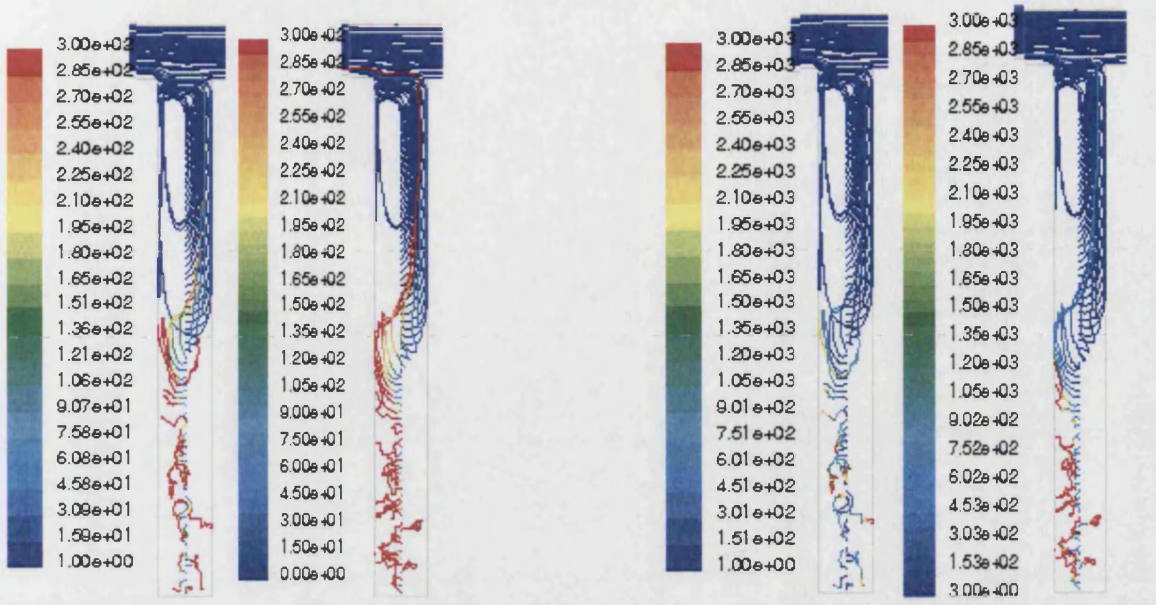

1320*l.h*$^{-1}$ transient 1340l.h^{-1} steady state 1320*l.h*$^{-1}$ transient 1340*l.h*$^{-1}$ steady state

(a) (b)

Figure 5.1.12: Comparison between path lines coloured by residence time released from a vertical line, coinciding with the central axis of the down stand, and the inlet surface for the transient cleaning of 1320*l.h*$^{-1}$ and the steady state of 1340*l.h*$^{-1}$ ranging from 1-300sec (a) and 1-3000sec (b).

5.1.3 Second electrical conductivity experiment and model

The second experiment was carried out with an initial salt concentration of 0.0025grml^{-1}, which is half the initial concentration of the previous experiment.

The properties of the water and steel walls are the same as for the previous flows.

The boundary conditions for the steady state model are:

u_{in}=0.336ms^{-1}

T_{in}= 297.5K

T_{env}=294K

h_{ver} = 5.8Wm^{-2}K^{-1}.

h_{hor} = 2.8Wm^{-2}K^{-1}.

Initially, with inlet temperature of 297.5K followed by cleaning for 3.5 minutes with deionised water at 292K. The temperature in the lab during that experiment was also approximately 292K. The comparison between model and experiment for the steady state is given on figure 5.1.13. The agreement is satisfactory with the plateau of constant temperature slightly extended further down the tube. At steady state, the temperature given by the 5th thermocouple (the closest to the electrical conductivity probe) is just below 296K

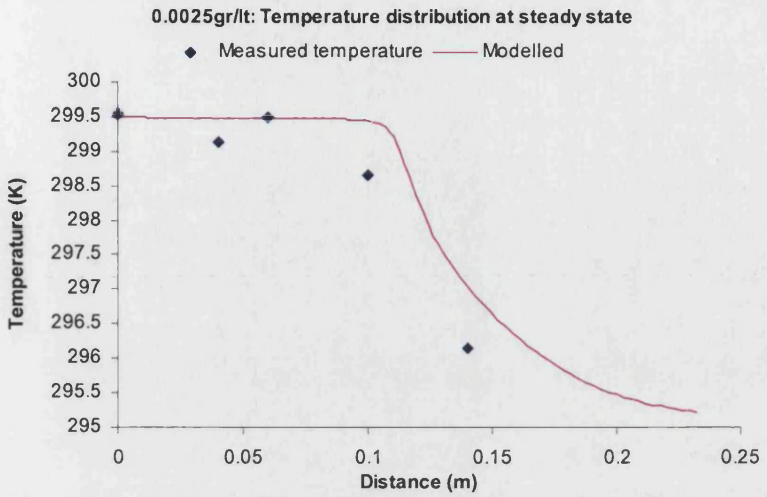

Figure 5.1.13: Temperature distribution comparison between model and 1st experiment in the centre of the vertical tube before cleaning.

Afterwards, cleaning follows at $1315 l.h^{-1}$ with the boundary conditions applied as:

$u_{in} = 0.722 ms^{-1}$

$T_{in} = 292K$

$T_{env} = 294K$

$h_{ver} = 3 Wm^{-2}K^{-1}$.

$h_{hor} = 2.1 Wm^{-2}K^{-1}$.

The temperature after flushing where the 5th thermocouple is located, reaches almost 294.5K (fig 5.1.14). The agreement is good again taking of course into account the fact that temperature variations are not significant.

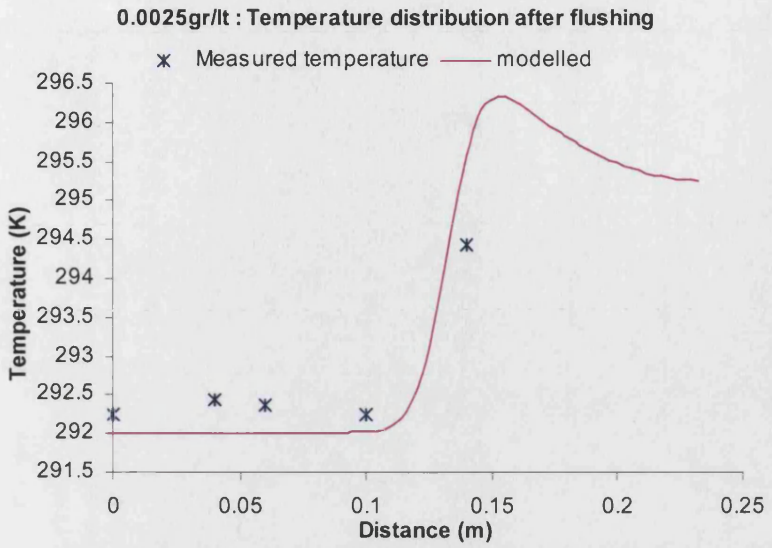

Figure 5.1.14: Temperature distribution comparison between model and 2nd experiment in the centre of the vertical tube after cleaning.

Figure 5.1.15 depicts temperature and velocity on the same plot. The first one (fig 5.1.15 (a)) gives the whole range of the two quantities and the other (fig 5.1.15 (b)) gives a narrower range and focuses on the values towards the bottom of the geometry. There we can see that the drop happens again at around the 15th cm after which, there are no changes and numbers stay low. This can be compared to the correspondent plot for the flow of 1340lthr^{-1}on figure 4.2.30. We see that velocity drops at the same point approximately, despite the trapped salt solution. Thus, at first glance, for this period of 3.5min and the specific fluid, the fluid already in the T-piece does not inhibit cleaning and the velocity profile in the centre is not considerably affected.

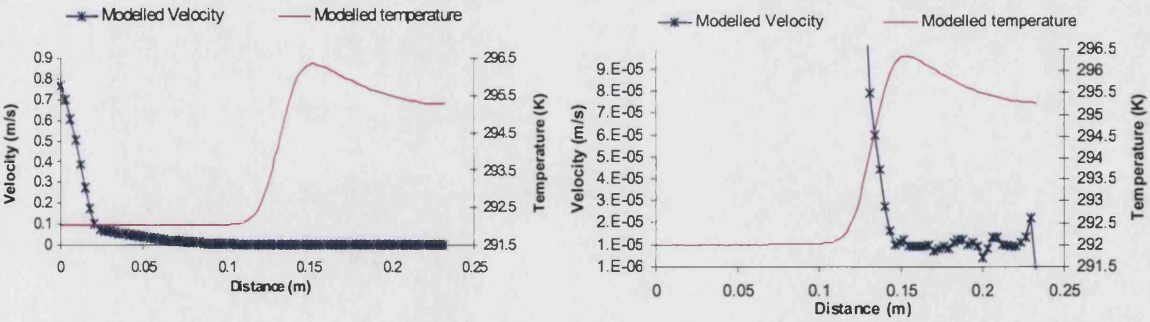

(a) (b)

Figure 5.1.15: Temperature and velocity distribution for the 2nd experiment in the centre of the vertical tube after flushing, where (a) is the whole range and (b) shows the length where velocity almost zeroes.

The calibration curve used is the one for 294.5K given in the Appendix 9. Before flushing electrical conductivity is 4.5mScm^{-1} and after cleaning has taken place for 3.5 minutes, 2.12mScm^{-1}. On the XY plot of figure 9.2 we can see that for 2.12mScm^{-1} at 294.5K

concentration is approximately 0.0017gl^{-1}. For that concentration figure 5.1.16 estimates the predicted length by FLUENT. In that case is approximately 14cm above the bottom of the T-piece. Therefore, again there is an overestimation of around 1.5 cm, which is a pretty similar deviation to the one noticed for the previous experiment. Again, it was observed during the experiment that the conductivity did not start dropping until cleaning was reaching its end. Hence, it is more likely that keeping the same flow for longer time we would have more removal of salt.

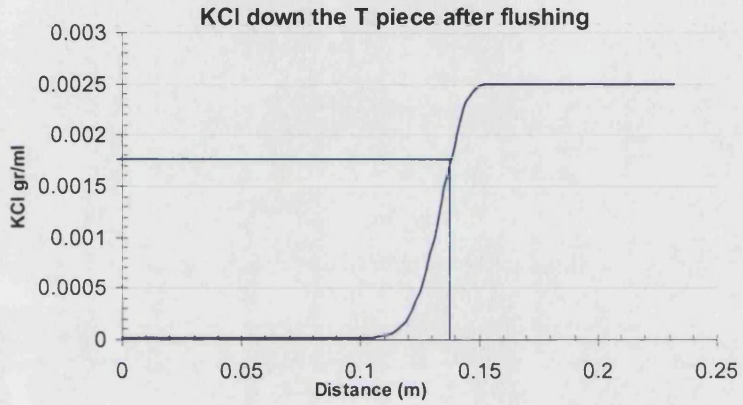

Figure 5.1.16: KCl mass concentration down the centre of the T-piece for the 2nd experiment predicted by FLUENT.

In order to get a better description of the flow, contours of temperature on a vertical cut surface are shown on figure 5.1.17. This is how the temperature distribution appears at steady state when salt concentration is homogeneously distributed and is also the initial condition when cleaning starts.

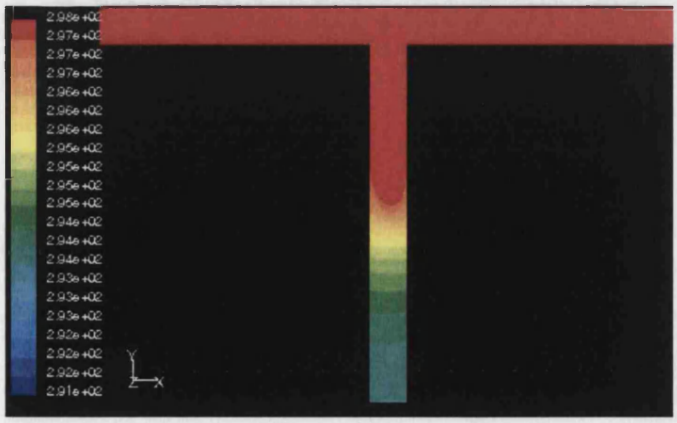

Figure 5.1.17 Contours of static temperature on a vertical cut surface across the T-piece at steady state for the 1st experiment

Hence, initial temperature distribution applies as shown on figure 5.1.17 and figure 5.1.18 shows how cleaning affects at various stages of the process. The result is similar to the images that correspond to the previous experiment.

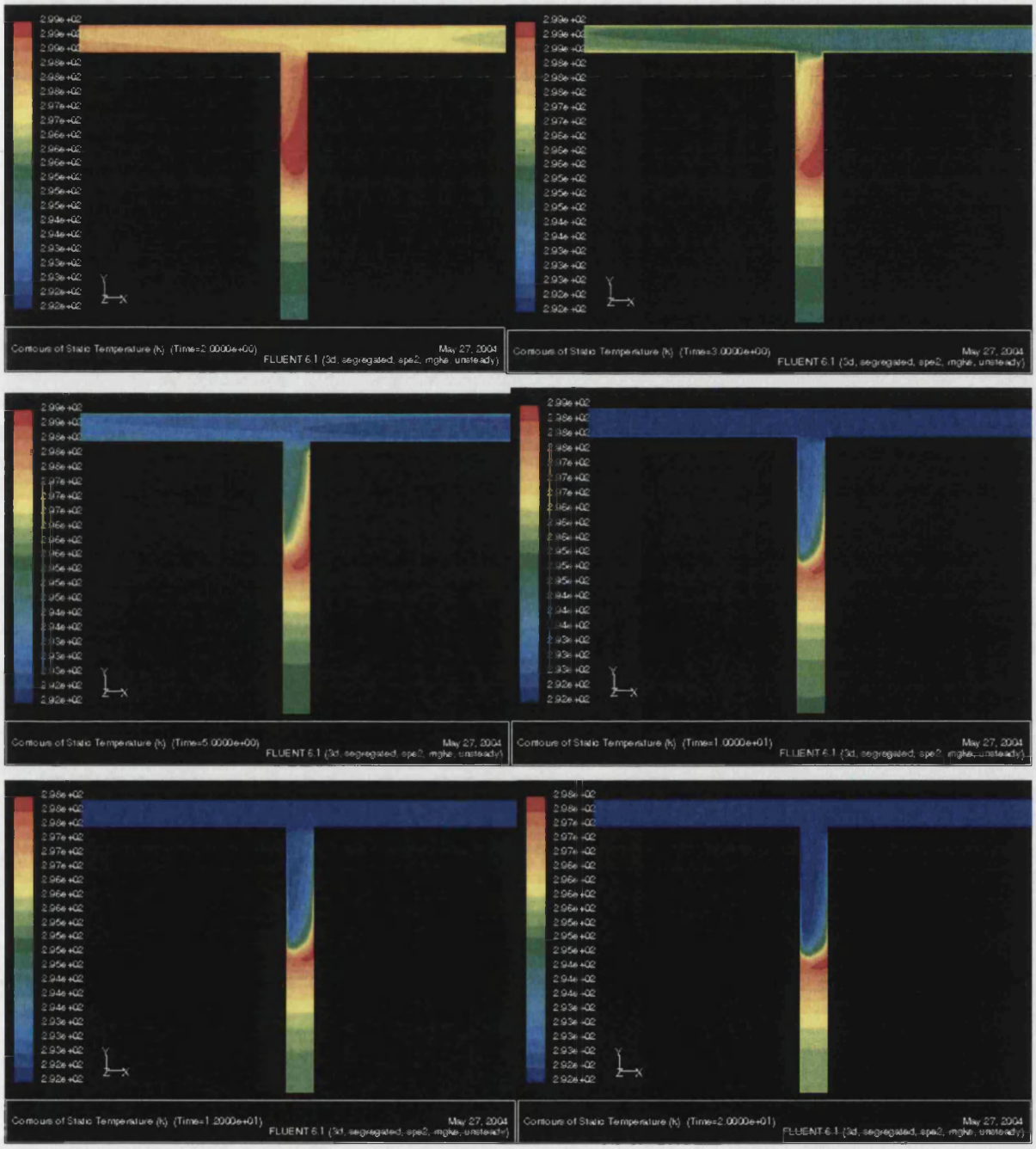

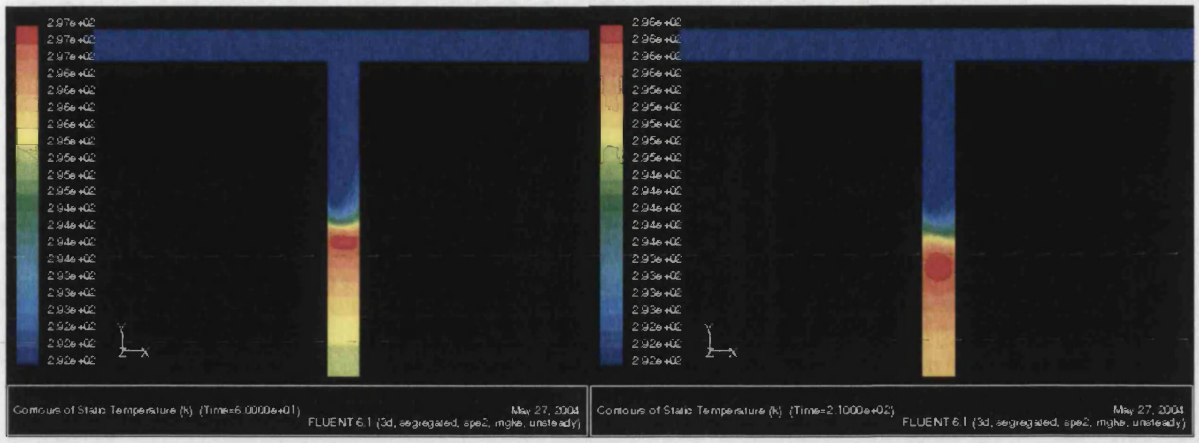

Figure 5.1.18: Contours of static temperature in the central area of the vertical tube for 1st experiment at different time steps of cleaning.

Comparing temperature contours between the similar flows of 1315$l.h^{-1}$ that lasted 3.5min and the 1340$l.h^{-1}$ where steady state was achieved, we can see that this period of time was not probably enough for temperature to reach the maximum depth (fig 5.1.19). We can see the hot spot formed for the transient case, which means that energy transfer phenomena are not complete and the temperature drop has not reached its maximum depth yet. This hotter area has the tendency to move downwards, as one can tell observing how it moves on figure 5.1.18 between 20sec, 1min and 3.5min. It is interesting to see how this warmer area compared to the rest fluid in the vertical tube, is formed surrounded by colder fields. From figure 5.1.19 it can be seen that the area where the threshold starts is further down for steady state. So, the amount of time given for cleaning is not adequate to reach the maximum depth possible. This can be observed better later on with the path lines (fig 5.1.21).

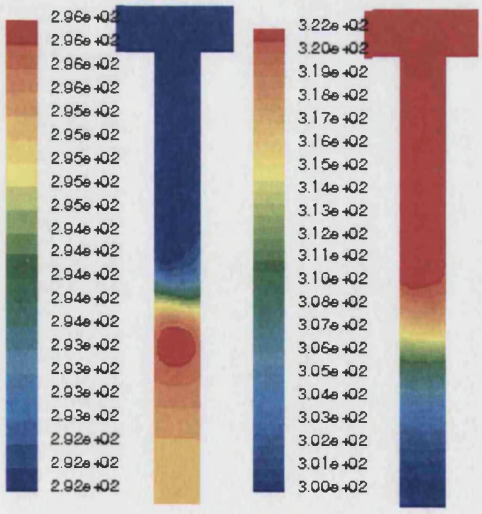

Figure 5.1.19: comparison between 3.5min cleaning at 1315lthr^{-1} and steady state 1340lthr^{-1}.

Taking contours of the potassium chloride mass fraction for the same time periods as above we see how removal and dilution zone progresses in the vertical pipe (fig 5.1.20). It is again clear

that once the cleaning solution is inside the down stand it penetrates very slowly compared to the circulation in the bulk flow in the horizontal tube.

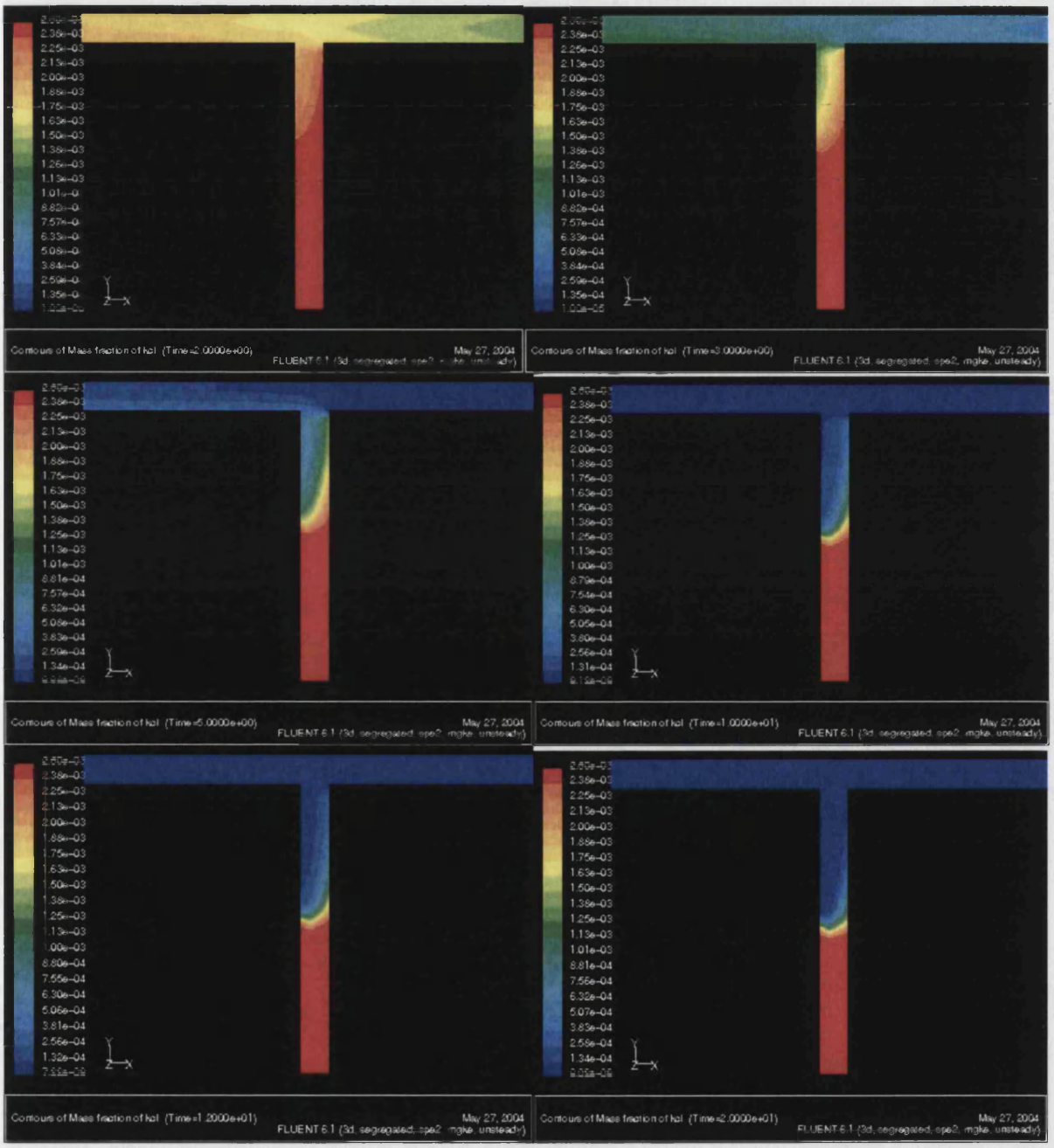

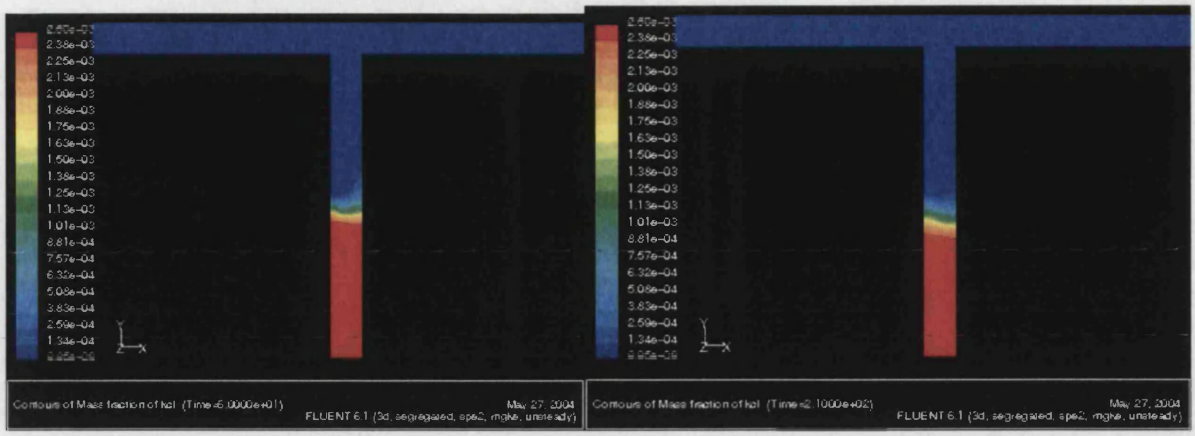

Figure 5.1.20: Contours of mass fractions in the central area of the vertical tube for 1st experiment at different time steps of cleaning.

It is very interesting to see the flow by observing the path lines of mass less particles coloured by velocity (fig 5.1.21 (a)) and by residence time (fig 5.1.21 (b)). The difference between the transient flow described here and the steady state condition of 1340lthr^{-1} is that the detachment of the eddy, formed in the vertical pipe, from the stagnant area happens at around 14.3cm, which is approximately 1.5cm higher compared to steady state. There are also some particles on the left that seem to be going to move upwards and escape but by that time it is not achieved. It can be seen that the height where velocity is practically zero is further down the pipe and so is the short residence time for the steady state. Consequently, like in the previous model described, the cleaning time was not enough to reach the maximum mass removal.

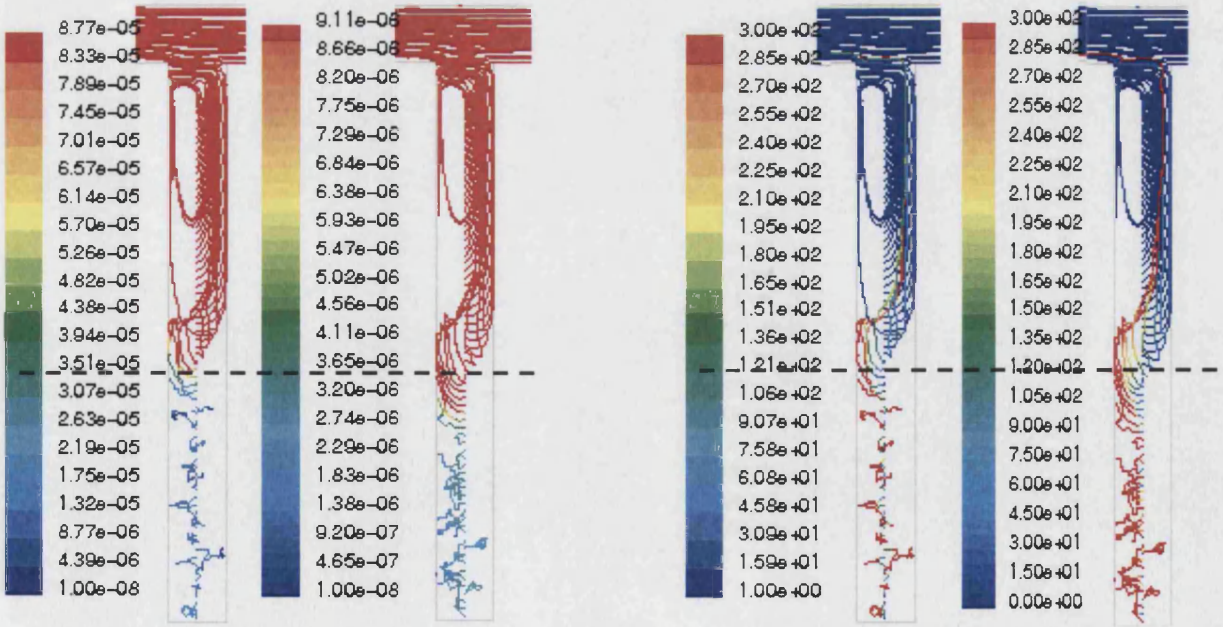

1315*l.h*$^{-1}$ transient 1340*l.h*$^{-1}$ steady state (a)

1315l.h^{-1} transient 1340*l.h*$^{-1}$ steady state (b)

Figure 5.1.21: Comparison between path lines coloured by velocity (a) and residence time (1-300sec) (b) released from a vertical line, coinciding with the central axis of the down stand, and the inlet surface for the transient cleaning of 1320$l.h^{-1}$ and the steady state of 1340$l.h^{-1}$.

5.1.4 Comments on the electrical conductivity experiments

The two experiments described above in combination with the CFD models show that in general there is good agreement between predictions and measurements. The salt is distributed homogeneously at steady state and temperature gradient is low. Large temperature variations were avoided in order to achieve better accuracy when it was coming to conductivity measurements. The probe was calibrated for various temperatures and potassium chloride concentrations. It was rather difficult to carry out these experiments and also analyse the results since the probe was not of great accuracy and due to high risk of leaking, where it was fitted, and high pressure developed in the T-piece it could not be moved in order to examine different distances within the vertical section.

The second part of the model is the transient solution, which is connected to cleaning and mass removal from part of the geometry. It is encouraging that a commercial CFD code, like FLUENT, can predict product removal from hygienically risky geometries, which are often encountered in the food industry. Although the estimations are not entirely quantitative but rather qualitative, it shows that in the turbulent regime, which is generally complicated, good choice of models can lead to reliable results, where in that case is the species model that includes mixing as well.

In the cases studied, the T-junction was not cleaned and there was salt remaining in the bottom of the dead leg. The simulation though showed that the longer the cleaning the lower the concentrations of KCl deeper down the tube, as can be seen by the contour images as the time was passing. Also, the fact that the 3.5 min for the specific flow was not an adequate amount of time can be proven by the comparison with the steady state computation for the similar flow of 1340$l.h^{-1}$.

A drawback of the experimental set up was the fact that temperature could not be monitored at the exact point where the probe was taking values. Hence, an assumption was made for the temperature and it was taken to be the same as read by the 5th thermocouple, which was closer to the bottom. Nevertheless, the predictions were very close to the experimental values despite the fact that there could be a difference of half degree of temperature for both experiments.

5.2 Bacterial kinetics based measurements

The next set of experiments is for bacterial kinetics. Hence, all the experiments are interesting from the time point of view and so are the simulations.

Firstly, a bacteria population was inoculated into a sterilised broth, of approximately 14-15lt, in an aseptic tank of 20lt capacity. Then, it was introduced into the rig under various temperature conditions, depending on the experiment. It was recirculated and after a certain chosen period of time three samples were taken from the down stand and one from the outlet. The results were compared to a sample taken from the outlet at the beginning of the experiment. The above process can be considered as the first part of each experiment.

Secondly, the rig was rinsed with deionised water and removal was measured by taking samples of the remaining fluid from the same ports, as before cleaning, and the outlet. This can be the second part.

Results are compared and growth or inactivation is observed, depending on the temperature conditions. In some cases there was no change in the concentration due to the fact that initially the solution was saturated (stationary phase 10^8-10^9). All the processes had to be done under hygienic conditions and the media used (broth, agar, syringes, needles etc.) were all autoclaved before use.

There are several experiments carried out with *Ps. fluorescens*, which is a spoilage bacterium, frequently encountered in the food processes. Pour and spread plate techniques were applied, as well as spectrophotometry.

The experiments were simulated as transient solutions in FLUENT, where the inactivation and growth kinetics are modelled as reaction equations that are temperature dependent. Not all the experiments were suitable for simulation due to lack of change in the concentrations. Hence there are three experiments chosen to be reproduced with CFD and there will be reference to the difficulties encountered while the simulation was running, including all these parameters and variables (e.g. temperature, concentrations, turbulence etc).

Before and after each experiment the rig was cleaned with peracetic acid 1000ppm in order to avoid contamination and the formation of biofilms. Avoidance of biofilms was also the reason for not running the experiments for very long times. After approximately 4 hours to notice growth of a couple of log numbers in the colony formed units was recorded.

5.2.1 First bacterial kinetics experiment

Temperatures during the run increased due to the pump adding heat into the system. The pump was not left to run for a long time, to avoid heating up the system to temperatures that would cause the death of the bacteria. The shape of the curves describing temperature versus time is exponential (fig 5.2.1) that plot T_{in} is the temperature recorded at the inlet, T_{out} at the outlet and T2, T3 and T5 are the thermocouples that remained in place at 4cm, 6cm and 14cm correspondingly.

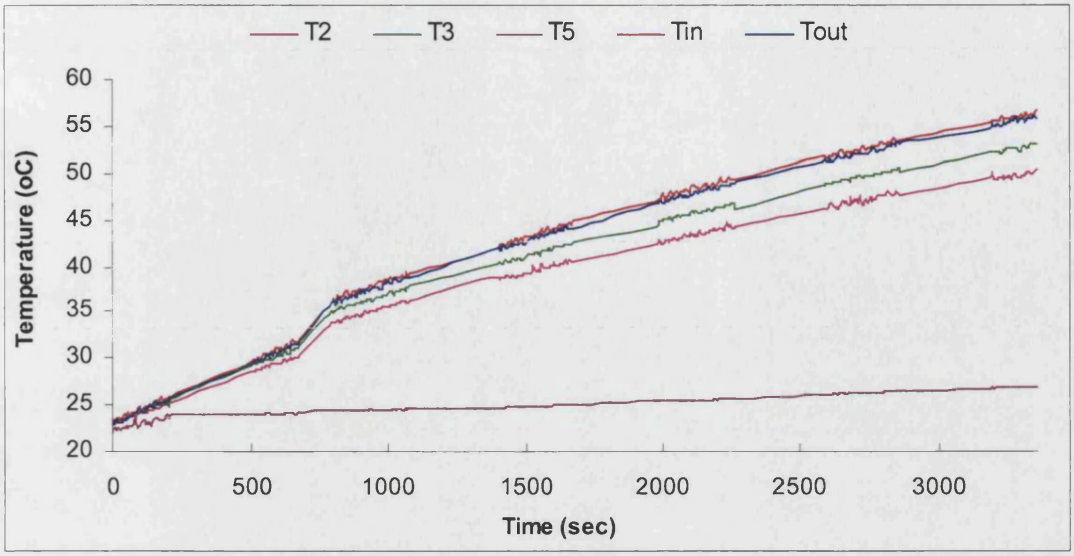

Figure 5.2.1: temperature vs. time for 1st experiment.

The microbial counts for this experiment were done with the pour plate technique. Compared to the spread plate, applied to previous experiments (data not presented), the growth appears more homogeneous in the agar Petri-dishes and this method was considered to be more efficient

This method gives generally higher numbers (probably up to one log number greater, compared to the spread plate method) and it takes longer for the bacteria to grow because there is less air supply (since *Pseudomonas* is aerobic). For this reason the counts were taken in two days time in total. First, colonies formed after approximately 38 hours were counted and then after 62 hours. This was done so that the colonies were taken into account at a time before any coalescence amongst them had occurred.

The duration of the first part of the experiment (before cleaning) is approximately 3351sec, (≈56min). The cleaning (second part of experiment) lasted 4min. The results of the plate counts and the spectrophotometry before and after flushing with water are given below in tables 5.2.1-5.2.3. In this experiment the bacteria were left overnight in the aseptic tank and maximum growth was obtained. The sample at the beginning of the experiment (feed) is taken for every experiment once the broth with the inoculum is introduced into the system and is allowed to recirculate into the rig for not long excluding from the system the T-piece, so that mixing is achieved. Table 5.2.1 gives the colony formed units per ml.

Table 5.2.1: Concentrations during the 1st experiment

Stage / **Position**	Feed ($cfuml^{-1}$)	Before cleaning($cfuml^{-1}$)	After cleaning ($cfuml^{-1}$)
Outlet	10^8	10^8	10^5
Top of vertical pipe	-	10^8	10^6
10cm	-	10^8	10^6

18cm	-	10^9	10^8

For comparison and additional verification the samples were put into the spectrophotometer at 640nm wavelength, once calibrating the machine with deionised water (table 5.2.2) and second time with sterile broth solution (table 5.2.3).

Table 5.2.2: Deionised water based spectrophotometry measurements for samples of 1st experiment.

Stage / **Position**	Feed (nm)	Before cleaning(nm)	After cleaning (nm)
Outlet	1.45	1.45	0.01
Top of vertical pipe	-	1.4	0.01
10cm	-	1.4	0.02
18cm	-	1.5	1.6

Table 5.2.3: Broth solution based spectrophotometry measurements for samples of 1st experiment.

Stage / **Position**	Feed (nm)	Before cleaning (nm)	After cleaning (nm)
Outlet	1.45	1.3	0.01
Top of vertical pipe	-	1.3	0
10cm	-	1.3	0
18cm	-	1.5	1.55

From the above results we can see that from the start (table 5.2.1) we already have the maximum growth into the tank, or it is very close, since it is 10^8cfuml^{-1}. Also neither growth, nor death of the bacteria was observed under the existing temperature conditions. After cleaning there is removal only down to the point where sample is taken out from the 10^{th} cm. Below that, counts show that concentration stays the same because, although it is counted to be one log number less concentrations between 10^8 and 10^9 are considered to saturate the dilution.

In spectrophotometry, as already mentioned (paragraph 3.3.2), the lower limit of detection is of the order of 10^6 cellsml^{-1} and that under conditions permitting consistent growth the stationary phase is typically of the order of 10^9 cellsml^{-1}, the onset of the stationary phase is not easily measurable (Mcmeekin et al. 1993). The relationship between log absorbance versus log (cell density) is only linear over a narrow range (~10^6-$10^{7.5}$). This is verified since for 10^8-10^9cfuml^{-1} concentrations we have absorbance between 1 and 1.5nm, which is above the linear relation (fig. 3.2.7). Moreover, 0.02nm, or even less, indicates concentrations below 10^6cfuml^{-1}. Therefore absorbance measurements are only a qualitative way to verify the results and similar log numbers have similar absorbance.

The above experiment can be modelled with the following boundary conditions:

Inlet: $10^8 cfuml^{-1}$,

Inlet flow: $300lthr^{-1}$

Inlet temperature is expressed by a profile. This means that temperature measurements were taken during the experiment and afterwards were used for the transient solution in FLUENT as a boundary condition at the inlet.

$u_{in}=0.164ms^{-1}$

Tenv=296K

$h_{hor}=2.7\ Wm^{-2}K^{-1}$

$h_{ver}=4\ Wm^{-2}K^{-1}$

The fluid, since it is an aqueous solution, is treated as water.

The microbial kinetics modelled using the *Species Transport Model*. So, in the flow there is water and at the inlet boundary conditions has to be set the mass fraction of the bacterium *Pseudomonas*. It is set to be 1.524exp (-4). This is calculated in the following way:

We find the mass fraction of *Ps. fluorescens* rods in a gram of water. In this experiment it contains 10^8 of Pseudomonas rods in a gram or in a cm^3 since the density of water is $1grcm^{-3}$.

The dimensions of one rod are (Bergey, 1974):

Diameter d $\approx 0.8\mu m$

Length h $\approx 2.5\mu m$

So, the volume of this cell is given by the following equation, which calculates the volume of a cylinder plus a sphere:

$$Vcyl = \frac{\pi d^2}{4}h + \frac{4}{3}\pi\left(\frac{d}{2}\right)^3 \qquad (5.2.1)$$

which gives V_{cyl} = 1.256exp(-18)+0.268exp(18) m^3 = 1.524exp(-18) m^3

Here we can make the assumption that the bacterium has the same density as the bulk flow, since the presence of the microbes does not affect the flow field. So, we have:

$\rho_{water} = \rho_{bugs} = 10^3 kgm^{-3}$.

By multiplying the density with the volume we get the weight of one cell: 1.524exp(-15)kg.

We start with 10^8 bacteria of Pseudomonas, which exist in one gram of water. The total mass will be:

1.524exp(-15)*10^8 = 1.524exp(-7) kg which is in 1gr or 0.001 kg of water.

So the initial mass fraction is 1.524exp(-7)/0.001 = 1.524exp(-4)

In order to describe the inlet mass fraction there was a UDF used taking the outlet area averaged mass fraction of the bacteria to apply it as inlet. This was done in order to keep the reaction continuous.

The reaction rates used were not from the same source, as already mentioned in paragraph 2.8.3. This caused problems of continuity in the solution and more specifically to the *Ps.*

fluorescens residuals that started increasing when the temperature became 320K, which is the point when inactivation starts.

Figure 5.2.2 shows the comparison of temperature down the T-piece between measurements and model. It is clear that in an hour, which is more or less the duration of the experiment before cleaning, the temperature profile is not fully developed since the drop where the 5th thermocouple is located has not reached low enough values, if we look at figure 4.2.10. The difference between the first and the next two measurements is because the sensor at the inlet, that corresponds to location zero on the graph and measurements of which are used as the inlet temperature profile in the model, is fixed on the rig and is different to the rest. For this reason deviations may occur. Again, we see the artefact the second thermocouple causes.

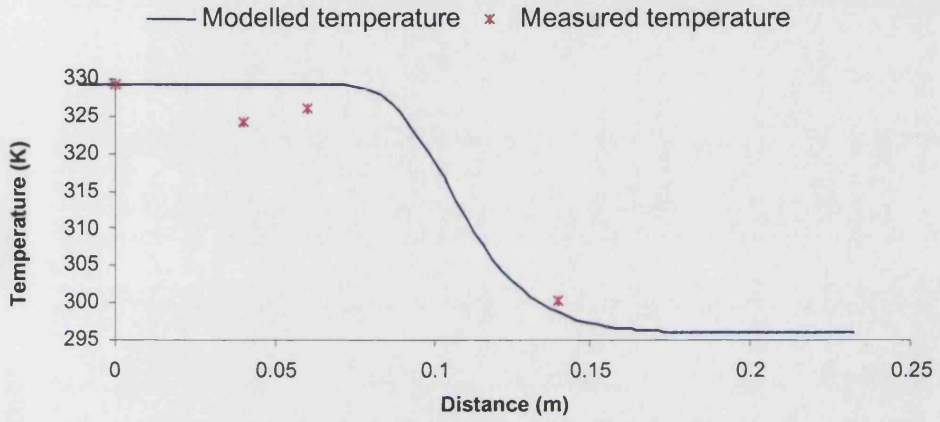

Figure 5.2.2: Temperature comparison between model and measurements for 1st bacterial experiment.

For the same conditions we take the profile of *Ps. fluorescens* profile down the tube (fig 5.2.3). We see that from the point where temperature is above 47°C (320 K) the drop is almost three log numbers. Hence, if 10^{-3} corresponds to 10^{8}cfuml^{-1} then the 10^{-5} is 10^{6}cfuml^{-1}. This is not in agreement with the experiment since the counting methods showed that there was no inactivation. Maybe it can be assessed that the equation used (Chiruta et al., 1997) to describe that phase is overestimating substantially the reaction rate. In addition, under the conditions of the experiment, which was pretty short, a large drop was not expected as the inactivation temperature was reached at around 1000sec before the experiment was stopped (~17min). This amount of time is not enough to cause such a substantial drop. The points in the vertical tube where samples were taken at the 10th and 18th cm give a mass fraction of around 10^{-3} with the one closer to the bottom being slightly higher. This corresponds to 10^{9} cfuml^{-1} giving a good agreement. So the model that describes growth is matching the experiment well.

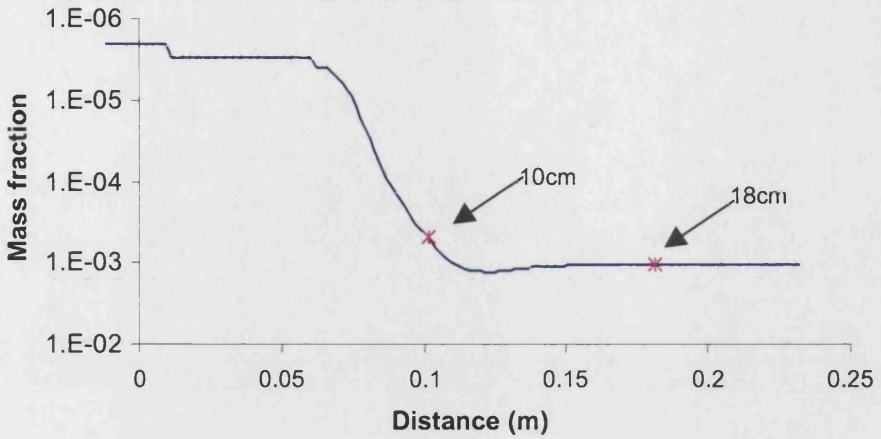

Figure 5.2.3: Predicted bacterial mass fraction distribution on the central axis of the vertical pipe for first experiment before cleaning.

This is shown also by the contours of temperature (fig 5.2.4) and the bacterial mass fraction (fig 5.2.5).

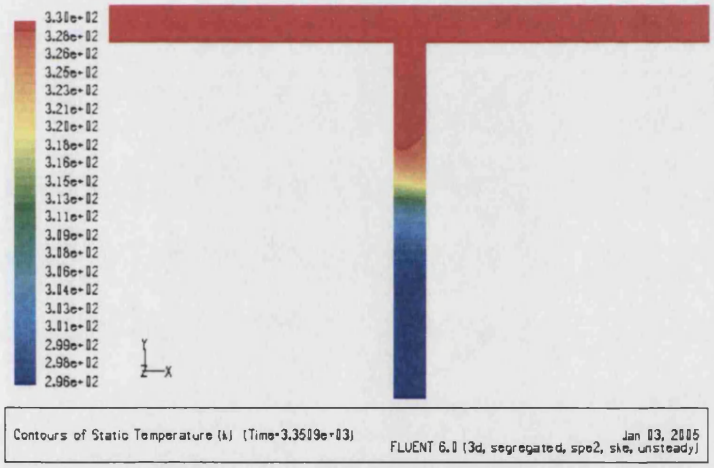

Figure 5.2.4: Contours of temperature after the first part of the first experiment on a vertical plane surface passing from the centre of the T-piece

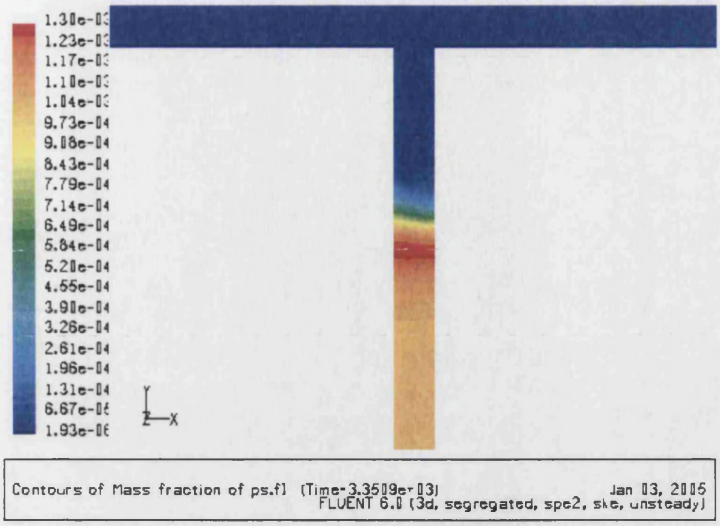

Figure 5.2.5: Contours of *Ps fluorescens* mass fraction after the first part of the first experiment on a vertical plane surface passing from the centre of the T-piece

Then cleaning followed for 4 min under the following conditions:

$u_{in}=0.73 ms^{-1}$

$T_{in}=293K$

$T_{env}=296K$

$h_{hor}=2.23\ Wm^{-2}K^{-1}$

$h_{ver}=2.7\ Wm^{-2}K^{-1}$

Here the species model was used but with three components this time: *Ps. fluorescens*, broth and water. The two first had mass fraction equal to zero (or very close in order to avoid divergence). However, since in the T-piece there was a wide range of temperature that was including the inactivation, there were during the solution many divergence problems. Hence, the time step had to remain quite low (~0.001), at least at the beginning of the run. This made the solution time consuming and difficult to be completed. This showed that all those parameters included and calculated added complexity to the set of equations solved by the program. Also the models used to describe the reactions were proven to be inconsistent since the divergence problems started when temperatures reached the values where inactivation commences.

The CFD calculation for cleaning came up with some interesting results. Figure 5.2.6 shows distribution of temperature and mass fraction of water and TSB (Trypton Soya Broth) in the central axis of the down stand after flushing. We see that the exchange of liquids is very clear: TSB is replaced by water and the point where this occurs is slightly before 15cm down the pipe. This point is almost in the middle of the exponential drop of the temperature where, as we know from the previous flows, the velocity had already dropped to a very low value.

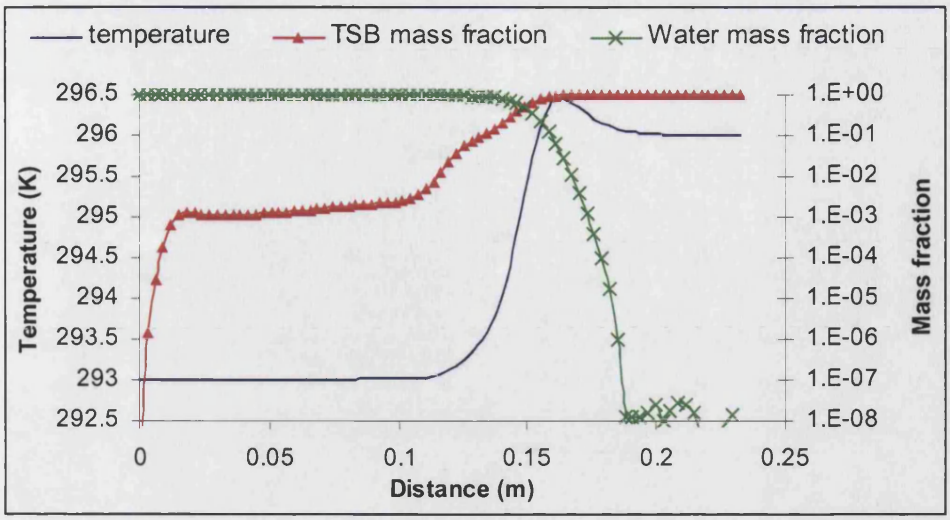

Figure 5.2.6: Temperature, TSB and water distribution predictions down the T-piece for the 1st experiment after cleaning.

From the plot that gives the bacteria mass fraction and the temperature down the pipe (fig 5.2.7) is observed that both exponential drops coincide as far it concerns the depth where they happen. On the mass fraction curve are illustrated the values that correspond to the depths where the samples were taken from (10 and 18cm). At 10cm mass fraction is just below 10^{-5} which is 10^{7}cfuml^{-1}. The 18th cm shows 10^{-3}, which corresponds to 10^{9}cfuml^{-1}. Both of them are close to the numbers given on table 5.2.1, with an overestimation of just one log number.

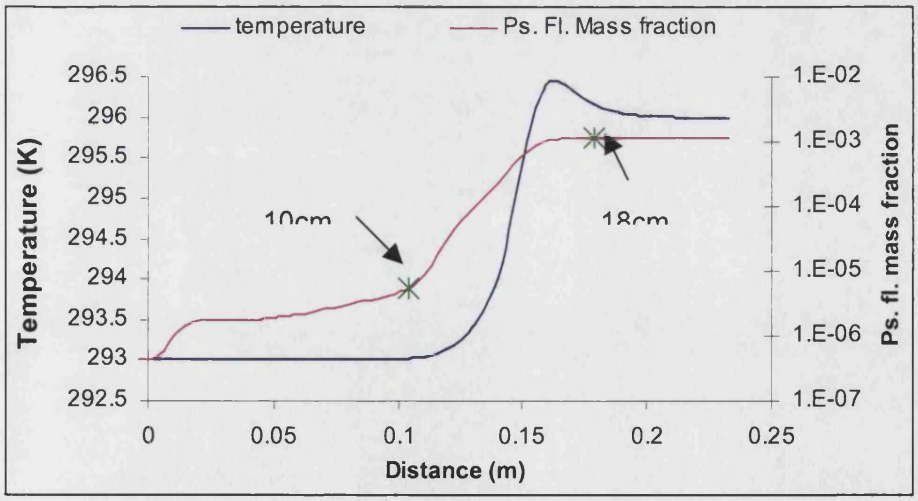

Figure 5.2.7: Predictions of temperature and *Ps. fluorescens* distribution predictions down the T-piece for the 1st experiment after cleaning.

In figure 5.2.8 we can see how temperature changes during cleaning. The mechanisms again are the same as in the previous set of experiments that introduced the transient solutions. First, forced convection that initiates heat transfer from the top takes place and pushes the cleaning

liquid into the down stand. Once the velocity domain is well established, a threshold is formed, beyond which, heat transfer occurs mainly with conduction since, there, velocity is practically zero. From that point in time and onwards temperature changes very slowly.

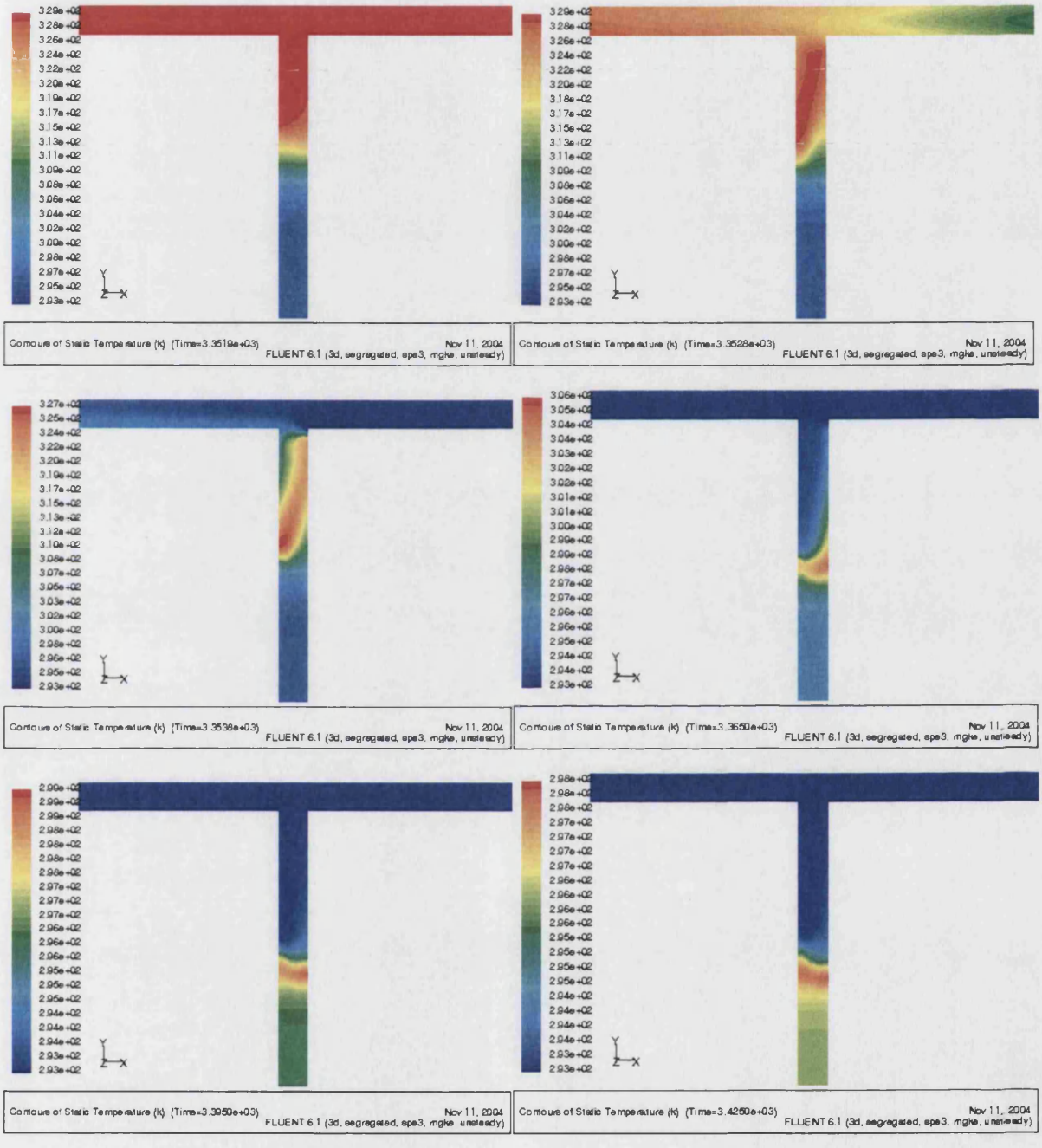

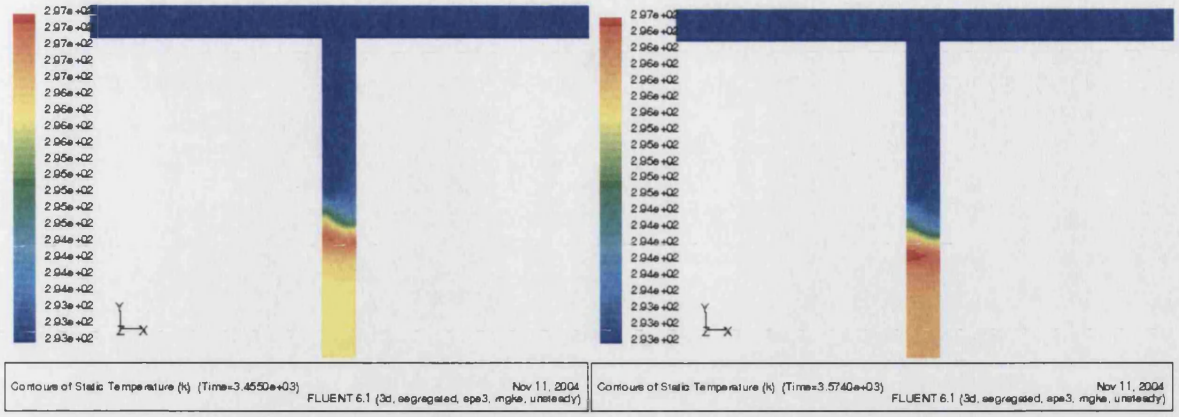

Figure 5.2.8: Temperature contours at various stages of flushing for the first experiment with bacteria.

For the *Ps. fluorescence* mass fraction contours (fig 5.2.9) is clear that the range stays the same during the whole process, since the bacteria had already dropped in numbers at the first part of the experiment. At the bottom is around 10^{-3}, which corresponds to 10^{9}cfuml^{-1}.

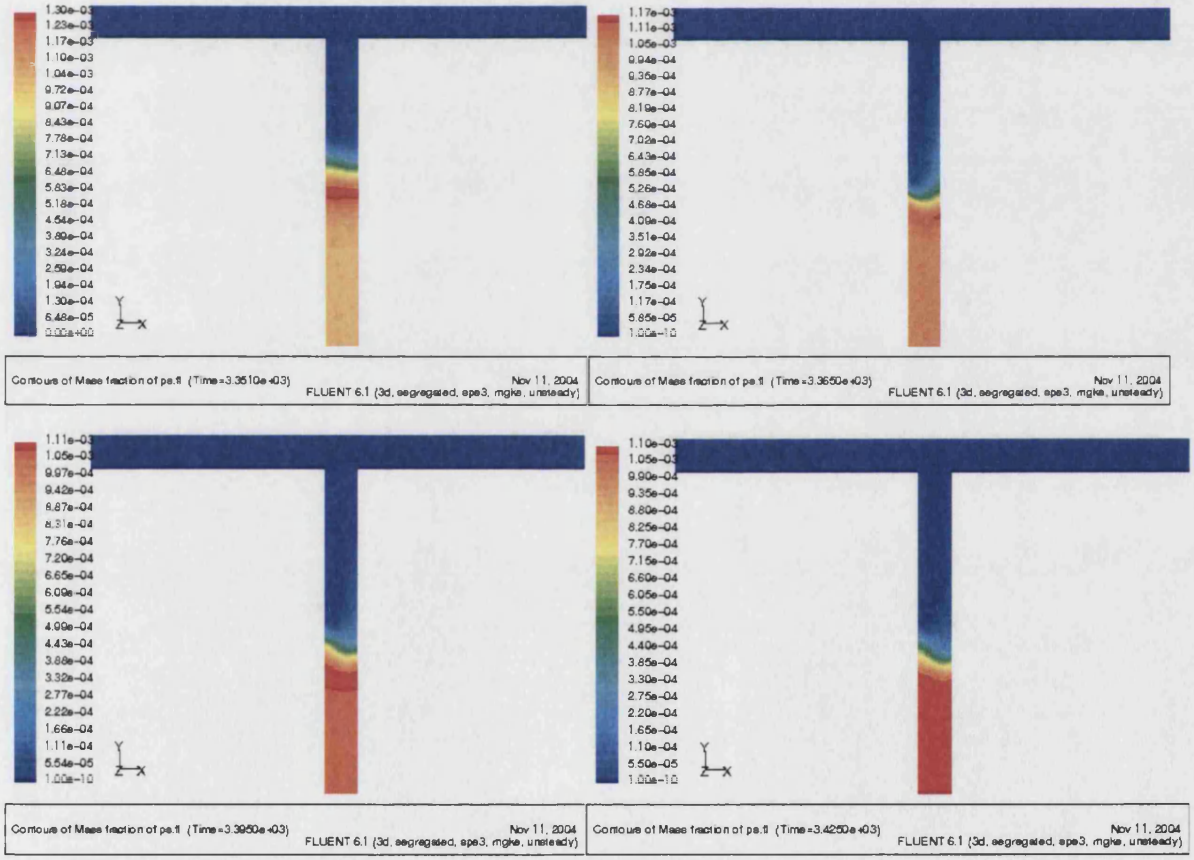

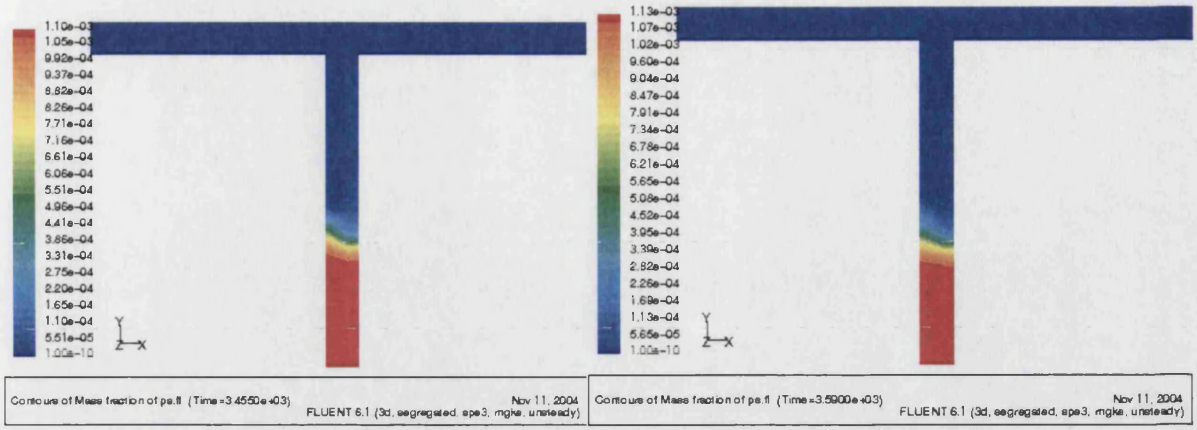

Figure 5.2.9: *Ps. fluorescens* mass fraction contours at various stages of flushing for the first experiment with bacteria.

At the beginning, the TSB (fig 5.2.10) is swept rapidly out of the dead end but after a certain point, where the flow is well establish, the mass removal takes place very slowly and contours colours are similar to the correspondent of the bacteria (fig 5.2.9).

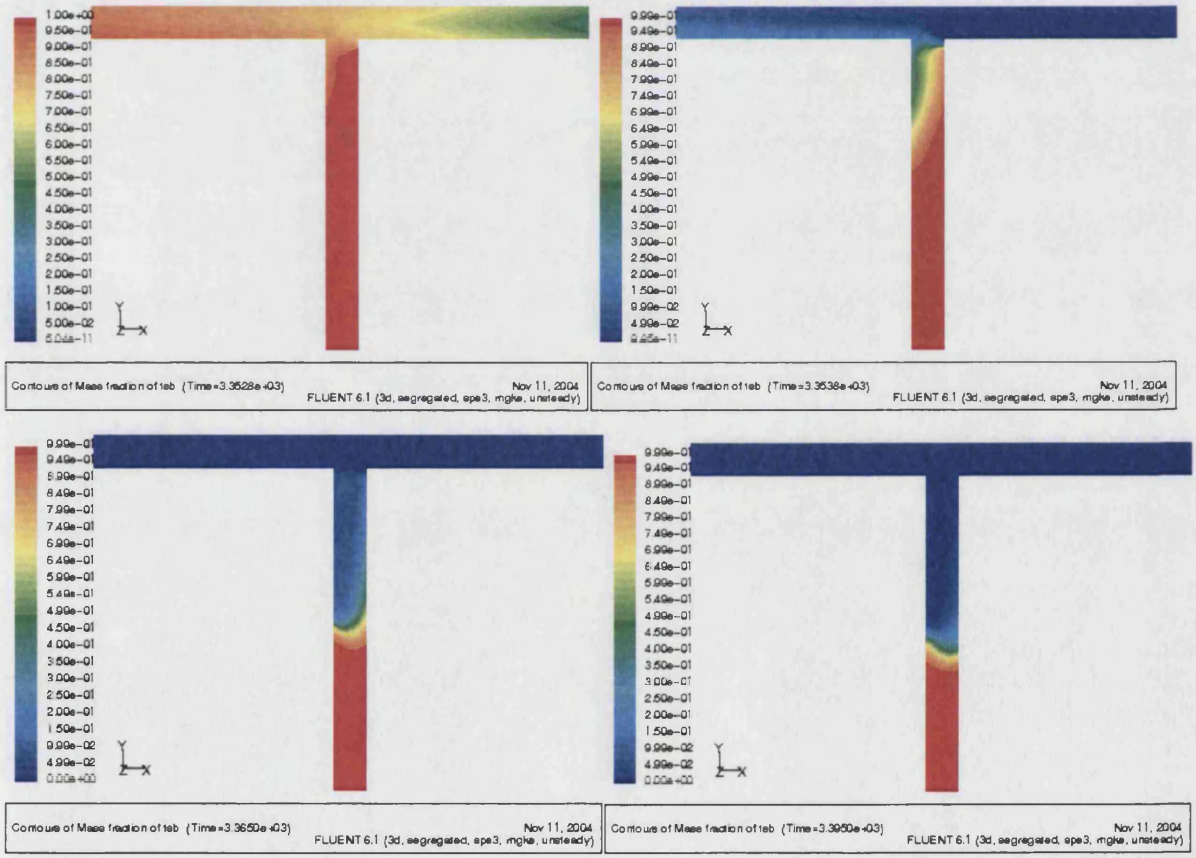

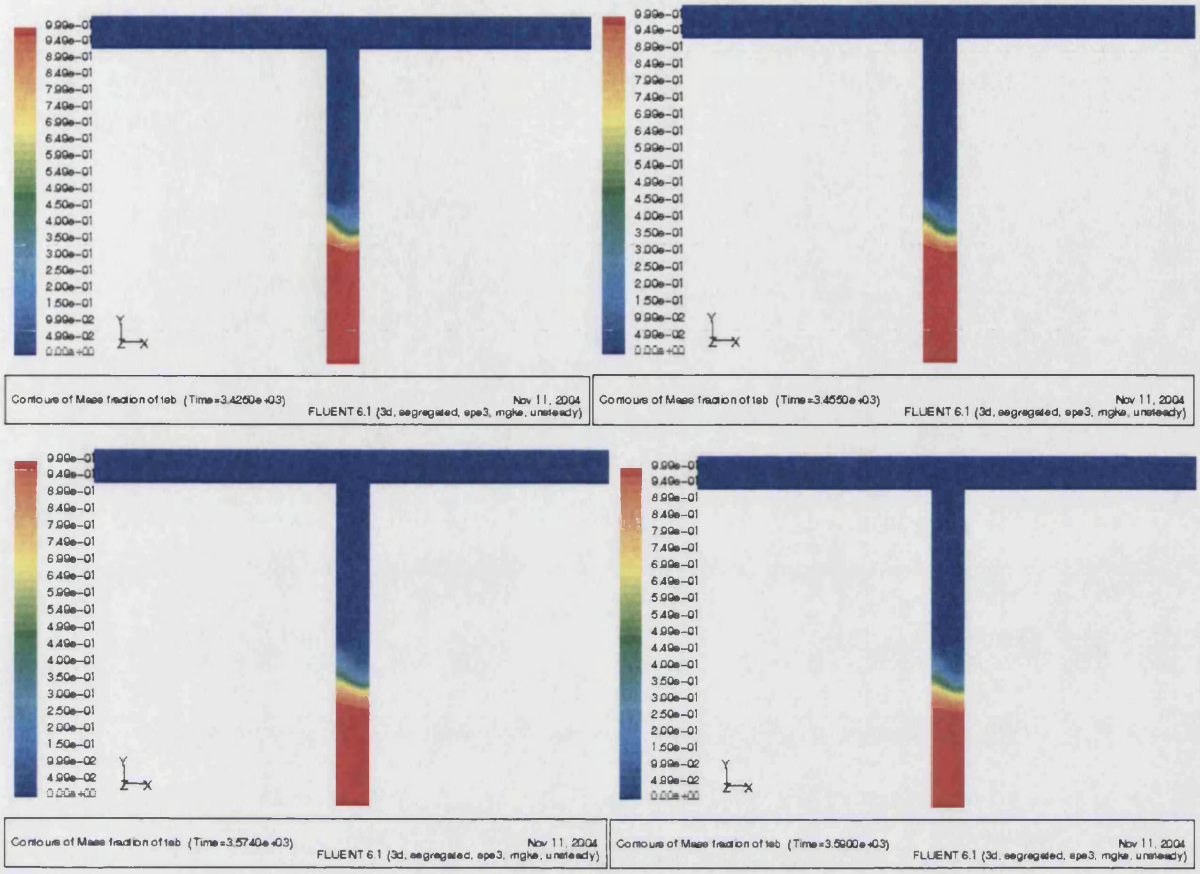

Figure 5.2.10: TSB mass fraction contours at various stages of flushing for the first experiment with bacteria.

Generally, the agreement between the experimental results and the models is good. Temperatures as well as bacteria concentrations give reliable comparisons. It is only when the inactivation takes place that the model reaction rate used is overestimating the rate of death, although under the existing conditions there was not expected significant loss. Additionally, while the simulation was taking place convergence difficulties took place and the system was complicated to solve. Time step had to stay low and a few minutes of real time cleaning took many hours of simulation.

5.2.2 Second bacterial kinetics experiment

This time the experiment was run for a longer period (approximately 4 hours). It was intended to get the bacteria into the system at the exponential phase so that some growth can be noticed within those 4 hours.

Hence, there was *Ps. fluorescens* inoculated into 250ml TSB (Trypton Soya Broth) and was left overnight to reach the stationary phase. At that stage we had approximately 10^8-10^9cfuml^{-1}. Afterwards, 50ml of the above was inoculated into 250ml TSB and was left for 1-2 hours, so that the bacteria could get used to the higher dilution.

The next step was to take 50ml of the new dilution and inoculate it into 12lt of TSB. It was left there for 1-2 hours again in order to avoid as much as possible the lag phase when the suspension is introduced into the system. The environmental temperature when the experiment started was around 22°C (while the experiment was running, after one or two hours the temperature reached 25°C). The first sample, which is considered the feed, was taken at temperature 33°C. So the pour plate method gave the numbers given on table 5.2.4.

Table 5.2.4: Concentrations during the 2nd experiment

Stage / **Position**	Feed ($cfuml^{-1}$)	Before cleaning($cfuml^{-1}$)	After cleaning ($cfuml^{-1}$)
Outlet	10^5	10^6	10^2
Top of vertical pipe	-	10^6	10^2
10cm	-	10^8	10^4
18cm	-	10^7	10^7

Spectrophotometry of the 9 samples gave the following results at 640nm after calibration with deionised water (tbl 5.2.5).

Table 5.2.5: Deionised water based spectrophotometry measurements for samples of 2nd experiment.

Stage / **Position**	Feed (nm)	Before cleaning(nm)	After cleaning (nm)
Outlet	0.045	0.475	0
Top of vertical pipe	-	0.406	0
10cm	-	0.27	0
18cm	-	0.206	0.45

From the above results it is clear that growth was detected. We started with 10^5 and at the horizontal pipe remained between 10^5 and 10^6, which makes sense because the temperature was quite high and relatively close to the inactivation limit. This would constrain and inhibit growth. At 10cm 10^8 was observed and at the bottom (18cm) 10^7. So, we can conclude that there was 2 to 3 log numbers growth. Some of the samples showed very low absorbance values that do not agree with the counted colonies. This is probably because the specific samples were not enough to fill the cell introduced into the spectrophotometer. Excluding those two the rest agree with the counts.

Figure 5.2.11 shows the temperature history during the experiment at the same location as described for the previous one. The inlet was kept below 50°C and around 45°C in order to get a temperature gradient but avoid inactivation at the same time. There is difference between the inlet and outlet since there was a part of the rig after the inlet substituted with a stainless steel coil emerged into a bucket containing water. This was used to remove excess heat generated by the pump. This was considered necessary because otherwise the horizontal tube would heat

up the broth excessively, leading to the death of the bacteria in a short time. The temperature in that part of the rig was the one named Tout, measured at the outlet since the pipe was insulated. Generally, the temperature stays around 45-47°C, which is very close to the threshold where growth stops and inactivation starts. T_2 and T_3 stay very close to the temperature at the top.

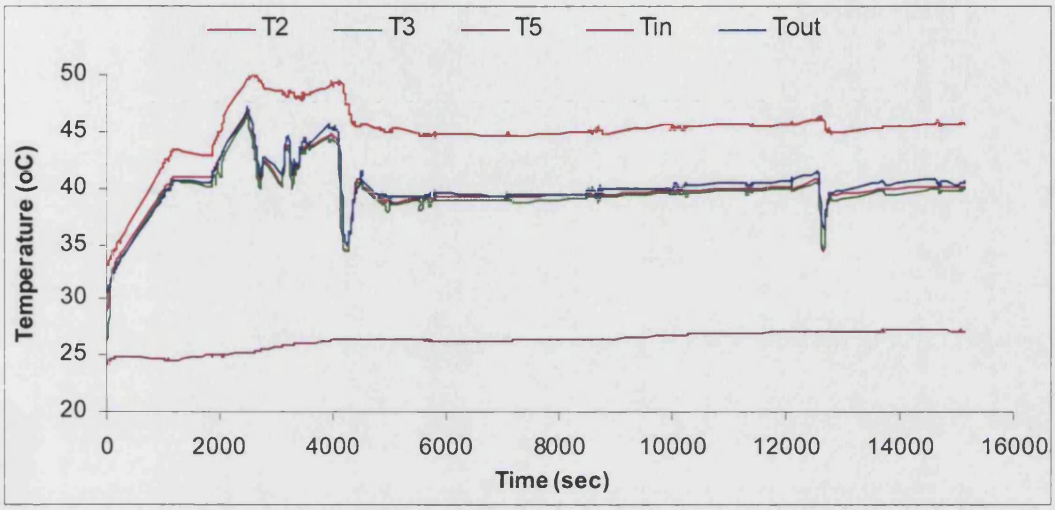

Figure 5.2.11: Temperature history during the 2nd experiment before cleaning.

Cleaning lasted 5min and 35sec since the attached coil dropped the flow to 1290lthr^{-1}. There was a four-log order drop in values before and after cleaning, as table 5.2.4 shows. This is not the case though for the sample taken from the port closest to the bottom. There the concentration stays the same, implying that no displacement of liquid has taken place.

The above experiment can be modelled with the following boundary conditions:

Inlet: 10^5 cfuml^{-1},

Inlet flow: 150 $l.h^{-1}$.

Inlet temperature is expressed by reading the profile of the outlet, which is located after the cooling section and the insulated rig, so we assume that temperature will be the same.

The duration of the experiment was 15150 sec (=252.5 min).

u_{in}=0.082 ms^{-1}

T_{in} was the profile taken from the experimental data.

T_{env}=298 K

h_{hor}=2.65 Wm^{-2}K^{-1}

h_{ver}=4 Wm^{-2}K^{-1}

The microbial kinetics are again modelled again using the *Species Transport Model.* So, in the flow there is water and at the inlet boundary conditions has to be set the mass fraction of the bacterium *Pseudomonas.* It is set to be 1.524exp (-7). This is calculated with the following way:

The dimensions of one rod are:

Diameter d $\approx 0.8\mu m$

Length h $\approx 2.5\mu m$

So, the volume of this cell is given by the following equation, which calculates the volume of a cylinder plus a sphere:

$$Vcyl = \frac{\pi d^2}{4} h + \frac{4}{3}\pi\left(\frac{d}{2}\right)^3 \qquad (5.2.1)$$

which gives V_{cyl} = 1.256exp(-18)+0.268exp(18) m^3 = 1.524exp(-18) m^3

Here we can make the assumption that the bacterium has the same density as the bulk flow, since the presence of the microbes does not affect the flow field. So, we have:

$p_{water} = p_{bugs} = 10^3 kg/m^3$.

By multiplying the density with the volume we get the weight of one cell: 1.524exp(-15)kg.

We start with 10^5 bacteria of Pseudomonas which exist in one gr of water. The total mass will be:

1.524exp (-15)*10^5 = 1.524exp (-10) kg which is in 1gr or 0.001 kg of water.

So the initial mass fraction is 1.524exp (-10)/0.001 = 1.524exp (-7)

According to the above conditions and using again a UDF for the inlet mass fraction (Appendix 10), the results of the simulation are presented.

On figure 5.2.12 we take the temperature distribution down the centre of the vertical pipe. We see that as time passes the heat diffuses more down the pipe and the whole profile has raised values. The position where the temperature starts dropping stays the same though, since after that point heat transfer is happening due to conduction. After approximately 2 hours the temperature profile is the same. Steady state is reached and no change occurs.

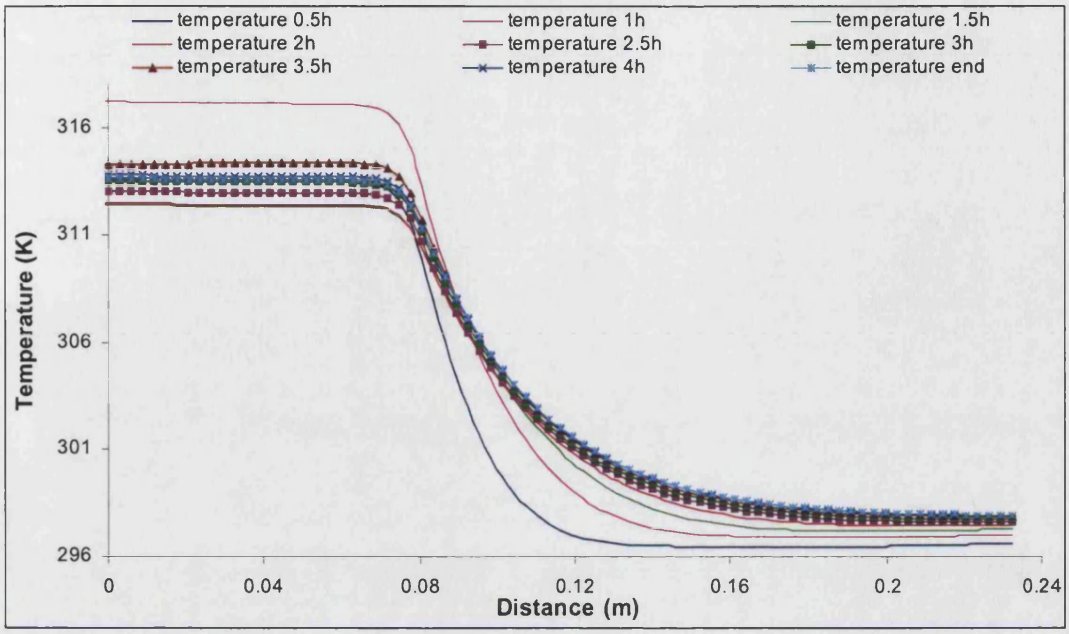

Figure 5.2.12: Temperature distribution down the vertical pipe for the 2nd experiment every 30min.

The following figure (fig 5.2.13) shows the mass fraction of the bacteria for the same time intervals and locations as for the above temperatures. Just before the 10th cm, between 8 and 9 cm we have the peak of the growth and after that depth, growth is still faster compared to the top of the pipe. This peak is moving slightly to the right for the first two hours, until temperature profile is established. Afterwards, differences are not significant and growth is uniform.

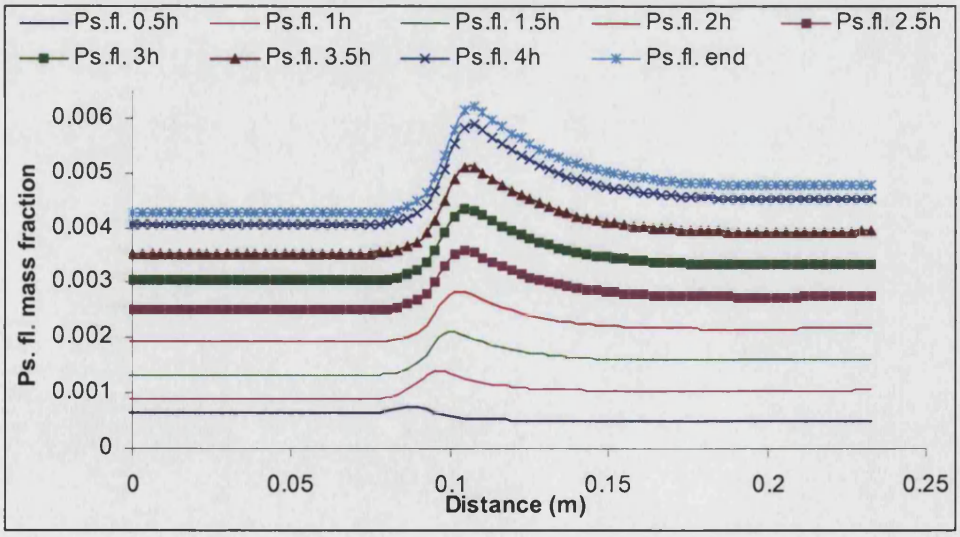

Figure 5.2.13: *Ps. fluorescens* mass fraction distribution down the vertical pipe for the 2nd experiment every 30min.

Similar correlations can be made between the contours for temperature (fig 5.2.14) and bacterial mass fraction (fig 5.2.15) that are taken every half an hour until the end of the experiment. It is noticed how slow the diffusion down the pipe progresses. The dark blue colour becomes light blue that corresponds to higher values. The temperature at the top was maintained at around 315K in order to achieve conditions closer to the heating processing where we have constant conditions in the heating sections to reach the adequate residence time.

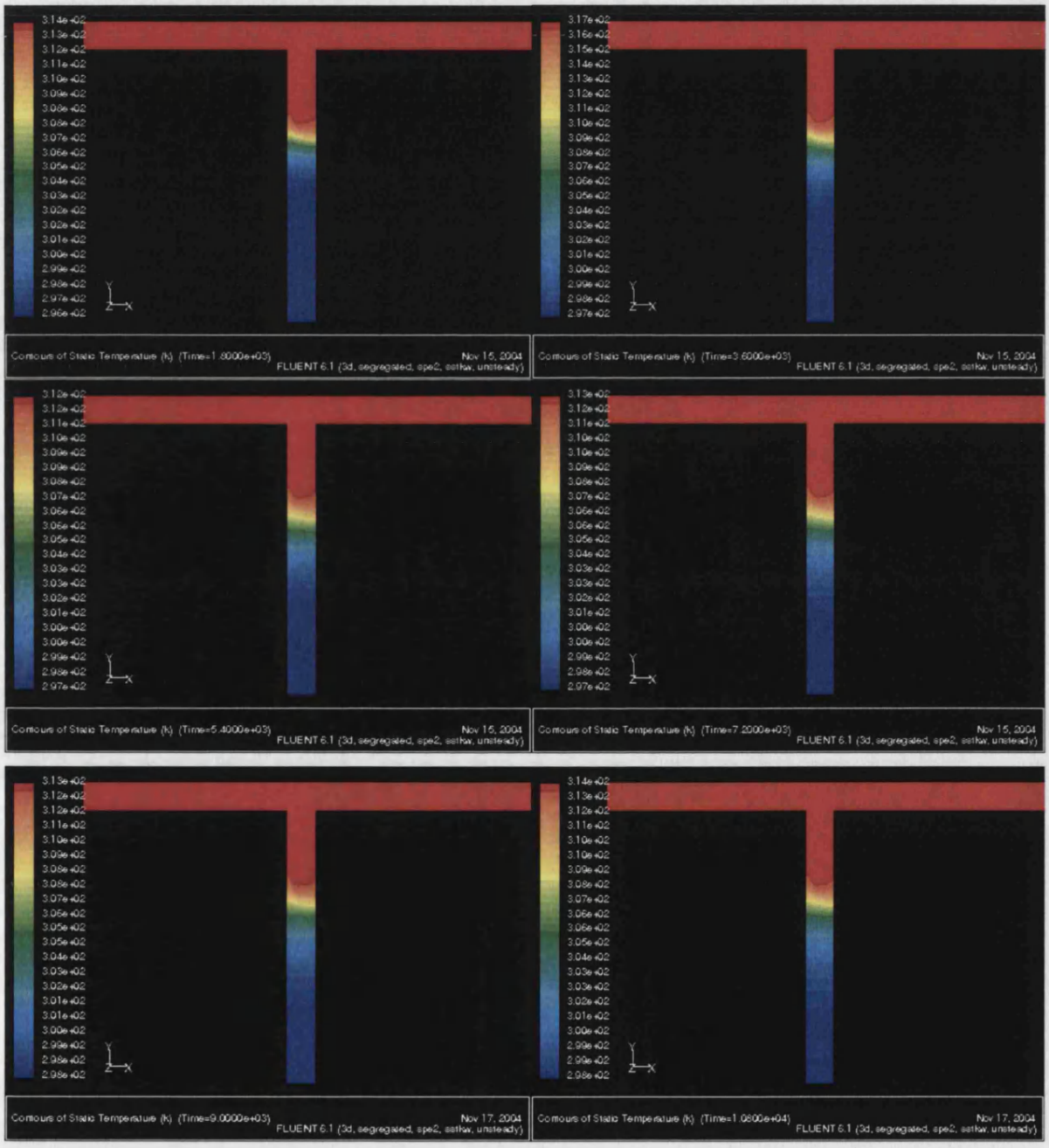

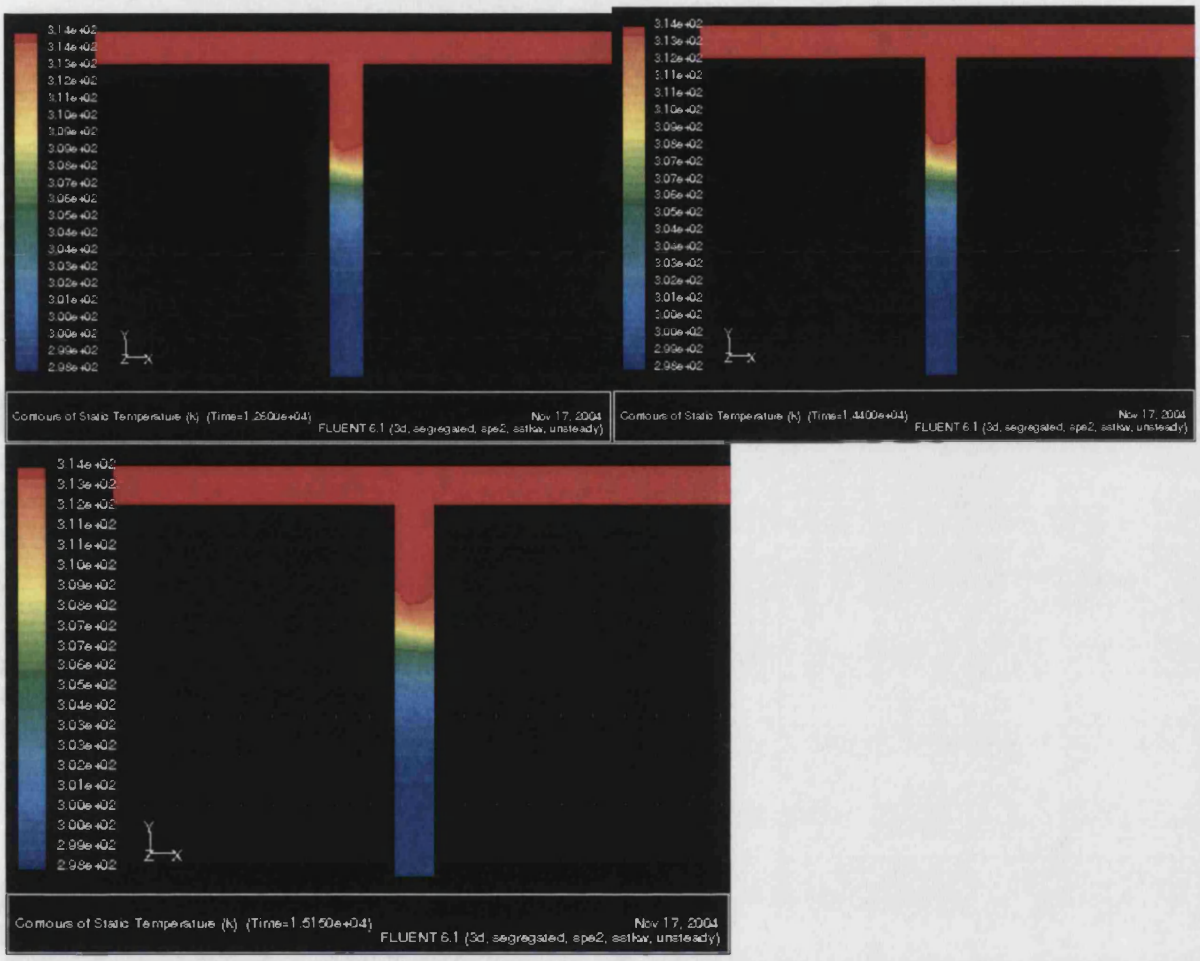

Figure 5.2.14: Contours of temperature on a vertical cut down the centre of the T-piece for the 2nd experiment taken every 30 min.

The corresponding contour values for the bacterial mass fraction (fig 5.2.15) show that at the top we have a change from 6.5×10^{-4} to approximately 4.3×10^{-3}. In the middle values go from 7.7×10^{-4} to 6.2×10^{-3} and towards the bottom from 5×10^{-4} to 5×10^{-3}. Hence, generally there is one order of magnitude increase in the mass fraction that corresponds to one log number of cfu growth and to 10^{8}-10^{9}cfuml^{-1}. This is in agreement with the counts at the middle and bottom but is overestimating the numbers at the rest of the locations. This is probably because the models used are not adequately describing growth when temperature is not absolutely constant or may be because the bacteria are under shock and are not getting used to the conditions in the rig. However, the plot on figure 5.2.13 shows that numbers are higher at around 10cm and towards the bottom compared to the top part of the pipe. This agrees with the counts where at the same areas we have corresponding growth.

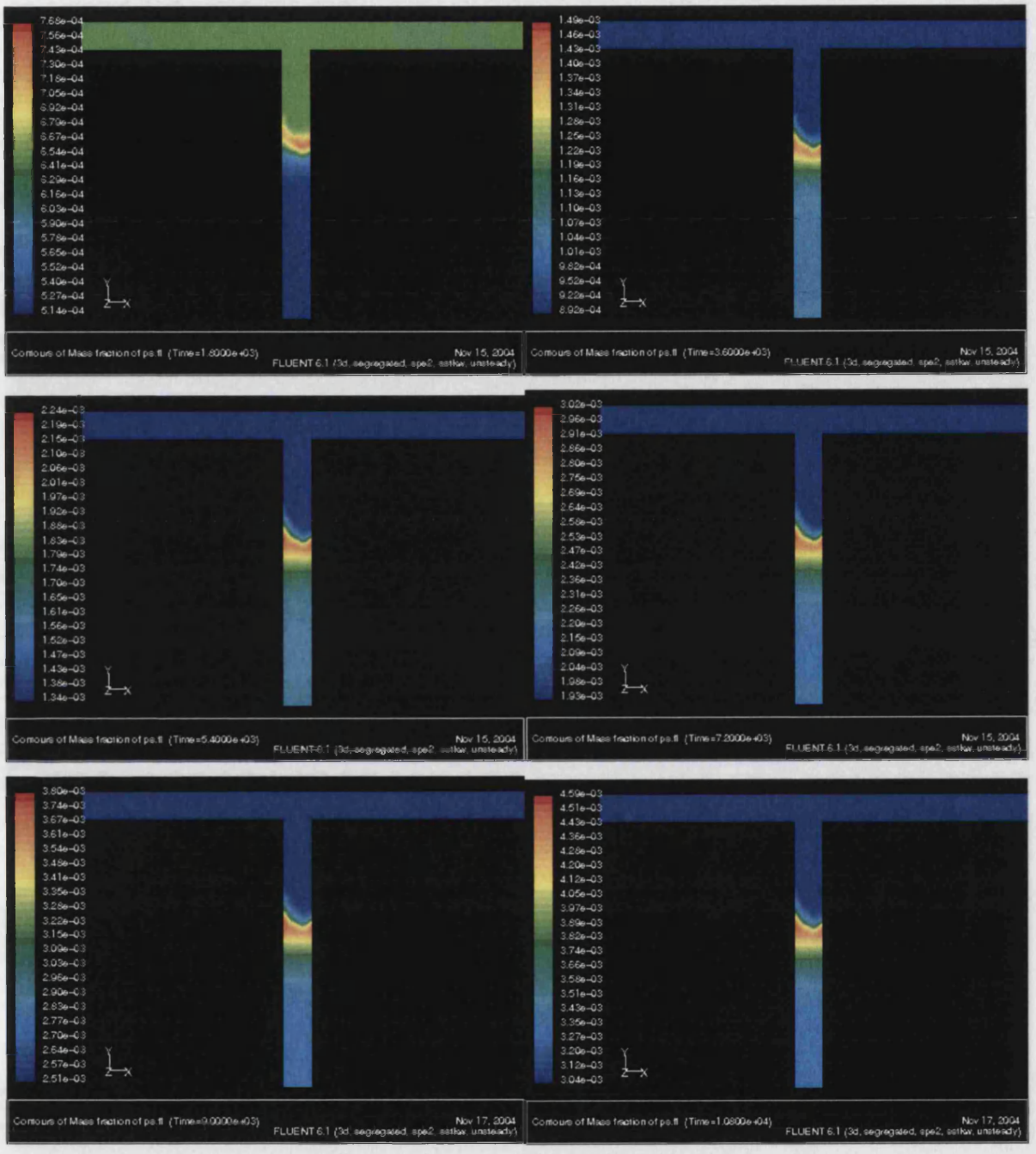
Contours of Mass fraction of ps.ti (Time=1.8000e-03)
Nov 15, 2004
FLUENT 6.1 (3d, segregated, spe2, sstkw, unsteady)
Contours of Mass fraction of ps.ti (Time=3.6000e-03)
Nov 15, 2004
FLUENT 6.1 (3d, segregated, spe2, sstkw, unsteady)
Contours of Mass fraction of ps.ti (Time=5.4000e-03)
Nov 15, 2004
FLUENT 6.1 (3d, segregated, spe2, sstkw, unsteady)
Contours of Mass fraction of ps.ti (Time=7.2000e-03)
Nov 15, 2004
FLUENT 6.1 (3d, segregated, spe2, sstkw, unsteady)
Contours of Mass fraction of ps.ti (Time=9.0000e-03)
Nov 17, 2004
FLUENT 6.1 (3d, segregated, spe2, sstkw, unsteady)
Contours of Mass fraction of ps.ti (Time=1.0800e-04)
Nov 17, 2004
FLUENT 6.1 (3d, segregated, spe2, sstkw, unsteady)

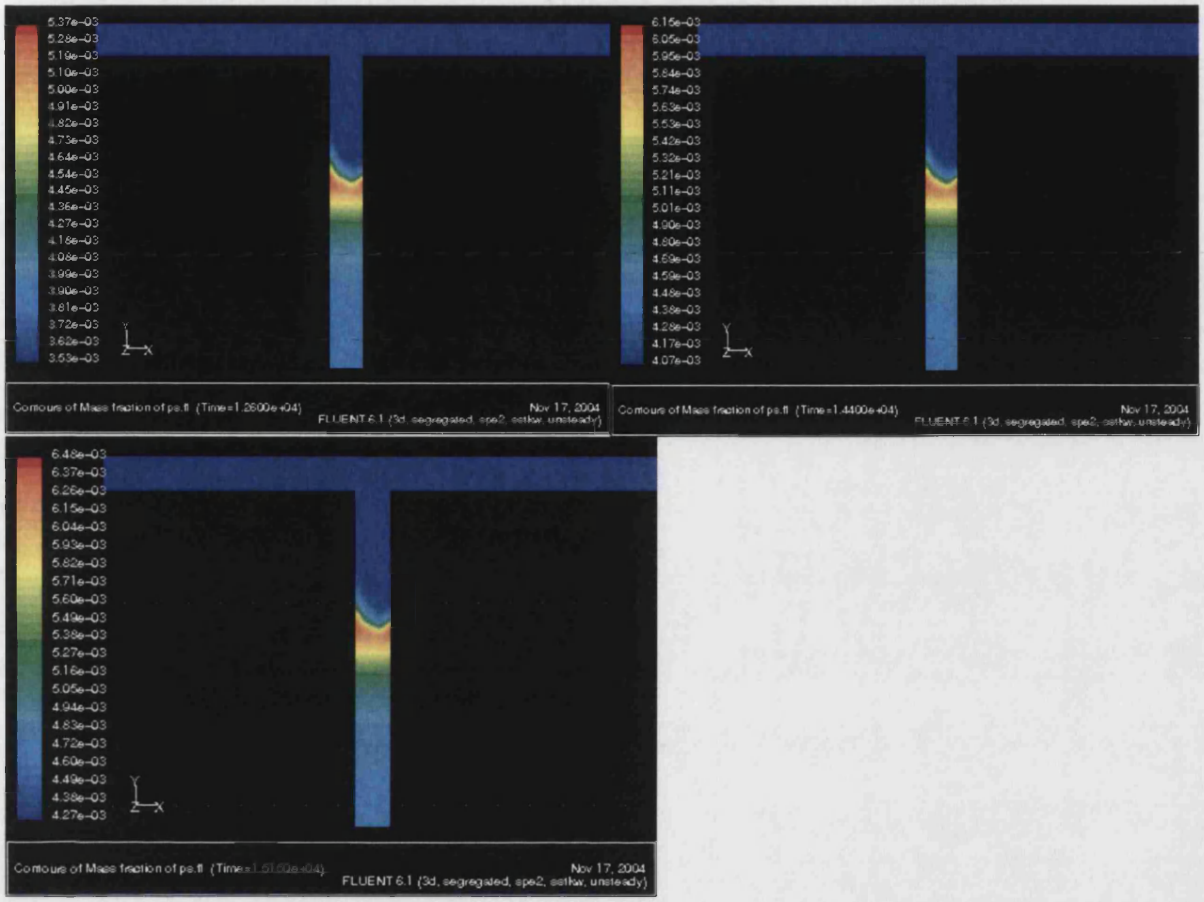

Figure 5.2.15: Contours of *Ps. fluorescens* mass fraction on a vertical cut down the centre of the T-piece for the 2nd experiment taken every 30 min.

Generally, the plots and contours shown above demonstrate that the *Ps. fluorescens* growth is overestimated. It is obvious that at the upper part of the dead end growth is slower but still the log numbers fluctuate at around 10^{-3}, which is 10^{9}cfuml^{-1}. Table 5.2.4 gives values between 10^{6} and 10^{8} cfuml^{-1} with the highest concentration located in the middle. Subsequently, qualitative agreement is achieved. Also, during the experiment, temperature fluctuations might have created a shock to the bacteria and growth was delayed. However, the post processing of the solution gives a good indication of how the growth proceeds. Another observation is that the horizontal tube was close to the inactivation temperature, where the model used to describe growth might not be appropriate.

Flushing takes a longer time than in the previous experiment and specifically 5min and 35sec.

Then cleaning followed under the following conditions:

u_{in}=0.7052ms^{-1}

T_{in}=295K

T_{env}=298K

h_{hor}=2.23 Wm^{-2}K^{-1}

h_{ver}=2.7 $Wm^{-2}K^{-1}$

As was expected, the velocity has dropped.

Figures 5.2.16 and 5.2.17 show temperature and mass fractions of water, TSB and bacteria according to their distribution in the central axis along the vertical pipe. At around 15cm down the tube the TSB is replaced by water and until around the 17th cm temperature is affected and has already dropped. Figure 5.2.17 shows the temperature together with the bacterial mass fraction. The later drops like TSB and at a depth that corresponds to the one where temperature stops dropping and remains as it was before cleaning (fig 5.2.12).

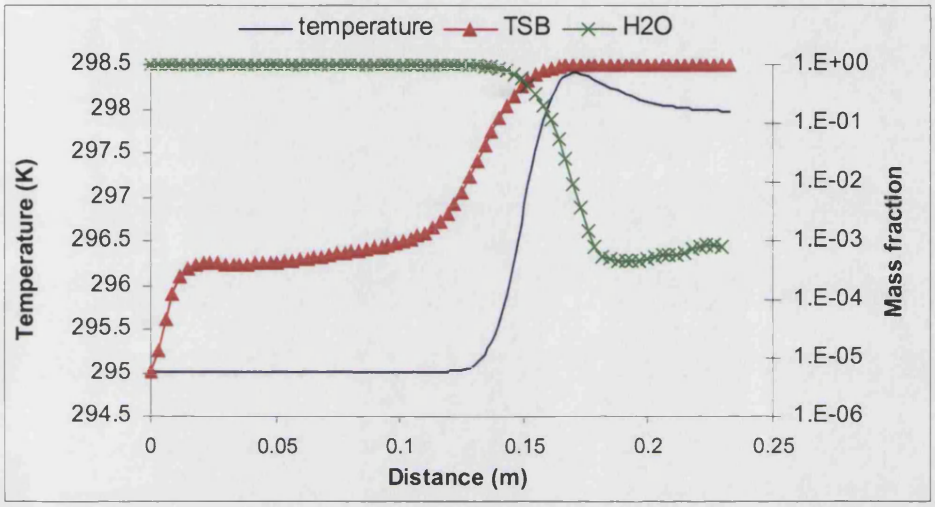

Figure 5.2.16: Temperature, TSB and water distribution predictions down the T-piece for the 2nd experiment after cleaning.

From the plot that shows the remaining microbes, we take the numbers predicted and compare them to the counts from table 5.2.4. At 10cm mass fraction is around 10^{-5} that means 10^{7}cfuml^{-1} and at 18cm is around 5×10^{-3} corresponding to 10^{9}cfuml^{-1}. So, the bottom of the T-piece is saturated with microbes, which agrees with the experiment (tables 5.2.4 and 5.2.5) and so does the top where it is 10^{-6} that is numerically the closest to zero FLUENT computes. In the middle (10cm) there is overestimation by approximately 2 log orders. The shape and numbers are similar to the ones for the cleaning of the first experiment (fig 5.2.17) especially at the sampling point at the 10th cm where the remaining mass fraction is almost the same.

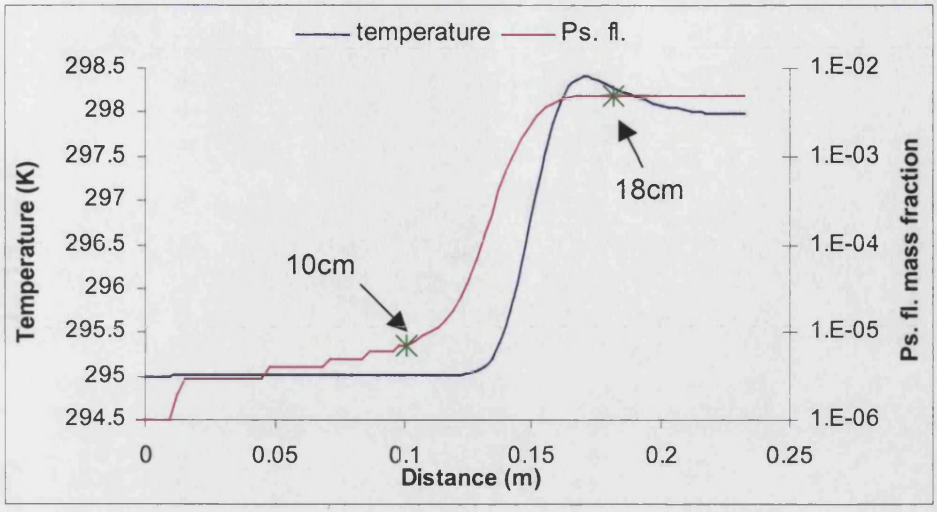

Figure 5.2.17: Temperature and *Ps. fluorescens* distribution predictions down the T-piece for the 2nd experiment after cleaning.

Temperature contours (fig 5.2.18) give the history of it and it is clear that at such short time period conduction does not play a significant role.

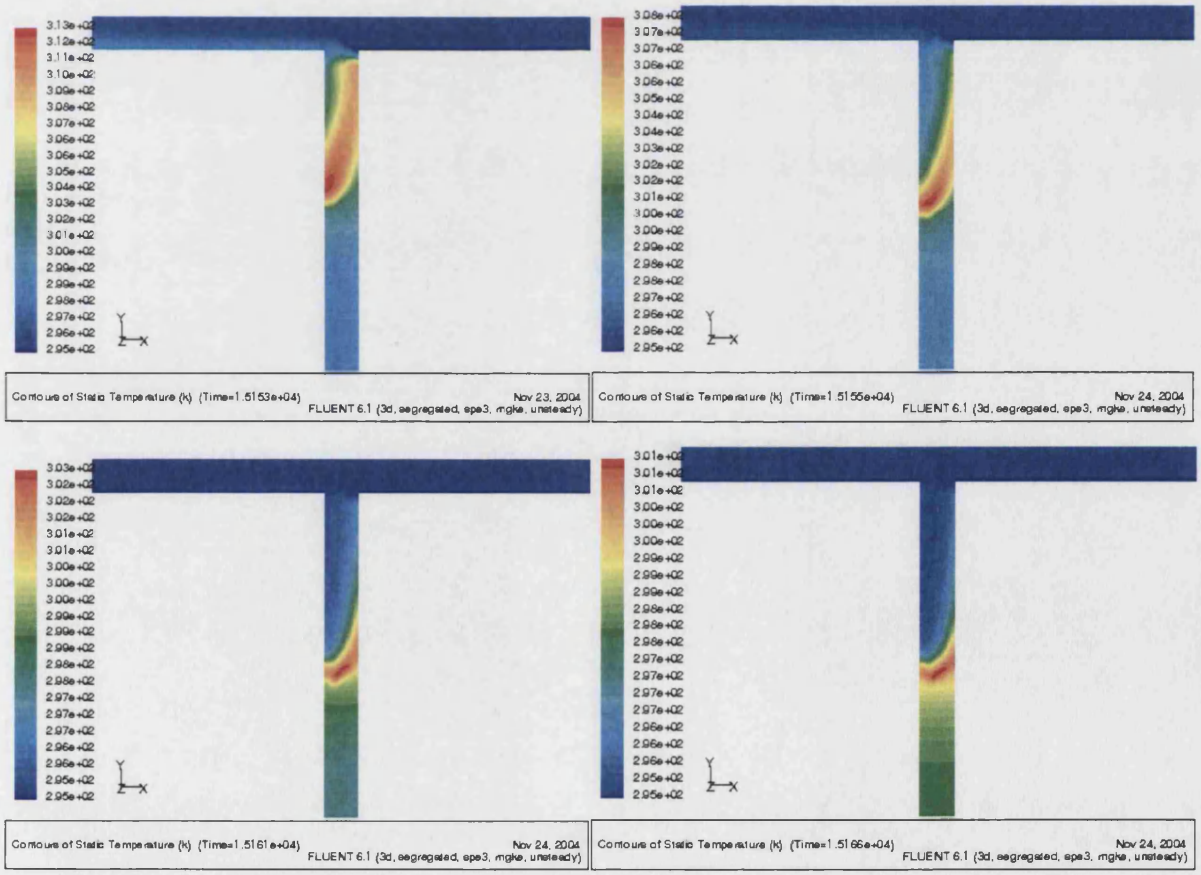

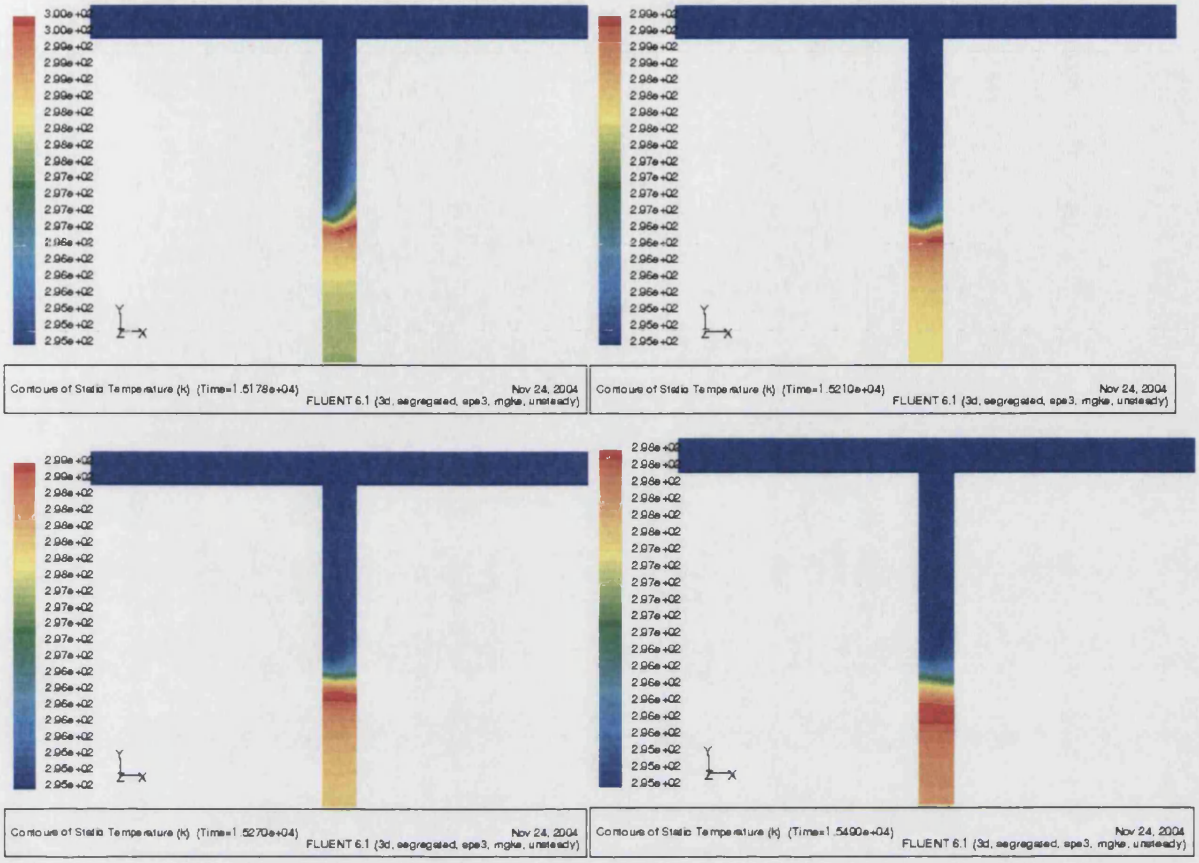

Figure 5.2.18: Temperature contours at various stages of flushing for the first experiment with bacteria.

Bacteria and TSB removal (fig 5.2.19 and 5.2.20) is happening quite slowly once the cleaning solution is into the tube. There is no death of bacteria since temperatures are not high and the only cleaning happens mechanically.

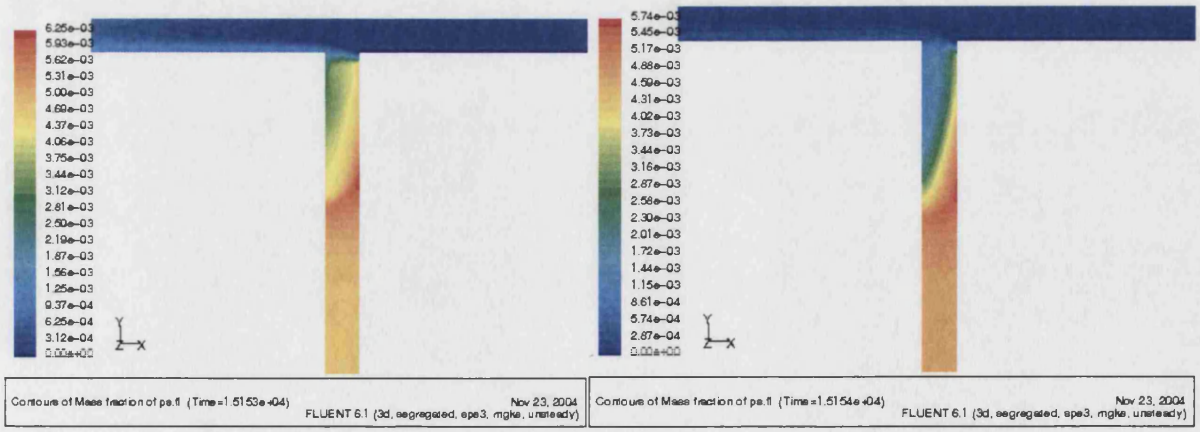

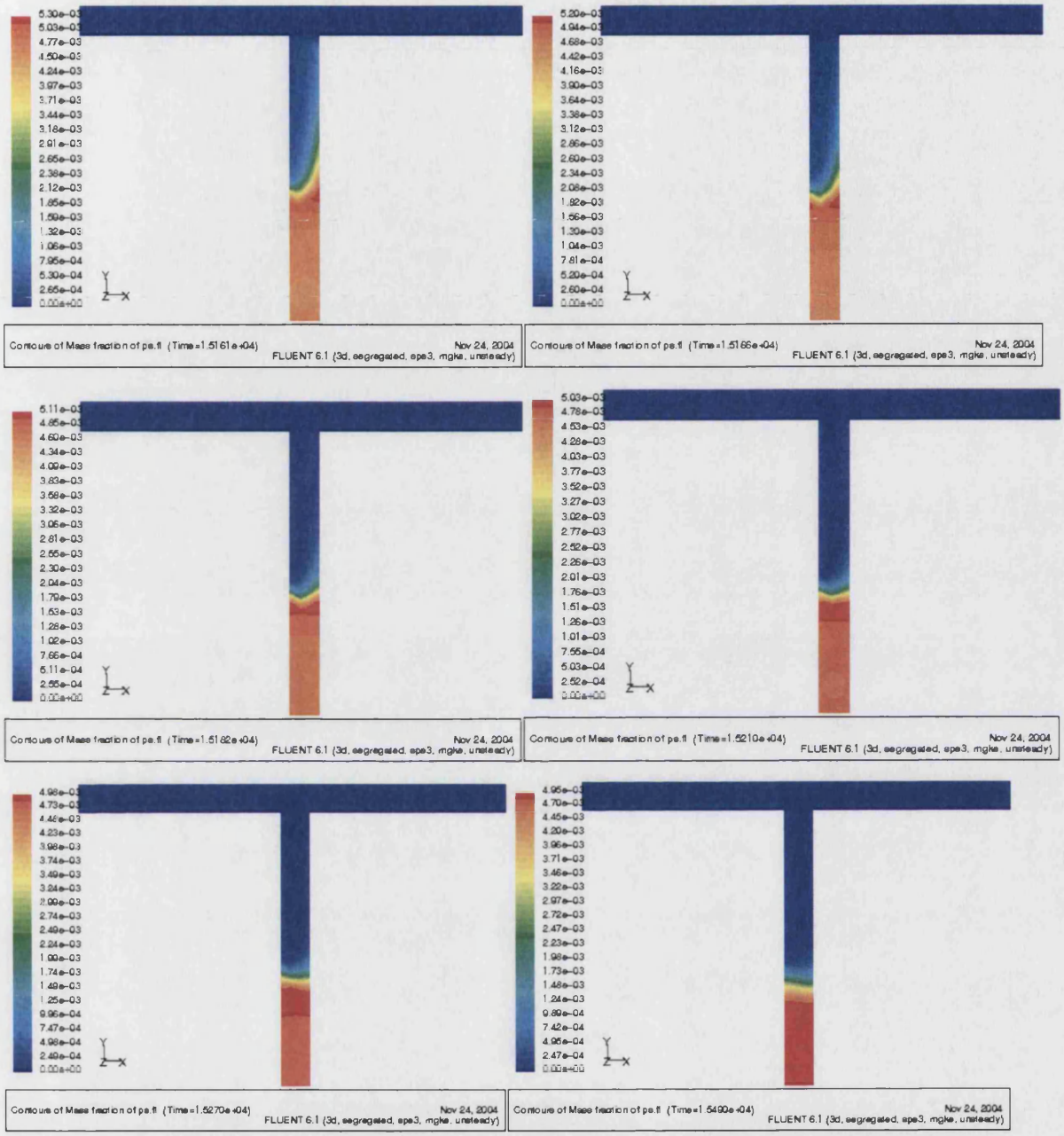

Figure 5.2.19: *Ps. fluorescens* mass fraction contours at various stages of flushing for the first experiment with bacteria.

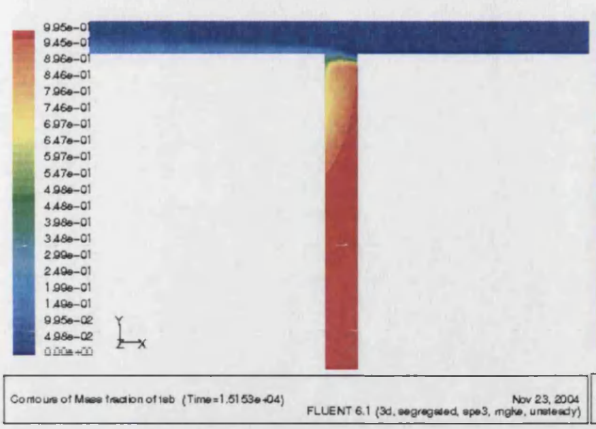

Contours of Mass fraction of tab (Time=1.5153e+04)
Nov 23, 2004
FLUENT 6.1 (3d, segregated, spe3, mgke, unsteady)

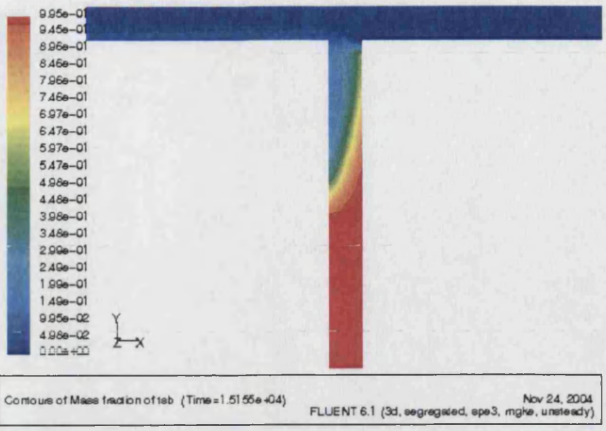

Contours of Mass fraction of tab (Time=1.5155e+04)
Nov 24, 2004
FLUENT 6.1 (3d, segregated, spe3, mgke, unsteady)

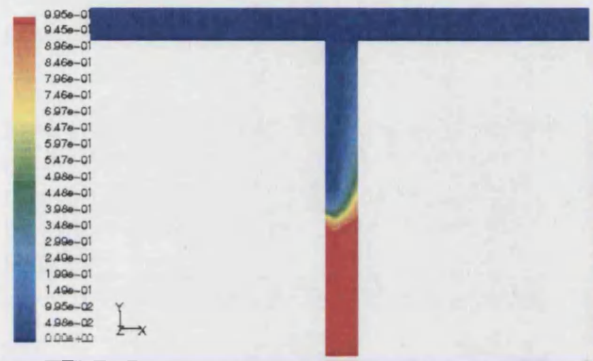

Contours of Mass fraction of tab (Time=1.5164e+04)
Nov 24, 2004
FLUENT 6.1 (3d, segregated, spe3, mgke, unsteady)

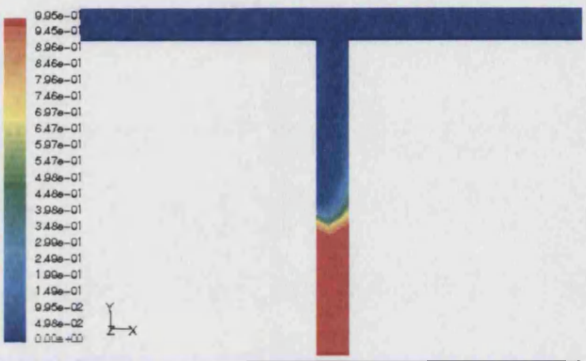

Contours of Mass fraction of tab (Time=1.5174e+04)
Nov 24, 2004
FLUENT 6.1 (3d, segregated, spe3, mgke, unsteady)

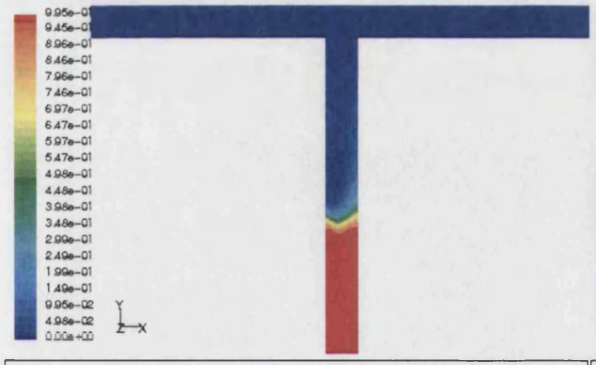

Contours of Mass fraction of tab (Time=1.5182e+04)
Nov 24, 2004
FLUENT 6.1 (3d, segregated, spe3, mgke, unsteady)

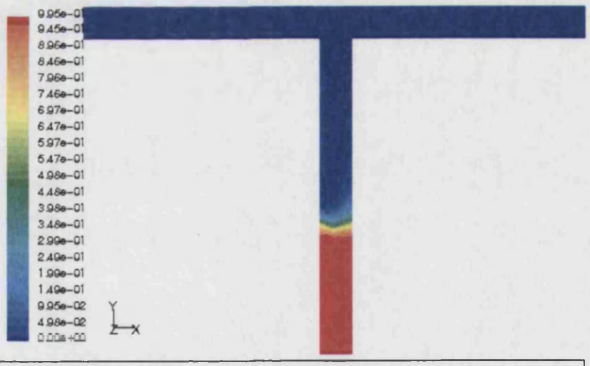

Contours of Mass fraction of tab (Time=1.5214e+04)
Nov 24, 2004
FLUENT 6.1 (3d, segregated, spe3, mgke, unsteady)

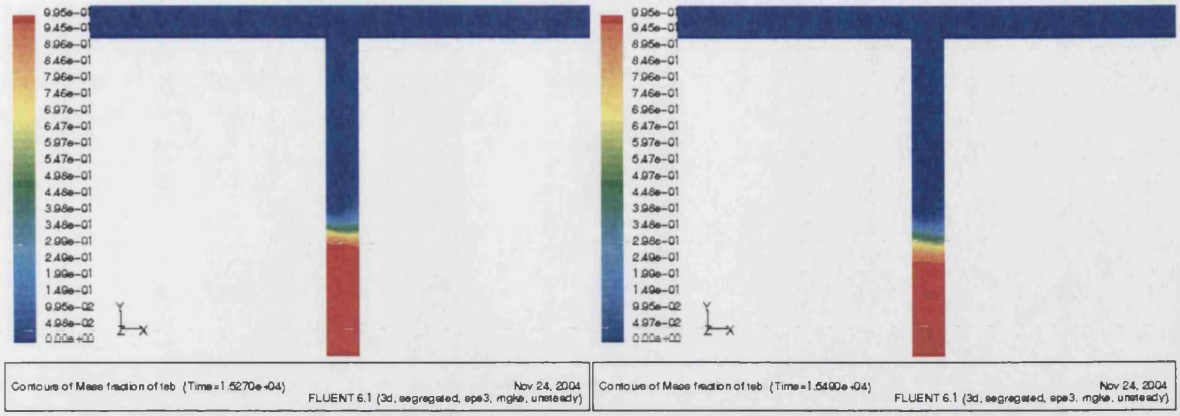

Figure 5.2.20: TSB mass fraction contours at various stages of flushing for the first experiment with bacteria.

By noticing the path lines of velocity and residence time, as they appear at the end of cleaning (fig 5.2.21 (a) and (b)), is obvious that at around 14.8cm down the pipe velocity slows down and mass removal does not occur below that point. Velocity path lines are distributed for low values in order to see the zone where the drop is sudden and mass does not recirculate and stops interacting with the bulk flow.

(a) (b)

Figure 5.2.21: Path lines of mass less particles at the end of cleaning for low ranged velocity vectors (a) and residence time (b) for the 2nd experiment with bacteria.

This experiment and model showed again the inconsistency between the whole biokinetic range that includes both growth and inactivation. In temperature values close to inactivation, but still

below that, the growth is overestimated. After cleaning concentration in the middle of the vertical pipe is again overestimated by a couple of log numbers. In general, though, the description of the kinetics are in good qualitative agreement with the experimental results and the errors that occurred are within the expected limits taking into account the fact that not all conditions can be reproduced in the simulation and not all parameters that affect microbial behaviour can be included in the models.

5.2.3 Third bacterial kinetics experiment

During this experiment the first attempt to cool down the system was made. For this reason the tank was jacketed with a flexible hose chilled with mixture of glycol and water coming out from a chiller. In this case the experiment lets the pump to carry on giving heat into the system. The cooling is very slow and not effective. It only provides a delay in the heating that allows observation of inactivation. Temperature values reached are so high that most of the bacteria stay under inactivation conditions for long enough to die.

The first part of the experiment lasted approximately 3 hours and the tank was saturated with bacteria from the beginning. Temperature reached 70°C within that period of time (fig 5.2.22). Tin and Tout are very close, so there are no heat losses along the horizontal pipe.

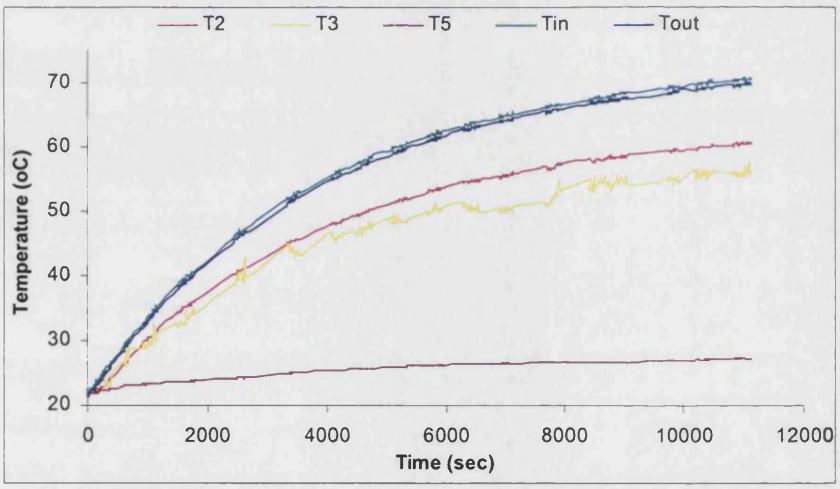

Figure 5.2.22: Temperature history during the 2nd experiment before cleaning.

Flow for the first part was 150 lthr^{-1}. T_{env} was around 23.5-24°C and feed sample was taken at around 21°C. Cooling did not work, as was already mentioned, and temperature reached 70°C within 3 hours. Flushing flux reached average of 1340 $l.h^{-1}$.

Table 5.2.6 shows the counts before and after cleaning, which lasted 4min. Generally the lower dilutions before cleaning were three and still gave 2 to 5 colonies. The rest gave practically nothing. So, it was concluded that the numbers were very low and bacteria were killed and went down to very low numbers. After cleaning, while flow reached 1350$l.h^{-1}$, counts were very low for all dilutions that correspond to the outlet and top. Concentration at the 10th cm dropped by 3 log numbers and at the bottom stayed the same.

Table 5.2.6: Concentrations during the 3rd experiment

Stage / Position	Feed ($cfuml^{-1}$)	Before cleaning ($cfuml^{-1}$)	After cleaning ($cfuml^{-1}$)
Outlet	10^9	10^4	10^2
Top of vertical pipe	-	10^4	10^2
10cm	-	10^9	10^6
18cm	-	10^9	10^9

Spectrophotometry measurements took place again (table 5.2.7) based on calibration with deionised water like for the previous experiments. Here we can see that absorption is high even where the log numbers are low before cleaning. This means that even the dead cells are included. That is why numbers dropped only after cleaning.

Table 5.2.7: Deionised water based spectrophotometry measurements for samples of 3rd experiment.

Stage / Position	Feed (nm)	Before cleaning (nm)	After cleaning (nm)
Outlet	1.12	1.11	0.02
Top of vertical pipe	-	1.1	0
10cm	-	1.04	0.04
18cm	-	1.07	1.06

The above experiment can be modelled with the following boundary conditions:

Inlet: $10^9 cfuml^{-1}$,

Inlet flow: $150 l.h^{-1}$

Inlet temperature is expressed by reading the profile during the experiment. The duration of the experiment was 11136sec, which means: 11136/60=185.6min more than 3 hours

$u_{in}=0.082ms^{-1}$

T_{in} was the profile taken from the experimental data.

Tenv=297K

$h_{hor}=2.7\ Wm^{-2}K^{-1}$

$h_{ver}=4.42\ Wm^{-2}K^{-1}$

The microbial kinetics are modelled using the *Species Transport Model*. So, in the flow there is water and at the inlet boundary conditions has to be set the mass fraction of the bacterium

Pseudomonas. It is set to be 1.524exp(-3). This is calculated with the same way as shown for the previous experiments.

Using the UDF to describe the inlet equal to the mass fraction coming out of the outlet and the temperature profile, the results of the temperature and bacterial mass fraction history are plotted (fig 5.2.23 and fig 5.2.24 (a) and (b)) for the central axis along the dead leg. Temperature rises in general, but it remains practically the same after approximately the 17th cm. This means that this area is not affected by the changes above and heat does not diffuse at those depths. It is also noticed that the threshold of the temperature drop is established very soon and is around 7.5cm.

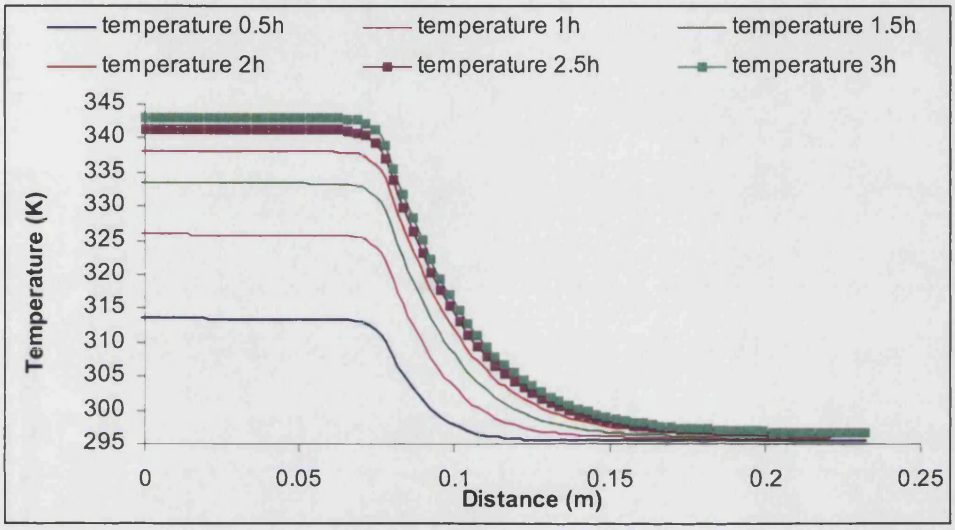

Figure 5.2.23: Temperature distribution down the vertical pipe for the 3rd experiment every 30min.

The mass fraction showed a very small growth the first 30min and then, when temperature reached the inactivation values, the drop was very fast. This again shows that the model used to express overestimates the death rate. The drop is of several orders of magnitude after an hour. Towards the end of the heating the numbers are practically zero. From the point where temperature does not change much and is not affected by the superjacent rises growth is more homogeneous. At the 10th and 18th cm at the end of this part of the experiment mass fraction is of around 10^{-3} that corresponds to 10^{9}cfuml^{-1}, agreeing very well with the counts on table 5.2.6.

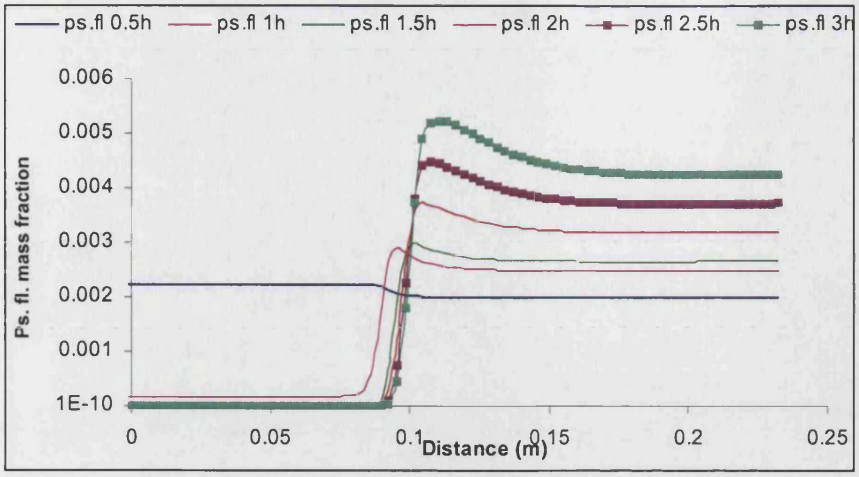

(a)

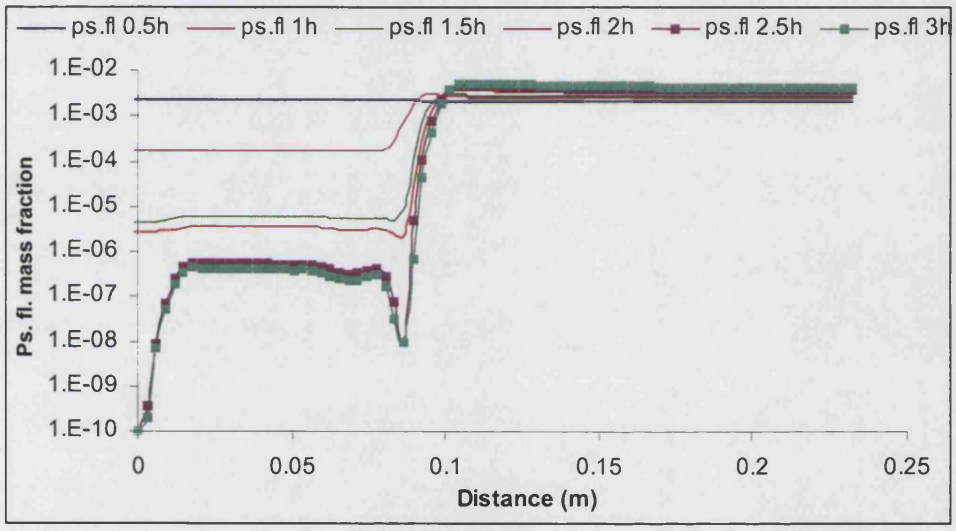

(b)

Figure 5.2.24: *Ps. fluorescens* mass fraction down the vertical pipe for the 2nd experiment every 30min (a) decimal scale, (b) logarithmic scale.

Cleaning is for 4min and the following boundary conditions are applied:

$u_{in}=0.738 ms^{-1}$

$T_{in}=294K$

$T_{env}=298K$

$h_{hor}=2.23\ Wm^{-2}K^{-1}$

$h_{ver}=2.7\ Wm^{-2}K^{-1}$

Again replacement of TSB with water is clear (fig. 5.2.25). The inclination of the exponential drop of TSB mass fraction coincides with that of temperature.

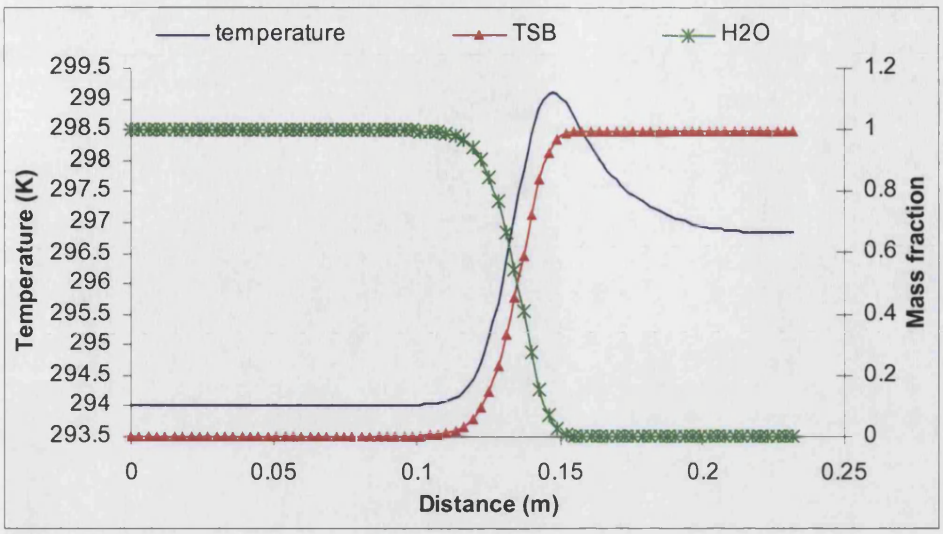

Figure 5.2.25: Temperature, TSB and water distribution down the T-piece for the 3rd experiment after cleaning.

This is not the case though for the bacteria mass fraction. Drop is exponential almost between the 15th cm and the 1.5cm where it is almost where the vertical tube starts. Thus, concentration is practically zeroed only where flow is in the horizontal pipe. This is in agreement with the counts on table 5.2.6 that give only 10^2cfuml^{-1}. At 10cm mass fraction is around 10^{-5} that is 10^7cfuml^{-1}, which is only one log number overestimation. At the bottom is 10^{-3}, which means 10^9cfuml^{-1} agreeing with the counts.

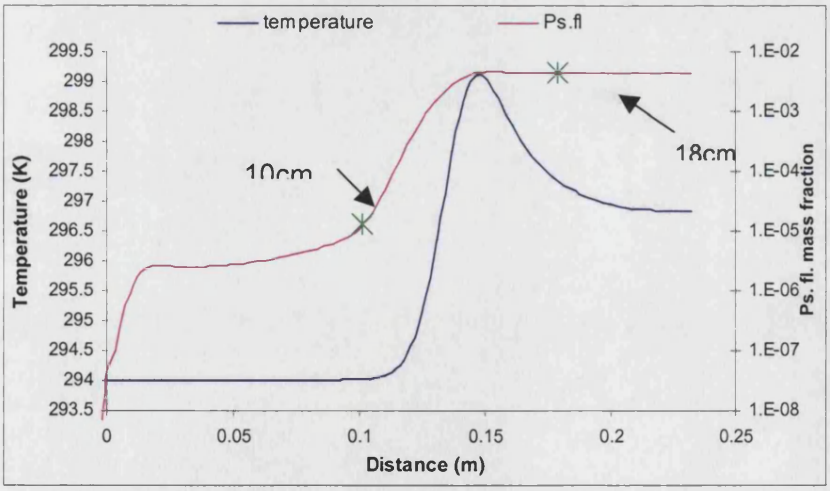

Figure 5.2.26: Temperature and Ps. fluorescens distribution down the T-piece for the 3rd experiment after cleaning.

Figure 5.2.27 (a) and (b) show the path lines of mass less particles released from the central axis of the dead end and the inlet. The recirculation zone stops at around the 15th cm but at

around 14cm down the pipe velocity slows down and mass removal does not occur below that point.

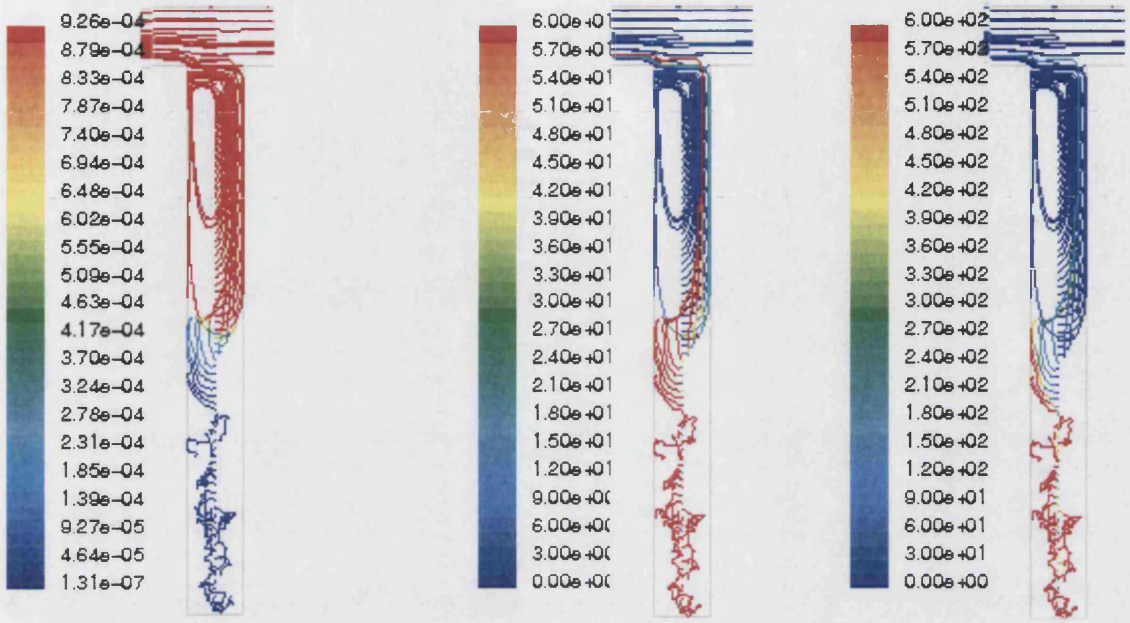

Figure 5.2.27: Path lines of mass less particles at the end of cleaning for low ranged velocity vectors (a) and residence time (b) for the 3rd experiment with bacteria.

5.2.4 Comments on the bacterial kinetics experiments

The models used to describe growth and inactivation are not continuous equations. They come from different sources and when the inactivation temperature regime was entered there were divergence problems because of inconsistency of the resulting reaction rates calculated by the UDF.

It was also found that inactivation rate was overestimating the death of the bacteria. Otherwise, the agreement was satisfactory, since the tendency of the kinetics predicted was the one counted and expected. When growth was involved the numbers that came out of the simulation were in good agreement with the experiment with one or two log numbers overestimation probably, which was consistent throughout the whole geometry.

The species model calculated as maximum mass fraction values around 0.001-0.005. This was observed after some trial runs in FLUENT where growth was let to carry on for much longer at the right temperature. This number corresponds to 10^9cfuml^{-1}, which is the saturated in bacteria broth solution.

Also, it is verified that cleaning is a combination of parameters: time and velocity. In the second experiment we have lower inlet velocity compared to the other two. However, the low velocity zone is slightly further down the tube since the cleaning lasted longer.

Experimental set up did not offer a lot of flexibility since there was a risk of cross contamination. The high pressures created in the T-piece made it impossible to fit both thermocouples and syringes for sampling in the same port. Also, the laboratory, where experiments were carried out, was not microbiology one. Hence, not all the necessary facilities were available and plating had to be done as soon as possible after the end of the experiment in order to avoid contamination. Additionally, not all the parameters affecting bacterial kinetics could be taken into account, neither in the UDF, nor in the CFD calculations (e.g. sudden temperature changes, possible shear stresses etc.).

Overall, the code was proven to give a good insight of the microbial conditions into such configurations, using temperature dependent kinetics and variable temperature so as to be as close as possible to real in line circumstances. A better model is probably necessary to be developed for temperatures around the inactivation area.

Also demand for accuracy differs between engineering and microbial calculations. In bacterial counts log orders are mentioned when it comes to counting, whereas engineering measurements need to be more precise, e.g. a deviation of a few of degrees in temperature during a heating process can lead to undesirable results.

The work presented in this chapter is the last sets of experiments that focus on transient flows. The results and comparison between the measurements and models give interesting correlations and observations. Combined with the steady state simulations results from chapter 4, they can provide a good assessment for the hygienic and safe design at parts of the configuration that might seem risky.

The following chapter discusses what these results mean for the food industry and the importance to the designers, engineers and microbiologists that share the same concerns and should work in strong collaboration.

6 Conclusions and Recommendations for further work

Hygiene in the food industry is a very important issue that, although it has drawn attention the last decades, it has not been improved considerably after the establishment of the main crucial points. It is an area that demands further investigation in order to save energy and meet product quality standards and process requirements.

6.1 Aims of this work

Because of the above and the small number of techniques existing so far to estimate and assess the hygienic design and safety of process lines, this work aimed at the investigation of applying CFD for such purposes. Computational Fluid Dynamics offer the possibility to follow the flow at any stage and time. Many parameters can be monitored, such as: velocity, temperature, concentrations, shear stresses etc. The user can set up his/her own equations to express one or more parameters in a different way or to introduce the calculation of a new one.

6.2 What was done

In summary, this work involved product and equipment interactions. It was a combination of CFD modelling and validation of it with experiments carried out at the Chemical Engineering Department Laboratory at the University of Bath and real time in-line measurements at a Unilever Factory.

Initially, temperature distribution was predicted down a T-piece. The horizontal pipe had a specific Newtonian flow field and temperature. The aim was to see how this was affecting the vertical pipe of the domain. There was a temperature difference between the top and the bottom and for each model and experiment there was a gradual increase to the velocity, moving from laminar to fully turbulent. The results were compared to experimental values that were taken from thermocouples along the dead end and the inlet and outlet of the horizontal part.

Heating was also validated for a series of Tube and Tube and Tube heat exchanger that included connecting bents for the flow of a non-Newtonian fluid. The aim was to see if heating was sufficient for the sterilisation of the product and to investigate the effect the geometry has on the flow. Both this and the above models were assuming steady state flow conditions.

The next set involved, apart from steady state, also transient flows and mass removal from the down stand. An electrical conductivity probe was fit at the bottom of the T-piece and salt concentrations were measured before and after cleaning with deionised water. This was compared to the CFD model where salt content was expressed with the Species model.

The last set of experiments together with the simulations involved only transient flows. Bacteria kinetics were included of single species. The microorganism used was *Ps. fluorescens*, a spoilage bacterium. Microbial growth and inactivation were expressed with temperature dependent equations and the number of bacteria predicted before and after cleaning was compared to counts taken out of the rig with plating techniques and spectrophotometry.

6.3 Summary of Results

The steady state calculations were carried out with various models available in FLUENT to solve turbulent and transitional flows. Those were compared to the experimental values and the one matching them best was accepted. The important thing to keep in mind here is that the models chosen to be solved were based on the flow expected in the horizontal tube since it is not clear what kind of development the flow is going to have in the vertical tube. The k-ω SST with transitional flow option was chosen for the low Reynolds number transitional flow, which was very close to the laminar model as well for the flow chosen. As velocities were increasing, the models moved from k-e STD for the $300 l.h^{-1}$ and $600 l.h^{-1}$ to k-e RNG for the fully developed turbulent flows of $1000 l.h^{-1}$ and $1340 l.h^{-1}$. Solutions were carried out with finer meshes as well for some of the flows. The result was that temperature values were overestimated down the tube and remained higher for longer lengths than in reality. Thus, although the finer the meshes the better the solution, in this case it was proven to be not only unnecessary but also misleading. This was probably because when the number of cells increased, the dead end domain was affected more computationally from the results in the horizontal tube.

The non-Newtonian flow in the TnTnT heater showed agreement between simulation and in line measurements only at the end of the whole process. The rest of the sensors were incorrectly located on the bends. Therefore, measurements were affected and second heating was appearing to lead the product to higher temperatures than the third. The simulation showed that the flow into the bends helped heat transfer, since the product was coming out at a higher temperature than the one it had at the entrance. This meant that there was mixing occurring in the bends that was distributing the temperature more homogeneously between the hotter product that was close to the walls and the colder in the centre. Generally, this model proved that CFD can provide reliable predictions for non-Newtonian fluid flows as well, although more data would offer definitely a better support to the predictions. However, this is not always possible when the data for validation comes from a real production line. Most of the time, it is not easy to make any alterations in order to fit thermocouples or any other probes along the line. Also, the processes are so demanding during production that any extra monitoring is a time consuming task that cannot be included into the everyday routine very successfully. The computational difficulties were lying in the fact that the configuration was complicated and the 6m long heaters were taking a significant time to converge.

The first transient flows modelled in this work were based on electrical conductivity measurements in order to assess mass removal from the T-piece experimentally. Temperature gradient down the vertical pipe was minimised in order to avoid big variations of the conductivity. The agreement between predictions and measurements was good having the model overestimating the location in the pipe where concentration corresponded to the one measured by approximately two centimetres upwards. This was a quite sensitive property to calculate accurately, using a probe that was not in-line but just one of laboratory application. The probe also could not be moved to various heights, which would be very interesting so as to see the concentration profile down the pipe and how it changes while cleaning is in progress.

Nevertheless, the species model used to express the salt concentration in the above models gave a good understanding for the set up of the following ones. Bacterial kinetics were taken into account at various stages of the biokinetic range. Cleaning followed again with deionised water. Plating techniques gave the colonies formed per one millilitre at various depths down the T-piece and at the outlet of the geometry being studied. These numbers were correlated to the mass fraction of the bacteria predicted by FLUENT, both before and after cleaning. The

comparison proved that the reaction models used to express the microbial kinetics were not consistent since they were taken from different literature sources. Specifically, the inactivation model was overestimating the death of the bacteria and the mass fraction was dropping rapidly. Due to the inconsistency of the whole biokinetic range, the time step had to be very low in order to avoid divergence of the solution. Also, some of the parameters that affect the microbial survival, such as pH, water activity etc. were not taken into account. The whole system is active and lag or stationary phase are not well described by the predictions or not sufficiently included at the assessments of the boundary conditions. Also, the broth with the *Ps. fluorescens* colonies underwent a lot of shear stresses in the rig (contractions, expansions, pump, plate heat exchanger etc.). Considering that the above were not included in the simulation, the estimations of the program solution was very close with only one to two log numbers divergence. It should also be taken into account that the counting plates technique is not of high accuracy, which is something that contributes to discrepancies.

6.4 Future Work

6.4.1 Temperature and mass removal in unhygienic geometries

The work that has been done here connects cleaning and disinfection to temperature and velocity predictions. That is why the experimental set up expanded from initial steady state cases, including temperature variations, to transient including mass removal and species modelling on top of the temperature measurements.

The simulations based on the T-piece configuration can be carried out with non-Newtonian products as well with various viscosity models. Temperature distribution is going to be different and cleaning is expected to be harder and less efficient when keeping the same experimental facilities. Mass removal is not going to be easy and penetration of the cleaning fluid might stop at a shorter length. This could be noticed better using probably a different kind of material for the T-piece. A kind of special glass, resistant enough to high pressures, could be used to visualise the mass removal and record it.

Also, geometry can change. Different ratios between the horizontal and the vertical pipe diameter can help to draw conclusions relating to the heat diffusion and cleaning regimes. A reasonable result would be to achieve better cleaning if the vertical pipe is broader. Unfortunately, this is not the case most of the time in practice.

Cleaning and high temperature can also be checked for crevices and pipe fittings. There bacteria can accumulate, so it is essential that they are effectively cleaned or disinfected, if they exist. Of course, such geometries are not acceptable normally and should be avoided. Sometimes, though, this is not feasible or there is no time to do it. Hence, assessing the existing line is a real necessity and CFD is proven to be a tool to help to do it.

All the above configurations, especially the up-stand and down-stand shapes, can be tried for products such as emulsions or products that include particles. Examples from the food industry are: soups, sauces, ice-cream etc. Every one of these has food particles such as meat, vegetables, starch and fibres. This composition gives a variety of thermophysical properties that can be integrated into the CFD code with the help of the UDFs (User Defined Functions). These food products are highly viscous and sensitive to heat treatment and high shear stresses. Very high temperature might damage them and not high temperatures could probably not be

sufficient for decontamination. CFD has models such as the Discrete phase and the Species one that can express all these particles and different phases in one foodstuff.

Lethality and Cook values could also be included and calculated as Custom Field Functions. This can give good information for microbiologists in order to estimate if there is going to be any survival after a heat treatment.

Hence, in general, similar geometries to the T-piece used here and viscous products can add more interest for the food industry applications. In a CFD code it is easier to keep the geometry constant and alter the product properties than change constantly the dimensions of the configuration in question. Thus, a database could be created with already existing domains that might be considered unhygienic for the production lines. Then, by changing the fluid properties and processing parameters the geometries can be kept as independent variables and check how they influence the flow.

6.4.2 Tube in Tube in Tube flow.

This part of the CFD modelling has proven to be very useful since it was based on a real process line and the results were directly compared to a sterilisation unit with a non-Newtonian fluid. Further investigation, as it has already been mentioned, would be to try and take more accurate measurements during the process from locations that are not affected by other forms of heat transfer outside the process modelled.

Different viscosities are also expected to give different flow patterns with those in the bends being the most affected. In particular, the race track effect will have different starting point probably for less viscous products. It is quite likely, for instance, that low viscosity fluids may not stay close to the wall, but instead make direct contract as they enter the bend and then follow a more vertical route or hit the wall and leads itself to the opposite direction. Then, heating will be distributed in a different way as well since the mixing pattern is not the same.

Cooling of the same or similar product could be of great interest since viscosity decreases and heating is going to be distributed in such a way that mixing is going to occur and affect even more the whole process comparing to the sterilisation. Of course, this is going to depend on the temperature difference.

Other geometry changes could be investigated as far as it concerns the heating sections. An example would be the effect it would have on the flow and heat, if tubes were not concentric but slightly removed from their original position, probably due to vibrations and long use of the system.

6.4.3 Electrical conductivity measurements improvements

For the electrical conductivity based experiments there are a few amendments that can give more data to be compared with the models. For instance, an in-line probe could give more time dependent results and cleaning would be monitored with more detail. Different depths also down the dead end would give an interesting investigation of the mass removal. The in-line system, though, is very expensive and a simple laboratory use probe was considered sufficient to get an idea of the bottom of the vertical tube as far as it concerns mass removal.

Having to deal with electrical conductivity, which is a very temperature sensitive property, makes the experiment difficult to be set up. Temperature differences down the T-piece can give big variations to conductivity. Calibration of the probe was also a difficult task since there were two parameters taken into account: temperature as well as concentration.

Coloured fluids could also be a way to visualise the cleaning process, using again a transparent T-piece and make estimations of the accuracy of the electrical conductivity values measured.

6.4.4 Bacterial models

This part of the work has a lot of potential to be improved or changed. These experiments, together with the models, are transient and microbial count measurements can be taken every hour almost, taking into account the fact that 20min is typical doubling time of the *Ps. fluorescens* bacteria. Sampling at that frequency would clearly give a better image of the growth or inactivation since the temperature track was constantly being kept. However, due to the fact that the laboratory was not microbiology one, plating was better if it was made the same day as the experiment since storage facilities were not aseptic. In the laboratory there were a lot of parameters that should be taken care of such as careful recirculation of the broth solution with the bacteria, correct timing of the temperature measurements etc.

Sampling was difficult since it was taken from the ports with specially chosen syringes and needles and due to the high pressures, the rig had to be stopped every time before and after cleaning in order to do the sampling. The samples had to be poured immediately into sterile flasks and stored in a cool place in order to avoid any growth while waiting for the whole experiment to finish and start the plating. Thus, more aseptic conditions would probably allow more samples to be taken. There was also a delay period before understanding the bacteria behaviour. Therefore, the first experiments could not be modelled since incorrect dilutions were made. Hence, knowing in advance the behaviour of the bacterial system in use, could speed up the process of the experiments. More temperature ranges could have been checked and also different initial concentrations.

The reaction models used to express the kinetics are not consistent. They were developed under more controlled conditions compared to the rig used. The square root model that gives the growth gives a better fit, while the inactivation one is leading to higher rates of destruction. A better model for the behaviour of the specific bacteria is required to improve the quality of the predictions.

In this work it is a monopopulation suspension used. In reality, there is a mixture of coexistent *Pseudomonas* species that demonstrate a different behaviour under the whole biokinetic range. Thus, the next step could probably be the use of such model cultures that represent better the reality in an industrial production line.

All the above are modelling steps that connect to one of the major problems of the food industry: biofouling. Suspended bacteria have the tendency to adhere on the wall equipment. Many researchers (de Jong, 2001, Characklis 1990) connected biofilm formation to bulk concentration, wall attachment and detachment rates. This showed how necessary is to have an estimation of the content of the main flow. Afterwards, using the biofilm formation equations, models can be developed within CFD and for various geometries in order to predict adhesion and cleaning forces.

Generally, comparison of experiments and models has proven to give good, qualitative mainly, agreement. CFD, though, is a tool that demands good engineering knowledge. Processing understanding is also crucial in order to estimate the important points for hygienic design and make CFD valuable and trustworthy where plain numerical calculations are not sufficient.

This kind of approach will contribute to dealing with hygienic issues with a risk assessment based method rather than with a prescriptive way. This is the first piece of work that looks both at production and cleaning process, including low viscosity products as well.

APPENDIX 1: Reynolds Equations Derivation for Turbulent Flow

For constant density ρ and transport property δ the general balance equation for the property is:

$$\frac{\partial \psi}{\partial t} + (U \cdot \nabla)\psi = \dot{\psi}_G + \delta(\nabla^2 \psi) \tag{1.1}$$

this equation can be applied in turbulent flow with instant velocity vector given as:

$$U = \overline{U} + U' \tag{1.2}$$

and the instant value of the property given by :

$$\psi = \overline{\psi} + \psi' \tag{1.3}$$

by substituting (1.2) and (1.3) to (1.1) we take the equation that comprises the mean components and fluctuations:

$$\frac{\partial \overline{\psi}}{\partial t} + \frac{\partial \psi'}{\partial t} + (\overline{U} \cdot \nabla)\overline{\psi} + (\overline{U} \cdot \nabla)\psi' + (U' \cdot \nabla)\overline{\psi} + (U' \cdot \nabla)\psi' = \overline{\dot{\psi}}_G + \dot{\psi}_G{}' + \delta(\nabla^2 \overline{\psi}) + \delta(\nabla^2 \psi') \tag{1.4}$$

if we take the mean values of the above equation we'll take the following equation after many algebraic operations:

$$\frac{\partial \overline{\psi}}{\partial t} + (\overline{U} \cdot \nabla)\overline{\psi} + \overline{(U' \cdot \nabla)\psi'} = \overline{\dot{\psi}}_G + \delta(\nabla^2 \overline{\psi}) \tag{1.5}$$

or

$$\frac{\partial \overline{\psi}}{\partial t} + (\overline{U} \cdot \nabla)\overline{\psi} = \overline{\dot{\psi}}_G + \delta(\nabla^2 \overline{\psi}) - [\nabla \cdot (\overline{U'\psi'})] \tag{1.6}$$

APPENDIX 2: Governing equation for mean flow kinetic energy K

An equation for the mean kinetic energy K can be obtained by multiplying the x-component Reynolds equation by U_x, the y component by U_y and the z-component by U_z. After adding the results together and a fair amount of algebra it can be shown that the time-average equation governing the mean kinetic energy of the flow is:

$$\frac{\partial \rho K}{\partial t} + div(\rho K \mathrm{U}) = div\left(-P\mathrm{U} + 2\mu \mathrm{UE}_{ij} - \rho \mathrm{U}\overline{u_i' u_j'}\right) - 2\mu E_{ij} \cdot E_{ij} + \rho \overline{u_i' u_j'} \cdot E_{ij} \qquad (2.1)$$

I II III IV V VI VII

I	II	III	IV	V	VI	VII
Rate of change of K	Transport of K by convection	Transport of K by pressure	Transport of K by viscous stresses	Transport of K by Reynolds stresses	Rate of dissipation of K	Turbulence production

Where E is the mean deformation of fluid element.

APPENDIX 3: Governing equation for turbulent kinetic energy k

Multiplication of each of the instantaneous Navier-Stokes equations by the appropriate fluctuating velocity components (i.e. x-component equation multiplied by u' etc.) and addition of all the results, followed by a repeat of this process on the Reynolds equations, subtraction of the two resulting equations and very substantial re-arrangement yields the equation for turbulent kinetic energy k:

$$\frac{\partial(\rho k)}{\partial t} + div(\rho k \mathrm{U}) = div\left(-\overline{\mathrm{p'u'}} + 2\mu\overline{u'e'_{ij}} - \rho\frac{1}{2}\overline{\mathrm{u'}\cdot_{\mathrm{i}}\,\mathrm{u'_i}u'_j}\right) - 2\mu\overline{e'_{ij}e'_{ij}} - \rho\overline{u'_iu'_j}\cdot E_{ij} \qquad (3.1)$$

I Rate of change of k

II Transport of k by convection

III Transport of k by pressure

IV Transport of k by viscous stresses

V Transport of k by Reynolds stresses

VI Rate of dissipation of k

VII Turbulence production

The rate of dissipation per unit mass, whose dimensions are m^2/s^3, is of vital importance in the study of turbulence dynamics and is denoted by

$$\varepsilon = 2\nu\overline{e'_{ij}\cdot e'_{ij}} \qquad (3.2)$$

It is always the main destruction term in the turbulent kinetic energy equation, of a similar order of magnitude to the production term and never negligible.

APPENDIX 4: Parameters in the transport equations of the K-ε models

Modeling Turbulent Production in the k-ε Models

The term G_k, representing the production of turbulence kinetic energy, is modeled identically for the standard, RNG, and realizable k-ε models. From the exact equation for the transport of k, this term may be defined as

$$G_k = -\rho\overline{u_i'u_j'}\frac{\partial u_j}{\partial x_i} \tag{4.1}$$

To evaluate G_k in a manner consistent with the Boussinesq hypothesis,

$$G_k = \mu_t S^2 \tag{4.2}$$

where S is the modulus of the mean rate-of-strain tensor, defined as

$$S \equiv \sqrt{2S_{ij}S_{ij}} \tag{4.3}$$

Effects of Buoyancy on Turbulence in the k-ε Models

When a non-zero gravity field and temperature gradient are present simultaneously, the k-ε models in FLUENT account for the generation of k due to buoyancy, and the corresponding contribution to the production of ε.

The generation of turbulence due to buoyancy is given by

$$G_b = \beta g_i \frac{\mu_t}{\mathrm{Pr}_t}\frac{\partial T}{\partial x_i} \tag{4.4}$$

where Pr_t is the turbulent Prandtl number for energy and g_i is the component of the gravitational vector in the *i*th direction. The coefficient of thermal expansion, β, is defined as

$$\beta = -\frac{1}{\rho}\left(\frac{\partial \rho}{\partial T}\right)_p \tag{4.5}$$

The degree to which ε is affected by the buoyancy is determined by the constant $C_{3\varepsilon}$. In FLUENT, $C_{3\varepsilon}$. is not specified, but is calculated as:

$$C_{3\varepsilon} = \tanh\left|\frac{\upsilon}{u}\right| \tag{4.6}$$

where υ is the component of the flow velocity parallel to the gravitational vector and u is the component of the flow velocity perpendicular to the gravitational vector. In this way, $C_{3\varepsilon}$ will become 1 for buoyant shear layers for which the main flow direction is aligned with the direction of gravity and zero for buoyant shear layers that are perpendicular to the gravitational vector.

APPENDIX 5: Parameters in the transport equations for the Standard k-ω model

Modeling the Effective Diffusivity

The effective diffusivities for the k-ω model are given by

$$\Gamma_k = \mu + \frac{\mu_t}{\sigma_k} \tag{5.1}$$

$$\Gamma_\omega = \mu + \frac{\mu_t}{\sigma_\omega} \tag{5.2}$$

where σ_k and σ_ω are the turbulent Prandtl numbers for k and ω, respectively. The turbulent viscosity, μ_t, is computed by combining k and ω as follows:

$$\mu_t = \alpha^* \frac{\rho k}{\omega} \tag{5.3}$$

Low-Reynolds-Number Correction

The coefficient α^* damps the turbulent viscosity causing a low-Reynolds-number correction. It is given by

$$\alpha^* = \alpha_\infty^* \left(\frac{\alpha_0^* + \mathrm{Re}_t / R_k}{1 + \mathrm{Re}_t / R_k} \right) \tag{5.4}$$

where

$$\mathrm{Re}_t = \frac{\rho k}{\mu \omega} \tag{5.5}$$

$R_k=6$ (5.6)

$$\alpha_0^* = \frac{\beta_i}{3} \tag{5.7}$$

$\beta i=0.072$ (5.8)

In the high-Reynolds-number form of the k-ω model, $\alpha^*=\alpha^*_\infty=1$.

Modeling the Turbulence Production

Production of k

The term G_k represents the production of turbulence kinetic energy. From the exact equation for the transport of k, this term may be defined as

$$G_k = -\rho\overline{u_i'u_j'}\frac{\partial u_j}{\partial x_i} \tag{5.9}$$

To evaluate Gk in a manner consistent with the Boussinesq hypothesis,

$$G_k = \mu_t S^2 \tag{5.10}$$

where S is the modulus of the mean rate-of-strain tensor, defined in the same way as for the k-ε model ($S \equiv \sqrt{2S_{ij}S_{ij}}$).

Production of ω

The production of ω is given by

$$G_\omega = \alpha\frac{\omega}{k}G_k \tag{5.11}$$

where G_k is given by equation 5.9.

The coefficient α is given by

$$\alpha = \frac{\alpha_\infty}{\alpha^*}\left(\frac{\alpha_0 + \mathrm{Re}_t/R_\omega}{1+\mathrm{Re}_t/R_\omega}\right) \tag{5.12}$$

where R_ω = 2.95. α^* and Re_t are given by equations 5.4 and 5.5, respectively.

In the high-Reynolds-number form of the k-ω model, $\alpha=\alpha_\infty=1$.

Modelling the Turbulence Dissipation

Dissipation of k is given by:

$$Y_k = \rho\beta^* f_{\beta^*} k\omega \tag{5.13}$$

where

$$f_{\beta^*} = \begin{cases} 1 & \chi_k \le 0 \\ \dfrac{1+680\chi_k^2}{1+400\chi_k^2} & \chi_k > 0 \end{cases} \tag{5.14}$$

where

$$\chi_k \equiv \frac{1}{\omega^3}\frac{\partial k}{\partial x_j}\frac{\partial \omega}{\partial x_j} \tag{5.15}$$

and

$$\beta^* = \beta_i^*\left[1+\zeta^* F(M_t)\right] \tag{5.16}$$

$$\beta_i^* = \beta_\infty^*\left(\frac{4/15+\left(\mathrm{Re}_t/R_\beta\right)^4}{1+\left(\mathrm{Re}_t/R_\beta\right)^4}\right) \tag{5.17}$$

$$\zeta^* = 1.5 \tag{5.18}$$

$$R_\beta = 8 \tag{5.19}$$

$$\beta^*_\infty = 0.09 \tag{5.20}$$

where Re_t is given by equation 5.5.

Dissipation of ω

Is given by:

$$Y_\omega = \rho\beta f_\beta \omega^2 \tag{5.21}$$

where

$$f_\beta = \frac{1+70\chi_\omega}{1+80\chi_\omega} \tag{5.22}$$

$$\chi_\omega = \left|\frac{\Omega_{ij}\Omega_{jk}S_{ki}}{\left(\beta^*_\infty\omega\right)^3}\right| \tag{5.23}$$

$$\Omega_{ij} = \frac{1}{2}\left(\frac{\partial u_i}{\partial x_j} - \frac{\partial u_j}{\partial x_i}\right) \tag{5.24}$$

$F(M_t)$ is the compressibility function and is given by the following equation:

$$f_{\beta^*} = \begin{cases} 0 & M_t \le M_{t0} \\ M_t^2 - M_{t0}^2 & M_t > M_{t0} \end{cases} \tag{5.25}$$

where

$$M_t^2 \equiv \frac{2k}{\alpha^2} \tag{5.26}$$

$$M_{t0} = 0.25 \tag{5.27}$$

$$\alpha = \sqrt{\gamma RT} \tag{5.28}$$

In the high-Reynolds-number form of the k-ω model, $\beta_i^* = \beta_\infty^*$. In the incompressible form:

$$\beta_i^* = \beta^* \tag{5.29}$$

Model constants

$$\alpha_\infty^* = 1,\ \alpha_\infty = 0.52,\ \alpha_0 = \frac{1}{9},\ \beta_\infty^* = 0.09,\ \beta_i = 0.072,\ R_\beta = 8,$$

$$R_k = 6,\ R_\omega = 2.95,\ \zeta^* = 1.5,\ M_{t0} = 0.25,\ \sigma_k = 2,\ \sigma_\omega = 2$$

APPENDIX 6: Parameters in the transport equations for the SST k-ω model

Modeling the Effective Diffusivity

The effective diffusivities for the SST k-ω model are given by

$$\Gamma_k = \mu + \frac{\mu_t}{\sigma_k} \tag{6.1}$$

$$\Gamma_\omega = \mu + \frac{\mu_t}{\sigma_\omega} \tag{6.2}$$

where σ_κ and σ_ω are the turbulent Prandtl numbers for k and ω, respectively. The turbulent viscosity is:

$$\mu_t = \alpha^* \frac{\rho k}{\omega} \frac{1}{\max\left[\frac{1}{\alpha^*}, \frac{\Omega F_2}{\alpha_1 \omega}\right]} \tag{6.3}$$

where

$$\Omega \equiv \sqrt{2\Omega_{ij}\Omega_{ij}} \tag{6.4}$$

$$\sigma_k = \frac{1}{F_1/\sigma_{k,1} + (1-F_1)/\sigma_{k,2}} \tag{6.5}$$

$$\sigma_\omega = \frac{1}{F_1/\sigma_{\omega,1} + (1-F_1)/\sigma_{\omega,2}} \tag{6.6}$$

Ω_{ij} is the mean rate-of-rotation tensor and α^* is defined in equation 5.4. The, F_1 and F_2 are blending functions.

Modelling the Turbulence Production

Production of k

The term G_k represents the production of turbulence kinetic energy, and is defined in the same manner as in the standard k-ω model (eq. 5.9)

Production of ω

The term G_ω represents the production of ω and is given by:

$$G_\omega = \frac{\alpha}{\nu_t} G_k \tag{6.7}$$

Note that this formulation differs from the standard k-ω model. The difference between the two models also exists in the way the term α_∞ is evaluated. In the standard k-ω model is defined as a constant (0.52). For the SST model, α_∞ is given by:

$$\alpha_\infty = F_1 \alpha_{\infty,1} + (1 - F_1)\alpha_{\infty,2} \tag{6.8}$$

where

$$\alpha_{\infty,1} = \frac{\beta_{i,1}}{\beta^*_\infty} - \frac{\kappa^2}{\sigma_{\omega,1}\sqrt{\beta^*_\infty}} \tag{6.9}$$

$$\alpha_{\infty,2} = \frac{\beta_{i,2}}{\beta^*_\infty} - \frac{\kappa^2}{\sigma_{\omega,2}\sqrt{\beta^*_\infty}} \tag{6.10}$$

where κ is 0.41 and:

$\beta_{i,1}=0.075$ (6.11)

$\beta_{i,2}=0.0828$ (6.12)

Modeling the Turbulence Dissipation

Dissipation of k

The term Y_k represents the dissipation of turbulence kinetic energy, and is defined in a similar manner as in the standard k-ω model. The difference is in the way the term f_β is evaluated. In the standard model, it is defined as a piecewise function. For the SST model, is a constant equal to 1. Thus,

$$Y_k = \rho\beta^* k\omega \tag{6.13}$$

Dissipation of ω

The term $Y\omega$ represents the dissipation of ω, and is defined in a similar manner as in the standard model. In the standard model, β_i is a constant (0.072) and is defined in equation 5.8. For the SST model, f_β is a constant equal to 1. Thus:

$$Y_k = \rho\beta\omega^2 \tag{6.14}$$

β_i is given by

$$\beta_i = F_1\beta_{i,1} + (1 - F_1)\beta_{i,2} \tag{6.15}$$

$\beta_{i,1}$ and $\beta_{i,2}$ are given by Equations 6.11 and 6.12, respectively.

Cross-Diffusion Modification

The SST model is based on both the standard k-ω model and the standard k-ε model. The standard k-ε model has been transformed into equations based on k and ω, so a cross-diffusion term is introduced:

$$D_\omega = 2(1 - F_1)\rho\sigma_{\omega,2}\frac{1}{\omega}\frac{\partial k}{\partial x_j}\frac{\partial \omega}{\partial x_j} \tag{6.16}$$

Model Constants

$\sigma_{k,1}=1.176$, $\sigma_{\omega,1}=2$, $\sigma_{k,2}=1$, $\sigma_{\omega,2}=1.168$, $\alpha_1=0.31$, $\beta_{\iota,1}=0.075$, $\beta_{\iota,2}=0.0828$

All additional model constants have the same values as for the standard k-ω model.

This term is given by

$$\Gamma = \sum_{i}^{N} \gamma_{i,r} C_j \tag{7.1}$$

where $\gamma_{j,r}$ is the third-body efficiency of the j_{th} species in the r_{th} reaction. By default, FLUENT does not include third-body effects in the reaction rate calculation. However, third-body efficiencies can be included, if there is any data for them.

APPENDIX 8: Calculation of B and ε values.

A more detailed analysis of the equation that was developed that relates the inlet velocity to the temperature profile down the T-piece.

The relation that was chosen to describe the profile given on figure 4.2.37, was of the form:

$$T = (T_{in} - T_{env}) \cdot e^{-B(x-\varepsilon)} + T_{env} \tag{8.1}$$

or

$$\frac{T - T_{env}}{T_{in} - T_{env}} = e^{-B(x-\varepsilon)} \tag{8.2}$$

The above is solved for each flow twice using pairs of values from the modelled distribution: one at the end of the curve and the other from the middle of the exponential drop. So, for each flow there was a simple set of two equations that needed to be solved where the two unknowns were B and ε.

Figures 8.1 and 8.2 show the plot of ε and B against velocity at the inlet, which is the value every time used at the inlet boundary conditions for the CFD model. From these graphs we can see the comparison between the values calculated analytically for the five flows (blue lines) and the ones from the asymptotic regression models. It is obvious that the trend for the ε reaches asymptotically a maximum value and the trendline describes it quite well.

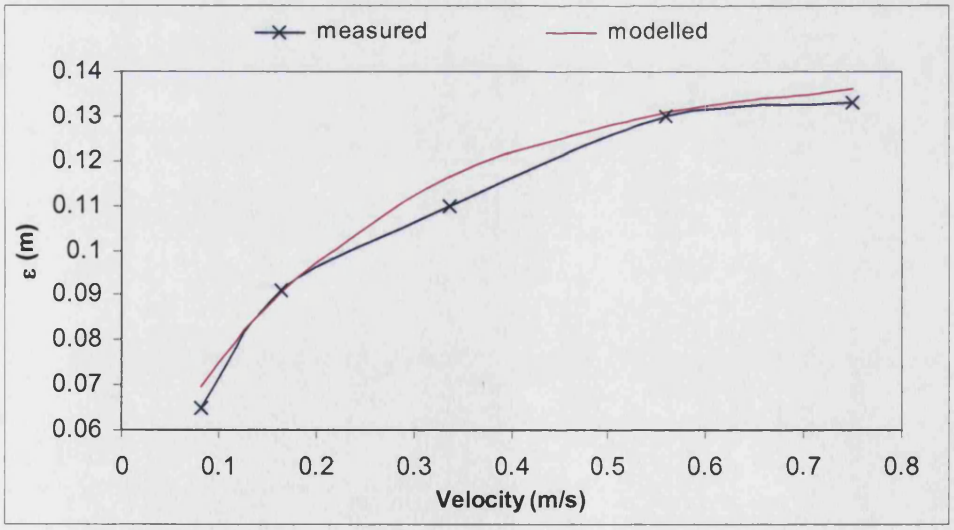

Figure 8.1: Measured and modelled ε values for the various flows.

For B the trend is not very clear although it is more likely that it is heading for a minimum value as velocity increases.

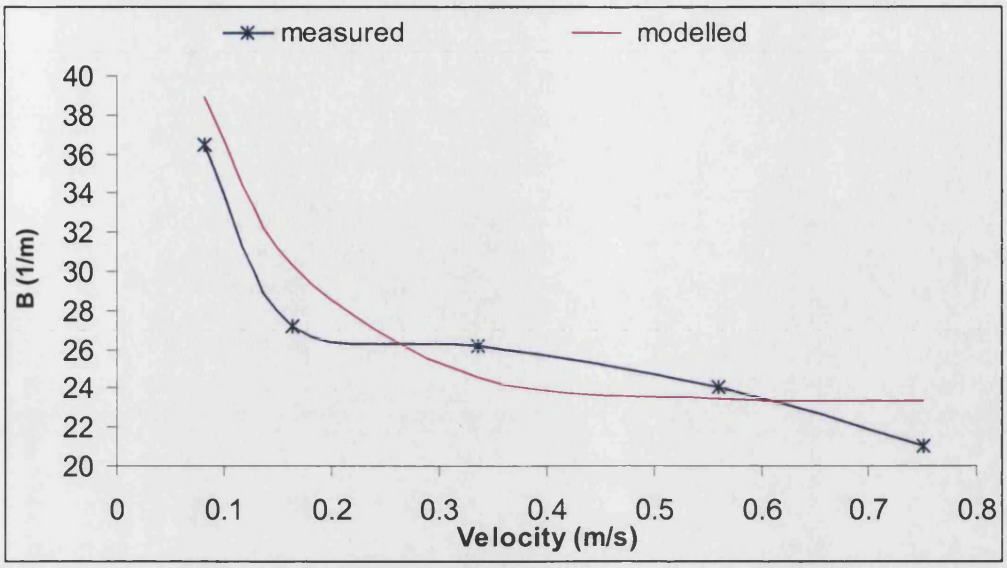

Figure 8.2: Measured and modelled B values for the various flows.

The RMSE ("root mean square error" = estimate of unexplained variation (sigma)) was 0.00387 for ε model and 5.81 for the B model (these are in the scale of the response variables).

However, the B model does not give a very good fit.

APPENDIX 9: Graphs correlating electrical conductivity of various concentration solutions at steady temperatures.

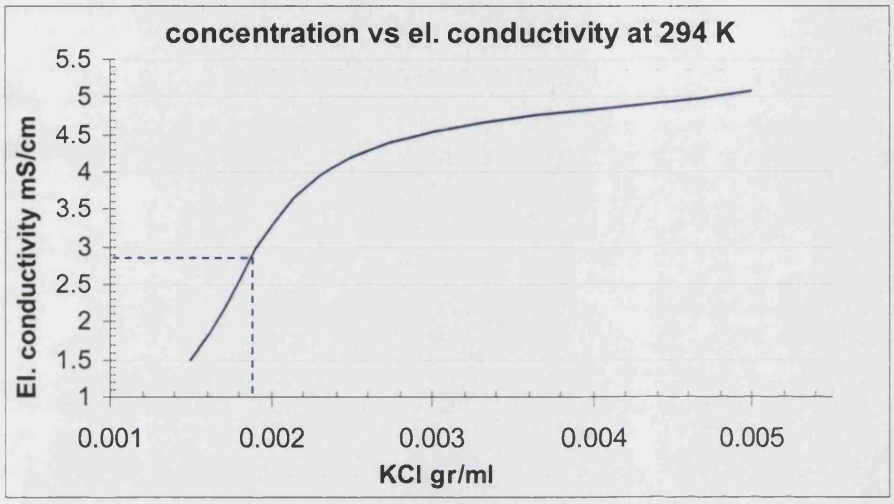

Figure 9.1: XY plot of KCl concentration vs el. Conductivity at 294K.

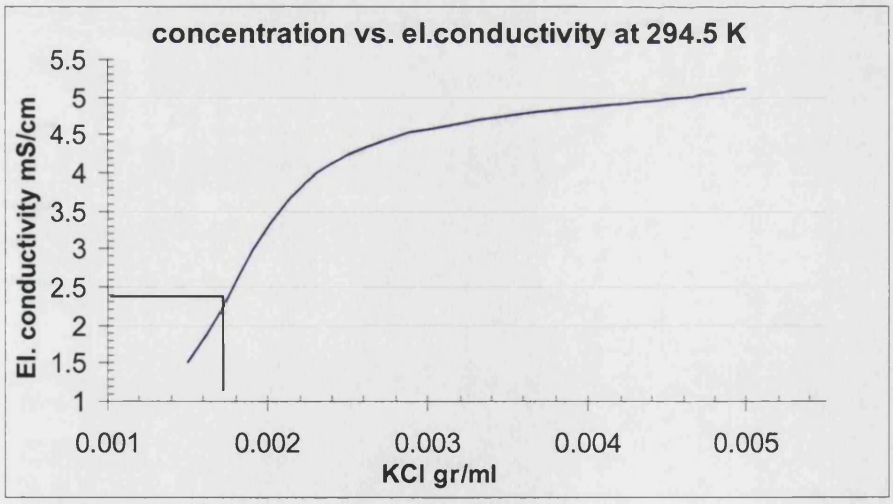

Figure 9.2: XY plot of KCl concentration vs el. Conductivity at 294.5K.

APPENDIX 10: UDFs used

```
/* udf to which reads area averaged mass fractions on a surface (such as outlet)
   and then applies it as BC on another surface such as inlet */

#include "udf.h"

#define EXIT_ID 4
#define INLET_ID 5

DEFINE_PROFILE(mass_frac_bc, inlet_face_thread, position)
{
  /* get access to domain which is not defined in this file */
  /* need domain for Lookup_Thread to access data */
 /*  extern Domain *domain; */
  Domain *domain = Get_Domain(1);

  /* look up all surface info */

  Thread *exit_face_thread = Lookup_Thread(domain, EXIT_ID);

  real area = 0.;
  real mag_area = 0.;
  real mass_frac = 0.;
  real avg_exit_mass_frac;
  real inlet_mass_frac;
  face_t f1;
  face_t f2;
  real A[ND_ND];

  /* data valid check prevents an attempt to calculate info from data not
     yet initialized */
  if(Data_Valid_P())
   {
```

```
    /* Loop through the faces of the exit surface */
    /* calculate the mass fraction of species 0 */
    begin_f_loop(f1, exit_face_thread)
     {
          F_AREA(A, f1, exit_face_thread);
        mag_area = NV_MAG(A);
          mass_frac += F_YI( f1, exit_face_thread, 0) * mag_area ;
        area += mag_area;
     }
    end_f_loop(f1, exit_face_thread);

    avg_exit_mass_frac = mass_frac/area;

/* Enter the F_YI_inlet as a function of FYI_exit here. */
/*******************************************************/
inlet_mass_frac = avg_exit_mass_frac ;

printf("setting inlet to %10.3e\n", inlet_mass_frac);

/* Loop through the faces of the inlet surface and define their
   inlet concentration. */
begin_f_loop(f2, inlet_face_thread)
 {
   F_PROFILE(f2, inlet_face_thread, position) = inlet_mass_frac;
 }
end_f_loop(f2, thread)
 }
else
 {
   printf("Please initialize solution.\n");
 }

}
```

```
DEFINE_VR_RATE(user_rate_new1, cell, thread, r, mole_weight, species_mf, rate, rr_t)
{

    real my_temp, my_ci;
    real my_b, my_Tmin, my_c, my_Tmax;
    real user_rate;

    my_temp = C_T(cell,thread);
    my_ci = C_R(cell, thread);
    my_b = 0.03*0.03/(3600*3600);
    my_Tmin = 279.0;
    my_c = 0.088;
    my_Tmax = 320.0;



  if(my_temp>=my_Tmin && my_temp<=my_Tmax)
    *rate = -my_b*pow((my_temp - my_Tmin), 2)*pow((1-exp(my_c*(my_temp-my_Tmax))),
2)*my_ci;

  else if(my_temp == my_Tmin && my_temp == my_Tmax)
    *rate = 0.000000000002;



  else
    *rate=(exp(116))*(exp(-41685/(my_temp)))*my_ci*exp(2.56*7)*exp(-0.25*7*7);

}
```

APPENDIX 11: Thermocouples error estimation.

In order to check the deviation of the thermocouples measurements the Standard Deviation Error is taken twice before the start of two experiments towards the end of all the experimental work. Hence, the environmental temperature (Tref) was taken at time 0 and was compared to all thermocoulpes 0.5mm (tables 11.1 and 11.2). All of them should give the same value equal to the environmental but they deviate slightly.

Table 11.1: Thermocouples error estimation for Tref 23.1°C

Thermocouples	T_1	T_2	T_3	T_4	T_5	T_6
°C	23.1	21.95	21.9	22.62	21.71	21.02
Average temperature:	22.36					
Standard Deviation:	0.58					
Standard Deviation Error:	0.24					

Table 11.2: Thermocouples error estimation for Tref 23.5°C

Thermocouples	T_1	T_2	T_3	T_4	T_5	T_6
°C	23.51	22.94	23.05	22.38	22.13	22.36
Average temperature:	22.73					
Standard Deviation:	0.52					
Standard Deviation Error:	0.21					

References

Alfa Laval, www.alfalaval.com, electronic citation

Allison D.G., Ruiz B., SanJose C., Jaspe Al. and Gilbert P., 1998, "Extracellular products as mediators of the formation and detachment of *Pseudomonas fluorescens* biofilms." FEMS Microbiology Letters 167 (1998) 179-184.

APV Fluid Components, "Fluid Handling Components", Product Catalogue, February 1995

Bakalis S., Cox P.W., & Fryer P.J 2001, "Modelling Thermal Processes: heating," in Food Process Modelling, 1st edn, Tijskens L.M.M., Hertog M.L.A.T.M, & Nicolai B.M., eds., Woodhead Publishing Limited, Boca Raton USA, p. 341--364.

Bakalis S., Cox P.W., & Fryer P.J., 2001, "Modelling Thermal Processes: heating," in Food Process Modelling, 1 edn, Tijskens L.M.M., Hertog M.L.A.T.M., & Nicolai B.M., eds., Woodhead Publishing Limited, Boca Raton USA, pp. 341-364.

Ball C.O. and Olson F.C.W., 1957, "Sterilisation in food technology", First edition, McGraw-Hill Book Company, Inc.

Baranyi J. and Pin C.,2001 "Modelling microbiological safety", in Food Process Modelling, 1 edn, Tijskens L.M.M., Hertog M.L.A.T.M., & Nicolai B.M., eds., Woodhead Publishing Limited, Boca Raton USA, pp. 382-401

Baranyi, J. & Roberts, T. A. 1995, "Mathematics of predictive food microbiology", International Journal of Food Microbiology, vol. 26,no. 2, pp. 199-218.

Baranyi, J. 2002, "Stochastic modelling of bacterial lag phase", International Journal of Food Microbiology, vol. 73,no. 2-3, pp. 203-206

Baranyi, J., Roberts, T. A., & McClure, P. 1993, "A non autonomous differential equation to model bacterial growth", Food Microbiology, vol. 10,no. 1, pp. 43-59.

Bellara, S. R., McFarlane, C. M., Thomas, C. R., & Fryer, P. J. 2000, "The growth of Escherichia coli in a food simulant during conduction cooling: combining engineering and microbiological modelling", Chemical engineering science, vol. 55,no. 24, pp. 6085-609.

Belova, S. E., Dorofeev, A. G., & Panikov, N. S. 1995, "Kinetics and Stoichiometry of Growth of Pseudomonas Fluorescens and Alcaligenes SP on a n agar containing medium", Microbiology, vol. 64, no. 3, pp. 289-294.

Bird M.R. and Bartlett M., 1995, "CIP Optimisation for the Food Industry", Trans IchemE, Vol 73, Part C, June 1995.

Bird M.R. and Espig S.W.P., 1998, "The Removal of crude oil from stainless steel surfaces using non-ionic surfactants", Fouling and cleaning in food processing '98, Proceedings of a conference held at Jesus college, Cambridge, 6 to 8 April 1998, published by European community.

Bishop An., 1997, "Cleaning In The Food Industry", Reprinted by permission of Wesmar Company Inc. from Basic Principles of Sanitation.

Boussinesq, J. (1877) "Theorie de l'ecoulement tourbillant"; Mem. Pres. Acad. Sci. Paris, vol 23, 46

Brodkey R.S. and Hersey H.C., 1988, "Transport Phenomena", McGraw-Hill, 1988, Translated in greek by Lavdakis K., A. Tziola E., 1990.

Brunskill R.E., Greenwood D.J. and Walker S.J., July 1993, "The effect of Temperature pH and Sodium Chloride on the Growth of *Pseudomonas spp.*", The Campden Food and Drink Research Association. Technical Memorandum No. 689.

Buchanan R.L & Cygnarowicz M., 1990, "A mathematical approach toward defining and calculating the duration of the lag phase", Food Microbiology, vol. 7, pp. 237-240

Bull Daniel, 2002, "The Quest for Sterilisation. Thermal Death Time and the F value." www.Hyperionresearch.com/tutorial/quest.html. 30-6-1999. 3-9-2002. Ref Type: Electronic Citation

Bull Daniel, 2002, "Temperature effects. The Z value.", www.hyperionresearch.com/ /tutorial/Zvalue.html. 30-6-1999. 3-9-2002. Ref Type: Electronic Citation

Cappuccino James G. & Sherman Natalie 2001, Microbiology A Laboratory manual, Sixth edition edn.

Casolari Antonio 1988, "Microbial Death" in *Physiological Models in Microbiology*, Michael J.bazin & James I.Prosser, eds., CRC PRESS, BOCA RATON, FLORIDA.

Casolari Antonio. "Food Sterilisation by Heat.", www.vency.com/sterilization.html . 1-5-2002. 1-5-2002. Ref Type: Electronic Citation

Casolari, A., 1994, "About Basic Parametres of Food Sterilisation Technology", 1994, Food Microbiology 11, 75-84

Chandler and McMeekin, 1985, "Temperature function integration and its relationship to the spoilage of pasteurised milk", The Australian Journal of Dairy Technology, March 1985.

Characklis W.G. & Cooksey L.E 1983, "Biofilms and Microbial Fouling", Advances in Applied Microbiology, by Academic Press, Inc, vol. Volume 29, pp. 93-138.

Characklis W.G. Marshall K.C. 1990, "Biofilms", A Wiley-Interscience Publication John Wiley & Sons, Inc., 1990.

Chen X.D., Yoo Jin-Ah, Benjamin Ad., & Turner M. 1998 "Study of Bacteria 'Transportation' in Model Milk Foulant and Bacteria Emission from Milk Fouling Layer into Streams of Rinse Water, Milk and Cleaning Chemical Solutions", Proceedings of conference on Fouling and Cleaning in Food processing '98. Wilson D.I., Fryer P.J., & Hasting A.P.M., eds., Office for Official Publications of the European Communities, Luxembourg, pp. 79-86. ISBN 92-828-5609-7.

Chiruta, J., Davey, K. R., & Thomas, C. J. 1997, "Thermal inactivation kinetics of three vegetative bacteria as influenced by combined temperature and pH in a liquid medium", Food and Bioproducts Processing, vol. 75,no. C3, pp. 174-180

Chiruta, J., Davey, K. R., & Thomas, C. J. 1997, "Thermal inactivation kinetics of three vegetative bacteria as influenced by combined temperature and pH in a liquid medium", Food and Bioproducts Processing, vol. 75, no. C3, pp. 174-180.

Christian G.K., Changani S.D. and Fryer P.J., 2002,"The effect of adding minerals on fouling from whey protein concentrate-Development of a model fouling fluid for a plate heat exchanger", Food and Bioproducts Processing, 80 (C4): 231-239 Dec 2002..

Clarke R.H. and Nicolas F. Cal Gavin Ltd., Alcester, UK, (2002) http:// www.technology. novem.nl/nl/heat-exchange/downloads/CFD%20Investigation %20of%20Maldistribution%20on %20Crude-oil%20Fouling.pdf

Cohen I., Golding I., Kozlovsky Y., & Ben-Jacob E. 1998, "Continuous and Discrete Models of Cooperation in Complex Bacterial Colonies", Inan E. & Markov K.Z., eds., World Scientific Publishing Co.

Combase, 2004, www.combase.cc.

Coulson J.M. and Richardson J.F., 1995, "Coulson & Richardson's CHEMICAL ENGINEERING", J.R. Backhurst and J.H. Harker, VOLUME 1 FIFTH EDITION Fluid Flow, Heat Transfer and Mass Transfer.

Coulson J.M., Richardson J.F., Backhurst J.R., & Harker J.H. 1995, Coulson & Richardson's CHEMICAL ENGINEERING, 5 edn, Butterworth-Heinemann.

Cousin M.A. Pseudomonas. Robinson R.K, Batt C.A., and Patel P.D. [Volume three], 1864-1867. 2000. Academic Press. Encyclopedia of Food Microbiology.

Danfoss. Product manual, MAGFLO Electromagnetic flowmeters. 1997. Danfoss A/S (IN-MSP) 10/1997.

Danfoss. Quick start manual, MAGFLO Electromagnetic flowmeter. 1999. Danfoss A/S (IN-MFC-KJ/SSS).

Daughtry B.J, Davey K.R. and King K.D., 1997, "Temperature dependence of growth kinetics of food bacteria." Food microbiology, 1997, 14, 21-30. Academic Press Limited

Davey, K. R. 1989, "A predictive model for combined temperature and water activity on microbial growth during the growth phase", Journal of Applied Bacteriology, vol. 67,no. 5, pp. 483-488.

Davey, K. R. 1989, "A Predictive Model for combined Temperature and Water Activity on Microbial Growth during the Growth phase", Journal of Applied Bacteriology, vol. 67, no. 5, pp. 483-488.

de Jong P., Giffel M.C., & Kiezebrink E.A. 2002, "Prediction of the adherence, growth and release of microorganisms in production chains.", International Journal of Food microbiology no. 74, pp. 13-25.

de Jong Peter, van der Horst H.C. and Waalewijn R., 1998 "Reduction of Protein and Mineral Fouling", Proceedings of conference on Fouling and Cleaning in Food processing '98. Wilson D.I., Fryer P.J., & Hasting A.P.M., eds., Office for Official Publications of the European Communities, Luxembourg, pp. 79-86. ISBN 92-828-5609-7.

Delignette-Muller M.L., 1998, "Relation between the generation time and the lag time of bacterial growth kinetics", International journal of Food Microbiology 43 (1998) 97-104)

den Aantrekker E.D., Boom R.M., Zwietering M.H., & van Schothorst M. 2003, "Quantifying recontamination through factory environments-a review", International Journal of Food microbiology no. 80, pp. 117-130.

Dhanasekharan, K.M., Grald, E.W. and Mathur, R., MARCH 2004, "How flow modelling benefits the food industry", Food Technology, vol. 58, No. 3: 32-35

Dubbelman S. & van Dijk M. 2004. Personal Communication

Dumont E., Fayolle F and Legrand J., 2000, "Flow regimes and wall shear rates determination within a scraped surface heat exchanger", Journal of Food Engineering 45 (2000) 195-207.

EHEDG 1993a, "Hygienic Design of Closed Equipment for the Processing of Liquid Food", Trends in Food Science & Technology, 4, 375-379

EHEDG 1993b, "Hygienic Equipment Design Criteria", Trends in Food Science & Technology, 4, 225-229

Farid M and Ghani A.G.A., 2004, "A new computational technique for the estimation of sterilisation time in canned foods", Chemical Engineering and Processing 43 (2004) 523-531.

Fernandez-Torres M.J., Fitzgerald M., Paterson W.R., & Wilson D.I. 2001, "A theoritical study of freezing fouling: limiting behaviour based on a heat and mass transfer analysis", Chemical Engineering and Processing 40 no. 40, pp. 335-344.

FLUENT Inc 2001a, FLUENT 6 User's Guide Volume 2 Lebanon.

FLUENT Inc 2001b, FLUENT 6 User's Guide Volume 3 Lebanon.

FLUENT news, 2003,"Customising Food Steamers", VOL XII ISSUE 1, SPRING 2003, pp. 24.

FLUENT, 2002, "Computational Fluid Dynamics (CFD)", http://www.fluent.com/ solutions/whatcfd.htm#2 2002. 15-11-2002., Ref Type: Electronic Citation

FLUENT, 2004, http://www.fluent.com/solutions/food

FMF/FMA, Joint Technical Committee, 1979, "Hygienic Design of Food Plant, A guide to Good Practice with Particular Reference to The Design of Tanks, Pumps and Pipework"

Foodlink, 2004 "Food Poisoning Fact File". Office of population Cencuses and Surveys, Scottish Centre for Infection and Environmental Health and Regional Information Branch, Department of Health and Social Security, Belfast http://www.foodlink.org.uk/factfile1.pdf

Friis A. and Jensen B.B.B., DEC 2002, "Prediction of hygiene in food processing equipment using flow modelling", Food and Bioproducts Processing, vol. 80 (C4): 281-285

Gaillard, S., Leguerinel, I., & Mafart, P. 1998, "Model for combined effects of temperature, pH and water activity on thermal inactivation of Bacillus cereus spores", Journal of Food Science , vol. 63,no. 5, pp. 887-889.

Georgiadis M.C, Rotstein G.E. and Macchietto S., 1998, "Modelling and Simulation of Shell and Tube Heat Exchangers under Milk Fouling", AIChE Journal, April 1998 Vol. 44, No. 4, pp: 959-971

Georgiadis M.C, Rotstein G.E. and Macchietto S., 1998, "Modelling and Simulation of Complex Plate Heat Exchanger Arrangements under Milk Fouling", Computers Chem. Engng Vol. 22, Suppl., pp. S331-S338, 1998.

Georgiadis M.C. and Macchietto S., 2000, "Dynamic modelling and simulation of plate heat exchangers under milk fouling", Chemical Engineering Science 55 (2000) 1605-1619

Ghani Abdul A.G., Farid M.M., Chen X.D., 2002c, "Theoritical and experimental investigation of the thermal destruction of Vitamin C in food pouches.", Computers and electronics in agriculture 34 (2002c) 129-143

Ghani Abdul A.G., Farid M.M., Chen X.D., Richards P., 1999a, "Numerical simulation of natural convection heating of canned food by computational fluid dynamics", Journal of food Engineering 41 (1999a) 55-64.

Ghani Abdul A.G., Farid M.M., Chen X.D., Richards P., 1999b, "An investigation of deactivation of bacteria in a canned liquid food during sterilisation using computational fluid dynamics (CFD)", Journal of Food Engineering 42 (1999) 207-214.

Ghani Abdul A.G., Farid M.M., Chen X.D., Richards P., 2000, "Thermal sterilization of canned food in a 3-D pouch using computational fluid dynamics", Journal of food engineering 48 (2000) 147-156.

Ghani Abdul A.G., Farid M.M., Chen X.D., Richards P., 2001, "A computational fluid dynamics study on the effect of sterilization temperatures on bacteria deactivation and vitamin destruction.", IMechE 2001., Proc Instn Mech Engrs Vol 215 Part E.

Ghani Abdul A.G., Farid M.M., Chen X.D., Richards P., 2002a, "Numerical simulation of transient temperature and velocity profiles in a horizontal can during sterilization using computational fluid dynamics.", Journal of Food Engineering 51, 77-83

Ghani Abdul A.G., Farid M.M., Chen X.D., Richards P., 2002b, "Theoretical and experimental investigation of the thermal inactivation of Bacillus stearothermophilus in food pouches.", Journal of Food Engineering 51, 221-228.

Ghani Abdul A.G., Farid M.M., Zarrouk S.J., 2003, "The effect of can rotation on sterilization of liquid food using computational fluid dynamics.", Journal of Food Engineering 57, 9-16

Gibson, A. M., Bratchell, N., & Roberts, T. A. 1987, "The effect of Sodium-Chloride and temperature on the rate and extent of growth of *Clostridium-botulinum* type-a in pasteurised pork slurry", Journal of Applied Bacteriology, vol. 62,no. 6, pp. 479-490.

Gillham CR, Wilson DI, Fryer PJ and Hasting APM, 1998, "Studies in cleaning of whey protein deposits", Fouling and cleaning in food processing '98, Proceedings of a conference held at Jesus college, Cambridge, 6 to 8 April 1998, published by European community.

Grasshoff Albrecht, 1989, "Environmental Aspects on the use of alkaline cleaning solutions", Fouling and Cleaning in the food processing, Kessler H.G. and Lund D.B., eds. Pp. 107-114, Proc. I.C.F.C. III, Prien

Grasshoff Albrecht, 1992, "Hygienic design – the basis for computer controlled automation", ICHEME Symposium Series No. 126, "Food Engineering in a Computer Climate", pp: 89-109.

Grasshoff Albrecht, 1994, "Efficiency assessment of a multiple stage CIP-procedure for cleaning a dairy plate heat exchanger", Proceedings of the Fouling and Cleaning in Food processing conference, March 1994, edited by Fryer P.J., Hasting A.P.M and Jeurnink J.M. published by the European Commission.

Grifoll J. and Giralt F., 2000, "The near wall mixing length formulation revisited", International Journal of Heat and Mass Transfer 43, 3742-3746

Hall J.E., Jones M.R and Timperley A.W., 1999, "Improving the Hygienic Design of Food Processing Equipment Using Modelling Approaches Based on Computational Fluid Dynamics", Confidential R&D Report No. 91 Project No. 29735, Campden & Chorleywood Food Research Association.

Hasting A.P.M 1999, "Fouling and Cleaning In the Food Industry: Introduction and Overview", Trans IChemE, vol. Vol 77, no. Part C, pp. 73-74.

Hasting A.P.M 2002, "Industrial experience of monitoring fouling and cleaning systems". Fouling, Cleaning and Disinfection in Food Processing, Proceedings of a conference held at Jesus College, Cambridge, ISBN 0-9542483-0-9

Hasting A.P.M 2002, Personal communication.

Hasting, A. P. M., Blackburn, C. D. W., & Crowther, J. S. 2001, "Mycobacterium paratuberculosis and the commercial pasteurization of milk", Food and Bioproducts Processing, vol. 79,no. C2, pp. 83-88.

Hendrickx, M., Silva, C., Oliveira, F., & Tobback, P. 1993, "Generilised (Semi)-empirical formulas for optimal sterilisation temperatures of conduction-heated foods with infinite surface heat-transfer coefficients", *Journal of Food Engineering*, vol. 19,no. 2, pp. 141-158.

Easter Regional Research centre, 2004, Information About the Pathogen Modeling Program, http://www.arserrc.gov/mfs/Information.htm

Food Standards Agency, 2004, "Maintenance and improvements of the Food MicroModel database", http://www.food.gov.uk/science/research/researchinfo/foodborneillness/microriskresearch/b13programme/b13list/b08002/.

Jensen B. B. B., September 2002, "Hygienic Design of Closed Processing Equipment by use of Computational Fluid Dynamics", Ph.D. Thesis, Lungby.

Jensen B.B.B. and Friis A., 2004a, "Prediction of Flow in Mix-Proof Valve by Use of CFD-Validation by LDA", Journal of Food Process Engineering 27, 65-85.

Jensen B.B.B. and Friis A., 2004b, "Critical wall shear stress for the EHEDG method", 2004, Chemical Engineering and Processing 43, 831-840.

Jennings W.G., McKillop A.A and Luick J.R., 1957, "Circulation Cleaning", Journal of Dairy Science, 40, 1471-1479

Jones, J. E. & Walker, S. J. 1993, "Advances in modelling microbial growth", Journal of Industrial Microbiology , vol. 12,no. 3-5, pp. 200-205.

Jung A. and Fryer P.J., 1999, "Optimising the quality of safe food: Computational modelling of a continuous sterilisation process", Chemical Engineering Science 54 (1999) 717-730.

Kane D.R and Middlemiss N.E., 1985, "Cleaning Chemicals-state of the knowledge in 1985", Fouling and Cleaning in the food processing, Lund D.B., Plett E and Sandu C., eds. pp. 312-355, Proc. I.C.F.C. II, Madison, Wisconsin

Karlsson C.A.C. 1999, "Fouling and Cleaning of Solid Surfaces. The influence of surface characteristics and operating conditions", PhD Thesis, Food Engineering Lund University Sweden.

Kirkpatrick J.P., McIntire L.V., & Characklis W.G. 1980, "Mass and Heat transfer in a circular Tube with Biofouling", Water Research, Pergamon Press Ltd, vol. Vol. 14, pp. 117-127.

Klijn N., A.A.P.M. Herrewegh and P. de Jong, 2001, "Heat Inactivation Data for Mycobacterium avium subsp. Paraturberculosis: Implications for Interpretation", Journal of Applied Microbiology, 91, 697-704,

Kolmogorov A.N., 1942, "Equations of motion of an incompressible turbulent fluid"; Izv Akad Nauk SSSR Ser Phys VI No 1-2, p56

Kumar Ashwini and Bhattacharya M., 1991, "Numerical analysis of aseptic processing of a non-Newtonian liquid food in a tubular heat exchanger", Chem. Eng. Comm., Vol. 103, pp. 27-51.

Kumar Ashwini and Bhattacharya M., 1991, "Transient temperature and velocity profiles in a canned non-Newtonian liquid food during sterilization in a still-cook retort", Int. J. Heat Mass Transfer. Vol. 34, No. 4/5, pp. 1083-1096.

Kumar Ashwini, Bhattacharya M. and Blaylock Jack, 1990, "Numerical Simulation of Natural Convection Heating of canned thick viscous liquid food products", University of Minnesota Supercomputing Institute Research Report UMSI 90/16, February 1990.

Langeveld L.P.M, van Montfort-Quasig R.M.G.E, Weerkamp A.H, Waalewijn R., & Wever J.S. 1995, "Adherence, Growth and Release of bacteria in a tube heat exchanger for milk", Netherlands Milk & Dairy Journal no. 49, pp. 207-220.

Launder B. and Spalding D., 1974, "The numerical computation of turbulent flows", Computer Methods in Applied Mechanics and Engineering 3, 269-289. Launder and Spalding 1974

Lazaridis Xaralampos N., "Food Engineering", Giahoudi-Giapouli Thessaloniki 2000.

Lelievre C., Antonini G., Faille C, & Benezech T 2002, "Cleaning in place: modelling of cleaning kinetics of pipes soiled by Bacillus spores". Fouling, Cleaning and Disinfection in Food Processing, Proceedings of a conference held at Jesus College, Cambridge, ISBN 0-9542483-0-9

Liao H-J., Rao M.A. and Datta A.K., 2000, "Role of thermo-rheological behaviour in simulation of continuous sterilisation of a starch dispersion.", Trans IChemE, Vol 78, Part C, March 2000

Lindsay, D. & von Holy, A. 1998, "Nutrient limitation affects growth and attachment of two food spoilage bacteria, Bacillus subtilis and Pseudomonas fluorescens", South African Journal of Science, vol. 94, no. 8, pp. 393-396.

Loisel C., Lecq G., Launay B and Ollivon M, 1997, "Tempering of chocolate in a scraped surface heat exchanger", Journal of Food Science, 61 (4): 773-780, Jul-Aug 1997.

Lowara, ITT Industries, Vertical multistage centrifugal pumps manual. 1999.

McClure P.J., Blackburn C.D., Cole M.B., Curtis P.S., Jones J.E., Legan J.D., Ogden I.D., Peck M.W., Roberts T.A, Sutherland J.P and Walker S.j., 1994. "Modelling the growth, survival and death of microorganisms in foods-The UK Food MicroModel approach.", International Journal of Food Microbiology, 23, 265-275..

McMeekin T.A., Olley J., Ratkowsky D.A. and Ross T., 2002, "Predictive microbiology: towards the interface and beyond", International Journal of food microbiology 73, 395-407

McMeekin, T. A., Olley, J., Ross, T., & Ratkowsky, D. 1993, "Predictive Microbiology: Theory and Application", 1 edn, RESEARCH STUDIES PRESS LTD.

Menter F.R. 1994, "Two-Equation Eddy-Viscosity Turbulence Models for Engineering Applications.", AIAA Journal, vol. 32, no. 8, pp. 1598-1605.

Messer J.W., Rice E.W., & Johnson C.H., 2000 "Total Viable Counts". Robinson R.K, Batt C.A. and Patel P.D. 2154-2159., Academic Press. Encyclopedia of Food Microbiology.

Mwaba Misheck Gift 2003. "Analysis of heat exchanger Fouling in Cane Sugar Industry", PhD Thesis, Technische Universiteit Eindhoven, The Netherlands.

Neumeyer K., Ross T. and McMeekin T., 1997 "Development of *Pseudomonas* Predictor", The Australian Journal of Dairy Technology, Vol 52-October 1997, pp:120-122

Panikov N.S. and Nikolaev Y.A., 2002, "Growth and Adhesion of Pseudomonas fluorescens in a Batch Culture: A Kinetic Analysis of the Action of Extracellular Antiadhesins", Microbiology, Vol. 71, No 5, 2002, pp. 532-540. Translated from Mikrobiologiya, Vol. 71, No. 5, pp. 619-628

Patrick A. "Thermophysical properties of tomato products". 2004. Personal Communication

Pereira M.O., Kuehn M., Wuertz S., Neu T and Melo L.F., 2002, "Effect of Flow Regime on the Architecture of a *Pseudomonas fluorescens* Biofilm" Biotechnology and Bioengineering, Volume 78 Issue 2 164-171.

Pereira, M. O., Kuehn, M., Wuertz, S., Neu, T., & Melo, L. F. 2002, "Effect of flow regime on the architecture of a Pseudomonas fluorescens biofilm", Biotechnology and Bioengineering, vol. 78, no. 2, pp. 164-171.

Prescott Lansing, Harley John, & Klein Donald 1999, "Chapter 6 Microbial Growth," in Microbiology, Fourth edition edn, McGraw-Hill, ed.

Pruitt, K. M. & Kamau, D. N., 1993, "Mathematical-models of bacterial growth, inhibition and death under combined stress conditions", Journal of Industrial Microbiology, vol. 12,no. 3-5, pp. 221-231.

Ratkowsky D.A., Lowry R.K, McMeekin T.A., Stokes A.N., 1983, "Model for Bacterial Culture Growth Rate Throughtout the entire biokinetic temperature rate" Journal of Bacteriology, June 1983, p. 1222-1226.

Ratkowsky, D. A., Lowry, R. K., McMeekin, T. A., Stokes, A. N., & Chandler, R. E. 1983, "Model for Bacterial Culture Growth rate throughout the entire Biokinetic Temperature Range", Journal of Bacteriology, vol. 154, no. 3, pp. 1222-1226.

Ratkowsky, D. A., Olley, J., McMeekin, T. A., & Ball, A., 1982, "Relationship between temperature and growth rate of bacterial cultures", Journal of Bacteriology, vol. 149,no. 1, pp. 1-5

Robbins P.T., Elliott B.L.., Belmar M.T. and Hasting A.P., 1999, "A comparison of milk and whey fouling in a pilot scale plate heta exchanger: Implications for modelling and mechanistic studies", Food and Bioproducts Processing, 77 (C2): 97-106, Jun 1999

Robinson Richard K., Batt Carl A.,. Pater Pradip D, 2000, "Encyclopedia of food microbiology", Volume three. ACADEMIC PRESS 2000

Ross T. and McMeekin T.A., 2003, "Modelling Microbial Growth within food safety risk assessments", Risk Analysis, Vol. 23, No. 1, 2003, p.179-197

Ross, T. 1993, "BELEHRADEK-TYPE MODELS", Journal of Industrial Microbiology, vol. 12,no. 3-5, pp. 180-189.

Rossi e Catelli, 2004, www.rossicatelli.com, electronic citation.

R-theta. 2004 "Extrusion Heatsinks", www.r-theta.com/products/extrusion/part1.pdf ..

Russell A.B., Burmester S.S.H. and Winch P.J., 1997, "Characterisation of shear thinning flow within a scraped surface heat exchanger", Food and Bioproducts Processing, 75 (C3): 191-197 Sep 1997

Schoolfield, R. M., Sharpe, P. J. H., & Magnuson, C. E., 1981, "Non-linear regression of biological temperature-dependent rate models based on absolute reaction-rate theory", *Journal of Theoretical Biology*, vol. 88,no. 4, pp. 719-731.

Scott G.M., 1992, "Computational Fluid Dynamics for the Food Industry", September 1992, Technical Bulletin No. 90 Project No. 6103 DTI Link, The Campden Food and Drink Research Association

Scott, G., Richardson, P., 1996, "Simulation of the Flow of Non-Newtonian Foods Using Computational Fluid Dynamics", R&D Report No. 34, Project No. 18724, Campden & Chorleywood Food Research Association September 1996.

Scott, G., Richardson, P., 1997, "The application of computational fluid dynamics in the food industry", Trends in Food Science & Technology, Vol. 8: 119-124 April 1997.

Smerage G.H. & Teixeira A.A. 1993, "Dynamics of heat destruction of spores: a new view", *Journal of Industrial Microbiology*, vol. 12, pp. 211-220.

Sondex, 2000, "Plate Heat Exchanger Operating & Instruction Manual".

Stumbo C.R., Purohit K.S. and Ramakrishman T.V., 1975, "Thermal process lethality guide for low-acid foods in metal containers.", J. Food Science 40, 1316-1323

Tewkwsbury H., Stapley A.G.F., Fryer P.J., 2000, "Modelling temperature distributions in cooling chocolate moulds", Chemical Engineering Science 55, 3123-3132.

Thackery P.A., 1980, "The cost of fouling in heat exchange plant", Effluent and Water Treatment Journal, Vol. 20, Issue 3, pp. 111-115.

Thorpe R.H. and Barker P.M., 1988, "Hygienic Design of Liquid Handling Equipment for the Food Industry", Technical Manual No. 17, Food Preservation Research Association, 1988.

Trulear M.G. & Characklis W.G. 1982, "Dynamics of biofilm processes", J.Water Pollut.Control Fed no. 54, pp. 1288-1301.

Tucker, G. & Heydon, C. 1998, "Food particle residence time measurement for the design of commercial tubular heat exchangers suitable for processing suspensions of solids in liquids", Food and Bioproducts Processing, vol. 76, no. C4, pp. 208-216.

Tyrer H., Ainsworth P., İbanoğlu Ş. And Bozkurt H., 2004, "Modelling the growth of Pseudomonas fluorescens and Candida sake in ready-to-eat meals", Journal of Food Engineering 65, 137-143..

U.S. Food and Drug Administration Center for Food Safety and Applied Nutrition (FDA/CFSAN), 2004, "Kinetics of Microbial Inactivation for Alternative Food Processing Technologies Overarching Principles: Kinetics and Pathogens of Concern for All Technologies." http://vm.cfsan.fda.gov/~comm/ift-toc.html

Van Leeuwen, P.J.M., "Method for applying a protective layer to which microorganisms do not adhere to vessels and utensils used in the food industry", patent 11 of January 1996, WO 96/00505.

Varga Szabolcs, Oliveira Jorge V., Smout Chantal and Hendrickx Mark E., 2000, "Modelling temperature variability in batch retorts and its impact on lethality distribution", Journal of Food Engineering 44, 163-174.

Verboven P., Nicolai Bart M., Scheelinck Nico and De Baerdemaeker Josse, 1997, "The local surface heat transfer coefficient in thermal food process calculations: a CFD approach", Journal of Food Engineering 33, 15-35

Verdteeg H.K. & Malalasekera W. 1995, "An introduction to Computational Fluid Dynamics The Finite Volume Method", UK: Addison - Wesley Longman Higher Education

Wang S., Ikediala J.N., Tang J., & Hansen J.D. 2002, "Thermal death kinetics and heating rate effects for fifth-instar codling moths (*Cydia pomonella* (L.)", Journal of stored Products Research, vol. 38, pp. 441-453.

Wang Y.Y., Russell A.B. and Stanley R.A., 2002, "Mechanical damage to food particles during processing in a scraped surface heat exchanger", Food and Bioproducts Processing, 80 (C1): 3-11 Mar 2002

Wilcox D.C., 1993, "Turbulence modelling for CFD" (2nd ed.) DCW Industries, La Cañada, California.

Wilcox D.C., 1994, "Simulation of Transition with a Two-Equation Turbulence Model", AIAA Journal, Vol. 32, No. 2, February 1994.

Wilcox, D. C. 1998, "Turbulence Modelling for CFD" La Canada, California.

Willocx, F., Mercier, M., Hendrickx, M., & Tobback, P. 1993, "Modelling the influence of temperature and carbon-dioxide upon the growth of Pseudomonas-fluorescens", Food Microbiology, vol. 10,no. 2, pp. 159-173.

Wirtanen G., Ahola H., & Mattila-Sandholm T. 1994, "Evaluation of cleaning procedures for elimination of biofilm from stainless steel surfaces in open process equipment". Proceedings of a conference on Fouling and Cleaning in food processing, Jesus College Cambridge 23 to 25 March 1994, ISBN 92-827-4360-8.

Wirtanen G., Ahola H., Mattila-Sandholm T., 1994, "Evaluation of cleaning procedures for elimination of biofilm from stainless steel surfaces in open process equipment", Fouling and Cleaning in Food Processing, Proceedings of a conference held at Jesus College, Cambridge 23 to 25 March 1994, pp. 167-177.

Woodall D.L., 2004, Personal communication.

Danish Institude for Fisheries Research, 2005, "Seafood Spoilage and Safety Predictor (SSSP) software version 1.0", www.dfu.min.dk/micro/sssp

Zwietering, M. H. & Hasting, A. P. M. 1997a, "Modelling the hygienic processing of foods - A global process overview", Food and Bioproducts Processing, vol. 75,no. C3, pp. 159-167

Zwietering, M. H. & Hasting, A. P. M. 1997b, "Modelling the hygienic processing of foods - Influence of individual process stages", Food and Bioproducts Processing, vol. 75,no. C3, pp. 168-173.

Zwietering, M. H., Dekoos, J. T., Hasenack, B. E., Dewit, J. C., & Vantriet, K. 1991, "Modelling of bacterial growth as a function oftemperature", Applied and Environmental Microbiology, vol. 57,no. 4, pp. 1094-1101.

Zwietering, M. H., Jongenburger I., Rombouts F.M., & Van 't Riet K. 1990, "Modelling of bacterial growth curve", Applied and Environmental Microbiology, vol. 56, pp. 1875-1881

Zwietering, M. H., Rombouts, F. M., & Vantriet, K. 1992, "Comparison of definitions of the lag phase and the exponential phase in bacterial growth", Journal of Applied Bacteriology, vol. 72,no. 2, pp. 139-145.